The role of the upper ocean for global ocean heat uptake and climate

Linus Vogt

Sorbonne Université

Ecole Doctorale 129 – Sciences de l'Environnement d'Ile de France

Laboratoire d'Océanographie et du Climat: Expérimentations et Approches Numériques (LOCEAN)

The role of the upper ocean for global ocean heat uptake and climate

Ph.D. thesis in oceanography and climate science

Linus Vogt

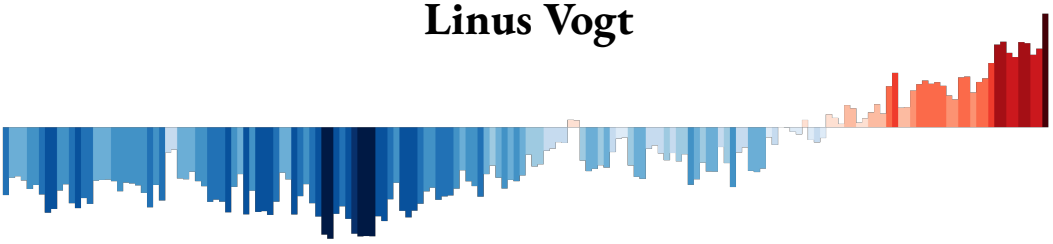

Defense held on December 6, 2024, before a jury composed of:

Jury president	Prof. Pascale Bouruet-Aubertot	Sorbonne Université, France
Reviewers	Prof. Laure Zanna	New York University, USA
	Prof. Jonathan M. Gregory	University of Reading, UK
Examiners	Dr. Céline Heuzé	University of Gothenburg, Sweden
	Dr. Helene Hewitt	Met Office, UK
Thesis supervisors	Dr. Jean-Baptiste Sallée	CNRS, France
	Dr. Casimir de Lavergne	CNRS, France

Sorbonne Université

Ecole Doctorale 129 – Sciences de l'Environnement d'Ile de France

Laboratoire d'Océanographie et du Climat: Expérimentations et Approches Numériques (LOCEAN)

Le rôle de l'océan de surface pour le stockage de chaleur océanique global et le climat

Thèse de doctorat en océanographie et sciences du climat

Linus Vogt

Soutenue le 6 décembre 2024 devant le jury composé de :

Présidente du jury	Prof. Pascale Bouruet-Aubertot	Sorbonne Université, France
Rapportrice	Prof. Laure Zanna	New York University, USA
Rapporteur	Prof. Jonathan M. Gregory	University of Reading, UK
Examinatrices	Dr. Céline Heuzé	University of Gothenburg, Suède
	Dr. Helene Hewitt	Met Office, UK
Directeurs de thèse	Dr. Jean-Baptiste Sallée	CNRS, France
	Dr. Casimir de Lavergne	CNRS, France

In memory of Klaus Koppe

Acknowledgements

I am indebted to a number of people without whom this work would not have been possible.

The members of the jury: thank you for having invested the time and effort to read my manuscript and provide helpful comments, as well as for an interesting discussion during the defense.

JB and Casimir: thank you for being great supervisors! I am thankful for your support, advice, and ideas during these three years, and I appreciate that you were open to let me work on things sometimes unrelated to your usual interests.

Jens Terhaar: thank you for inviting me to Woods Hole in 2023, and for the very fruitful collaboration ever since. Also thanks for forwarding JB's Twitter ad in 2021, which is how I found this PhD position!

Juliette Mignot and Ric Williams: thank you for your ideas and advice as part of my PhD committee, which has provided me with much-needed guidance during the early part of the PhD.

Vincent Lam and Julie Jebeile (et al.): thank you for the interesting course on "Philosophical issues in modeling climate change" during my master's in Bern, which has motivated and inspired parts of the Introduction of this thesis.

B. B. Cael: thank you for a brief exchange which has partly inspired the ideas for Chapter 4.

My previous teachers and mentors: Thomas Frölicher, thank you for getting me into oceanography and climate science in the first place, and for letting me sit at KUP during my visits to Bern. Mathias Aschwanden, thank you for giving me a crash course in scientific Python in my first research days and being a role model for good coding practices ever since. Sven Huber, thank you for your effort and patience during my high school years.

Lab friends: thanks for the amazing time we had during my three years in Paris. I'm not putting a huge list of names here (because I don't like picking favorites, and because I hope the people concerned know how much I appreciate them, and because no one reads this anyway!), but know that I will never forget what we had.

My parents: thank you for your unconditional support and for giving me the freedom to pursue the things I really wanted.

Natacha: bisou!

This document was typeset in LaTeX by adapting the `latex-mimosis` template originally developed by Bastian Rieck using `KOMA-script`.

The image on the title page is adapted from the "warming stripes" visualisation by Prof. Ed Hawkins at the University of Reading (www.showyourstripes.info) and shows a timeseries of global mean sea surface temperature anomalies over the period 1850–2023 relative to a 1961–2010 baseline using UK Met Office data. The original image including axis labels is shown in Figure A.1 in Appendix A.

Abstract

The Earth's climate is currently undergoing rapid and widespread changes. Human activities in the industrial era, in particular the emission of CO_2 into the atmosphere through the burning of fossil fuels, have led to an enhanced greenhouse effect which has caused an increase in the global average surface air temperature of 1.1 °C in 2011–2020 relative to 1850–1900. A further consequence is the warming of the global ocean: it has absorbed over 90% of the excess energy stored in the Earth system due to the increased radiative forcing.

This global ocean heat uptake (OHU) is a critical climate process and plays a dual role for anthropogenic climate change. On the one hand, OHU is a measure of the cumulative effects of transient climate change, and scales with negative impacts such as sea level rise and the frequency of oceanic extreme events. On the other hand, OHU provides a crucial service by shielding the atmosphere from large amounts of heat that would otherwise cause much greater global warming than currently observed.

Despite their importance, many of the physical processes controlling OHU are still poorly understood, including in state-of-the-art numerical climate models used for international climate change assessments. In this thesis, we address this problem using climate simulations of models participating in the Coupled Model Intercomparison Project (CMIP). In a first study, we provide improved future projections of global OHU by the end of the 21st century by identifying an emergent relationship across an ensemble of CMIP models linking the simulated baseline climate state of the Southern Hemisphere to future global OHU. By combining this relationship with observational data, we obtain constrained projections showing that future OHU is likely larger than previously thought. In a second study, we clarify the processes involved in setting the ocean heat uptake efficiency (OHUE) which quantifies the amount of OHU per degree of global surface warming. We reconcile a number of previous attempts at explaining controls on OHUE, and show that the upper ocean stratification in the Southern Ocean is a key property setting its value in CMIP climate models. Last, we present an exploratory analysis combining the approaches of these two studies, and perform a statistical analysis of simulations from a large multi-model ensemble with the goal of constraining OHUE.

Beyond these concrete results concerning global OHU, we also discuss some of the methodological issues related to the interpretation of uncertainties arising from multi-model ensembles more generally.

Résumé

Le climat terrestre connaît actuellement des changements rapides et généralisés. Les activités humaines depuis l'ère industrielle, en particulier les émissions de CO_2 dans l'atmosphère dues à la combustion de combustibles fossiles, ont intensifié l'effet de serre. Cela a entraîné une augmentation de la température moyenne de l'air à la surface du globe de 1.1 °C en 2011–2020 par rapport à 1850–1900. Une autre conséquence majeure est le réchauffement des océans mondiaux, qui ont absorbé plus de 90% de l'énergie excédentaire accumulée dans le système climatique en raison de l'augmentation du forçage radiatif.

L'absorption de chaleur par l'océan mondial (OHU) est un processus climatique clé qui joue un double rôle dans le changement climatique d'origine anthropique. D'une part, l'OHU constitue en soi une mesure clé du changement climatique, qui est directement associée à des impacts négatifs tels que l'élévation du niveau de la mer et l'augmentation de la fréquence des événements extrêmes dans l'océan. D'autre part, l'OHU fournit un service climatique essentiel en épargnant l'atmosphère de grandes quantités de chaleur, sans lequel le réchauffement atmosphérique serait bien plus marqué que celui que nous observons actuellement.

Malgré leur importance, de nombreux processus physiques qui contrôlent l'OHU restent mal compris, même dans les modèles climatiques numériques utilisés dans les évaluations internationales du changement climatique. Dans cette thèse, nous avançons sur ce problème en nous appuyant sur des simulations climatiques issues de modèles participant au Projet d'intercomparaison des modèles couplés (CMIP).

Dans une première étude, nous produisons des estimations améliorées de l'OHU global d'ici à la fin du XXIe siècle en identifiant une relation émergente dans un ensemble de modèles CMIP, qui relie l'état climatique présent de l'hémisphère sud à l'OHU futur. En combinant cette relation avec des données d'observation, nous obtenons des projections mieux contraintes qui montrent que l'OHU futur pourrait être plus important qu'estimé précédemment.

Dans une deuxième étude, nous clarifions les processus à l'origine de l'efficacité d'absorption de la chaleur océanique (OHUE), qui quantifie la quantité d'OHU par degré de réchauffement de la surface terrestre. Nous réconcilions plusieurs tentatives antérieures d'explication des facteurs influençant l'OHUE, et montrons que la stratification de l'océan Austral supérieur est une propriété clé qui contrôle l'OHUE dans les modèles climatiques CMIP.

Enfin, nous présentons une analyse exploratoire combinant les approches de ces deux études, et menons une analyse statistique des simulations d'un grand ensemble multi-modèle dans le but de contraindre l'OHUE.

Au-delà de ces résultats concrets concernant l'OHU global, nous discutons également de certaines questions méthodologiques liées à l'interprétation des incertitudes découlant des ensembles multi-modèles de manière plus générale.

Plain language summary

It is now an unequivocal fact that human activities in the industrial era (i.e., since around 1760) have caused significant changes to Earth's climate. The burning of fossil fuels and changes in land use such as deforestation have led to the emission of greenhouse gases into the atmosphere. These gases, which include carbon dioxide (CO_2) and methane (CH_4), act as an insulating blanket and reduce the radiation emitted from Earth to space, which in turn leads to increased surface temperatures. The Intergovernmental Panel on Climate Change (IPCC) has recently assessed that the globally averaged surface air temperature has warmed by 1.1 °C compared to its level in the late 19th century. However, not only the air has warmed: the world's oceans have taken up over 90% of the additional heat energy trapped in the climate system. This is both due to the ocean's tremendous mass as well as the particularly high capacity of water to absorb energy.

This ocean heat uptake (OHU; measured in Joules) is the subject of this Ph.D. thesis. One the one hand, OHU leads to widespread negative impacts: for example, the melting of ice sheets and the expansion of water as it warms lead to sea level rise, and warmer ocean temperatures increase the frequency of destructive marine heatwaves with harmful consequences for marine ecosystems. On the other hand, OHU provides a great service: it removes heat from the atmosphere and stores it at depth, which greatly reduces the magnitude of the surface warming that humans experience compared to a hypothetical world with zero OHU.

In this thesis, we use three-dimensional numerical computer models of the climate system to better understand the physical processes contributing to OHU, as well as to obtain future OHU projections with reduced uncertainties. In a first study, we combine simulations from an ensemble of 28 different climate models with observational data to obtain constrained OHU projections by the end of the 21st century, and show that future OHU will likely be greater than previously appreciated. In a second study, we reconcile a number of previous studies which tried to identify the physical mechanisms controlling the efficiency of OHU at removing heat from the atmosphere. Last, we identify potential ways to constrain this efficiency by performing a statistical analysis of simulation output from an ensemble of over 100 climate model simulations.

Beyond these concrete results concerning global OHU, we also discuss some of the methodological issues related to the interpretation of uncertainties arising from ensembles consisting of different climate models more generally.

Résumé simplifié

Il est désormais établi que les activités humaines de l'ère industrielle (c'est-à-dire depuis 1760 environ) ont provoqué des changements significatifs dans le climat de la Terre. La combustion de combustibles fossiles et les changements dans l'utilisation des sols, tels que la déforestation, ont entraîné l'émission de gaz à effet de serre dans l'atmosphère. Ces gaz, qui comprennent le dioxyde de carbone (CO_2) et le méthane (CH_4), agissent comme une couverture isolante et réduisent le rayonnement émis de la Terre vers l'espace, ce qui entraîne une augmentation des températures de surface. Le groupe d'experts intergouvernemental sur l'évolution du climat (GIEC) a récemment estimé que la température moyenne de l'air à la surface du globe s'est réchauffée de 1,1 degré Celsius par rapport à son niveau de la fin du XIXe siècle. Cependant, l'air n'est pas le seul à s'être réchauffé : les océans ont absorbé plus de 90% de l'énergie thermique supplémentaire créée par le changement climatique. Ce phénomène est dû à la fois à la masse considérable des océans et à la capacité particulièrement élevée de l'eau à absorber l'énergie.

Cette absorption de chaleur par les océans (OHU ; mesurée en joules) est le sujet de cette thèse de doctorat. D'un côté, l'OHU a des effets négatifs considérables : par exemple, la fonte des calottes glaciaires et l'expansion de l'eau lorsqu'elle se réchauffe entraînent une élévation du niveau de la mer, et les températures océaniques plus élevées augmentent la fréquence des vagues de chaleur marine destructrices, avec des conséquences néfastes pour les écosystèmes marins. De l'autre côté, l'OHU rend un grand service : il retire la chaleur de l'atmosphère et la stocke en profondeur, ce qui réduit considérablement l'ampleur du réchauffement de surface que subissent les humains par rapport à un monde hypothétique où l'OHU serait nulle.

Dans cette thèse, nous utilisons des modèles numériques tridimensionnels du système climatique pour mieux comprendre les processus physiques contribuant à l'OHU, ainsi que pour obtenir des projections futures de l'OHU avec des incertitudes réduites. Dans une première étude, nous combinons les simulations d'un ensemble de 28 modèles climatiques différents avec des données d'observation pour obtenir des projections contraintes de l'OHU d'ici la fin du 21ème siècle, et nous montrons que l'OHU futur sera probablement plus important que ce que l'on pensait jusqu'à présent. Dans une deuxième étude, nous réconcilions un certain nombre d'études antérieures qui ont tenté d'identifier les mécanismes physiques contrôlant l'efficacité de l'OHU à limiter le réchauffement de l'atmosphère. Enfin, nous identifions des moyens potentiels de mieux connaîtrmieux connaître cette efficacité en effectuant une analyse statistique des résultats d'un ensemble de plus de 100 simulations de modèles climatiques.

Au-delà de ces résultats concrets concernant l'OHU global, nous discutons également de certaines questions méthodologiques liées à l'interprétation des incertitudes découlant d'ensembles constitués de différents modèles climatiques de manière plus générale.

Scientific activities during the Ph.D.

Published/accepted articles

- **L. Vogt**, F. A. Burger, S. M. Griffies and T. L. Frölicher. 2022. "Local Drivers of Marine Heatwaves: A Global Analysis With an Earth System Model." Frontiers in Climate 4:847995. https://doi.org/10.3389/fclim.2022.847995 ⊕
- SO-CHIC consortium, J.-B. Sallée et al. (including **L. Vogt**). 2023. "Southern Ocean Carbon and Heat Impact on Climate." Philosophical Transactions of the Royal Society A: Mathematical, Physical and Engineering Sciences 381 (2249): 20220056. https://doi.org/10.1098/rsta.2022.0056. ⊕
- A. Minière, K. von Schuckmann, J.-B. Sallée, and **L. Vogt**. 2023. "Robust Acceleration of Earth System Heating Observed over the Past Six Decades." Scientific Reports 13 (1): 22975. https://doi.org/10.1038/s41598-023-49353-1. ⊕
- J. Terhaar, **L. Vogt**, and N. P. Foukal. 2025. "Atlantic overturning inferred from air-sea heat fluxes indicates no decline since 1960." Nature Communications 16, 222. https://doi.org/10.1038/s41467-024-55297-5 ⊕
- J. Terhaar, F. Burger, **L. Vogt**, T. L. Frölicher, and T. F. Stocker. "Record sea surface temperature jump in 2023/24 unlikely but not unexpected." Accepted for publication in *Nature*. ⊕

Articles in review

- **L. Vogt**, C. de Lavergne, J.-B. Sallée, L. Kwiatkowski, T. Frölicher, and J. Terhaar. In review. "Increased future ocean heat uptake constrained by Antarctic sea ice extent." Preprint: https://doi.org/10.21203/rs.3.rs-3982037/v1
- **L. Vogt**, J.-B. Sallée, and C. de Lavergne. In review. "Stratification and overturning circulation are intertwined controls on ocean heat uptake efficiency in climate models." Preprint: https://doi.org/10.5194/egusphere-2024-3442

Updated January 22, 2025. Studies marked by the symbol ⊕ were conducted at least in part during the time of the Ph.D. project but are not included in this thesis.

Summer schools

- *Physics of the Ocean*, Bad Honnef, Germany. July 2023, one week.
- *Southern Ocean Summer School*, Cargèse, Corsica (France). May 2024, two weeks.

Research visits

- Guest Student at Woods Hole Oceanographic Institution (WHOI), Woods Hole, USA. March–May 2023. Host: Dr. Jens Terhaar

Seminars

- **L. Vogt** et al. 2024. Southern Ocean stratification and overturning circulation controls on ocean heat uptake efficiency.
  Oral presentation: SO-CHIC annual meeting 2024, Paris, France.
- **L. Vogt** et al. 2024. Understanding and constraining ocean heat uptake with climate models.
  Invited talk: Max-Planck-Institute for Meteorology / University of Hamburg.
- **L. Vogt** et al. 2023. Antarctic sea ice predicts ocean heat uptake in climate simulations.
  Oral presentation: SO-CHIC annual meeting 2023, Paris, France.
- **L. Vogt** et al. 2022. Stratification feedbacks on ocean heat uptake in CMIP6.
  Oral presentation: SO-CHIC annual meeting 2022, Paris, France.

International conferences

- **L. Vogt** et al. 2024. Increased future ocean heat uptake constrained by Antarctic sea ice extent.
  Oral presentation: European Geosciences Union 2024, Vienna, Austria.
- **L. Vogt** et al. 2022. Local Drivers of Marine Heatwaves: A Global Analysis With an Earth System Model.
  Oral presentation: European Geosciences Union 2022, Vienna, Austria.
- **L. Vogt** et al. 2022. Local Drivers of Marine Heatwaves: A Global Analysis With an Earth System Model.
  Oral presentation: Ocean Sciences Meeting 2022, virtual.

Contents

List of Figures

List of Tables

Acronyms

AABW	Antarctic Bottom Water
AAIW	Antarctic Intermediate Water
ACC	Antarctic circumpolar current
AMOC	Atlantic meridional overturning circulation
AOGCM	Atmosphere-ocean general circulation model
CMIP	Coupled Model Intercomparison Project
CMIP6	CMIP phase 6 (in general, CMIP*n* for phases $n = 1, 2, 3, 5,$ and 6)
EBM	Energy balance model
EC	Emergent constraint
ECS	Equilibrium climate sensitivity
EEI	Earth energy imbalance
EEP	Eastern Equatorial Pacific
EffCS	Effective climate sensitivity
ENSO	El Niño–Southern Oscillation
ERF	Effective radiative forcing
ESM	Earth system model
GCM	General circulation model
GHG	Greenhouse gas
GO-SHIP	Global Ocean Shipbased Hydrographic Investigations Program
ICE	Initial condition ensemble
IMR	Inter-model relationship
IPCC	Intergovernmental Panel on Climate Change
IPCC AR6	IPCC sixth assessment report
IPCC AR6 WG1	IPCC AR6 Working Group I ("The Physical Science Basis")
MHW	Marine heatwave
MIP	Model intercomparison project
MME	Multi-model ensemble
NADW	North Atlantic Deep Water
NPP	Net primary production

NWP	Numerical weather prediction
OHC	Ocean heat content
OHU	Ocean heat uptake
OHUE	Ocean heat uptake efficiency
PDO	Pacific Decadal Oscillation
PPE	Perturbed parameter ensemble
SAF	Snow albedo feedback
SAMW	Subantarctic Mode Water
SAT	Surface air temperature
SLR	Sea level rise
SST	Sea surface temperature
TCRE	Transient climate response to emissions
TEOS-10	Thermodynamic Equation of SeaWater 2010
TOA	Top of the atmosphere
WEP	Western Equatorial Pacific
WOCE	World Ocean Circulation Experiment

I Introduction and Methods

Today, the reality of anthropogenic climate change is unequivocal (Masson-Delmotte et al. 2021a). Human activities in the industrial era, in particular the burning of fossil fuels and changes in land use, have caused increasing concentrations of greenhouse gases (GHGs) such as carbon dioxide (CO_2), methane (CH_4), and nitrous oxide (N_2O) in the atmosphere. The resulting enhanced greenhouse effect has led to an effective radiative forcing at the top of the atmosphere of 2.72 W m^{-2} over 1750–2019, resulting in global mean surface warming of 1.09 °C in 2011–2020 relative to 1850–1900, and an additional 435 ZJ (Zettajoules, 1 ZJ = 10^{21} J) of energy stored in the Earth system over the period 1971–2018 (Forster et al. 2021). Over 90% of this energy has been stored in the ocean through ocean heat uptake (OHU, Fig. 1.1; Schuckmann et al. 2020). The ocean thus plays a crucial buffering role in contemporary climate change by absorbing and redistributing heat that would otherwise warm the atmosphere.

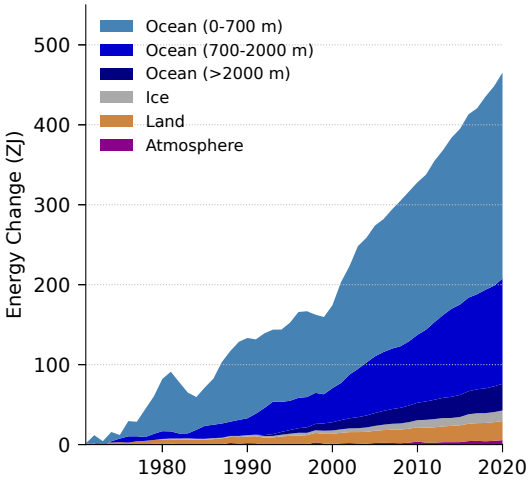

Figure 1.1: Observed changes in the Earth energy inventory for the period 1971–2020. Adapted from Forster et al. (2023) (Fig. 4a).

This chapter is structured into two parts. In section 1.1, we review the role of OHU in the climate system based on a conceptual distinction between two ways of thinking about OHU. In section 1.2, we review the structure and functioning of modern numerical climate models, which are the principal tools used in the main chapters of this thesis.

1.1 Ocean heat uptake and its role in the climate system

1.1.1 The ocean as a climate system component

Before turning to ocean heat uptake, we begin with an overview situating the functioning and circulation of the ocean as a component of the full climate system, and introduce a number of terms used throughout this thesis.

With a surface area of around 361 million km^2 (71% of the Earth's surface area) and an average depth of roughly 3730 meters, the global ocean contains 1.3×10^{18} m^3 of water, representing more than 95% of the water available to participate in the global hydrological cycle (Stocker 2013). Seawater has a high specific heat capacity of $c_p = 3992\,\mathrm{J\,kg^{-1}\,K^{-1}}$ and an average density of $\rho_w = 1027\,\mathrm{kg\,m^{-3}}$ (compared to the values of around $c_p = 700\,\mathrm{J\,kg^{-1}\,K^{-1}}$ and $\rho_a = 1.2\,\mathrm{kg\,m^{-3}}$ for air), making the ocean by far the largest reservoir of heat in the climate system (for a precise definition of the concept of "heat content", see Sec. 1.1.3.1 below), with the upper 100 m having a heat capacity around 30 times larger than that of the entire atmosphere (Canadell et al. 2021).

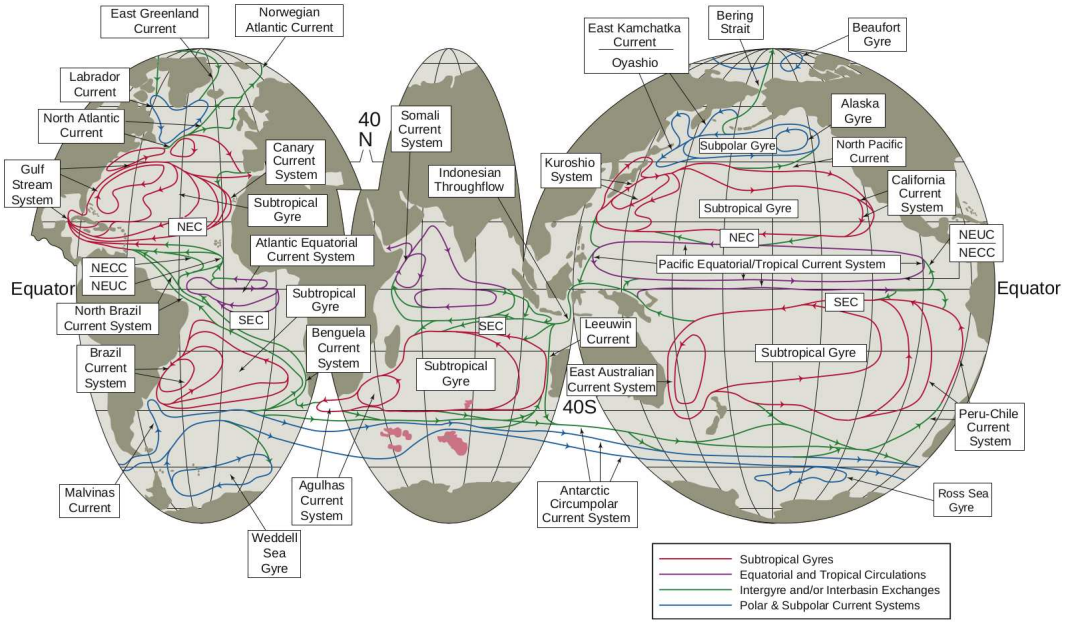

Figure 1.2: Schematic of the surface ocean circulation. Reprinted from Talley et al. (2011) (Fig. 14.1), originally modified from Schmitz (1996).

At its surface, the ocean is in contact with the atmosphere and continually exchanges mass (mainly water vapor), momentum (through winds), heat (through radiation as well as sensible and latent heat fluxes), and gases including oxygen and carbon dioxyde. These exchanges span a vast range of spatial and temporal scales, from millimeters and seconds for turbulent gas exchange

to global and multi-millenial scales for freshwater storage over glacial cycles, and they represent a crucial group of processes for climate dynamics. For example, the supply of water vapor to the atmosphere is a key ingredient for the establishment of the natural greenhouse effect which increases the average atmospheric surface temperature by around 33 °C compared to an equivalent planet with no atmosphere (Marshall and Plumb 2008), and is thus partly responsible for the habitability of Earth to organic life.

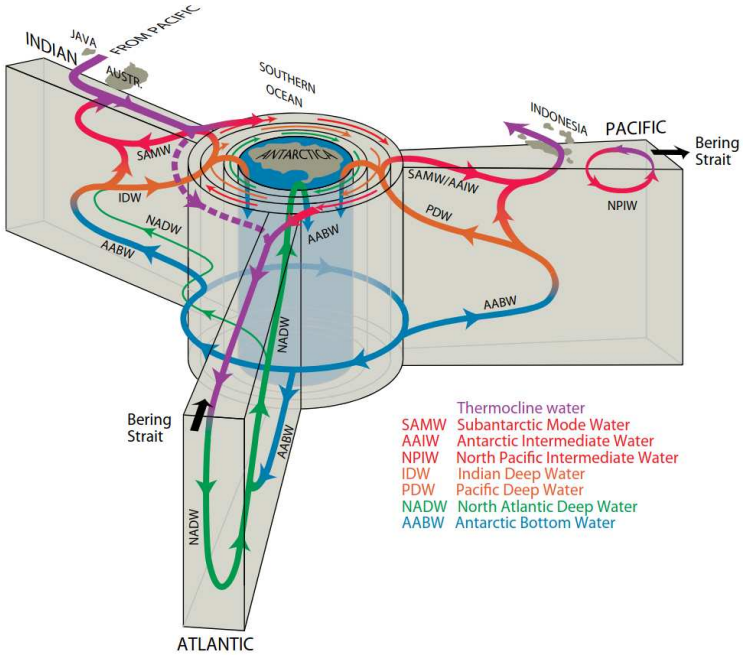

Figure 1.3: Schematic of the global overturning circulation centered on the Southern Ocean. Reprinted from Talley (2013) (Fig. 4).

The action of winds on the surface ocean drives large scale currents in the upper ocean (Fig. 1.2; Munk 1950). Since, unlike the atmosphere, the ocean is laterally bounded by continents at most latitudes, surface wind stress leads to the formation of large-scale rotating gyres at subtropical and subpolar latitudes in all major ocean basins (the red and blue streamlines in Fig. 1.2, respectively), with intense currents at their western boundaries due to the effects of planetary rotation (Stommel 1948). An exception to this behavior is found in the Southern Ocean, defined roughly as the region south of 35°S, where strong westerly winds create the Antarctic Circumpolar Current (ACC) which flows largely unimpeded by continental boundaries and represents around 173 Sv (Donohue et al. 2016, Sverdrups, 1 Sv = 1×10^6 m^3 s^{-1}) of volume transport, making it the strongest ocean current globally. In addition to these wind-driven currents, air-sea fluxes of heat and freshwater force the ocean circulation by changing the density of seawater at the surface. Cooling and evaporation of water in high latitude regions such as the Labrador Sea in the North Atlantic or

the Weddell Sea in the Southern Ocean can cause the water column to become gravitationally unstable, triggering vertical convection. Together with wind-driven upwelling and turbulent mixing in the ocean interior, this effect produces a large-scale meridional overturning cell in the Atlantic known as the Atlantic Meridional Overturning Circulation (AMOC; Toggweiler and Samuels 1998; Cimoli et al. 2023). The AMOC transports large amounts of mass and heat northwards in the Atlantic surface ocean, and returns towards the Southern Ocean via a deeper southward branch of North Atlantic Deep Water (NADW). In the Southern Ocean, divergent wind-induced surface Ekman flow leads to upwelling of water from the deep ocean which returns to depth following either the "upper cell" through the formation of Subantarctic Mode Water (SAMW) and Antarctic Intermediate Water (AAIW), or the "lower cell" which fills the abyssal ocean with cold and dense Antarctic Bottom Water (AABW; Marshall and Speer 2012) This global overturning circulation is depicted in Fig. 1.3 and regulates regional and global climate through the redistribution of heat, carbon, and other tracers (Talley 2013). In particular, Fig. 1.3 highlights the role of the Southern Ocean as a central hub connecting all major ocean basins, as well as the upper and deep oceans. As we will see in Chapters 2 and 3, the Southern Ocean is also a key region for ocean heat uptake, in large part due to its circulation features described above.

1.1.2 Two conceptions of ocean heat uptake

Although one can perhaps not ascribe a normative value to an abstract technical concept such as OHU, there do exist two distinct views of thinking about OHU in the literature: in the first, OHU is considered as "negative" or "detrimental", and in the second OHU is considered as "good" or "beneficial". These views are not contradictory, however, as they merely consider two different aspects of the role of OHU for the climate system.

The first view considers OHU simply as the *total increase in ocean heat content* (either locally or globally integrated), measured in Joules, relative to some baseline. This definition directly measures the energy stored by the ocean through warming and is directly related to negative impacts such as regional and global sea level rise, which is why OHU in this sense could be considered as detrimental.

The second view defines the crucial *ocean heat uptake efficiency* (OHUE) metric, defined as the amount of OHU per degree of global warming and measured in units of $\mathrm{W\,m^{-2}\,K^{-1}}$, which broadly quantifies the role of the ocean in buffering climate change by removing heat from the atmosphere, and could thus be considered as beneficial.

These two views will structure the remainder of this thesis. The concept of total OHU is the focus of chapter 2, where we present a novel emergent constraint on future total OHU by the end of the century. The concept of OHUE is treated in chapter 3, where we analyze the oceanic

controls on OHUE in climate models under idealized forcing. In the remainder of the present section, we will introduce these two notions in more detail by reviewing existing studies on historical observations and future projections of these quantities, as well as physical process understanding and the research gaps addressed in chapters 2 and 3.

1.1.3 Total ocean heat uptake

1.1.3.1 Some definitions

For the sections that follow, it is necessary to define a few central terms, in particular the variables ocean heat content (OHC) and ocean heat uptake (OHU).

§ Ocean heat content The term "heat content"—widely used in oceanography—may seem unconventional at first, since, as many introductory texts on thermodynamics will emphasize, heat is usually defined as a type of *flux* of energy between thermodynamic systems, not as the energy *content* of any system. More precisely, heat is not a state function like temperature or volume, and a parcel of seawater cannot classically be said to "have" or "contain" a certain amount of heat. This is why in the first law of thermodynamics, which expresses the conservation of energy, the change in heat Q is sometimes expressed as an inexact differential (denoted here by ∂):

$$\mathrm{d}U = \partial Q - p\,\mathrm{d}V \tag{1.1}$$

where $\mathrm{d}U$ is the exact differential of internal energy U, and $\partial W = p\,\mathrm{d}V$ is the thermodynamic work done by the system (due to a change in volume V at pressure p). This notation emphasizes the fact that the integrated change in internal energy, a state function, only depends on the initial and final states of a thermodynamic process, while the integrated change in heat and work is path dependent.

However, since seawater is nearly incompressible, work done on the ocean by pressure is small, and furthermore kinetic energy is small relative to internal and potential energy, making it possible to find a sensible definition of "heat content" (Vallis 2017). The term heat content as it is used in oceanography refers not to heat in the above sense, but refers to another quantity: *potential enthalpy*. Enthalpy H is defined as $H = U + pV$. At constant pressure ($\mathrm{d}p = 0$), this definition implies that a change in enthalpy is equal to the amount of heat transferred:

$$\mathrm{d}H = \mathrm{d}U + \mathrm{d}(pV) \overset{(1.1)}{=} \partial Q. \tag{1.2}$$

Enthalpy is preferred over internal energy U because the energy transfer between water parcels is associated with a flux of enthalpy and not of internal energy, since enthalpy accounts for the work

done by pressure forces and is not affected by effects such as cabbeling (McDougall 1987; Vallis 2017). *Potential* enthalpy is then defined as the enthalpy of a water parcel brought to a constant reference pressure $p_{\text{ref}} = 0$ at the sea surface without the exchange of heat or salt. The potential enthalpy per unit mass is denoted by h^0. McDougall 2003 has shown that the use of potential enthalpy as a measure of "heat content" has several advantages: (i) unlike internal energy, h^0 is very nearly conservative except for negligible error terms (i.e. it is neither created nor destroyed by mixing at constant pressure), (ii) interior fluxes of h^0 are balanced exactly by air-sea heat fluxes (since the reference pressure $p_{\text{ref}} = 0$ is at the sea surface) and nearly exactly by geothermal heating at the ocean bottom, and (iii) h^0 almost exactly obeys a conservation equation of the form

$$\rho \frac{\mathrm{D}h^0}{\mathrm{D}t} = \nabla \cdot \vec{F}, \tag{1.3}$$

where ρ is in-situ density and $\vec{F}$ is the flux of potential enthalpy, such that ρh^0 can be usefully regarded as the "heat content" per unit volume (Vallis 2017). Based on potential enthalpy, McDougall 2003 further defined *conservative temperature* Θ, a highly conserved temperature variable (Graham and McDougall 2013) which can be computed from observational data or ocean model output using efficient algorithms (McDougall and Barker 2011) or directly inferred from potential temperature (McDougall 2003; McDougall et al. 2021). Using conservative temperature, potential enthalpy can be written as $h^0 = c_p^0 \Theta$, where $c_p^0 = 3991.87\,\mathrm{J\,kg^{-1}\,K^{-1}}$ is a constant heat capacity defined by the TEOS-10 standard (McDougall and Barker 2011), and ocean heat content in some ocean volume A can be calculated in the following simple form (Griffies et al. 2016):

$$\mathrm{OHC} = \int_A \rho\, c_p^0\, \Theta \,\mathrm{d}V. \tag{1.4}$$

In practice, OHC can also be calculated according to the definition above using model output of potential temperature θ, which is the temperature of a water parcel when brought to the sea surface without the exchange of heat and is used as the prognostic temperature variable in many ocean models, instead of conservative temperature Θ (McDougall 2003; Griffies et al. 2016; McDougall et al. 2021).

§ Ocean heat uptake Following this rather detailed definition of OHC, total ocean heat uptake (OHU) can now be easily defined as the time rate of change of OHC. OHU at time t is defined as the increase in OHC relative to some baseline time t_0,

$$\mathrm{OHU}(t) = \mathrm{OHC}(t) - \mathrm{OHC}(t_0), \tag{1.5}$$

or, in some applications, relative to a baseline time period t_0–t_1:

$$\mathrm{OHU}(t) = \mathrm{OHC}(t) - \frac{1}{t_1 - t_0} \int_{t_0}^{t_1} \mathrm{OHC}(t')\,\mathrm{d}t'. \tag{1.6}$$

This results in a value of OHU measured in Joules, the unit of OHC. Alternatively, OHU can be expressed as an equivalent heat flux into the ocean in units of W m^{-2} by dividing OHU by the global ocean surface area A_{oc} and by the length of the considered time period:

$$\mathrm{OHU}_{\mathrm{W\,m^{-2}\,s^{-1}}}(t) = \frac{1}{A_{\mathrm{oc}}(t - t_0)} \mathrm{OHU}_{\mathrm{J}}(t), \tag{1.7}$$

where $\mathrm{OHU}_{\mathrm{J}}$ is the OHU measured in Joules from Eq. (1.5). These two unit conventions are equivalent and are both used in the literature.

1.1.3.2 Historical observations and future projections

Total OHU is a key indicator of the rate of ongoing climate change. Anthropogenic GHG forcing manifests itself fundamentally through anomalous radiative forcing at the top of the atmosphere (TOA). This flux anomaly, the Earth energy imbalance (EEI), gives the rate of energy uptake by the Earth system. The EEI has increased over recent decades, leading to an acceleration of global warming (Forster et al. 2021; Minière et al. 2023). The most accurate method of measuring the EEI consists of a stocktake of the energy budget of each of the climate system's components (the ocean, land, cryosphere, and atmosphere; Meyssignac et al. 2019). (Other approaches include measuring energy fluxes at TOA or at the surface using satellites, or running climate model simulations.) Around 91% of this energy flux over the period 1971–2018 has entered the ocean through OHU, making the ocean by far the dominant reservoir of excess heat in the climate system (Forster et al. 2021), while the atmosphere has taken up only 1.3%, and the land and cryosphere have taken up 5.0% and 2.7%, respectively (Fig. 1.1). This is a consequence of the ocean's large heat capacity due to the combination of the high specific heat capacity of water and the ocean's tremendous mass, as well as the ocean's large surface area, low albedo, and relatively efficient mixing. Thus, total OHU directly quantifies the amplitude of climate change, and the accuracy of EEI estimates obtained by constraining each climate system reservoirs' energy budgets relies principally on the accuracy of OHC estimates.

There are four principal methods for observing OHC (Meyssignac et al. 2019): (i) *in situ* measurements of seawater temperature and calculation of OHC through Eq. (1.4); (ii) satellite measurements of air-sea heat fluxes at the ocean surface; (iii) satellite altimetry measurements of sea level rise due to thermal expansion; and (iv) the construction of ocean reanalyses by combining models and observations. The availability and relative importance of these methods has changed

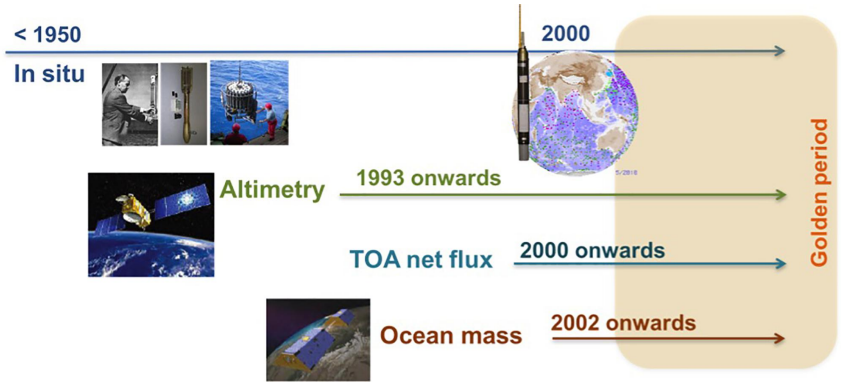

Figure 1.4: Schematic timeline of the evolution of ocean heat content observing systems. Reprinted from Meyssignac et al. (2019) (Fig. 1).

over time due to the invention and deployment of new observation techniques. This is illustrated in Fig. 1.4, which divides the history of OHC observations into three periods (Meyssignac et al. 2019): (i) an initial period with relatively sparse shipboard *in situ* measurements; (ii) an intermediate period, starting with the deployment of satellite altimetry in 1993, characterized by a more complementary observing system combining satellites, ships, autonomous platforms and models; and finally (iii) an ongoing "golden era" of OHC measurements initiated by the start of the Argo program (Wong et al. 2020) of autonomous profiling floats in the early 2000s. This development is illustrated by the number of subsurface temperature measurements recorded each year which has drastically increased in the early 2000s (Fig. 1.5a), with data coverage to increasing depths and especially over the top 2000m covered by Argo floats (Fig. 1.5b). (Also visible in Fig. 1.5b is the impact on international research campaigns of the two world wars in 1914–18 and 1939–45.)

The advancement of this observing system has been driven by the continuous introduction and improvement of new measurement techniques and sensors. One of the first global subsurface ocean temperature observation campaigns was undertaken during the Challenger expedition (1873–1876) which circumnavigated the globe and recorded surface-to-bottom temperature profiles (Abraham et al. 2013). Due to the instrumentation available at the time, temperature measurements were time consuming and could only be taken at discrete depth levels, which remained a general issue with ocean temperature observations until the invention of the mechanical bathythermograph (MBT) in 1939 and later the conductivity-temperature-depth (CTD) instruments in 1955 (Abraham et al. 2013). A general limitation of these shipboard measurements is their geographical and seasonal bias, with more observations available in the Northern hemisphere and during summer. This bias has decreased over time (see Fig. 1.6 for the geographical coverage of SST observations) but remains a problem especially in difficult environments such as the South-

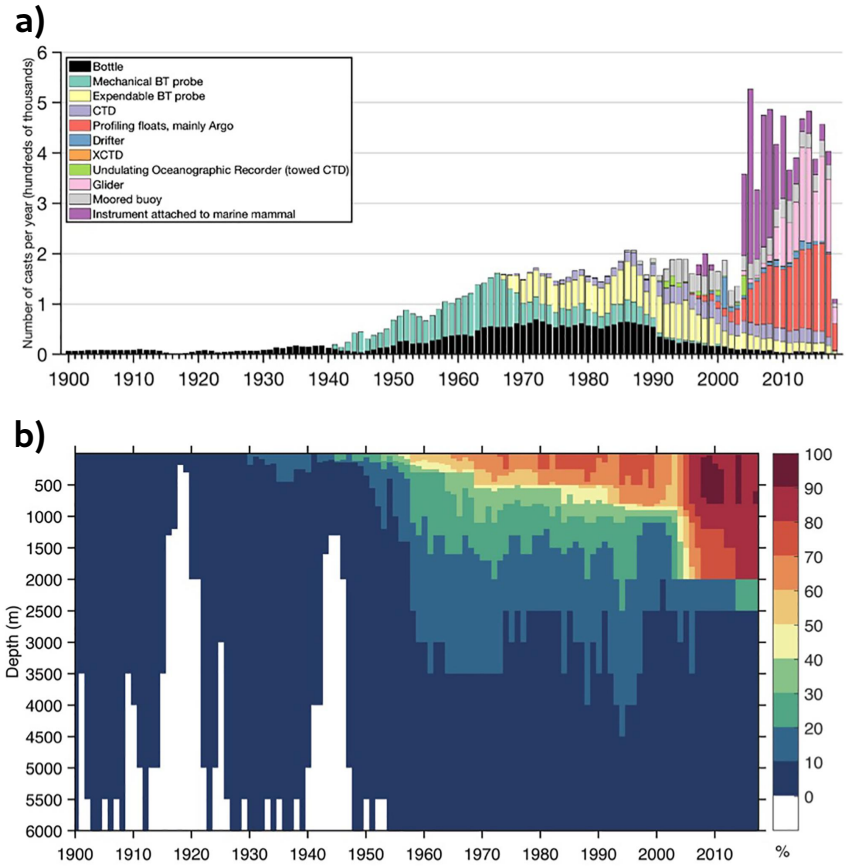

Figure 1.5: Increasing number of ocean temperature measurements over time. **a)** Number of subsurface ocean temperature profiles per year over the period 1900–2017. BT, Bathythermograph; CTD, Conductivity-Temperature-Depth; XCTD, Expendable CTD. **b)** Percentage of global data coverage counted in 3° × 3° latitude-longitude boxes as a function of depth and time. Adapted from Meyssignac et al. (2019) (Fig. 2).

ern Ocean during winter. The deployment of autonomous Argo floats since 2000 has improved the global and seasonal coverage of upper ocean temperature measurements.

Fig. 1.7a shows time series of estimated upper ocean (0–2000 m) OHU from 1955 to 2021 relative to a 2005–2019 baseline from a number of studies. The OHC above 2000 m has increased by an estimated 365 ZJ over the period 1971–2018, with 61% of this energy stored above 700 m (Forster et al. 2021). The equivalent OHU has increased over time from 7.6 ZJ/yr over 1971–2018 to 9.6 ZJ/yr over 2006–2018 (Fig. 1.7b Forster et al. 2021), indicating an acceleration of OHU (Minière et al. 2023). The observational uncertainty associated with these estimates has decreased over time due to improved sensors and coverage and more consistent quality control (Fig. 1.7a).

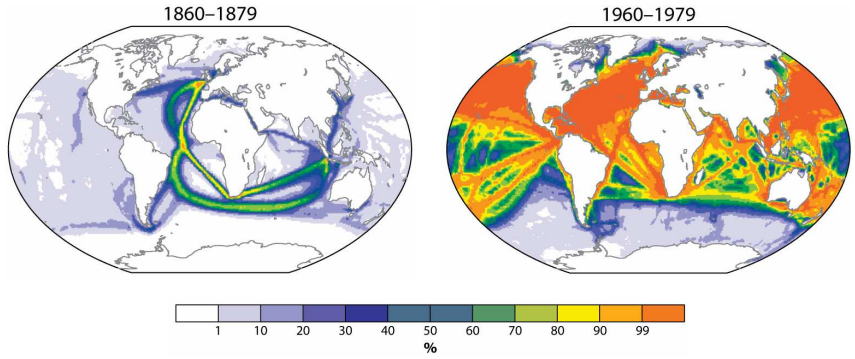

Figure 1.6: Percentage of months with at least one sea surface temperature measurement in 2°×2° latitude-longitude boxes in the International Comprehensive Ocean Atmosphere Data Set (Worley et al. 2005) for the periods 1860–1879 and 1960–1979. Adapted from Deser et al. (2010) (Fig. 3).

Climate model simulations of historical OHU agree reasonably well with these observed values when averaged over the members of the CMIP5 or CMIP6 ensembles, but there is substantial spread across members within each ensemble (Fig. 1.7b). Future projections of OHU strongly depend on the assumed future emission scenario, with diverging OHU evolution between high- and low-mitigation scenarios, and the inter-model spread for each scenario spans a wide range.

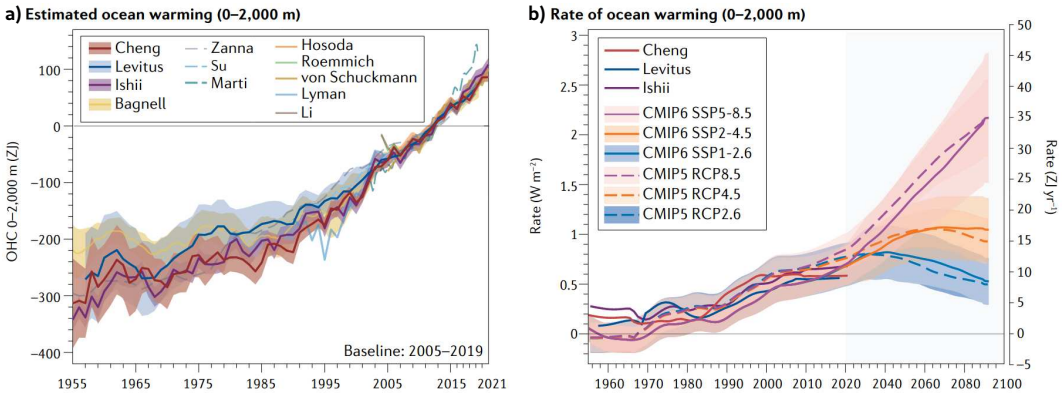

Figure 1.7: a) Observed change in global 0–2000 m OHC from 1955 to 2021 from various sources. Solid and dashed lines are direct and indirect estimates, respectively, and shading indicates 90% confidence intervals. **b)** Observed (1955–2021) and simulated (1955–2100) global 0–2000 m OHU. Solid lines indicate ensemble mean, shading represents 1σ inter-model spread. Adapted from Cheng et al. (2022) (Fig. 2).

The observed increase in OHC is greatest in the Southern Ocean and the low- to mid-latitude Atlantic Ocean (Fig. 1.8a). The ocean south of 35°S accounts for around 36% of the total increase in OHC, with warming concentrated to the north of the ACC, where mode and intermediate water formation subducts large amounts of excess heat (Armour et al. 2016; Sallée 2018; Li et al. 2023). In the Atlantic north of 35°S, warming is strongest in the Gulf Stream which displays the greatest

warming rates of any region globally. The subpolar North Atlantic is the only major region with marked cooling and displays a "warming hole" mostly attributed to heat redistribution due to circulation changes (Keil et al. 2020).

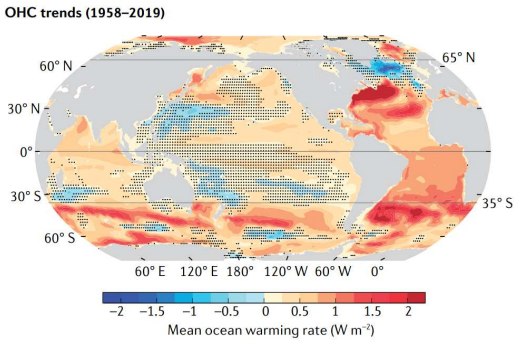

Figure 1.8: Observed local OHC trends from 1958–2019. Stippling indicates trends not significantly different from zero at the 90% confidence level. Adapted from Cheng et al. (2022) (Fig. 3).

However, OHU is not restricted to the upper ocean. The ocean below 2000 m has taken up 31 ZJ or around 8% of the total OHC increase over 1971–2018 (Forster et al. 2021). Deep ocean warming is detectable even in Antarctic Bottom Water (AABW) below 4000 m depth (Fig. 1.9; Purkey and Johnson 2010).

1.1.3.3 Physical, biological, and socio-economic impacts of ocean warming

One crucial reason for studying total ocean heat uptake (as opposed to ocean heat uptake efficiency, as discussed below in Sec. 1.1.4) is that the magnitude of total OHU directly scales with a number of major negative impacts (Cheng et al. 2022; Venegas et al. 2023). Ocean warming due to ocean heat uptake has widespread consequences not only for the physical functioning of the ocean and coupled climate system, but also for marine biogeochemical cycles, marine ecosystems, and ultimately the human socio-economic systems that depend on their services.

§ Sea level rise One immediate impact of a warmer ocean is regional and global sea level rise (SLR). Ocean warming causes SLR both directly through the thermal expansion of seawater as it warms, as well as indirectly through freshwater input from land due to the melting of ice sheets (Pritchard et al. 2012) and glaciers (Kochtitzky and Copland 2022), which are in turn partly caused by ocean warming. Thermosteric SLR (i.e., due to reduced water density from thermal expansion; Gregory et al. 2019) is responsible for around one third of global mean SLR over the period 1900–2018, while the remaining two thirds are due to barystatic SLR (i.e., due to input of water mass from outside the ocean; Gregory et al. 2019), including the melting of glaciers, the Greenland and Antarctic ice sheets, and changes in terrestrial water storage (Frederikse et al. 2020). In total, these contributions have resulted in global mean SLR of 0.20 m over 1901–2018, with an accelerating trend of 3.7 mm yr^{-1} over 2006–2018 compared to 2.3 mm yr^{-1} over 1971–2018 (Fox-Kemper et al. 2021). This SLR comes with negative consequences for humans, in particular for the over 10% of the

world population living in low-elevation coastal zones (Reimann et al. 2023), since it causes changes in shorelines due to coastal erosion, increased marine flooding, as well as salt-water intrusions into coastal aquifers (FitzGerald et al. 2008; Cazenave and Cozannet 2014).

§ Stratification, CO_2, and oxygen The observed magnitude of ocean warming is highest in the upper ocean and decays with depth (Schuckmann et al. 2020); this has resulted in increased upper ocean density stratification (Yamaguchi and Suga 2019; Li et al. 2020; Sallée et al. 2021; Olmedo et al. 2022). Increased stratification has not only led to changes in the physical circulation of the ocean (e.g., intensified upper ocean currents, Peng et al. 2022), but also perturbs the supply of nutrients and oxygen to marine ecosystems (Bopp et al. 2013). However, this is not the only mechanism through which ocean warming impacts marine ecosystems. Through changes in ocean circulation, biologial processes, and reduced solubility of oxygen and carbon dioxide at higher temperatures, ocean warming leads to deoxygenation (Keeling et al. 2010; Bopp et al. 2013; Deutsch et al. 2015; Schmidtko et al. 2017) as well as reduced net uptake of CO_2 by the ocean (DeVries 2022; Gruber et al. 2023; Müller et al. 2023).

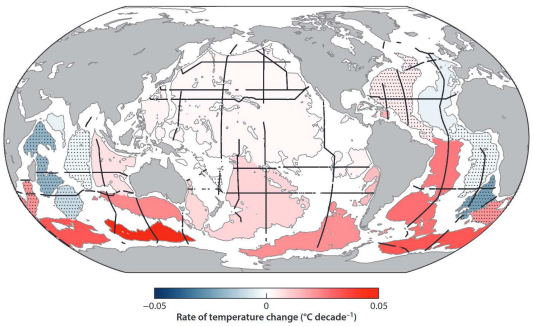

Figure 1.9: Observed mean warming rates below 4000 m centered on 1992–2005. Stippling indicated rates not significantly different from zero at 95% confidence. The black lines show the paths of repeat oceanographic transects from the WOCE and GO-SHIP programs. Reprinted from Talley et al. (2016) (Fig. 1), originally from Purkey and Johnson (2010).

§ Multiple stressors and biology The effect of ocean warming on marine ecosystems is compounded by the convergence of multiple stressors (Breitburg and Riedel 2005; Bopp et al. 2013; Gunderson et al. 2016), including increased ocean acidification due to oceanic uptake of CO_2. The combined effect of ocean warming and other stressors has led to changed structure and geographical distribution of key marine habitats such as kelp forests (Smale 2020) and seagrasses (Nguyen et al. 2021), as well as negative impacts on marine invertebrates at all developmental stages (Byrne and Przeslawski 2013). Some marine species adapt to ocean warming by shifting their geographical range both in the horizontal (i.e., poleward Wernberg et al. 2011) and in the vertical (i.e., to greater depths Jorda et al. 2020), with potentially distinct responses at different depth levels (Santana-Falcón and Séférian 2022). Ocean warming has also resulted in decreased phytoplankton biomass (Boyce et al. 2010), but the effects of ocean warming on phytoplankton are not fully understood due their great ecological diversity (Huertas et al. 2011; Henson et al. 2021) and associated adaptation strate-

gies (Thomas et al. 2012; Irwin et al. 2015), as well as the combination of multiple stressors (Winder and Sommer 2012; Lewandowska et al. 2014). A decrease in net primary production (NPP; Behrenfeld et al. 2006), partly linked to OHU, has been inferred, but observational estimates and future model projections of NPP still suffer from large uncertainties (Sarmiento et al. 2004; Kwiatkowski et al. 2020; Tagliabue et al. 2021).

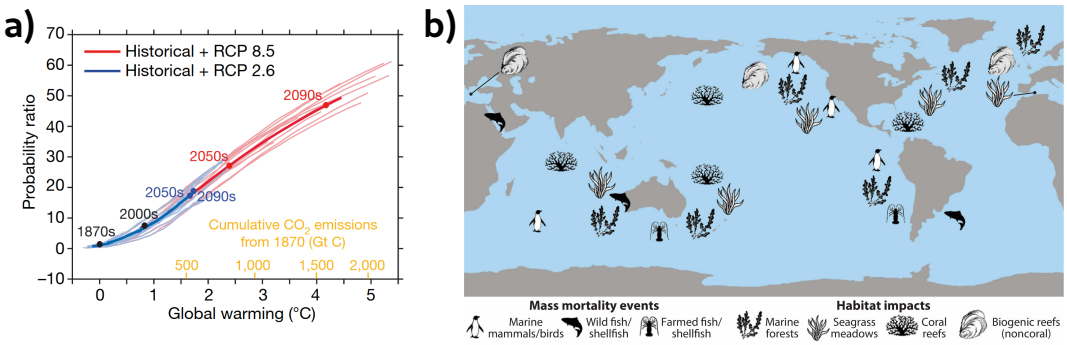

Figure 1.10: Increased frequency of MHWs under global warming and associated biological impacts. **a)** Global annual mean probability ratio of MHW occurrence under historical, RCP2.6 and RCP8.5 forcing in 12 CMIP5 models. **b)** Overview of mass mortality events and habitat impacts due to MHWs. Panel **a)** adapted from Frölicher et al. (2018) (Fig. 1), panel **b)** adapted from Smith et al. (2023) (Fig. 3).

§ Extreme events A further major consequence of ocean warming is the increased occurrence of prolonged extreme warm seawater temperature events termed marine heatwaves (MHWs; Oliver et al. 2021). Marine heatwaves have become more frequent, more intense, and longer-lasting over the past century (Fig. 1.10a; Frölicher et al. 2018; Oliver et al. 2018), which is attributed to the mean increase in ocean temperatures (Frölicher and Laufkötter 2018; Oliver 2019). These extreme events have had major biological and socio-economic consequences (Fig. 1.10b Smale et al. 2019; Smith et al. 2021; 2023), including impacts on important foundation species (Wernberg et al. 2011; Arias-Ortiz et al. 2018; Filbee-Dexter et al. 2020), coral bleaching (Hughes et al. 2017; 2018), range shifts of marine species (Jacox et al. 2020; Santora et al. 2020), and impacts on fisheries (Cheung and Frölicher 2020). In addition, MHWs often occur as "compound events" in concert with extreme events in other variables such as low chlorophyll concentration (Le Grix et al. 2021), decreased NPP (Le Grix et al. 2022), acidification (Burger et al. 2022) and deoxygenation (Li et al. 2024), leading to increased negative consequences on marine ecosystems (Gruber et al. 2021).

These impacts are all directly or indirectly caused by increasing ocean temperatures due to total ocean heat uptake, a motivation for the quantification of future OHU undertaken in Chapter 2.

1.1.4 Ocean heat uptake efficiency

We now turn to the ocean heat uptake efficiency, a key metric of transient climate change best introduced using a basic model of global-mean climate change. The simplest model of the global mean temperature response to CO_2 forcing is the following zero-dimensional energy balance model (EBM; all quantities are global means):

$$N = F + \lambda T, \tag{1.8}$$

where F is the instantaneous radiative forcing (in $\mathrm{W\,m^{-2}}$) at the top of the atmosphere (TOA), N is the TOA radiative anomaly relative to the unperturbed state, T is the surface temperature anomaly, and λ is the climate feedback parameter (in $\mathrm{W\,m^{-2}\,K^{-1}}$). On time scales relevant to climate change, almost all of the energy is taken up by the ocean due to its large heat capacity compared to the atmosphere, cryosphere, and land surface, so N can be identified with ocean heat uptake (Palmer and McNeall 2014). The term λT represents the radiation of energy back to space at increased global mean temperatures due to climate feedbacks (it is essentially the first term in a Taylor expansion of the radiative response as a function of T; Roe 2009; Knutti and Rugenstein 2015; Rose and Rayborn 2016). The radiative forcing F is thus partitioned between heat loss to space (λT) and OHU (N; Raper et al. 2002). The value of λ assessed in the most recent IPCC AR6 is $\lambda = -1.16\,\mathrm{W\,m^{-2}\,K^{-1}}$ (Forster et al. 2021, 90% confidence interval: -1.81 to $-0.51\,\mathrm{W\,m^{-2}\,K^{-1}}$,), which implies a stabilizing net climate feedback under this sign convention. The principal stabilizing process is the Planck feedback (enhanced thermal radiation to space at higher temperatures, $\lambda_{\mathrm{Planck}} = -3.22\,\mathrm{W\,m^{-2}\,K^{-1}}$), while changes in water vapor, lapse rate, surface albedo and clouds all contribute positive values which amplify the warming response. These contributions λ_i are assumed to be independent to first order and summed to obtain the net feedback parameter λ.

Assuming that λ is constant, one can compute the global warming at equilibrium (where $N = 0$) resulting from any given radiative perturbation, for example the equilibrium climate sensitivity (ECS) defined as the global mean surface temperature change at steady state following a doubling of atmospheric CO_2 concentration:

$$\mathrm{ECS} = T_{2\times\mathrm{CO_2}} = -\frac{F_{2\times\mathrm{CO_2}}}{\lambda}. \tag{1.9}$$

The ECS in this model depends on the strength of the initial perturbation, F, as well as of the acting climate feedbacks as quantified by λ. In coupled atmosphere-ocean general circulation models (AOGCMs), ECS can be calculated by running simulations under perturbed forcing to equilibrium (e.g., Stouffer and Manabe 1999), but this is computationally expensive due to the long equilibration time scale of the deep ocean. Alternatively, ECS can be estimated by coupling an at-

mospheric GCM to a "slab" ocean model (a simplified zero-dimensional thermodynamic mixed layer model, e.g.; Senior and Mitchell 2000), which is more computationally efficient than running the full AOGCM but neglects the effect of ocean dynamics on climate feedbacks (Winton et al. 2010). A more cost-effective and robust method is to compute an *effective climate sensitivity* (EffCS; Murphy 1995; Watterson 2000) by fitting the radiative response to warming in a step-forcing run of an AOGCM, which can be visualized in a T–N graph sometimes called "Gregory plot" (Gregory et al. 2004; Rose and Rayborn 2016). An example of this is shown in Fig. 1.11 for data from the CESM model and the CMIP5 ensemble.

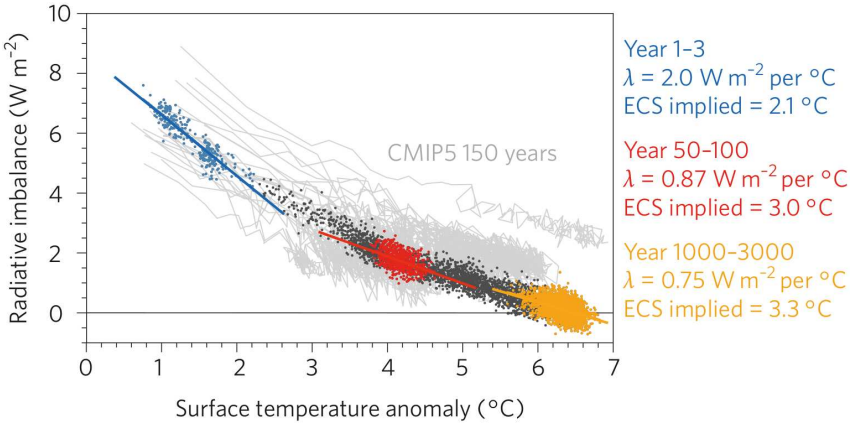

Figure 1.11: Radiative imbalance N as a function of global mean temperature T after abrupt quadrupling of atmospheric CO_2 concentrations (`abrupt-4xCO2` experiment) in 22 CMIP5 models run for 150 years (grey lines) and in a CESM simulation of 3675 years (black and colored dots). The linear fits for three different time periods in CESM are shown as colored lines, their slope is the climate feedback parameter λ (Gregory et al. 2004). Reprinted from Knutti et al. (2017a) (Fig. 4).

The slope of the regression of N onto T yields the climate feedback parameter λ, while the y- and x-intercept give the effective radiative forcing (ERF; Williams et al. 2008) and the EffCS, respectively. The ERF includes not only the direct radiative forcing of CO_2, but also considers "fast" responses (on the order of months), such as adjustments in stratospheric temperature or aerosol-cloud interactions that do not change surface temperature, as part of the forcing (instead of as part of the response; Hansen et al. 1997; Knutti and Hegerl 2008; Sherwood et al. 2015; Smith et al. 2020). However, it is clear from the curvature in Fig. 1.11 that λ diagnosed from this method is not constant but tends to increase in time in all models, resulting in increasing EffCS with time (Senior and Mitchell 2000). It has been shown that this behavior is intimately linked to OHU as well as ocean surface warming patterns and their interaction with climate feedbacks. OHU influences sea surface temperature (SST) patterns by damping surface warming more in regions of effective heat uptake (Manabe et al. 1991; Marshall et al. 2015; Armour et al. 2016), especially in the high latitudes where forcing is most impactful at driving climate change (Hansen et al. 1997; Rose et al.

2014) through its impact on climate feedback and especially cloud feedback (Winton et al. 2010). The time evolution of λ and EffCS is thus strongly influenced by evolving OHU and SST patterns as the climate system approaches equilibrium (e.g., the initial emergence and subsequent slow decay of high latitude intensified OHU; Armour et al. 2013; Rose and Rayborn 2016). As a consequence, discrepancies between modelled and observed SST patterns lead to considerable biases in projections of climate feedback and climate sensitivity (this is the so-called "pattern effect", see also the discussion section 5.2.1; Andrews et al. 2018; Dong et al. 2020; Zhou et al. 2021; Andrews et al. 2022; Alessi and Rugenstein 2023; Rugenstein et al. 2023; Armour et al. 2024).

One way of formalizing this influence of OHU on the time-dependence of the climate feedback parameter is via the concept of forcing *efficacy*. In the context of radiative forcing from GHGs, it has been found that some forcing agents are more effective (e.g., methane) or less effective (e.g., ozone) than CO_2 at driving surface warming for a given amount of induced radiative forcing (Hansen et al. 2005). Winton et al. (2010) proposed to apply this concept to OHU (thus considering OHU as a forcing instead of a response), and found that the efficacy of OHU in GCMs is generally greater than 1, meaning that global warming is more sensitive to OHU than to CO_2 forcing, which is attributed to the spatial pattern of OHU and its interaction with climate feedback.

An equivalent formulation (Watanabe et al. 2013) of this effect is via a time-dependent *ocean heat uptake efficiency*, a term which we will introduce now. Under steadily increasing radiative forcing (e.g., idealized CO_2 forcing or 21st century emissions scenarios), the OHU term N in Eq. (1.8) is nearly proportional to T with proportionality factor κ:

$$N = \kappa T. \tag{1.10}$$

The factor $\kappa = N/T$ defines the *ocean heat uptake efficiency* (OHUE; introduced by Gregory and Mitchell 1997, although they did not yet use the term "efficiency") and is assumed to be constant in this approximation. OHUE is a concept inherently only applicable to transient climate change, as the relationship in Eq. (1.10) breaks down as the climate approaches equilibrium (since $N \to 0$ but $T \to T_{eq} \neq 0$). Combining Eqs. (1.8) and (1.10) gives

$$T = \frac{F}{\lambda + \kappa}, \tag{1.11}$$

which is an expression for transient warming similar to Eq. 1.9 for equilibrium warming, except that the OHUE κ is added to the climate feedback parameter λ, damping the transient warming compared to the equilibrium temperature response (Dufresne and Bony 2008). Another way of

seeing this is to consider the fraction of realized warming relative to the equilibrium warming (Raper et al. 2002) by dividing Eq. 1.11 by $T_{\mathrm{eq}} = F/\lambda$:

$$\frac{T}{T_{\mathrm{eq}}} = \frac{\lambda}{\lambda + \kappa} = \frac{1}{1 + \kappa/\lambda}. \tag{1.12}$$

Thus, at any given time, the fraction of realized warming relative to equilibrium is smaller for a higher sensitivity (less negative λ; Siegenthaler and Oeschger 1984; Hansen et al. 1985; Stouffer et al. 2006) as well as for more efficient OHU (larger κ; Raper et al. 2002).

The physical interpretation of OHUE as an oceanic process can also be seen by considering a simple two-layer model extension of the EBM (1.8):

$$C\frac{\mathrm{d}T}{\mathrm{d}t} = F + \lambda T - H \tag{1.13}$$

$$C_D\frac{\mathrm{d}T_D}{\mathrm{d}t} = H, \tag{1.14}$$

where T and T_D are the temperature anomalies of the upper and deep layer with heat capacities C and C_D, respectively (Gregory 2000; Held et al. 2010). The upper layer mainly represents the upper ocean mixed layer but also includes the atmosphere and land surface which exchange with the upper ocean on fast time scales and have negligible heat capacity compared to the upper and deep oceans. The term

$$H = \gamma(T - T_D) \tag{1.15}$$

is the heat transfer between the upper and deep layer with thermal coupling coefficient γ. In the limit of a deep ocean with infinite heat capacity $C_D \to \infty$, $T_D \to 0$ and

$$\gamma \to \kappa. \tag{1.16}$$

The OHUE κ in this limit is equal to the thermal coupling coefficient γ (Yoshimori et al. 2016).

However, the assumption that OHUE is constant is often insufficient, since κ is found to decline on long time scales in AOGCMs. The weakening of OHUE is an inevitable response to increased stratification and reduced thermal coupling between the upper and deep oceans (Giorgetta et al. 2013; Watanabe et al. 2013), although its value may be state dependent (Stolpe et al. 2019). This contributes to the "cold start" effect of initially slower atmospheric warming after perturbing a model with increasing CO_2 from steady state (Gregory et al. 2015), and increased OHUE has been advanced as a cause for the 1998–2012 global warming hiatus (Easterling and Wehner 2009; Meehl et al. 2011; Watanabe et al. 2013; Chen and Tung 2014; Drijfhout 2018). In observations, OHUE has instead been found to have increased since 1970 (Cael 2022), a finding attributed to increased vertical

temperature gradients which lead to more efficient downward mixing of heat, although OHUE is expected to eventually decline also in the real world as the ocean equilibrates to the imposed forcing. Furthermore, Sohail et al. (2023) has found that the "aerosol-only" contribution to OHUE has decreased since 1980, meaning that the ocean cools less for a given aerosol-driven surface cooling.

Given the important role of climate feedbacks and OHU in transient and equilibrium climate change, what is their relative importance for controlling inter-model spread in GCM warming projections? Boé et al. (2009) found that polar mixed layer depths, which quantify vertical mixing and are important for OHU, correlate with deep ocean warming and with the transient climate response (TCR; the global mean surface air temperature anomaly at the time of CO_2 doubling under idealized exponentially increasing atmospheric CO_2 concentration forcing) across Coupled Model Intercomparison, phase 3 (CMIP3; see Sec. 1.2.4) models, with stronger correlations than between TCR and ECS (which is a measure of climate feedback strength). This led the authors to conclude that OHU is as important as climate feedbacks for controlling the inter-model spread in future warming, but the study may have been influenced by outlier models (Kuhlbrodt and Gregory 2012). Dufresne and Bony (2008) have shown that OHU indeed has an impact on warming projections which is comparable in size to the contribution of cloud feedback and of the combined water vapor–lapse rate feedback, but the inter-model spread was found to be dominated by differences in cloud feedback, and this result has continued to hold from the early days of coupled climate modeling (Cess et al. 1990) to the most recent generation of climate models (Williams et al. 2020; Zelinka et al. 2020). Nevertheless, the ocean retains a key role in the transient climate response to CO_2 emissions, both due to its dominant mean response (taking up the vast majority of the excess energy), and its secondary control on inter-model spread (second to cloud feedback, which is influenced by surface ocean warming).

The inter-model spread in OHUE in particular has been the subject of a number of studies. OHUE is an inherently oceanic quantity and is correlated with an effective deep ocean diffusion parameter in simplified models (Wigley and Schlesinger 1985; Sokolov et al. 2003). It is sensitive to the parameterization of mixing and mesoscale eddies (Winton et al. 2014; Romanou et al. 2017; Saenko et al. 2018; Newsom et al. 2023) and to the resulting density stratification (Liu et al. 2023; Newsom et al. 2023), in particular in the Southern Ocean (Kuhlbrodt and Gregory 2012; Bourgeois et al. 2022). OHUE has also been found to correlate with AMOC strength across models (Rugenstein et al. 2013; Kostov et al. 2014; Winton et al. 2014; He et al. 2017; Romanou et al. 2017; Saenko et al. 2018), although this is likely not due to the direct effect of AMOC on OHU, but due to their common control by stratification and mixing (see Chapter 3; Gregory et al. 2023). Furthermore, OHUE is influenced by surface warming patterns, with warming at locations with efficient ventilation (such as in the Southern Ocean) leading to higher OHUE, although this effect cannot explain the inter-model spread (Newsom et al. 2020).

1.2 Climate models

Scientific practice is sometimes thought of as revolving around the interplay between two principal pillars of the scientific method: theory and experiment. According to this view, observing the behavior of processes occuring in Nature allows scientists to inductively form hypotheses about the presumed general rules governing these processes, which can be formalized into scientific theories that can then be tested and potentially falsified through controlled experiments. However, this step-by-step recipe for scientific research can be considered as too simplistic (Hepburn and Andersen 2021), and this can be illustrated by the pivotal role of models, in particular numerical computer models, in contemporary climate science (Storch 2010; Winsberg 2022). Thanks to the exponential progress in computer technology since the mid-twentieth century, computer models have become essential tools not only for numerical weather prediction, but also for advancing our basic understanding of the atmosphere, ocean, and other Earth system components. These models do not neatly fall into either of the categories of theory or experiment: they are in large parts explicitly constructed based on physical theory (e.g., the theory of geophysical fluid dynamics), but at the same time they provide a means of testing hypotheses through targeted simulations that would be impossible to realize in the real world (and these simulations are in fact often referred to as "experiments"; Sacks et al. 1989; Jebeile 2017). Although such models can not be verified in a practical sense, since many of their projections are by definition currently unobservable, they can be tested by comparison to observations (Oreskes et al. 1994; Hargreaves and Annan 2014), and find a wide use in contexts such as climate prediction, hypothesis testing, process understanding, and data assimilation (Storch 2010).

We start this section with a historical overview of the development of models of the climate system (Sec. 1.2.1). We then review the notion of model ensembles (Sec. 1.2.3), which is central for this thesis, before introducing the Coupled Model Intercomparison Project (Sec. 1.2.4) and the method of emergent constraints (Sec. 1.2.5) which is used in Chapter 2.

1.2.1 Historical perspective

The complex numerical models currently used in climate research are the result of a long scientific tradition of (climate) model development. (The term "model" as used here should be understood to signify any *representation* of the climate system, whether conceptual, analytical, or numerical; Frigg and Hartmann (2024).)

Climate modeling in this broad sense began already with the conceptual models of Earth's climate proposed by ancient Greek philosophers (Edwards 2011). Eratosthenes (3rd century BC), recognizing the implications of Earth's spherical shape, divided the planet into several latitude bands defined by their length of day (thus introducing the word "climate"; Heymann 2010; Edwards

2011). This geographical view differed from the "causal" climatology previously described by Hippocrates (5th century BC), who focused on the effects of environmental factors on human health (a subject still very much of relevance today; Cissé et al. 2022) as well as on cultural differences between peoples (Heymann 2010). These and other ancient conceptual "models" of climate and weather, especially as laid out in Aristotle's treatise *Meteorologica* (ca. 340 BC), remained highly influential for many centuries until the "scientific revolution" of the 16th and 17th century (Frisinger 1973; Heymann 2010). The first major conceptual advances in this era were obtained for the global atmospheric circulation by Halley in the 17th century and later amended by Hadley and Ferrel in the two following centuries, yielding the Hadley, Ferrel and polar cells now standard as conceptual models of the global atmospheric overturning circulation (Edwards 2011).

The first mathematical models of climate were energy balance models (EBMs), i.e., sets of analytically solvable equations for the atmospheric temperature which balance the radiative energy entering and leaving the Earth system based on simplified parameterizations of energy fluxes (North et al. 1981). Arrhenius (1896) famously used this approach to investigate the influence of atmospheric CO_2 on temperature, resulting in the first estimate of equilibrium climate sensitivity of 5 °C–6 °C (determined with 10'000 to 100'000 manual calculations; Uppenbrink 1996). In the 1960s, a new type of zonal average EBM was developed in parallel by Budyko (Budyko 1961; 1969) and Sellers (Sellers 1969), and was used for example to show that small variations in the solar constant could lead to the onset of a new ice age (Budyko 1969; Sellers 1969). This "Budyko–Sellers" type of EBM proved very influential and was adapted and refined in the following decades (North 1975).

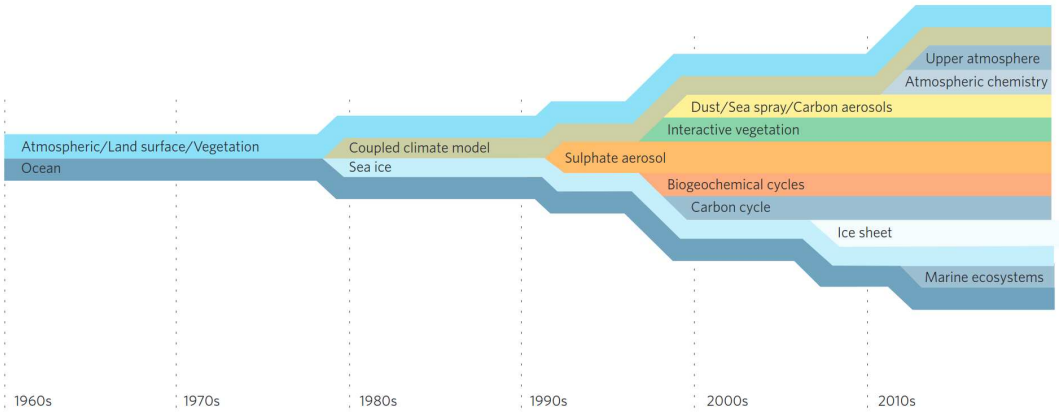

Figure 1.12: Timeline of increasing climate model complexity through the inclusion of processes and model components. Reprinted from Jakob (2014) (Fig. 1).

It was around the same time that the first numerical AOGCMs were being developed. Numerical climate modeling began in the form of numerical weather prediction (NWP) in the early 20th

century. In 1922, Richardson performed a weather forecast through numerical integration of the primitive equations laid out earlier by V. Bjerknes (Richardson 1922), but was unsuccessful due to errors in the input observations and numerical instabilities in his method (and it took 6 weeks of manual calculations to produce an 8-hour forecast; Pearce 2018). Following this failed attempt, NWP was practically abandoned for two decades until the invention of digital computers in the 1940s. In the 1950s, 60s, and 70s, several major modeling institutions were founded in the United States with funding from US military and civilian agencies (Edwards 2011; Pearce 2018). These decades saw the development of the first atmospheric GCM (Phillips 1956), the first 3D ocean model (Bryan and Cox 1967), and finally the first coupled AOGCM (Manabe and Bryan 1969; Bryan et al. 1975; Manabe et al. 1975). Following the development of several GCMs at different institutions, the Atmospheric Model Intercomparison Project (AMIP) was born in 1989 (Gates et al. 1999), followed by the first Coupled Model Intercomparison Project (CMIP) in 1996 (Meehl et al. 1997; 2000).

Fig. 1.12 shows the increase in model complexity over time as more processes were included in GCMs. Starting from the atmosphere-only and later ocean-only models of the 1960s, new model components were developed and coupled to the existing models to produce more complete representations of the climate system, including the effects of processes such as sea ice dynamics (Hibler 1979), sulphate aerosols (Jones et al. 1994), land vegetation (Henderson-Sellers 1993), and the carbon cycle (Cox et al. 2000). This has resulted in the fully coupled Earth System Models (ESMs) used for climate projections today, though it must be noted that "uncoupled" single model components such as ocean models remain vital for process studies.

1.2.2 Structure of modern climate models

Modern climate models are constructed in a modular fashion, with several submodels for different climate components combined via a "coupler". Fig. 1.13 illustrates an example of this coupling from Alexander and Easterbrook (2015) for the CESM1-BGC model (Lindsay et al. 2014), with the size of each bubble corresponding to the amount of software code contained in each component. In this model, the atmosphere, ocean, sea ice and land components are each simulated by a distinct submodel. These submodels communicate with each other through a coupler which handles fluxes of energy, momentum and matter and ensures e.g. the correct interpolation of fluxes to respect conservation laws. In addition, each submodel may contain further subcomponents, such as a marine biogeochemistry (BGC) component in the ocean model (Fig. 1.13). However, this is not the only possible configuration of model components, and there is a diversity of model structures found in current climate models. For example, models may differ in their focus on particular components (as quantified by the amount of code), or couple certain components directly without passing through a coupler (Alexander and Easterbrook 2015).

Due to the historical emergence of climate model development from NWP, the largest GCM component is often the atmospheric model (Alexander and Easterbrook 2015), but for the purpose of this introduction we will focus on the ocean component. An ocean model generally contains a dynamical core which numerically solves the Navier–Stokes equations of fluid motion, often in the *primitive equations* approximation (Griffies et al. 2000; Vallis 2017). These equations are discretized onto a three-dimensional grid and solved numerically at discrete time intervals. Fig. 1.14 shows an illustration of a regular latitude-longitude grid with vertical levels of constant altitude (for the atmosphere in this case). The model cannot *resolve* processes occuring at scales smaller than the size of individual grid cells and must rely on parameterizations (i.e., representations of unresolved processes as a function of the resolved state; see Sec. 1.2.3.2). Examples of processes that are unresolved in coarse resolution ocean models and thus require parameterization include vertical mixing in the upper ocean (Large et al. 1994), advection and diffusion by mesoscale eddies (Redi 1982; Gent and McWilliams 1990), or the air-sea exchange of CO_2 (Wanninkhof 1992).

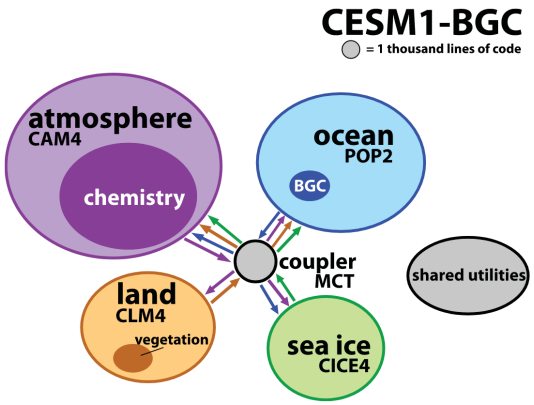

Figure 1.13: Software architecture diagram for the CESM1-BGC model (Lindsay et al. 2014). Reprinted from Alexander and Easterbrook (2015) (Fig. 1).

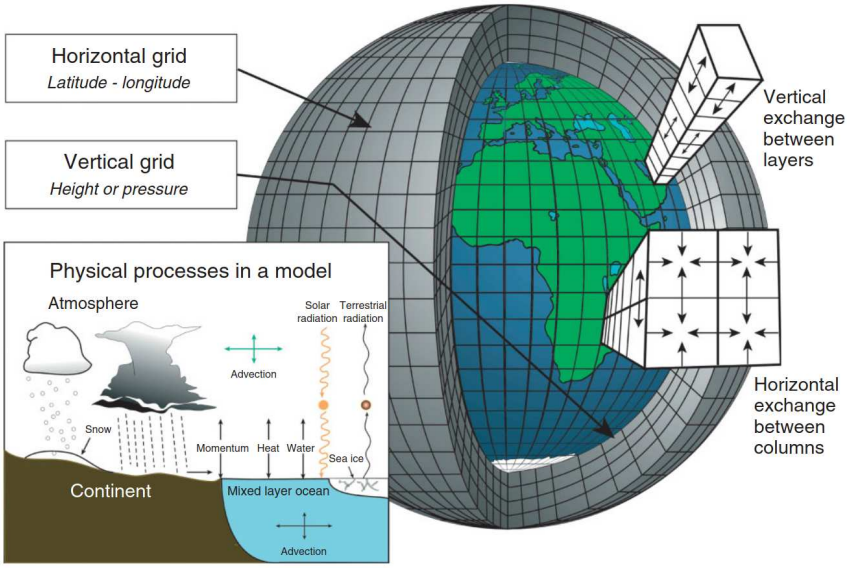

Figure 1.14: Schematic of a typical GCM grid structure and relevant processes. Reprinted from Edwards (2011) (Fig. 2).

1.2.3 Using model ensembles as research tools

We have seen that today, large parts of the dynamics of the climate system are relatively well understood, and their representation in climate models is solidly based on classical (e.g., the Navier–Stokes equations) and modern physics (e.g., radiative transfer). Despite this common basis, there is currently a large number of different climate models being actively developed and used in climate research, and no single model can be considered ideal for all applications (or indeed for *any* given application). Increasingly, modeling studies produce and analyze model output not from single climate models, but from *ensembles* of several models or model configurations (called *ensemble members*).

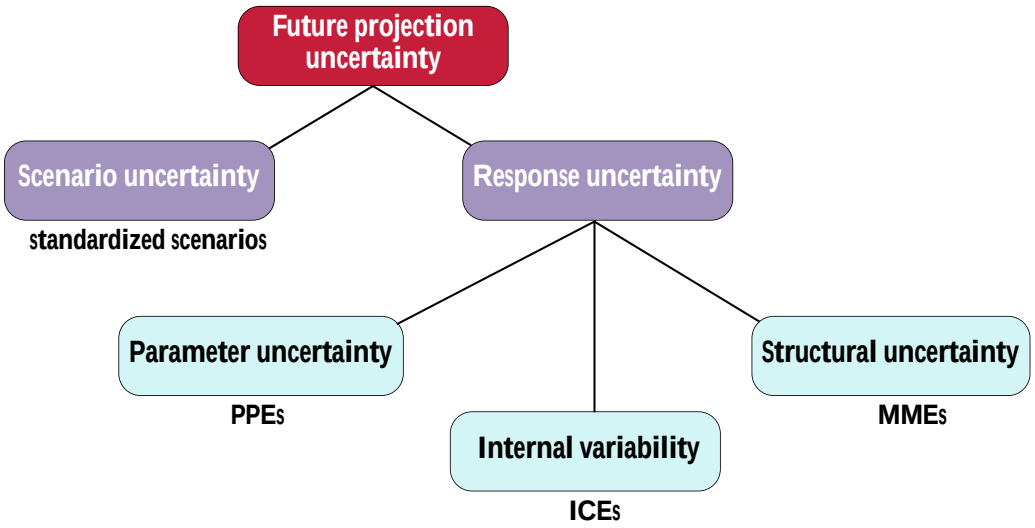

Figure 1.15: Types of future projection uncertainty in climate model projections as classified by e.g. Parker (2013), and types of model ensembles used to quantify these uncertainties: perturbed parameter ensembles (PPEs; Sec. 1.2.3.2), initial condition ensembles (ICEs; Sec. 1.2.3.1), and multi-model ensembles (MMEs; Sec. 1.2.3.3).

There are diverse reasons for using model ensembles as research tools, but fundamentally all ensemble modeling studies have in common that they allow to quantify and address certain types of *uncertainty*. In the context of future climate projections—which are the focus of this thesis—Parker (2013) and others have offered a classification of the types of uncertainties affecting climate model simulations (see the schematic in Fig. 1.15). As an example, consider the projection of future global OHU by the end of the 21st century using state-of-the-art climate models (this is the goal of Chapter 2). It is clear that the exact value of this quantity will strongly depend on the future trajectory of anthropogenic greenhouse gas (GHG) emissions; a business-as-usual scenario will have more GHG emissions and lead to increased energy storage in the ocean compared to

a drastic mitigation scenario. This introduces *scenario uncertainty* into the projection, as these GHG trajectories depend on future political choices and societal developments which are currently practically unknown. However, even if the future emissions trajectory of GHGs (and of other agents such as aerosols) was known exactly, we could not obtain a perfect estimate of future OHU, since we cannot fully predict the response of the climate system to these forcings. This *response uncertainty* is illustrated by simulations of the recent historical period, for which we have relatively accurate observational data for all anthropogenic and natural forcings (Meinshausen et al. 2017), but where many models struggle to accurately simulate the observed evolution of the climate system (Wills et al. 2022). Uncertainty in the response of the climate system to forcing stems from several factors: (i) simulations are sensitive to initial conditions due to the chaotic nature of the climate system, leading to *initial condition uncertainty*, (ii) simulations are sensitive to the choice of unknown physical parameters, leading to *parameter uncertainty*, and (iii) it is unclear how to best formulate an "ideal" climate model, leading to *structural uncertainty*. In practice, these three types of uncertainty are each addressed using different ways of constructing model ensembles, which are separately discussed further below: initial condition uncertainty is quantified with *initial condition ensembles* (ICEs; Sec. 1.2.3.1), parameter uncertainty is quantified with *parameter perturbation ensembles* (PPEs; Sec. 1.2.3.2), and structural uncertainty is quantified with *multi-model ensembles* (MMEs; Sec. 1.2.3.3). In this thesis, we make extensive use of MMEs coordinated by the Coupled Model Intercomparison Project (CMIP), which has also produced ICEs and PPEs for individual models (see Sec. 1.2.4). It should be noted that one could consider our limited theoretical understanding of certain climate processes (such as turbulence) to be a further source of uncertainty (Knutti et al. 2010), but for the purposes of this discussion this is subsumed under structural and parameter uncertainty.

The relative importance of these sources of uncertainty is not fixed in time. Fig. 1.17 shows the fraction of total uncertainty contributed by scenario, structural, and initial condition uncertainty as a function of time in simulations of future surface air temperature (SAT) over 2020–2100 using 20 climate models under six scenarios (from Watson-Parris (2021)). (Note that this decomposition does not explicitly include parameter uncertainty, which should be understood to be a part of structural uncertainty in this case.) On short timescales of around 0–10 years, initial condition uncertainty is the dominant contribution: this is the timescale of weather forecasting and decadal climate prediction, where synoptic weather systems and interannual climate variability dominate differences across models and scenarios. On centennial timescales, the relative role of initial condition uncertainty vanishes, and the dominant factor is scenario uncertainty (for the range of scenarios considered in Watson-Parris (2021)), as diverging trajectories of atmospheric GHG concentrations become more important than differences in internal variability. Structural uncertainty is largest at intermediate timescales of ca. 20–30 years, but remains substantial (ca. 20%) even until

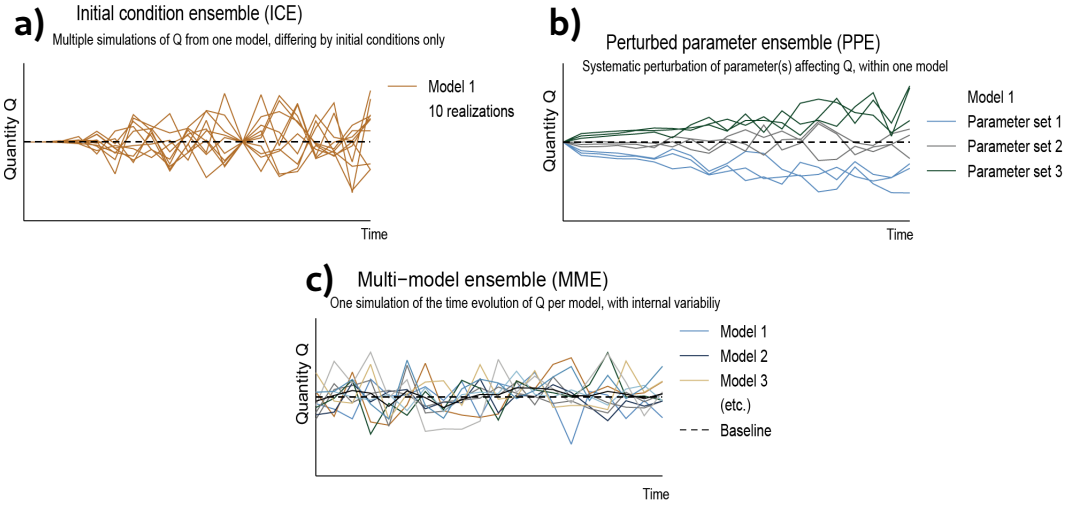

Figure 1.16: Idealized example of three types of model ensemble. Adapted from Chen et al. (2021) (Fig. 1.21).

the end of the century, such that inter-model differences are the main source of uncertainty for any given scenario on long timescales.

1.2.3.1 Initial condition ensembles (ICEs)

Ever since the seminal work of E. Lorenz in the 1960s, it is recognized that the climate system is *chaotic*. This is to say that, although the (coupled and nonlinear) differential equations governing the fluid dynamics of the atmosphere and ocean—the Navier–Stokes equations—are deterministic, their solutions are highly dependent on the initial conditions (Lorenz 1963), a behavior popularly known as the "butterfly effect" (Palmer 2024). As a consequence, when initializing e.g. an atmospheric model for numerical weather prediction (NWP), even small observational errors in the initial state will increase exponentially over the course of the simulation, leading to large errors after a finite period of time (Lorenz 1965), which is the main reason why weather forecasts are not trustworthy for lead times of more than a few days. This is because errors in the unresolved small scales will eventually feed back onto the larger scales resolved by the model, but even increasing the model resolution indefinitely will not achieve perfect forecast skill (Lorenz 1969; Palmer 2024).

This problem does not only beset atmospheric NWP models, but also and especially global climate models, which couple more processes and typically have coarser grid resolutions. In order to quantify initial condition uncertainty and to obtain more accurate projections, climate models can be run as initial condition ensembles (ICEs). For this, a single model is run several times under identical forcing but initialized with slightly different initial conditions, such as taken from different starting points in a control simulation (e.g., Bonnet et al. 2021) or from different days in

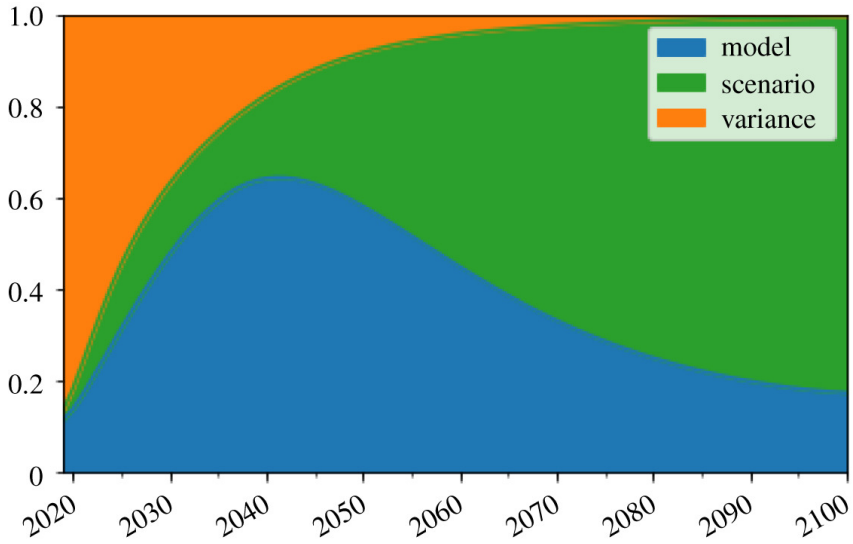

Figure 1.17: Fractional uncertainty as a function of time in future projections of global annual mean surface air temperature in 20 CMIP6 models across six scenarios, due to structural uncertainty ("model"), scenario uncertainty, and internal variability ("variance"). Figure reprinted from Watson-Parris (2021) (Fig. 1), original method by Hawkins and Sutton (2009).

the observational record (e.g., Deser et al. 2012). The resulting spread in projections can be solely attributed to differences in internal variability in each member, since other factors such as model version and forcing are held constant. This approach can be used for studies aiming at the detection and attribution of climate changes to anthropogenic activity (e.g., Silvy et al. 2022), as the spread between ensemble members provides an envelope of natural variability outside of which changes can be considered as likely caused by external forcing. Using the average output of many ensemble members (as single model initial-condition large ensembles or "SMILEs"; Maher et al. 2021) can also increase the fidelity of future projections since fluctuations due to internal variability are "averaged out" for a sufficient number of members (Krishnamurti et al. 2000).

Fig. 1.18 shows an example of such an ICE from Bonnet et al. (2021). The IPSL-CM6A-LR climate model is run under preindustrial forcing to obtain a long quasi-stationary control simulation exhibiting a bicentennial mode of global temperature variability (orange and red curves in Fig. 1.18a). From this, 32 ensemble members are initialized at different points in the control run and run under historical forcing. This results in considerable spread in the simulated global mean SAT over the historical period (Fig. 1.18b) which persists over the whole course of the simulation.

1.2.3.2 Perturbed parameter ensembles (PPEs)

The dynamical equations governing the climate system must be discretized onto finite grids in order to be solved by numerical models. As the computational cost of running such simulations

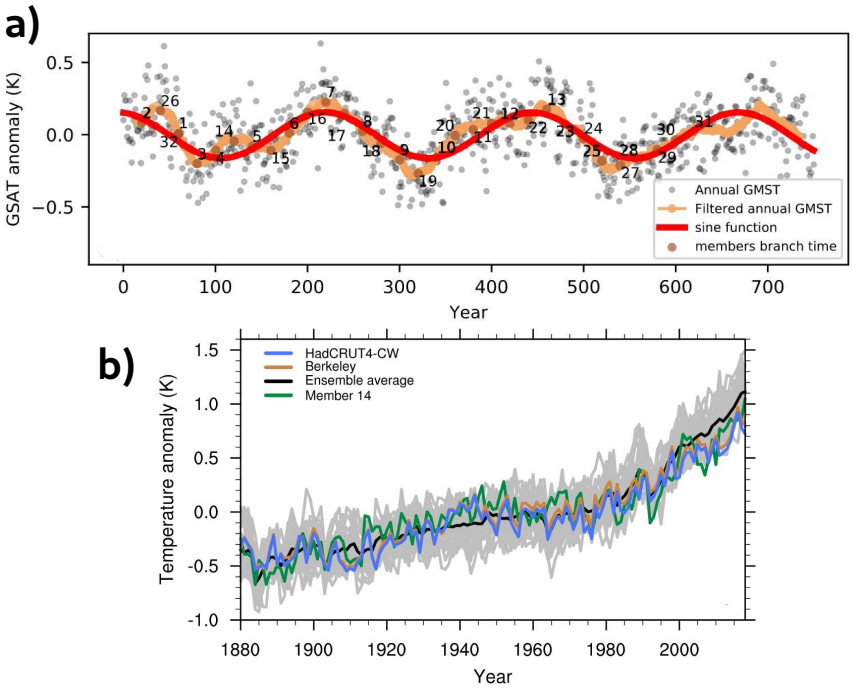

Figure 1.18: Example of an initial condition ensemble using the IPSL-CM6A-LR climate model. **a)** The initialisation procedure, where ensemble members are branched off at different points (brown circles) of a preindustrial control simulation (grey circles). **b)** Global annual mean surface air temperature anomaly relative to 1880–2018 for each member (grey lines) compared to observations (blue and brown lines), as well as the ensemble member closest to observations (green line). Figure reprinted from Bonnet et al. (2021) (Figs. 1 and 3).

increases with increasing grid resolution as well as with the number of processes included in the model, most climate models currently used for long-term climate simulations employ horizontal grid resolutions on the order of 50–100 km in the ocean and 100–200 km in the atmosphere (Gutiérrez and Treguier 2021). (Ocean models require higher resolution than their atmospheric counterparts because of the smaller Rossby radius of the ocean compared to the atmosphere; Vallis 2017) This means that processes occuring at spatial scales that are comparable or smaller than the size of the individual grid cells are not explicitly resolved by these models. Examples for such processes include turbulent heat transfer in the atmospheric boundary layer and (sub-)mesoscale eddies in the ocean. These processes must be accounted for using *parameterizations*, that is, theoretical or quasi-empirical representations of the effects of unresolved processes given the resolved large scales (these are also termed *closures*).

In the case of oceanic mesoscale eddies, which arise from flow instabilities e.g. from horizontal shear, a large number of ocean models employ a parameterization scheme developed by Gent and McWilliams (1990) which quantifies the effect of eddies on resolved circulation and stratification

by flattening the slope of isopycnal layers and effectively introducing an "eddy-induced velocity". The strength of this parameterized effect crucially depends on the value of the parameter κ_{GM}, sometimes termed "thickness diffusivity" parameter (Gent 2011), which was introduced in the formulation of the Gent and McWilliams (1990) scheme.

The dependence on parameter values such as κ_{GM} is a fundamental property of parameterizations. Fully coupled climate models employ a diversity of parameterizations of unresolved processes in all model components, resulting in tens to hundreds of uncertain parameters (Parker 2013), some of which are not simple constants but vary in space (as is the case for κ_{GM} in modern ocean models). As these parameters have major impacts on the resulting climate simulations (Kawai et al. 2022), an important question is how to choose their values. It is often unclear which parameter value results in the most accurate results, as (i) some parameters, such as κ_{GM}, are idealized constructions and do not have a "true" value which could be measured in reality, and (ii) even parameters which directly correspond to measureable quantities, such as the fall speed of ice crystals in clouds, do not necessarily give the best simulation results when set to their "true" values (Parker 2010). This is because the imperfect representation of the underlying behavior can cause an improvement in one parameterization to be offset by a deterioration in another parameterization or resolved process.

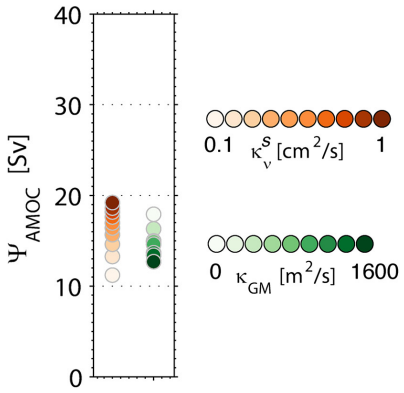

Figure 1.19: Example of a perturbed parameter ensemble using the MITgcm ocean model. The circles give the strength of the simulated Atlantic Meridional Overturning Circulation (AMOC) in MITgcm members forced by identical surface fields but using different values of the Gent-McWilliams parameter κ_{GM} and of the vertical diffusion coefficient κ_v. Figure adapted from Huber and Zanna (2017) (Fig. 4).

In order to quantify the sensitivity of climate simulations to such parameter choices, studies employ perturbed-parameter ensembles (PPEs). In such an ensemble, a single model is run several times under identical forcing and initial conditions, but with the value of one or several parameters in question set to a different value for each ensemble member. The resulting spread in simulations can be used to determine which parameters are most impactful on the overall simulation characteritics, to produce probabilistic estimates of unknown quantities (e.g., Piani et al. 2005; Murphy et al. 2007; Wagman and Jackson 2018), or to "tune" parameters to their ideal values (Hourdin et al. 2017). PPEs can also include ICEs in their setup, where each parameter choice is run with several perturbed initial conditions, which can further isolate the role of parameter choices relative to internal variability. However, it is important to acknowledge that a PPE based on a single

model cannot account for structural bias in the model, i.e., errors inherent in the model configuration that cannot be reduced for any parameter choice (McNeall et al. 2016; Sanderson et al. 2021); this issue can only be addressed (albeit only partially) in multi-model ensembles (see Sec. 1.2.3.3 below).

Fig. 1.19 shows an example of a PPE from Huber and Zanna (2017). In this study, the MITgcm ocean model was run several times using identical surface forcing fields (of temperature, salinity, and fluxes of heat, momentum and freshwater), but using different value choices for the Gent-McWilliams parameter κ_{GM} and for the vertical diffusion coefficient κ_v (each parameter was varied separately). The red and green points in Fig. 1.19 indicate that the simulated Atlantic Meridional Overturning Circulation (AMOC) strength increases with increasing vertical diffusion and decreases with increasing κ_{GM}. We do not discuss these results further here, but it should be noted that this dependence of the AMOC strength on mixing parameters also has important implications for OHU (Newsom et al. 2023), see Chapter 3.

1.2.3.3 Multi-model ensembles (MMEs)

We now turn to multi-model ensembles (MMEs), the main type of ensemble coordinated by the Coupled Model Intercomparison Project (CMIP; see Sec. 1.2.4), and the one used most extensively in this thesis. MMEs consist of several different models, either developed by separate modeling groups or representing distinct versions of the same model (e.g. obtained by coupling different model components), run under identical forcing and initial conditions. The ensemble members may thus differ in the processes they include, their grid resolution, the parameterizations and parameter values they employ (see Sec. 1.2.3.2 above), as well as their numerical implementation and the computer hardware they are run on (Parker 2013). The multi-model average of a simulated quantity is often more accurate (when referenced to observations) than the output of any single model, especially when optimizing the accuracy of multiple target variables simultaneously (Hagedorn et al. 2005; Knutti et al. 2010). MMEs further allow to explore the sensitivity of simulations to model structure, which, as we have seen (Fig. 1.17), is the leading source of uncertainty in future climate projections on long scales for a given scenario.

§ Inferring response uncertainty and best estimates from MMEs Given a MME of simulations of a climate quantity, such as future OHU by the end of the 21st century (as in Sec. 2), how can we quantify both the quantity's central estimate as well as its uncertainty?

The most common approach to obtain a central estimate is to simply average each member's prediction with equal weight in a kind of "model democracy" where each member is considered as providing an independent estimate (Knutti 2010). However, this method can be problematic for some applications as the ensemble members are often not truly independent (see the paragraph be-

low) and since some members could be considered more useful than others based on their performance and agreement with observations (Abramowitz et al. 2019). For this reason, several methods have been developed to select subsets of models with desirable properties such as agreement with observations and model independence (e.g., Chiew et al. 2009; Ruane and McDermid 2017; Herger et al. 2018). Another approach is to compute a weighted average of each member's prediction, with the weights again based on model performance (e.g., Gillett 2015; Haughton et al. 2015; Knutti et al. 2017b; Eyring et al. 2019). In addition, more advanced statistical (in particular Bayesian) methods have been developed to combine climate model simulations with information from observations (e.g., Forest et al. 2002; Giorgi and Mearns 2002), including the method of *emergent constraints* (Hall and Qu 2006) introduced in Sec. 1.2.5 and used in Chapter 2.

There are several approaches to infer uncertainty from a MME Parker (2013): (i) the spread between ensemble members can be considered a lower bound on the true uncertainty range since factors other than model structure are expected to add additional uncertainty (Hourdin et al. 2023), (ii) one can compute formal statistical probabilities of future changes based on information from observations (e.g., the emergent constraint method), or (iii) information from models can be combined with other lines of evidence such as expert judgement to produce confidence intervals (e.g., Sherwood et al. 2020; Masson-Delmotte et al. 2021a).

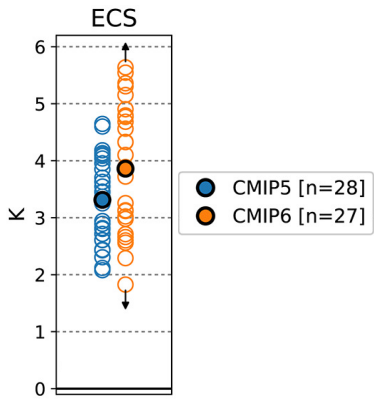

Figure 1.20: Example of a multi-model ensemble using the CMIP5 (blue) and CMIP6 (orange) ensembles. The circles give the equilibrium climate sensitivity (ECS) in K for each ensemble member. Figure adapted from Zelinka et al. (2020) (Fig. 1).

§ Methodological issues of MMEs Although the use of MMEs for climate projections and process studies has become increasingly widespread, there exist several potentially problematic methodological issues concerning the construction and interpretation of MMEs.

When computing a multi-model average of some simulated quantity as described above, the average can exhibit characteristics not found in any of the individual members: for example, a nonlinear relationship between two variables can be obscured by averaging, or the amplitude of a response underestimated due to the averaging of positive and negative contributions of greater magnitude (Knutti et al. 2010).

More fundamentally, when constructing a model ensemble for a study addressing structural uncertainty, it is unclear how to best sample this uncertainty space (Parker 2010; 2013). For PPEs

(Sec. 1.2.3.2), the parameter space is usually an interval of real numbers (e.g., Fig. 1.19) which can be sampled systematically using well-defined statistical procedures (e.g., MacDougall and Knutti 2016). In contrast, the space of possible MME members consists in principle of all possible model configurations, including all possible combinations of model components, processes, parameterizations and numerical settings. It is clear that this space cannot be sampled systematically, not least because of computational limits. Instead, MMEs are always "ensembles of opportunity", which consist of a number of currently available models that may differ or resemble each other in systematic ways (Tebaldi and Knutti 2007). Modeling groups often only publish their "best" model versions (Knutti et al. 2010) while withholding alternative model versions and thus reducing the amount of outlier or extreme models in the resulting MME (Hourdin et al. 2023).

Ensemble members in common MMEs such as CMIP cannot be considered to give independent estimates, since all models are developed based on shared literature and use similar or identical parameterizations and observational evaluation data sets, and in some cases even share model code (Sanderson et al. 2015a; Abramowitz et al. 2019). As a consequence, model biases relative to observations can be correlated, such that a multi-model mean bias persists even when adding more models to the ensemble and even in the theoretical limit of an infinite number of models (Knutti et al. 2010). Another way of expressing this is that the "effective number" of models in a MME is smaller than the actual number of models included (Jun et al. 2008; Pennell and Reichler 2011). This effect has been shown by Masson and Knutti (2011) and Knutti et al. (2013) for the CMIP3 and CMIP5 MMEs, respectively. Using unsupervised hierarchical clustering on preindustrial surface temperature and precipitation output from these model ensembles, they showed that model output tends to be similar for models developed by the same group, for models sharing model components, and for successive versions of a single model (Masson and Knutti 2011). Rauser et al. (2015) has thus argued for the use of cross-generational multi-model ensembles, e.g. by combining models from successive CMIP phases, since models are too similar across generations. Nevertheless, Annan and Hargreaves (2010) have argued that MMEs should be interpreted under the paradigm of a *statistically indistinguishable ensemble*, i.e., by assuming that the real climate system is drawn from the same statistical distribution as the models in an MME. They showed that under this framework, the CMIP3 MME can be considered a relatively "good" sample in terms of statistical properties, in contrast to the traditional paradigm where MME members are assumed to be drawn from a distribution centered on the truth and which suffers from the above mentioned issues (Annan and Hargreaves 2010), although these two paradigms may be complementary (Sanderson and Knutti 2012). In addition, weighting methods have been devised which take model interdependence into account (Bishop and Abramowitz 2013; Abramowitz and Bishop 2015; Sanderson et al. 2015b; 2017).

§ The notion of inter-model relationships A crucial concept used in this thesis is that of an *inter-model relationship* (IMR) between two variables. An IMR exists when two simulated variables x and y (for example, AMOC strength and OHUE as in Chapter 3) covary across ensemble members of a MME. This is similar but conceptually distinct from the kind of relationship in Fig. 1.19, which showed the dependence of a simulated climate quantity (AMOC strength) on model parameters (κ_{GM} and κ_v). It is also separate from the relationship between two variables across time or space, for example the relationship between the ENSO index and remote precipitation as determined from observations or model simulations (e.g., Alexander et al. 2002).

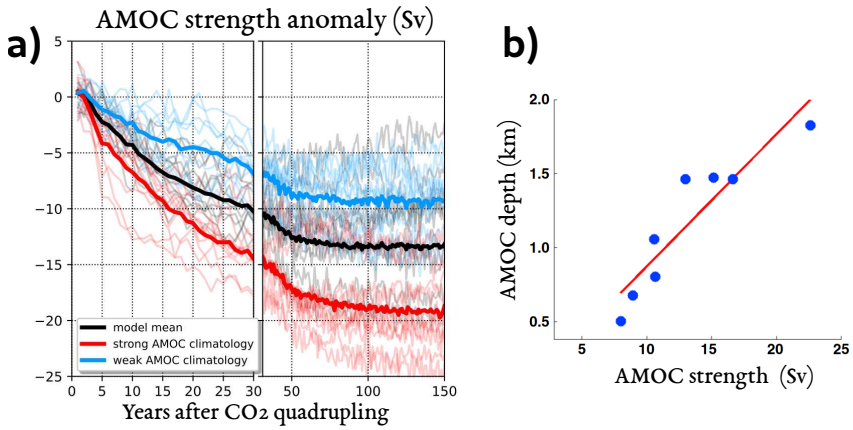

Figure 1.21: Examples of inter-model relationships between quantities related to AMOC. **a)** AMOC weakening in 31 CMIP6 model simulations after abrupt quadrupling of atmospheric CO_2 (`abrupt-4xCO2` simulation), with lines colored by climatological preindustrial AMOC strength. **b)** Scatter plot between AMOC strength and AMOC depth (defined as the average depth of the 5 Sv and 10 Sv streamlines north of 35°S in the Atlantic) in eight CMIP5 models over 150 years of `abrupt-4xCO2` forcing. The correlation is $r = 0.92$ ($p < 0.01$). Panel **a)** adapted from Lin et al. (2023) (Fig. 1), panel **b)** adapted from Kostov et al. (2014) (Fig. 3).

In the simplest case, an IMR can be quantified as a linear correlation between two variables across MME members and can be visualized e.g. in a scatter plot. As an illustration, we will consider examples from the literature that have identified inter-model relationships between AMOC strength and other climate variables. Fig. 1.21a shows timeseries of AMOC strength anomaly in 31 CMIP6 models forced by an abrupt quadrupling of atmospheric CO_2 concentrations (Lin et al. 2023). The lines are divided into three groups according to each model's climatological (unperturbed) AMOC strength. It is apparent that models with strong climatological AMOC tend to have a greater AMOC decrease under this forcing than models with a weak initial AMOC. This result, which Lin et al. (2023) show is related to stratification and mixing in the Labrador sea, is a first example of an IMR between two quantities (climatological AMOC strength and future AMOC decline), although this is shown only visually in Fig. 1.21a and not quantified statisti-

cally. In Fig. 1.21b, AMOC strength in eight CMIP5 models is plotted against the depth of the AMOC overturning cell (Kostov et al. 2014). Models with a stronger AMOC tend to have a deeper AMOC, as these two variables are highly correlated (Pearson's $r = 0.92$).

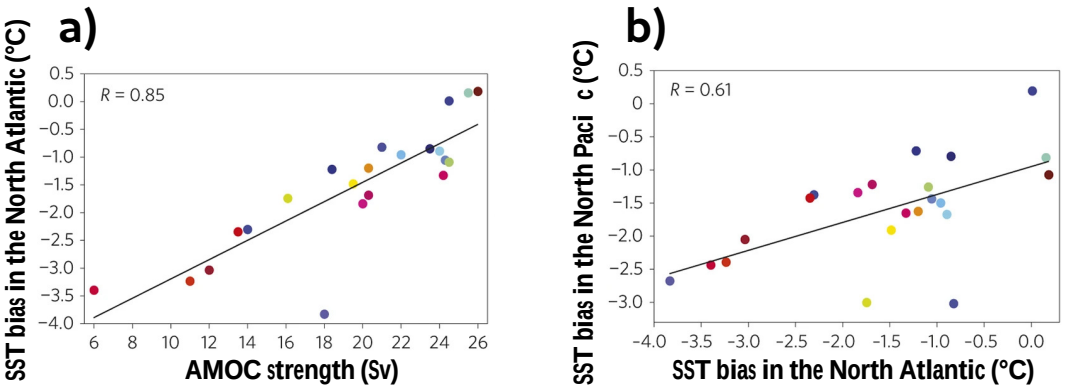

Figure 1.22: Examples of inter-model relationships between AMOC and regional SST. **a)** Scatter plot between historical AMOC strength and North Atlantic SST bias relative to observations in 22 CMIP5 models. **b)** As panel a), but between North Atlantic SST bias and North Pacific SST bias. Adapted from Wang et al. (2014) (Fig. 2).

However, IMRs are not restricted to relationships between intrinsically linked variables (such as AMOC strength, depth, and future decline), but can appear between any two physically linked variables (relationships occurring due to chance are of course not of interest). Keeping the AMOC as an example, Wang et al. (2014) found a significant IMR between AMOC strength and SST bias in the North Atlantic in an ensemble of 22 CMIP5 models (Fig. 1.22a). Models with a weaker AMOC were found to have a more negative (cold) SST bias, which is consistent with the role of the AMOC in transporting heat from low latitudes to the subpolar North Atlantic, and has been used to construct AMOC proxies based on SST in this region (Caesar et al. 2018). The North Atlantic SST bias was in turn found to be correlated with the SST bias in the North Pacific (Fig. 1.22b). These results illustrate the important point that climate model biases can be linked between variables and across remote geographical regions. This means that improving model biases in a specific variable or in a single region can have remote effects due to the coupled nature of the (simulated) climate system (Wang et al. 2014).

1.2.4 The Coupled Model Intercomparison Project (CMIP)

The Coupled Model Intercomparison Project (CMIP) was established in 1995 by the World Climate Research Programme (Meehl et al. 1997). Its purpose is to coordinate climate simulations using coupled general circulation models (GCMs) under standardized forcing protocols and make the model output freely available in order to advance our understanding of the climate system

and inform the development and improvement of GCMs. In addition, CMIP also provides crucial information to the assessment reports of the Intergovernmental Panel on Climate Change (IPCC) of the United Nations, which inform policymakers about the scientific consensus knowledge on the physical basis of climate change as well as its impacts and related adaptation and mitigation strategies (Meehl 2023). Like the cycles of the IPCC, CMIP is organized in phases: the first phase (CMIP1) began in 1996 (Meehl et al. 1997), and successive phases were initiated in 1997 (CMIP2; Meehl et al. 2000), 2003 (CMIP3; Meehl et al. 2007), 2008 (CMIP5; Taylor et al. 2012) and 2013 (CMIP6; Eyring et al. 2016). The intermediate CMIP4 was not a major CMIP phase and only consisted of simulations supplementary to CMIP3 (Stouffer et al. 2017). The next phase, CMIP7, is currently in planning (e.g., Funke et al. 2024).

In this thesis, we make extensive use of model simulations from the most recent CMIP6 phase (Meehl et al. 2014; Eyring et al. 2016), on which we will focus here. CMIP6 has a federated structure (Fig. 1.23), with a number of core experiments including a historical simulation and a group of simulations called DECK (for Diagnostic, Evaluation and Characterization of Klima) which are mandatory for any model participating in the excercise, and a number of endorsed secondary model intercomparison projects (MIPs) addressing more specialized research questions. The CMIP6 `historical` simulations span the period 1850–2014 and use a forcing dataset of historical atmospheric GHG concentrations for 43 GHG species (Meinshausen et al. 2017) as well as observed anthropogenic and natural forcings (e.g., land use change, solar forcing, and stratospheric aerosol from volcanic activity; Zanchettin et al. 2016; Matthes et al. 2017; Hoesly et al. 2018; Ma et al. 2020). The DECK consists of four experiments: (i) an `amip` experiment (for Atmospheric Model Intercomparison Project; Gates et al. 1999) where each GCM's atmospheric model component is forced by observed SSTs and sea ice concentrations over the period 1979–2014; (ii) a `piControl` control experiment where the coupled GCMs are forced by preindustrial GHG concentrations for at least 500 simulation years; (iii) an `abrupt-4xCO2` experiment where atmospheric CO_2 concentrations are abruptly quadrupled from their preindustrial value and the coupled GCMs run for at least 150 years; and

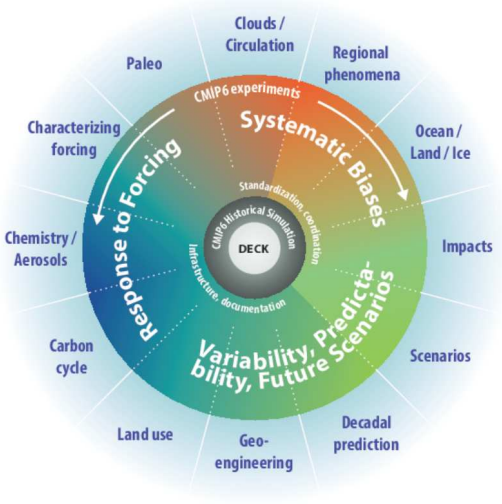

Figure 1.23: Schematic of the CMIP6 project structure and science goals. The core historical and DECK experiments are mandatory, the outer topics are addressed by endorsed MIPs. Reprinted from Eyring et al. (2016) (Fig. 2).

(iv) a `1pctCO2` experiment where atmospheric CO_2 concentrations rise exponentially from their preindustrial value at a rate of 1% per year for at least 150 years.

Over 130 models from 53 modeling centers contributed output to CMIP6 (Durack et al. 2014), providing a wide variety of model configurations and grid resolutions (Fig. 1.24). Importantly, all GCMs are subjected to identical forcing fields for any given CMIP experiment, such that differences in the resulting simulations are principally due to structural differences between models (see Sec. 1.2.3.3). Modeling centers may additionally choose to perform a given experiment with multiple ensemble members initialized with perturbed initial conditions (Sec. 1.2.3.1) or with different physical parameter choices (Sec. 1.2.3.2).

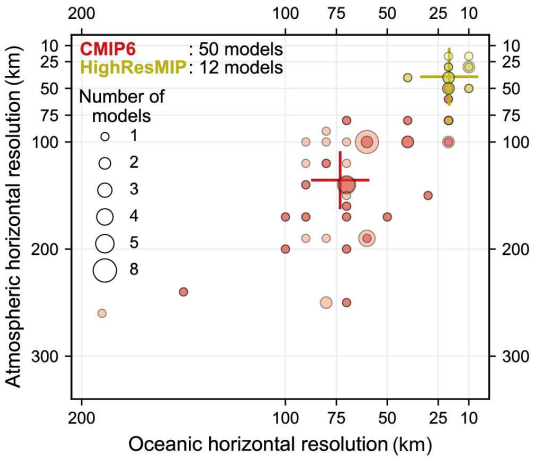

Figure 1.24: Horizontal resolution of the atmospheric and oceanic components of CMIP6 and HighResMIP GCMs. Reprinted from Chen et al. (2021) (Fig. 1.19).

These CMIP6 standard experiments are intended to serve distinct but complementary purposes. The `historical` experiment allows model output to be compared with observations, thus enabling systematic model evaluation and observational constraint methodologies (see Sec. 1.2.5). The `amip` experiment is designed for atmospheric model intercomparison and can be used to quantify differences between forced and fully coupled simulations of the same GCM (e.g. Andrews et al. 2022). The preindustrial control experiment (`piControl`) is used to quantify unforced internal variability in each GCM and is used as a baseline to compute anomalies of climate variables under the GHG forcing of other CMIP experiments. Finally, the `abrupt-4xCO2` and `1pctCO2` experiments are idealized representations of CO_2-driven climate change and can be used to calculate idealized climate properties such as the effective climate sensitivity (EffCS; Gregory et al. 2004) and the transient climate response (Raper et al. 2002).

In addition to these mandatory historical and DECK experiments, CMIP6 includes 21 "endorsed" secondary MIPs which address a variety of more specialized topics. For example, the Ocean Model Intercomparison Project (Griffies et al. 2016; Orr et al. 2017; Tsujino et al. 2020) defines an experimental protocol for ocean model simulations forced by common atmospheric surface fields, analogous to AMIP for the atmospheric components, and a set of supplementary physical and biogeochemical output variables requested from participating models. Other endorsed MIPs focus on topics such as cloud feedback (CFMIP; Webb et al. 2017), high resolution simula-

tions (HighResMIP; Haarsma et al. 2016), paleoclimate (PMIP; Kageyama et al. 2018), or the carbon cycle (Jones et al. 2016, C4MIP,).

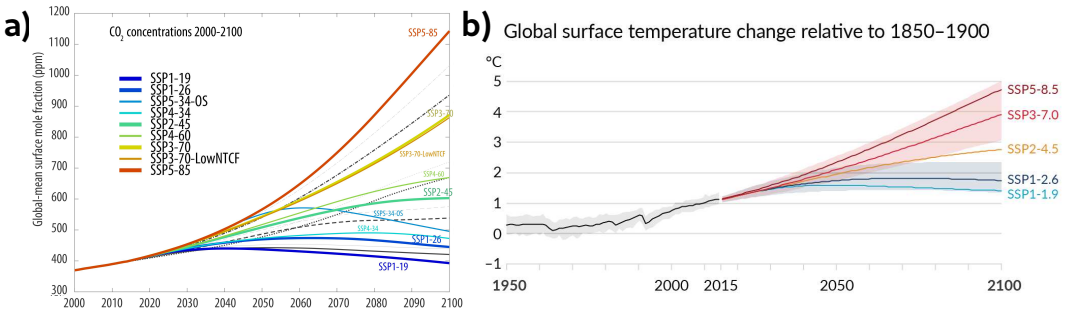

Figure 1.25: **a)** Atmospheric CO_2 concentrations and **b)** global SAT change in different SSP scenarios. Panel **a)** adapted from Meinshausen et al. (2020) (Fig. 3), panel **b)** adapted from Masson-Delmotte et al. (2021b) (Fig. SPM.8).

The MIP most important for future climate projections and in particular for informing the IPCC is the ScenarioMIP (O'Neill et al. 2016). For ScenarioMIP, a number of future GHG emission trajectories were created based on socioeconomic scenarios obtained from integrated assessment models (simplified numerical models of physical, economical and social interactions). These scenarios consist of Shared Socioeconomic Pathways (SSPs; Riahi et al. 2017; Gidden et al. 2019; Meinshausen et al. 2020) which are an update of the Representative Concentration Pathways of atmospheric GHG concentrations used in CMIP5 (RCPs; Vuuren et al. 2011). They span a range from the "2°C scenario" SSP1-2.6 (the "sustainability" SSP1 pathway with approximately 2.6 W m^{-2} of radiative forcing anomaly by 2100) to the "business as usual scenario" SSP5-8.5 (the "fossil-fuel development" SSP5 pathway with approximately 8.5 W m^{-2} of radiative forcing anomaly by 2100). Fig. 1.25 shows the atmospheric CO_2 concentrations used in each SSP (Fig. 1.25a), and the resulting global mean surface air temperature evolution over the 21st century (Fig. 1.25b). The ensemble spread across scenarios in the multi-model ensemble or within a given GCM can be used to quantify scenario uncertainty and provide future projections under plausible future development pathways or at given global warming levels. In particular, it can be exploited via the method of emergent constraints, which are introduced in the following section.

1.2.5 Emergent constraints

Comparing the output of model simulations to real-world observations is a fundamental part of model evaluation and a prerequisite for their confident use for future projections (Hall et al. 2019). Even before model evaluation, observations are already used to inform the model development process when tuning parameters (Hourdin et al. 2017). Although model performance has steadily

increased with successive CMIP phases and IPCC reports (Chen et al. 2021), the ensemble spread in certain key future climate variables has hardly decreased. A prominent example is equilibrium climate sensitivity (ECS; Knutti and Hegerl 2008), the global mean surface temperature change at steady state following a doubling of atmospheric CO_2 concentration, whose uncertainty has remained stubbornly large across CMIP cycles and IPCC assessment reports (Maslin and Austin 2012). Inter-model spread in ECS has even increased in CMIP6 compared to previous model generations (Meehl et al. 2020), and the *very likely* range (>90% probability) assessed by IPCC AR6 of 2 K to 5 K is similar to the range assessed in the "Charney report" in 1979 (1.5 K–4.5 K; National Research Council 1979), which is due to persistent uncertainties in the climate feedback parameter λ (Zelinka et al. 2020).

Although ECS is an idealized quantity, it quantifies the climate system's sensitivity to CO_2 forcing and thus has direct implications for more plausible future scenarios of climate change; hence, there is a crucial need to reduce its uncertainty. However, it has been argued that, from the perspective of ensemble modeling, reducing inter-model spread is less important than increasing model independence (Jebeile and Barberousse 2021). Reduced ensemble spread alone does not guarantee robustness, since the participating models may suffer from common biases. Instead, greater model independence may initially lead to increased ensemble spread, but also enables the use of sophisticated methods to reduce projection uncertainty by incorporating information from observations. Currently most prominent among these is the method of *emergent constraints* (ECs), which we use in Chapter 2 to reduce uncertainties in future global OHU, and which we now introduce in the present section.

1.2.5.1 Concept

Consider a situation with a climate variable of interest, Y, whose projection from an MME has considerable ensemble spread due to structural uncertainty. This variable may be difficult to observe in the present climate or an inherently unobservable response to future forcing such as global OHU by the end of the 21st century (as in Chapter 2). An *emergent constraint* consists of identifying a relationship between a *predictor* variable, X, and the variable of interest Y (the *predictand*), across the members of the MME. This relationship is of the general form

$$Y = f(X) + \varepsilon, \tag{1.17}$$

where f is the functional form of the relationship and ε is a small random error term. If the predictor X is an observable quantity of the present-day or historical climate, observations of X can be combined with Eq. (1.17) to obtain a constrained estimate of Y. The relationship (1.17) is not contained in any single model, but "emerges" from the combination of structurally different

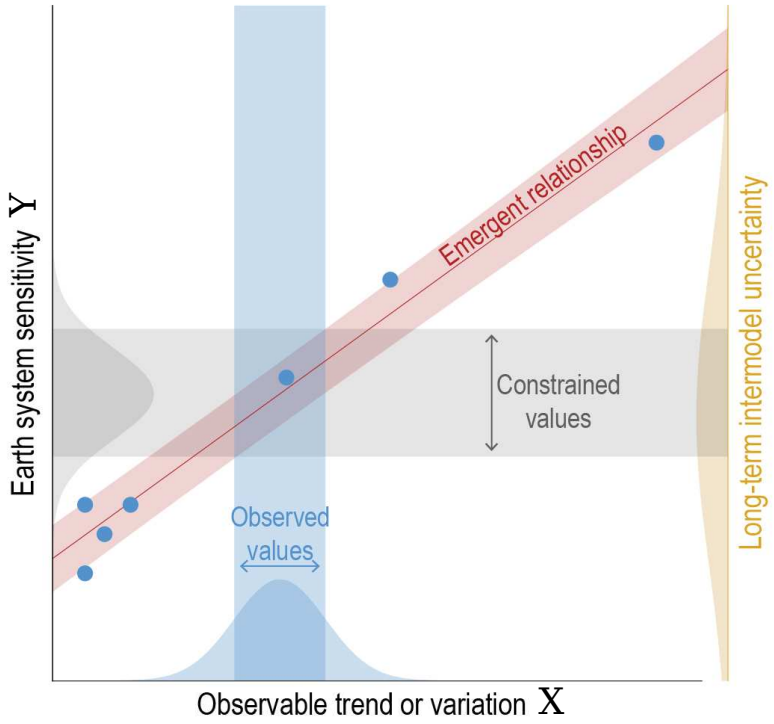

Figure 1.26: Illustration of the emergent constraint method. The emergent relationship f (red) is combined with the observational distribution of the predictor X (blue) to obtain an estimate of the predictand Y (left y-axis) that is more constrained than the prior multi-model mean (right y-axis). Adapted from Chen et al. (2021) (Fig. 1.23), originally from Eyring et al. (2019) (Box 1).

models of an MME (the first use of the term *emergent constraint* in the context of climate projections is likely due to Allen and Ingram (2002)). In order for an EC to be trustworthy, it is important that the underlying relationship is based on a verifiable physical mechanism and not due to chance (Hall et al. 2019, this is discussed in more detail below, Sec. 1.2.5.5). Given the relationship (1.17) and an observational estimate (including observational uncertainty) of the predictor X, an updated estimate of Y can be obtained using statistical methods. The simplest and most used approach (and the approach adopted in Chapter 2) is to estimate f using linear regression and to simply project the distribution of X onto the Y-axis using the estimate of f (see Fig. 1.26), taking into account uncertainty in the observations of X and in the regression model for f (Eyring et al. 2019; Brient 2020; Chen et al. 2021). However, since this method of statistical inference has a number of potential shortcomings (as will be discussed below; Sec. 1.2.5.6), more sophisticated methods of obtaining constrained estimates from X and f have been developed, such as methods based on Bayesian inference (e.g., Hargreaves et al. 2012; Renoult et al. 2020) or on information theory (e.g., Brient and Schneider 2016).

1.2.5.2 Examples of published ECs

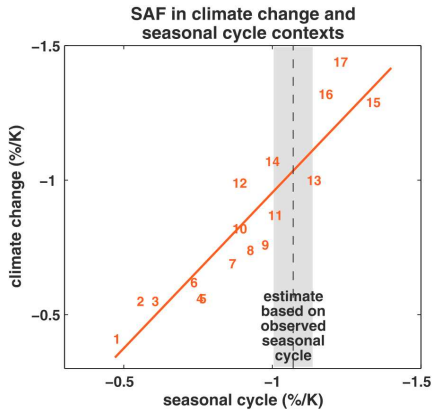

Figure 1.27: Emergent constraint on snow albedo feedback (SAF), defined here as the response of snow albedo $\Delta\alpha_s$ (in %) to surface warming ΔT_s (in K). The SAF under future climate change (y-axis) is constrained using observations of SAF in the seasonal cycle (x-axis) based on a linear inter-model regression (orange line; compare Fig. 1.26). Figure reprinted from Hall and Qu (2006) (Fig. 3).

Perhaps the first successful application of the EC method to climate projections is due to Hall and Qu (2006). In that study, the strength of future snow albedo feedback (SAF, increased surface warming due to melting of snow caused by an initial warming; Thackeray and Fletcher 2016) was constrained using observations of the strength of SAF in the context of the seasonal cycle, which was shown to be highly correlated across models with future SAF (Fig. 1.27; Hall and Qu 2006; Qu and Hall 2014). Since then, the EC method has been applied to a wide range of uncertain climate variables, in particular to ECS and related quantities such as cloud feedback (see Brient (2020) for an exhaustive list of ECs published before 2020, and Knutti et al. (2017a) for constraints on ECS). The EC method was also considered in IPCC AR5 for projections of near-term global warming until 2035 (Kirtman et al. 2013; Gillett 2015), and in the most recent IPCC AR6 to constrain e.g. ECS (Forster et al. 2021) and quantities related to the carbon cycle (Canadell et al. 2021).

1.2.5.3 Types of ECs

Although the fundamental idea of ECs is the same for all of the above examples, there is a large diversity in the literature in the statistical methods employed to obtain constrained estimates as well as in the types of observable variables chosen as predictors. Sanderson et al. (2021) have proposed a classification of ECs into three kinds: (i) "bias persistence" or trend-on-trend ECs, where X and Y are of the same nature (e.g., past warming and future warming; Tokarska et al. 2020; Lyu et al. 2021), and the model bias in X is assumed to persist into the future; (ii) process-based ECs, where a leading-order physical process is identified which controls Y and whose strength can be quantified with X (e.g., ocean surface density constraining Arctic Ocean acidification Terhaar et al. 2020); and (iii) "frequency substitution" or variability-based ECs, where the future response of Y is constrained using its response to shorter-term forcing quantified by X (e.g., the seasonal cycle, interannual variability, or volcanic and paleo forcing Hall and Qu 2006; Renoult et al. 2020). In Chapter 2, we make use of a

process-based EC to constrain future global OHU, improving on previous approaches employing trend-on-trend constraints.

1.2.5.4 Why do ECs "emerge" from model ensembles?

It is natural to ask why functional relationships between climate variables such as f in Eq. 1.17 appear to be found so frequently in MMEs. Brient (2020) noted that ECs arise due to the interaction of local structural uncertainties and (possibly remote, e.g., Wang et al. 2014) biases in large-scale dynamics. A trivial possibility is that such relationships can appear simply by chance: due to the high dimensionality of GCMs, which include hundreds of variables on millions of gridcells (Williamson et al. 2021), significant correlations between pairs of variables can be found by data mining especially in the presence of model interdependence (Caldwell et al. 2014), even though these relationships may often not be grounded on physical processes and thus not applicable to reduce uncertainties in the predictand. Hall et al. (2019) have instead proposed two physically-based sources for the emergence of ECs from MMEs. The first source relies on the Fluctuation-Dissipation Theorem, a fundamental result from statistical physics which relates variability in a variable to its sensitivity to forcing (Callen and Welton 1951; Kubo 1966; Leith 1975; Williamson et al. 2018). This principle is especially applicable to GCM ensembles in the presence of conservation principles (Hall et al. 2019) such as global mean radiative balance imposed by model tuning (Siler et al. 2018; Brient 2020). The second source of emergent relationships between variables across GCMs mentioned in Hall et al. (2019) is the potential similarity between the response of a variable to forcing on short timescales (e.g., over the seasonal cycle) to its response to forcing on longer and slower timescales. This is the reasoning behind variability-based constraints introduced above. A more mathematical view has been advanced by Huntingford et al. (2023), who suggested that ECs are fundamentally due to the implicit presence of large-scale bulk differential equations describing the Earth system which arise from an aggregation of the effect of physics coded into the model at the grid scale. In this view, the application of an EC amounts to determining the implicit value of a parameter contained in such a bulk differential equation.

1.2.5.5 Validity criteria

The possibility of spurious ECs arising due to chance calls for solid criteria for the evaluation of the validity of any proposed EC. Such criteria have been previously proposed (e.g., Klein and Hall 2015; Hall et al. 2019; Brient 2020; Sanderson et al. 2021), and can be summarized as three major points: (i) an EC requires the identification of a plausible and verifiable physical mechanism which explains the relationship between predictor and predictand; (ii) observations of the predictor must be sufficiently constrained and adequately compared to GCM values; and (iii) the EC

should be robust to out-of-sample testing. A proposed constraint fulfilling these criteria could be considered to be a "confirmed" EC (Hall et al. 2019), although ECs can never be fully confirmed due to the possibility of missing processes in GCMs or biased sampling of structural uncertainty in MMEs. First, the verification of a proposed mechanism can be attempted through additional analysis of model output (as in Chapter 2) or through targeted simulations such as PPEs, although the greater structural diversity in MMEs compared to PPEs lends greater confidence to ECs arising from MMEs (Klein and Hall 2015). Such analysis must explain how and why the inter-model spread relates in a similar way to both the predictor and the predictand. Second, observations of the predictor must be sufficiently constrained to allow a narrowing of the predictands uncertainty, and in particular should not encompass the entire inter-model spread (Knutti and Tomassini 2008). The observational period must be long enough and sufficiently resolved to capture the time scale of the mechanism or feedback at play in the longer future projection (e.g., Wittenberg 2009). Furthermore, observations of the predictor must be directly comparable to simulated values of the predictor, e.g. when using pixel-level data for a large-scale predictor (Winkler et al. 2019) or when comparing satellite cloud observations to GCM output (e.g., Myers et al. 2021), which requires the use of satellite simulators for faithful comparison (Bodas-Salcedo et al. 2011). Third and last, a proposed EC must hold in an out-of-sample test, e.g. by replication in a different model ensemble (such as the CMIP5 ensemble for a constraint proposed using CMIP6, see Chapter 2), which ensures that the identified relationship is not due to sampling bias in the chosen MME. Numerous previously proposed ECs have been subsequently shown to be weaker or invalid in newer MMEs (e.g., Schlund et al. 2020; Williamson et al. 2024), while others have been replicated and thus strengthened in their trustworthiness using newer ensembles (e.g., Bracegirdle and Stephenson 2012).

1.2.5.6 Potential issues

Despite their recent success and increased use as a research method, ECs are subject to a number of potential issues impacting their applicability and credibility. Fundamentally, in many cases it is unknown whether model performance is stationary in the sense that present model behavior can be used to infer future model behavior (Abe et al. 2009). The processes controlling the predictand may be state dependent or change with time (Klein and Hall 2015), for example due to the emergence of slowly acting feedbacks (Eyring et al. 2019). For example, Marvel et al. (2018) have found that constraints on ECS based on the historical record are generally biased low, because historical climate feedback has been weaker than that expected under long-term climate change (e.g., Andrews et al. 2018; 2022). Since models in "ensembles of opportunity" such as the CMIP6 MME are not independent (see Sec. 1.2.3.3), the inclusion of similar or nearly duplicate models in an EC can artificially increase the correlation between predictor and predictand without

adding independent information (Sanderson et al. 2015a; 2021). The participating models may also all have a common deficiency, such as a missing process or a shared parameterization, which causes a systematic bias in the prediction (Klein and Hall 2015). Still, an EC allows to reduce at least one source of model error, but the results should be carefully interpreted. A related issue is that some observational products such as reanalysis estimates of cloud properties rely themselves on parameterizations or model assumptions to produce their output, challenging their use as independent estimates in ECs (Brient 2020). Considering the statistical inference method applied to estimate the predictand, using a linear regression to estimate f in Eq. 1.17 can give outsize influence to outlier models which are inconsistent with observations of the predictand, and little weight to models consistent with observations but lying off the regression line (Brient 2020). A possible solution is to use methods not based on linear regression as detailed above (e.g., Brient and Schneider 2016). However, any statistical method can potentially be impacted by selection bias since analysis parameters may be actively chosen by researchers to maximize the correlation between predictor and predictand, which leads to an underestimation of the fit uncertainty. Lastly, in the case where multiple variables influence the predictand (which is especially the case for compound variables such as ECS), errors in each of the influences may compensate each other, again leading to uncertainty underestimation. For this case, approaches have been developed to use multiple predictors using multivariate methods (e.g., Renoult et al. 2020) or to combine existing ECs (e.g., Bretherton and Caldwell 2020).

Despite these potential issues, a careful application of the EC methodology remains a powerful tool to constrain future projections of important climate quantities, and can help identify priorities for model development and observational programs.

1.3 Scientific aims and outline of this thesis

1. How can we constrain future global OHU?

Given the major role of total OHU as an indicator of past and future climate change (Sec. 1.1.3.2) as well as its direct connection to widespread climate impacts (Sec. 1.1.3.3), accurate future OHU projections are of vital importance. However, there remains substantial uncertainty in projections of future OHU over the 21st century, both due to scenario uncertainty and due to structural uncertainty across climate models for a given scenario (Cheng et al. 2022). Following our discussion of the emergent constraint method in Section 1.2.5, it is therefore tempting to search for potential predictor variables to be used in a formal observational constraint on future OHU. This is the goal of Chapter 2, where we identify a physics-based emergent constraint among CMIP5/6 models on future OHU by the end of the 21st century under various emissions scenarios. This constraint is

based on interlinked climate model biases in the Southern Hemisphere including Antarctic sea ice extent, Southern Ocean cloud cover, and the temperature of waters upwelling from the deep ocean to the surface. We find that the historical state of these variables precondition each model's response to future climate change, in particular through global-scale cloud feedbacks, such that observations of present-day sea ice extent can be used to predict future OHU. The underlying mechanism also carries implications for global surface warming and cloud feedback, and predicts slightly more OHU, higher warming, and stronger cloud feedback than the raw CMIP6 predictions. These conclusions are at odds with previously published constraints based on past warming trends (Tokarska et al. 2020; Lyu et al. 2021), and this is discussed in Chapter 2.

At the time of writing (January 18, 2025), this article is under review at *Science Advances* (submitted on June 6, 2024).

2. What processes control the OHU efficiency?

Recalling the conceptual split between total OHU and OHU efficiency (OHUE) introduced in Section 1.1.2, we aim to obtain process understanding also for OHUE, which could then potentially be used in a separate constraint on OHUE. Total OHU and OHUE are not necessarily determined by the same processes, since total OHU integrates the amplitude of climate feedbacks and surface warming, whereas the definition of OHUE partly "normalizes" these effects by scaling OHU by global warming (see Eq. 1.10). Furthermore, the processes controlling OHUE are less explored in the literature and partly inconsistent (e.g., Boé et al. 2009; Kostov et al. 2014; Gregory et al. 2023), although recent studies are converging on the importance of upper ocean density stratification and mesoscale eddy parameterizations on setting OHUE in climate models (Gregory et al. 2023; Liu et al. 2023; Newsom et al. 2023). In Chapter 3, we thus investigate the linkages between proposed controls on OHUE in an ensemble of climate models. This analysis reveals how interhemispheric connections of model biases, especially in ocean stratification, can explain and partly reconcile these proposed mechanisms.

At the time of writing (January 18, 2025), this article is under review at *Ocean Science* (submitted on November 5, 2024).

3. Can we use this process understanding to constrain OHU (efficiency)?

Following the analysis of the factors controlling OHUE in climate models in Chapter 3, it is then natural to look for an emergent constraint on OHUE based on these variables. Due to the relatively large number of potential predictors found in Chapter 3, their interdependence, as well as the confounding influence of model interdependence (Sec. 1.2.5.6), we opt for a systematic statistical approach using a maximum number of available model members. This preliminary analysis

is presented in the Outlook Chapter 4, where we process model output of around ten predictors for over 100 CMIP6 members in each of four scenarios, and apply both unsupervised and supervised statistical learning methods to better understand the ensemble structure as well as to potentially obtain constrained projections of OHUE.

4. What is the effect of climate model biases on future projections, and how do different biases relate to each other?

A more general overarching issue pervading all chapters of this thesis is the impact of climate model biases on future projections, and in particular their linkage across different models and model members. Although enormous progress has been made in all areas of climate model development (see Sec. 1.2.1), the representation of the climate system in even the most advanced models still suffers from substantial errors and biases which form the subject of ongoing research. While we do not propose explicit measures to directly alleviate these biases in this thesis, we analyze their implications in detail and provide both conceptual and quantitative advances in their understanding. In Chapter 2, we exploit the inter-model spread in a number of Southern Hemisphere variables to obtain improved future OHU projections; in Chapter 3, we analyze how such biases can be linked across hemispheres and impact the global climate response; and in Chapter 4, we make use of dimensionality reduction and clustering techniques to analyze the structure of inter-ensemble variance in key climate variables.

Bibliography

Abe, M. et al. (2009). "Correlation between Inter-Model Similarities in Spatial Pattern for Present and Projected Future Mean Climate". *SOLA* 5. Publisher: Meteorological Society of Japan, pp. 133–136. ISSN: 1349-6476. DOI: 10.2151/sola.2009-034.

Abraham, J. P. et al. (2013). "A review of global ocean temperature observations: Implications for ocean heat content estimates and climate change". *Reviews of Geophysics* 51:3. _eprint: https://onlinelibrary.wiley.com/doi/pdf/10.1002/rog.20022, pp. 450–483. ISSN: 1944-9208. DOI: 10.1002/rog.20022.

Abramowitz, G. and C. H. Bishop (2015). "Climate Model Dependence and the Ensemble Dependence Transformation of CMIP Projections". Section: Journal of Climate. DOI: 10.1175/JCLI-D-14-00364.1.

Abramowitz, G. et al. (2019). "ESD Reviews: Model dependence in multi-model climate ensembles: weighting, sub-selection and out-of-sample testing". *Earth System Dynamics* 10:1. Publisher: Copernicus GmbH, pp. 91–105. ISSN: 2190-4979. DOI: 10.5194/esd-10-91-2019.

Alessi, M. J. and M. A. A. Rugenstein (2023). "Surface Temperature Pattern Scenarios Suggest Higher Warming Rates Than Current Projections". *Geophysical Research Letters* 50:23. _eprint: https://onlinelibrary.wiley.com/doi/pdf/10.1029/2023GL105795, e2023GL105795. ISSN: 1944-8007. DOI: 10.1029/2023GL105795.

Alexander, K. and S. M. Easterbrook (2015). "The software architecture of climate models: a graphical comparison of CMIP5 and EMICAR5 configurations". *Geoscientific Model Development* 8:4. Publisher: Copernicus GmbH, pp. 1221–1232. ISSN: 1991-959X. DOI: 10.5194/gmd-8-1221-2015.

Alexander, M. A. et al. (2002). "The Atmospheric Bridge: The Influence of ENSO Teleconnections on Air–Sea Interaction over the Global Oceans". Section: Journal of Climate. ISSN: 1520-0442.

Allen, M. R. and W. J. Ingram (2002). "Constraints on future changes in climate and the hydrologic cycle". *Nature* 419:6903. Publisher: Nature Publishing Group, pp. 224–232. ISSN: 1476-4687. DOI: 10.1038/nature01092.

Andrews, T. et al. (2018). "Accounting for Changing Temperature Patterns Increases Historical Estimates of Climate Sensitivity". *Geophysical Research Letters* 45:16. _eprint: https://onlineli-

brary.wiley.com/doi/pdf/10.1029/2018GL078887, pp. 8490–8499. ISSN: 1944-8007. DOI: 10.1029/2018GL078887.

Andrews, T. et al. (2022). "On the Effect of Historical SST Patterns on Radiative Feedback". *Journal of Geophysical Research: Atmospheres* 127:18. _eprint: https://onlinelibrary.wiley.com/doi/pdf/10.1029/2022JD036675, e2022JD036675. ISSN: 2169-8996. DOI: 10.1029/2022JD036675.

Annan, J. D. and J. C. Hargreaves (2010). "Reliability of the CMIP3 ensemble". *Geophysical Research Letters* 37:2. _eprint: https://onlinelibrary.wiley.com/doi/pdf/10.1029/2009GL041994. ISSN: 1944-8007. DOI: 10.1029/2009GL041994.

Arias-Ortiz, A. et al. (2018). "A marine heatwave drives massive losses from the world's largest seagrass carbon stocks". *Nature Climate Change* 8:4. Number: 4 Publisher: Nature Publishing Group, pp. 338–344. ISSN: 1758-6798. DOI: 10.1038/s41558-018-0096-y.

Armour, K. C., C. M. Bitz, and G. H. Roe (2013). "Time-Varying Climate Sensitivity from Regional Feedbacks". *Journal of Climate* 26:13. Publisher: American Meteorological Society Section: Journal of Climate, pp. 4518–4534. ISSN: 0894-8755, 1520-0442. DOI: 10.1175/JCLI-D-12-00544.1.

Armour, K. C., J. Marshall, J. R. Scott, A. Donohoe, and E. R. Newsom (2016). "Southern Ocean warming delayed by circumpolar upwelling and equatorward transport". *Nature Geoscience* 9:7. Number: 7 Publisher: Nature Publishing Group, pp. 549–554. ISSN: 1752-0908. DOI: 10.1038/ngeo2731.

Armour, K. C. et al. (2024). "Sea-surface temperature pattern effects have slowed global warming and biased warming-based constraints on climate sensitivity". *Proceedings of the National Academy of Sciences* 121:12. Publisher: Proceedings of the National Academy of Sciences, e2312093121. DOI: 10.1073/pnas.2312093121.

Arrhenius, S. (1896). "On the Influence of Carbonic Acid in the Air upon the Temperature of the Ground". *Philosophical Magazine and Journal of Science* 41:251, pp. 237–276.

Behrenfeld, M. J. et al. (2006). "Climate-driven trends in contemporary ocean productivity". *Nature* 444:7120. Publisher: Nature Publishing Group, pp. 752–755. ISSN: 1476-4687. DOI: 10.1038/nature05317.

Bishop, C. H. and G. Abramowitz (2013). "Climate model dependence and the replicate Earth paradigm". *Climate Dynamics* 41:3, pp. 885–900. ISSN: 1432-0894. DOI: 10.1007/s00382-012-1610-y.

Bodas-Salcedo, A. et al. (2011). "COSP: Satellite simulation software for model assessment". Section: Bulletin of the American Meteorological Society. DOI: 10.1175/2011BAMS2856.1.

Boé, J., A. Hall, and X. Qu (2009). "Deep ocean heat uptake as a major source of spread in transient climate change simulations". *Geophysical Research Letters* 36:22. _eprint: https://onlineli-

brary.wiley.com/doi/pdf/10.1029/2009GL040845. ISSN: 1944-8007. DOI: 10.1029/2009GL040845.

Bonnet, R. et al. (2021). "Presentation and Evaluation of the IPSL-CM6A-LR Ensemble of Extended Historical Simulations". *Journal of Advances in Modeling Earth Systems* 13:9. _eprint: https://onlinelibrary.wiley.com/doi/pdf/10.1029/2021MS002565, e2021MS002565. ISSN: 1942-2466. DOI: 10.1029/2021MS002565.

Bopp, L. et al. (2013). "Multiple stressors of ocean ecosystems in the 21st century: projections with CMIP5 models". *Biogeosciences* 10:10. Publisher: Copernicus GmbH, pp. 6225–6245. ISSN: 1726-4170. DOI: 10.5194/bg-10-6225-2013.

Bourgeois, T., N. Goris, J. Schwinger, and J. F. Tjiputra (2022). "Stratification constrains future heat and carbon uptake in the Southern Ocean between 30°S and 55°S". *Nature Communications* 13:1. Bandiera_abtest: a Cc_license_type: cc_by Cg_type: Nature Research Journals Number: 1 Primary_atype: Research Publisher: Nature Publishing Group Subject_term: Biogeochemistry;Carbon cycle;Marine chemistry;Physical oceanography Subject_term_id: biogeochemistry;carbon-cycle;marine-chemistry;physical-oceanography, p. 340. ISSN: 2041-1723. DOI: 10.1038/s41467-022-27979-5.

Boyce, D. G., M. R. Lewis, and B. Worm (2010). "Global phytoplankton decline over the past century". *Nature* 466:7306. Publisher: Nature Publishing Group, pp. 591–596. ISSN: 1476-4687. DOI: 10.1038/nature09268.

Bracegirdle, T. J. and D. B. Stephenson (2012). "On the robustness of emergent constraints used in multimodel climate change projections of arctic warming". *Journal of Climate* 26:2. Place: Boston MA, USA Publisher: American Meteorological Society, pp. 669–678. DOI: 10.1175/JCLI-D-12-00537.1.

Breitburg, D. L. and G. F. Riedel (2005). *Multiple stressors in marine systems*. Accepted: 2015-04-09T16:47:38Z. Island Press. ISBN: 978-1-59726-771-7.

Bretherton, C. S. and P. M. Caldwell (2020). "Combining Emergent Constraints for Climate Sensitivity". *Journal of Climate* 33:17. Publisher: American Meteorological Society Section: Journal of Climate, pp. 7413–7430. ISSN: 0894-8755, 1520-0442. DOI: 10.1175/JCLI-D-19-0911.1.

Brient, F. (2020). "Reducing Uncertainties in Climate Projections with Emergent Constraints: Concepts, Examples and Prospects". *Advances in Atmospheric Sciences* 37:1, pp. 1–15. ISSN: 1861-9533. DOI: 10.1007/s00376-019-9140-8.

Brient, F. and T. Schneider (2016). "Constraints on Climate Sensitivity from Space-Based Measurements of Low-Cloud Reflection". Section: Journal of Climate. DOI: 10.1175/JCLI-D-15-0897.1.

Bryan, K. and M. D. Cox (1967). "A numerical investigation of the oceanic general circulation". *Tellus* 19:1. _eprint: https://onlinelibrary.wiley.com/doi/pdf/10.1111/j.2153-3490.1967.tb01459.x, pp. 54–80. ISSN: 2153-3490. DOI: 10.1111/j.2153-3490.1967.tb01459.x.

Bryan, K., S. Manabe, and R. C. Pacanowski (1975). "A Global Ocean-Atmosphere Climate Model. Part II. The Oceanic Circulation". Section: Journal of Physical Oceanography. ISSN: 1520-0485.

Budyko, M. I. (1961). "The Heat Balance of the Earth's Surface". *Soviet Geography* 2:4. Publisher: Routledge _eprint: https://doi.org/10.1080/00385417.1961.10770761, pp. 3–13. ISSN: 0038-5417. DOI: 10.1080/00385417.1961.10770761.

– (1969). "The effect of solar radiation variations on the climate of the Earth". *Tellus* 21:5. _eprint: https://onlinelibrary.wiley.com/doi/pdf/10.1111/j.2153-3490.1969.tb00466.x, pp. 611–619. ISSN: 2153-3490. DOI: 10.1111/j.2153-3490.1969.tb00466.x.

Burger, F. A., J. Terhaar, and T. L. Frölicher (2022). "Compound marine heatwaves and ocean acidity extremes". *Nature Communications* 13:1. Publisher: Nature Publishing Group, p. 4722. ISSN: 2041-1723. DOI: 10.1038/s41467-022-32120-7.

Byrne, M. and R. Przeslawski (2013). "Multistressor Impacts of Warming and Acidification of the Ocean on Marine Invertebrates' Life Histories". *Integrative and Comparative Biology* 53:4, pp. 582–596. ISSN: 1540-7063. DOI: 10.1093/icb/ict049.

Cael, B. B. (2022). "Ocean Heat Uptake Efficiency Increase Since 1970". *Geophysical Research Letters* 49:19. _eprint: https://onlinelibrary.wiley.com/doi/pdf/10.1029/2022GL100215, e2022GL100215. ISSN: 1944-8007. DOI: 10.1029/2022GL100215.

Caesar, L., S. Rahmstorf, A. Robinson, G. Feulner, and V. Saba (2018). "Observed fingerprint of a weakening Atlantic Ocean overturning circulation". *Nature* 556:7700. Number: 7700 Publisher: Nature Publishing Group, pp. 191–196. ISSN: 1476-4687. DOI: 10.1038/s41586-018-0006-5.

Caldwell, P. M. et al. (2014). "Statistical significance of climate sensitivity predictors obtained by data mining". *Geophysical Research Letters* 41:5. _eprint: https://onlinelibrary.wiley.com/doi/pdf/10.1002/2014GL059205, pp. 1803–1808. ISSN: 1944-8007. DOI: 10.1002/2014GL059205.

Callen, H. B. and T. A. Welton (1951). "Irreversibility and Generalized Noise". *Physical Review* 83:1. Publisher: American Physical Society, pp. 34–40. DOI: 10.1103/PhysRev.83.34.

Canadell, J. G. et al. (2021). "Global carbon and other biogeochemical cycles and feedbacks". In: *Climate Change 2021: The Physical Science Basis. Contribution of Working Group I to the Sixth Assessment Report of the Intergovernmental Panel on Climate Change*. Ed. by V. Masson-Delmotte et al. Cambridge University Press, Cambridge, United Kingdom and New York, NY, USA, pp. 673–816. DOI: 10.1017/9781009157896.001.

Cazenave, A. and G. L. Cozannet (2014). "Sea level rise and its coastal impacts". *Earth's Future* 2:2. _eprint: https://onlinelibrary.wiley.com/doi/pdf/10.1002/2013EF000188, pp. 15–34. ISSN: 2328-4277. DOI: 10.1002/2013EF000188.

Cess, R. D. et al. (1990). "Intercomparison and interpretation of climate feedback processes in 19 atmospheric general circulation models". *Journal of Geophysical Research: Atmospheres* 95, D10. _eprint: https://onlinelibrary.wiley.com/doi/pdf/10.1029/JD095iD10p16601, pp. 16601–16615. ISSN: 2156-2202. DOI: 10.1029/JD095iD10p16601.

Chen, D. et al. (2021). "Framing, context, and methods". In: *Climate Change 2021: The Physical Science Basis. Contribution of Working Group I to the Sixth Assessment Report of the Intergovernmental Panel on Climate Change*. Ed. by V. Masson-Delmotte et al. Cambridge University Press, Cambridge, United Kingdom and New York, NY, USA, pp. 147–286. DOI: 10.1017/9781009157896.001.

Chen, X. and K.-K. Tung (2014). "Varying planetary heat sink led to global-warming slowdown and acceleration". *Science* 345:6199. Publisher: American Association for the Advancement of Science, pp. 897–903. DOI: 10.1126/science.1254937.

Cheng, L. et al. (2022). "Past and future ocean warming". *Nature Reviews Earth & Environment*. Publisher: Nature Publishing Group, pp. 1–19. ISSN: 2662-138X. DOI: 10.1038/s43017-022-00345-1.

Cheung, W. W. L. and T. L. Frölicher (2020). "Marine heatwaves exacerbate climate change impacts for fisheries in the northeast Pacific". *Scientific Reports* 10:1. Number: 1 Publisher: Nature Publishing Group, p. 6678. ISSN: 2045-2322. DOI: 10.1038/s41598-020-63650-z.

Chiew, F. H. S., J. Teng, J. Vaze, and D. G. C. Kirono (2009). "Influence of global climate model selection on runoff impact assessment". *Journal of Hydrology* 379:1, pp. 172–180. ISSN: 0022-1694. DOI: 10.1016/j.jhydrol.2009.10.004.

Cimoli, L. et al. (2023). "Significance of Diapycnal Mixing Within the Atlantic Meridional Overturning Circulation". *AGU Advances* 4:2. _eprint: https://onlinelibrary.wiley.com/doi/pdf/10.1029/2022AV000800, e2022AV000800. ISSN: 2576-604X. DOI: 10.1029/2022AV000800.

Cissé, G. et al. (2022). "Health, wellbeing and the changing structure of communities". In: *Climate Change 2022: Impacts, Adaptation and Vulnerability. Contribution of Working Group II to the Sixth Assessment Report of the Intergovernmental Panel on Climate Change*. Ed. by H.-O. Pörtner et al. Cambridge University Press.

Cox, P. M., R. A. Betts, C. D. Jones, S. A. Spall, and I. J. Totterdell (2000). "Acceleration of global warming due to carbon-cycle feedbacks in a coupled climate model". *Nature* 408:6809. Publisher: Nature Publishing Group, pp. 184–187. ISSN: 1476-4687. DOI: 10.1038/35041539.

Deser, C., M. A. Alexander, S.-P. Xie, and A. S. Phillips (2010). "Sea Surface Temperature Variability: Patterns and Mechanisms". *Annual Review of Marine Science* 2, Volume 2, 2010. Pub-

lisher: Annual Reviews, pp. 115–143. ISSN: 1941-1405, 1941-0611. DOI: 10.1146/annurev-marine-120408-151453.

Deser, C., A. Phillips, V. Bourdette, and H. Teng (2012). "Uncertainty in climate change projections: the role of internal variability". *Climate Dynamics* 38:3, pp. 527–546. ISSN: 1432-0894. DOI: 10.1007/s00382-010-0977-x.

Deutsch, C., A. Ferrel, B. Seibel, H.-O. Pörtner, and R. B. Huey (2015). "Climate change tightens a metabolic constraint on marine habitats". *Science* 348:6239. Publisher: American Association for the Advancement of Science, pp. 1132–1135. DOI: 10.1126/science.aaa1605.

DeVries, T. (2022). "The Ocean Carbon Cycle". *Annual Review of Environment and Resources* 47, Volume 47, 2022. Publisher: Annual Reviews, pp. 317–341. ISSN: 1543-5938, 1545-2050. DOI: 10.1146/annurev-environ-120920-111307.

Dong, Y. et al. (2020). "Intermodel Spread in the Pattern Effect and Its Contribution to Climate Sensitivity in CMIP5 and CMIP6 Models". *Journal of Climate* 33:18. Publisher: American Meteorological Society Section: Journal of Climate, pp. 7755–7775. ISSN: 0894-8755, 1520-0442. DOI: 10.1175/JCLI-D-19-1011.1.

Donohue, K. A., K. L. Tracey, D. R. Watts, M. P. Chidichimo, and T. K. Chereskin (2016). "Mean Antarctic Circumpolar Current transport measured in Drake Passage". *Geophysical Research Letters* 43:22. _eprint: https://onlinelibrary.wiley.com/doi/pdf/10.1002/2016GL070319, pp. 11, 760–11, 767. ISSN: 1944-8007. DOI: 10.1002/2016GL070319.

Drijfhout, S. (2018). "The relation between natural variations in ocean heat uptake and global mean surface temperature anomalies in CMIP5". *Scientific Reports* 8:1. Publisher: Nature Publishing Group, p. 7402. ISSN: 2045-2322. DOI: 10.1038/s41598-018-25342-7.

Dufresne, J.-L. and S. Bony (2008). "An Assessment of the Primary Sources of Spread of Global Warming Estimates from Coupled Atmosphere–Ocean Models". *Journal of Climate* 21:19. Publisher: American Meteorological Society Section: Journal of Climate, pp. 5135–5144. ISSN: 0894-8755, 1520-0442. DOI: 10.1175/2008JCLI2239.1.

Durack, P. J., P. J. Gleckler, F. W. Landerer, and K. E. Taylor (2014). "Quantifying underestimates of long-term upper-ocean warming". *Nature Climate Change* 4:11. Number: 11 Publisher: Nature Publishing Group, pp. 999–1005. ISSN: 1758-6798. DOI: 10.1038/nclimate2389.

Easterling, D. R. and M. F. Wehner (2009). "Is the climate warming or cooling?" *Geophysical Research Letters* 36:8. _eprint: https://onlinelibrary.wiley.com/doi/pdf/10.1029/2009GL037810. ISSN: 1944-8007. DOI: 10.1029/2009GL037810.

Edwards, P. N. (2011). "History of climate modeling". *WIREs Climate Change* 2:1. _eprint: https://onlinelibrary.wiley.com/doi/pdf/10.1002/wcc.95, pp. 128–139. ISSN: 1757-7799. DOI: 10.1002/wcc.95.

Eyring, V. et al. (2016). "Overview of the Coupled Model Intercomparison Project Phase 6 (CMIP6) experimental design and organization". *Geoscientific Model Development* 9:5, pp. 1937–1958. ISSN: 1991-9603. DOI: 10.5194/gmd-9-1937-2016.

Eyring, V. et al. (2019). "Taking climate model evaluation to the next level". *Nature Climate Change* 9:2. Number: 2 Publisher: Nature Publishing Group, pp. 102–110. ISSN: 1758-6798. DOI: 10.1038/s41558-018-0355-y.

Filbee-Dexter, K. et al. (2020). "Marine heatwaves and the collapse of marginal North Atlantic kelp forests". *Scientific Reports* 10:1. Number: 1 Publisher: Nature Publishing Group, p. 13388. ISSN: 2045-2322. DOI: 10.1038/s41598-020-70273-x.

FitzGerald, D. M., M. S. Fenster, B. A. Argow, and I. V. Buynevich (2008). "Coastal Impacts Due to Sea-Level Rise". *Annual Review of Earth and Planetary Sciences* 36, Volume 36, 2008. Publisher: Annual Reviews, pp. 601–647. ISSN: 0084-6597, 1545-4495. DOI: 10.1146/annurev.earth.35.031306.140139.

Forest, C. E., P. H. Stone, A. P. Sokolov, M. R. Allen, and M. D. Webster (2002). "Quantifying Uncertainties in Climate System Properties with the Use of Recent Climate Observations". *Science* 295:5552. Publisher: American Association for the Advancement of Science, pp. 113–117. DOI: 10.1126/science.1064419.

Forster, P. et al. (2021). "The Earth's energy budget, climate feedbacks, and climate sensitivity". In: *Climate Change 2021: The Physical Science Basis. Contribution of Working Group I to the Sixth Assessment Report of the Intergovernmental Panel on Climate Change*. Ed. by V. Masson-Delmotte et al. Cambridge University Press, Cambridge, United Kingdom and New York, NY, USA, pp. 923–1054. DOI: 10.1017/9781009157896.001.

Forster, P. M. et al. (2023). "Indicators of Global Climate Change 2022: annual update of large-scale indicators of the state of the climate system and human influence". *Earth System Science Data* 15:6. Publisher: Copernicus GmbH, pp. 2295–2327. ISSN: 1866-3508. DOI: 10.5194/essd-15-2295-2023.

Fox-Kemper, B. et al. (2021). "Ocean, cryosphere, and sea level change". In: *Climate Change 2021: The Physical Science Basis. Contribution of Working Group I to the Sixth Assessment Report of the Intergovernmental Panel on Climate Change*. Ed. by V. Masson-Delmotte et al. Cambridge University Press, Cambridge, United Kingdom and New York, NY, USA, pp. 1211–1362. DOI: 10.1017/9781009157896.001.

Frederikse, T. et al. (2020). "The causes of sea-level rise since 1900". *Nature* 584:7821. Publisher: Nature Publishing Group, pp. 393–397. ISSN: 1476-4687. DOI: 10.1038/s41586-020-2591-3.

Frigg, R. and S. Hartmann (2024). "Models in Science". In: *The Stanford Encyclopedia of Philosophy*. Ed. by E. N. Zalta and U. Nodelman. Fall 2024. Metaphysics Research Lab, Stanford University.

Frisinger, H. H. (1973). "Aristotle's legacy in meteorology". Section: Bulletin of the American Meteorological Society. ISSN: 1520-0477.

Frölicher, T. L., E. M. Fischer, and N. Gruber (2018). "Marine heatwaves under global warming". *Nature* 560:7718. Number: 7718 Publisher: Nature Publishing Group, pp. 360–364. ISSN: 1476-4687. DOI: 10.1038/s41586-018-0383-9.

Frölicher, T. L. and C. Laufkötter (2018). "Emerging risks from marine heat waves". *Nature Communications* 9:1. Number: 1 Publisher: Nature Publishing Group, p. 650. ISSN: 2041-1723. DOI: 10.1038/s41467-018-03163-6.

Funke, B. et al. (2024). "Towards the definition of a solar forcing dataset for CMIP7". *Geoscientific Model Development* 17:3. Publisher: Copernicus GmbH, pp. 1217–1227. ISSN: 1991-959X. DOI: 10.5194/gmd-17-1217-2024.

Gates, W. L. et al. (1999). "An Overview of the Results of the Atmospheric Model Intercomparison Project (AMIP I)". Section: Bulletin of the American Meteorological Society. ISSN: 1520-0477.

Gent, P. R. (2011). "The Gent–McWilliams parameterization: 20/20 hindsight". *Ocean Modelling*. Modelling and Understanding the Ocean Mesoscale and Submesoscale 39:1, pp. 2–9. ISSN: 1463-5003. DOI: 10.1016/j.ocemod.2010.08.002.

Gent, P. R. and J. C. McWilliams (1990). "Isopycnal Mixing in Ocean Circulation Models". *Journal of Physical Oceanography* 20:1. Publisher: American Meteorological Society Section: Journal of Physical Oceanography, pp. 150–155. ISSN: 0022-3670, 1520-0485. DOI: 10.1175/1520-0485(1990)020<0150:IMIOCM>2.0.CO;2.

Gidden, M. J. et al. (2019). "Global emissions pathways under different socioeconomic scenarios for use in CMIP6: a dataset of harmonized emissions trajectories through the end of the century". *Geoscientific Model Development* 12:4. Publisher: Copernicus GmbH, pp. 1443–1475. ISSN: 1991-959X. DOI: 10.5194/gmd-12-1443-2019.

Gillett, N. P. (2015). "Weighting climate model projections using observational constraints". *Philosophical Transactions of the Royal Society A: Mathematical, Physical and Engineering Sciences* 373:2054. Publisher: Royal Society, p. 20140425. DOI: 10.1098/rsta.2014.0425.

Giorgetta, M. A. et al. (2013). "Climate and carbon cycle changes from 1850 to 2100 in MPI-ESM simulations for the Coupled Model Intercomparison Project phase 5". *Journal of Advances in Modeling Earth Systems* 5:3. _eprint: https://onlinelibrary.wiley.com/doi/pdf/10.1002/jame.20038, pp. 572–597. ISSN: 1942-2466. DOI: 10.1002/jame.20038.

Giorgi, F. and L. O. Mearns (2002). "Calculation of Average, Uncertainty Range, and Reliability of Regional Climate Changes from AOGCM Simulations via the "Reliability Ensemble Averaging" (REA) Method". Section: Journal of Climate. ISSN: 1520-0442.

Graham, F. S. and T. J. McDougall (2013). "Quantifying the Nonconservative Production of Conservative Temperature, Potential Temperature, and Entropy". Section: Journal of Physical Oceanography. DOI: 10.1175/JPO-D-11-0188.1.

Gregory, J. M. (2000). "Vertical heat transports in the ocean and their effect on time-dependent climate change". *Climate Dynamics* 16:7, pp. 501–515. ISSN: 0930-7575, 1432-0894. DOI: 10.1007/s003820000059.

Gregory, J. M., T. Andrews, and P. Good (2015). "The inconstancy of the transient climate response parameter under increasing CO2". *Philosophical transactions. Series A, Mathematical, physical, and engineering sciences* 373:2054, p. 20140417. ISSN: 1364-503X. DOI: 10.1098/rsta.2014.0417.

Gregory, J. M. and J. F. B. Mitchell (1997). "The climate response to CO2 of the Hadley Centre coupled AOGCM with and without flux adjustment". *Geophysical Research Letters* 24:15. _eprint: https://onlinelibrary.wiley.com/doi/pdf/10.1029/97GL01930, pp. 1943–1946. ISSN: 1944-8007. DOI: 10.1029/97GL01930.

Gregory, J. M. et al. (2004). "A new method for diagnosing radiative forcing and climate sensitivity". *Geophysical Research Letters* 31:3. _eprint: https://onlinelibrary.wiley.com/doi/pdf/10.1029/2003GL018747. ISSN: 1944-8007. DOI: 10.1029/2003GL018747.

Gregory, J. M. et al. (2019). "Concepts and Terminology for Sea Level: Mean, Variability and Change, Both Local and Global". *Surveys in Geophysics* 40:6, pp. 1251–1289. ISSN: 1573-0956. DOI: 10.1007/s10712-019-09525-z.

Gregory, J. M. et al. (2023). "A new conceptual model of global ocean heat uptake". *Climate Dynamics*. ISSN: 1432-0894. DOI: 10.1007/s00382-023-06989-z.

Griffies, S. M. et al. (2000). "Developments in ocean climate modelling". *Ocean Modelling* 2:3, pp. 123–192. ISSN: 1463-5003. DOI: 10.1016/S1463-5003(00)00014-7.

Griffies, S. M. et al. (2016). "OMIP contribution to CMIP6: experimental and diagnostic protocol for the physical component of the Ocean Model Intercomparison Project". *Geoscientific Model Development* 9:9. Publisher: Copernicus GmbH, pp. 3231–3296. ISSN: 1991-959X. DOI: 10.5194/gmd-9-3231-2016.

Gruber, N., P. W. Boyd, T. L. Frölicher, and M. Vogt (2021). "Biogeochemical extremes and compound events in the ocean". *Nature* 600:7889. Number: 7889 Publisher: Nature Publishing Group, pp. 395–407. ISSN: 1476-4687. DOI: 10.1038/s41586-021-03981-7.

Gruber, N. et al. (2023). "Trends and variability in the ocean carbon sink". *Nature Reviews Earth & Environment*. Publisher: Nature Publishing Group, pp. 1–16. ISSN: 2662-138X. DOI: 10.1038/s43017-022-00381-x.

Gunderson, A. R., E. J. Armstrong, and J. H. Stillman (2016). "Multiple Stressors in a Changing World: The Need for an Improved Perspective on Physiological Responses to the Dynamic Marine Environment". *Annual Review of Marine Science* 8, Volume 8, 2016. Publisher: Annual Reviews, pp. 357–378. ISSN: 1941-1405, 1941-0611. DOI: 10.1146/annurev-marine-122414-033953.

Gutiérrez, J. M. and A.-M. Treguier (2021). "Annex II: Models". In: *Climate Change 2021: The Physical Science Basis. Contribution of Working Group I to the Sixth Assessment Report of the Intergovernmental Panel on Climate Change*. Ed. by V. Masson-Delmotte et al. Cambridge University Press, Cambridge, United Kingdom and New York, NY, USA, pp. 2087–2138. DOI: 10.1017/9781009157896.001.

Haarsma, R. J. et al. (2016). "High Resolution Model Intercomparison Project (HighResMIP v1.0) for CMIP6". *Geoscientific Model Development* 9:11. Publisher: Copernicus GmbH, pp. 4185–4208. ISSN: 1991-959X. DOI: 10.5194/gmd-9-4185-2016.

Hagedorn, R., F. J. Doblas-Reyes, and T. N. Palmer (2005). "The rationale behind the success of multi-model ensembles in seasonal forecasting – I. Basic concept". *Tellus A* 57:3. _eprint: https://onlinelibrary.wiley.com/doi/pdf/10.1111/j.1600-0870.2005.00103.x, pp. 219–233. ISSN: 1600-0870. DOI: 10.1111/j.1600-0870.2005.00103.x.

Hall, A., P. Cox, C. Huntingford, and S. Klein (2019). "Progressing emergent constraints on future climate change". *Nature Climate Change* 9:4. Number: 4 Publisher: Nature Publishing Group, pp. 269–278. ISSN: 1758-6798. DOI: 10.1038/s41558-019-0436-6.

Hall, A. and X. Qu (2006). "Using the current seasonal cycle to constrain snow albedo feedback in future climate change". *Geophysical Research Letters* 33:3. _eprint: https://onlinelibrary.wiley.com/doi/pdf/10.1029/2005GL025127. ISSN: 1944-8007. DOI: 10.1029/2005GL025127.

Hansen, J., M. Sato, and R. Ruedy (1997). "Radiative forcing and climate response". *Journal of Geophysical Research: Atmospheres* 102, D6. _eprint: https://onlinelibrary.wiley.com/doi/pdf/10.1029/96JD03436, pp. 6831–6864. ISSN: 2156-2202. DOI: 10.1029/96JD03436.

Hansen, J. et al. (1985). "Climate Response Times: Dependence on Climate Sensitivity and Ocean Mixing". *Science* 229:4716. Publisher: American Association for the Advancement of Science, pp. 857–859. DOI: 10.1126/science.229.4716.857.

Hansen, J. et al. (2005). "Efficacy of climate forcings". *Journal of Geophysical Research: Atmospheres* 110, D18. _eprint: https://onlinelibrary.wiley.com/doi/pdf/10.1029/2005JD005776. ISSN: 2156-2202. DOI: 10.1029/2005JD005776.

Hargreaves, J. C. and J. D. Annan (2014). "Can we trust climate models?" *WIREs Climate Change* 5:4. _eprint: https://onlinelibrary.wiley.com/doi/pdf/10.1002/wcc.288, pp. 435–440. ISSN: 1757-7799. DOI: 10.1002/wcc.288.

Hargreaves, J. C., J. D. Annan, M. Yoshimori, and A. Abe-Ouchi (2012). "Can the Last Glacial Maximum constrain climate sensitivity?" *Geophysical Research Letters* 39:24. Publisher: John Wiley & Sons, Ltd. ISSN: 0094-8276. DOI: 10.1029/2012GL053872.

Haughton, N., G. Abramowitz, A. Pitman, and S. J. Phipps (2015). "Weighting climate model ensembles for mean and variance estimates". *Climate Dynamics* 45:11, pp. 3169–3181. ISSN: 1432-0894. DOI: 10.1007/s00382-015-2531-3.

Hawkins, E. and R. Sutton (2009). "The Potential to Narrow Uncertainty in Regional Climate Predictions". Section: Bulletin of the American Meteorological Society. DOI: 10.1175/2009BAMS2607.1.

He, J., M. Winton, G. Vecchi, L. Jia, and M. Rugenstein (2017). "Transient Climate Sensitivity Depends on Base Climate Ocean Circulation". *Journal of Climate* 30:4. Publisher: American Meteorological Society Section: Journal of Climate, pp. 1493–1504. ISSN: 0894-8755, 1520-0442. DOI: 10.1175/JCLI-D-16-0581.1.

Held, I. M. et al. (2010). "Probing the Fast and Slow Components of Global Warming by Returning Abruptly to Preindustrial Forcing". Section: Journal of Climate. DOI: 10.1175/2009JCLI3466.1.

Henderson-Sellers, A. (1993). "Continental vegetation as a dynamic component of a global climate model: a preliminary assessment". *Climatic Change* 23:4, pp. 337–377. ISSN: 1573-1480. DOI: 10.1007/BF01091622.

Henson, S. A., B. B. Cael, S. R. Allen, and S. Dutkiewicz (2021). "Future phytoplankton diversity in a changing climate". *Nature Communications* 12:1. Publisher: Nature Publishing Group, p. 5372. ISSN: 2041-1723. DOI: 10.1038/s41467-021-25699-w.

Hepburn, B. and H. Andersen (2021). "Scientific Method". In: *The Stanford Encyclopedia of Philosophy*. Ed. by E. N. Zalta. Summer 2021. Metaphysics Research Lab, Stanford University.

Herger, N. et al. (2018). "Selecting a climate model subset to optimise key ensemble properties". *Earth System Dynamics* 9:1. Publisher: Copernicus GmbH, pp. 135–151. ISSN: 2190-4979. DOI: 10.5194/esd-9-135-2018.

Heymann, M. (2010). "The evolution of climate ideas and knowledge". *WIREs Climate Change* 1:4. _eprint: https://onlinelibrary.wiley.com/doi/pdf/10.1002/wcc.61, pp. 581–597. ISSN: 1757-7799. DOI: 10.1002/wcc.61.

Hibler, W. D. (1979). "A Dynamic Thermodynamic Sea Ice Model". *Journal of Physical Oceanography* 9:4, pp. 815–846. ISSN: 0022-3670, 1520-0485. DOI: 10.1175/1520-0485(1979)009<0815:ADTSIM>2.0.CO;2.

Hoesly, R. M. et al. (2018). "Historical (1750–2014) anthropogenic emissions of reactive gases and aerosols from the Community Emissions Data System (CEDS)". *Geoscientific Model Development* 11:1. Publisher: Copernicus GmbH, pp. 369–408. ISSN: 1991-959X. DOI: 10.5194/gmd-11-369-2018.

Hourdin, F. et al. (2017). "The Art and Science of Climate Model Tuning". Section: Bulletin of the American Meteorological Society. DOI: 10.1175/BAMS-D-15-00135.1.

Hourdin, F. et al. (2023). "Toward machine-assisted tuning avoiding the underestimation of uncertainty in climate change projections". *Science Advances* 9:29. Publisher: American Association for the Advancement of Science, eadf2758. DOI: 10.1126/sciadv.adf2758.

Huber, M. B. and L. Zanna (2017). "Drivers of uncertainty in simulated ocean circulation and heat uptake". *Geophysical Research Letters* 44:3. _eprint: https://onlinelibrary.wiley.com/doi/pdf/10.1002/2016GL pp. 1402–1413. ISSN: 1944-8007. DOI: 10.1002/2016GL071587.

Huertas, I. E., M. Rouco, V. López-Rodas, and E. Costas (2011). "Warming will affect phytoplankton differently: evidence through a mechanistic approach". *Proceedings of the Royal Society B: Biological Sciences* 278:1724. Publisher: Royal Society, pp. 3534–3543. DOI: 10.1098/rspb.2011.0160.

Hughes, T. P. et al. (2017). "Global warming and recurrent mass bleaching of corals". *Nature* 543:7645. Number: 7645 Publisher: Nature Publishing Group, pp. 373–377. ISSN: 1476-4687. DOI: 10.1038/nature21707.

Hughes, T. P. et al. (2018). "Spatial and temporal patterns of mass bleaching of corals in the Anthropocene". *Science* 359:6371. Publisher: American Association for the Advancement of Science Section: Report, pp. 80–83. ISSN: 0036-8075, 1095-9203. DOI: 10.1126/science.aan8048.

Huntingford, C., P. M. Cox, M. S. Williamson, J. J. Clarke, and P. D. L. Ritchie (2023). "Emergent constraints for the climate system as effective parameters of bulk differential equations". *Earth System Dynamics* 14:2. Publisher: Copernicus GmbH, pp. 433–442. ISSN: 2190-4979. DOI: 10.5194/esd-14-433-2023.

Irwin, A. J., Z. V. Finkel, F. E. Müller-Karger, and L. Troccoli Ghinaglia (2015). "Phytoplankton adapt to changing ocean environments". *Proceedings of the National Academy of Sciences* 112:18. Publisher: Proceedings of the National Academy of Sciences, pp. 5762–5766. DOI: 10.1073/pnas.1414752112.

Jacox, M. G., M. A. Alexander, S. J. Bograd, and J. D. Scott (2020). "Thermal displacement by marine heatwaves". *Nature* 584:7819. Number: 7819 Publisher: Nature Publishing Group, pp. 82–86. ISSN: 1476-4687. DOI: 10.1038/s41586-020-2534-z.

Jakob, C. (2014). "Going back to basics". *Nature Climate Change* 4:12. Publisher: Nature Publishing Group, pp. 1042–1045. ISSN: 1758-6798. DOI: 10.1038/nclimate2445.

Jebeile, J. (2017). "Computer Simulation, Experiment, and Novelty". *International Studies in the Philosophy of Science* 31:4. Publisher: Routledge _eprint: https://doi.org/10.1080/02698595.2019.1565205, pp. 379–395. ISSN: 0269-8595. DOI: 10.1080/02698595.2019.1565205.

Jebeile, J. and A. Barberousse (2021). "Model spread and progress in climate modelling". *European Journal for Philosophy of Science* 11:3, p. 66. ISSN: 1879-4920. DOI: 10.1007/s13194-021-00387-0.

Jones, A., D. L. Roberts, and A. Slingo (1994). "A climate model study of indirect radiative forcing by anthropogenic sulphate aerosols". *Nature* 370:6489. Publisher: Nature Publishing Group, pp. 450–453. ISSN: 1476-4687. DOI: 10.1038/370450a0.

Jones, C. D. et al. (2016). "C4MIP – The Coupled Climate–Carbon Cycle Model Intercomparison Project:experimental protocol for CMIP6". *Geoscientific Model Development* 9:8, pp. 2853–2880. ISSN: 1991-9603. DOI: 10.5194/gmd-9-2853-2016.

Jorda, G. et al. (2020). "Ocean warming compresses the three-dimensional habitat of marine life". *Nature Ecology & Evolution* 4:1. Publisher: Nature Publishing Group, pp. 109–114. ISSN: 2397-334X. DOI: 10.1038/s41559-019-1058-0.

Jun, M., R. Knutti, and D. W. Nychka (2008). "Spatial Analysis to Quantify Numerical Model Bias and Dependence: How Many Climate Models Are There?" *Journal of the American Statistical Association* 103:483. Publisher: ASA Website _eprint: https://doi.org/10.1198/016214507000001265, pp. 934–947. ISSN: 0162-1459. DOI: 10.1198/016214507000001265.

Kageyama, M. et al. (2018). "The PMIP4 contribution to CMIP6 – Part 1: Overview and overarching analysis plan". *Geoscientific Model Development* 11:3. Publisher: Copernicus GmbH, pp. 1033–1057. ISSN: 1991-959X. DOI: 10.5194/gmd-11-1033-2018.

Kawai, H., K. Yoshida, T. Koshiro, and S. Yukimoto (2022). "Importance of Minor-Looking Treatments in Global Climate Models". *Journal of Advances in Modeling Earth Systems* 14:10. _eprint: https://agupubs.onlinelibrary.wiley.com/doi/pdf/10.1029/2022MS003128, e2022MS003128. ISSN: 1942-2466. DOI: 10.1029/2022MS003128.

Keeling, R. F., A. Körtzinger, and N. Gruber (2010). "Ocean Deoxygenation in a Warming World". *Annual Review of Marine Science* 2:1. _eprint: https://doi.org/10.1146/annurev.marine.010908.163855, pp. 199–229. DOI: 10.1146/annurev.marine.010908.163855.

Keil, P. et al. (2020). "Multiple drivers of the North Atlantic warming hole". *Nature Climate Change* 10:7. Number: 7 Publisher: Nature Publishing Group, pp. 667–671. ISSN: 1758-6798. DOI: 10.1038/s41558-020-0819-8.

Kirtman, B. et al. (2013). "Near-term climate change: Projections and predictability". In: *Climate change 2013: The physical science basis. Contribution of working group I to the fifth assessment report of the intergovernmental panel on climate change*. Ed. by T. Stocker et al. Section: 11 Type: Book Section. Cambridge University Press, Cambridge, United Kingdom and New York, NY,

USA, pp. 953–1028. ISBN: ISBN 978-1-107-66182-0. DOI: 10.1017/CBO9781107415324.023.

Klein, S. A. and A. Hall (2015). "Emergent Constraints for Cloud Feedbacks". *Current Climate Change Reports* 1:4, pp. 276–287. ISSN: 2198-6061. DOI: 10.1007/s40641-015-0027-1.

Knutti, R. (2010). "The end of model democracy?" *Climatic Change* 102:3, pp. 395–404. ISSN: 1573-1480. DOI: 10.1007/s10584-010-9800-2.

Knutti, R., R. Furrer, C. Tebaldi, J. Cermak, and G. A. Meehl (2010). "Challenges in Combining Projections from Multiple Climate Models". *Journal of Climate* 23:10, pp. 2739–2758. ISSN: 1520-0442, 0894-8755. DOI: 10.1175/2009JCLI3361.1.

Knutti, R. and G. C. Hegerl (2008). "The equilibrium sensitivity of the Earth's temperature to radiation changes". *Nature Geoscience* 1:11, pp. 735–743. ISSN: 1752-0894, 1752-0908. DOI: 10.1038/ngeo337.

Knutti, R., D. Masson, and A. Gettelman (2013). "Climate model genealogy: Generation CMIP5 and how we got there". *Geophysical Research Letters* 40:6. _eprint: https://agupubs.onlinelibrary.wiley.com/doi/pdf/10.1002/grl.50256, pp. 1194–1199. ISSN: 1944-8007. DOI: 10.1002/grl.50256.

Knutti, R. and M. A. A. Rugenstein (2015). "Feedbacks, climate sensitivity and the limits of linear models". *Philosophical Transactions of the Royal Society A: Mathematical, Physical and Engineering Sciences* 373:2054. Publisher: Royal Society, p. 20150146. DOI: 10.1098/rsta.2015.0146.

Knutti, R., M. A. A. Rugenstein, and G. C. Hegerl (2017a). "Beyond equilibrium climate sensitivity". *Nature Geoscience* 10:10. Publisher: Nature Publishing Group, pp. 727–736. ISSN: 1752-0908. DOI: 10.1038/ngeo3017.

Knutti, R. and L. Tomassini (2008). "Constraints on the transient climate response from observed global temperature and ocean heat uptake". *Geophysical Research Letters* 35:9. _eprint: https://onlinelibrary.wiley.com/doi/pdf/10.1029/2007GL032904. ISSN: 1944-8007. DOI: 10.1029/2007GL032904.

Knutti, R. et al. (2017b). "A climate model projection weighting scheme accounting for performance and interdependence". *Geophysical Research Letters* 44:4. _eprint: https://onlinelibrary.wiley.com/doi/pdf/10.1002/2016GL072012, pp. 1909–1918. ISSN: 1944-8007. DOI: 10.1002/2016GL072012.

Kochtitzky, W. and L. Copland (2022). "Retreat of Northern Hemisphere Marine-Terminating Glaciers, 2000–2020". *Geophysical Research Letters* 49:3. _eprint: https://onlinelibrary.wiley.com/doi/pdf/10.1029/2021GL096501, e2021GL096501. ISSN: 1944-8007. DOI: 10.1029/2021GL096501.

Kostov, Y., K. C. Armour, and J. Marshall (2014). "Impact of the Atlantic meridional overturning circulation on ocean heat storage and transient climate change". *Geophysical Research Letters* 41:6. _eprint: https://onlinelibrary.wiley.com/doi/pdf/10.1002/2013GL058998, pp. 2108–2116. ISSN: 1944-8007. DOI: 10.1002/2013GL058998.

Krishnamurti, T. N. et al. (2000). "Multimodel Ensemble Forecasts for Weather and Seasonal Climate". Section: Journal of Climate. ISSN: 1520-0442.

Kubo, R. (1966). "The fluctuation-dissipation theorem". *Reports on Progress in Physics* 29:1, p. 255. ISSN: 0034-4885. DOI: 10.1088/0034-4885/29/1/306.

Kuhlbrodt, T. and J. M. Gregory (2012). "Ocean heat uptake and its consequences for the magnitude of sea level rise and climate change". *Geophysical Research Letters* 39:18. _eprint: https://onlinelibrary.wiley.com/doi/pdf/10.1029/2012GL052952. ISSN: 1944-8007. DOI: 10.1029/2012GL052952.

Kwiatkowski, L. et al. (2020). "Twenty-first century ocean warming, acidification, deoxygenation, and upper-ocean nutrient and primary production decline from CMIP6 model projections". *Biogeosciences* 17:13. Publisher: Copernicus GmbH, pp. 3439–3470. ISSN: 1726-4170. DOI: 10.5194/bg-17-3439-2020.

Large, W. G., J. C. McWilliams, and S. C. Doney (1994). "Oceanic vertical mixing: A review and a model with a nonlocal boundary layer parameterization". *Reviews of Geophysics* 32:4. _eprint: https://onlinelibrary.wiley.com/doi/pdf/10.1029/94RG01872, pp. 363–403. ISSN: 1944-9208. DOI: 10.1029/94RG01872.

Le Grix, N., J. Zscheischler, C. Laufkötter, C. S. Rousseaux, and T. L. Frölicher (2021). "Compound high-temperature and low-chlorophyll extremes in the ocean over the satellite period". *Biogeosciences* 18:6. Publisher: Copernicus GmbH, pp. 2119–2137. ISSN: 1726-4170. DOI: 10.5194/bg-18-2119-2021.

Le Grix, N., J. Zscheischler, K. B. Rodgers, R. Yamaguchi, and T. L. Frölicher (2022). "Hotspots and drivers of compound marine heatwaves and low net primary production extremes". *Biogeosciences* 19:24. Publisher: Copernicus GmbH, pp. 5807–5835. ISSN: 1726-4170. DOI: 10.5194/bg-19-5807-2022.

Leith, C. E. (1975). "Climate Response and Fluctuation Dissipation". Section: Journal of the Atmospheric Sciences. ISSN: 1520-0469.

Lewandowska, A. M. et al. (2014). "Effects of sea surface warming on marine plankton". *Ecology Letters* 17:5. _eprint: https://onlinelibrary.wiley.com/doi/pdf/10.1111/ele.12265, pp. 614–623. ISSN: 1461-0248. DOI: 10.1111/ele.12265.

Li, C. et al. (2024). "The ocean losing its breath under the heatwaves". *Nature Communications* 15:1. Publisher: Nature Publishing Group, p. 6840. ISSN: 2041-1723. DOI: 10.1038/s41467-024-51323-8.

Li, G. et al. (2020). "Increasing ocean stratification over the past half-century". *Nature Climate Change* 10:12. Number: 12 Publisher: Nature Publishing Group, pp. 1116–1123. ISSN: 1758-6798. DOI: 10.1038/s41558-020-00918-2.

Li, Z., M. H. England, and S. Groeskamp (2023). "Recent acceleration in global ocean heat accumulation by mode and intermediate waters". *Nature Communications* 14:1. Number: 1 Publisher: Nature Publishing Group, p. 6888. ISSN: 2041-1723. DOI: 10.1038/s41467-023-42468-z.

Lin, Y.-J., B. E. J. Rose, and Y.-T. Hwang (2023). "Mean state AMOC affects AMOC weakening through subsurface warming in the Labrador Sea". *Journal of Climate* -1, aop. Publisher: American Meteorological Society Section: Journal of Climate, pp. 1–44. ISSN: 0894-8755, 1520-0442. DOI: 10.1175/JCLI-D-22-0464.1.

Lindsay, K. et al. (2014). "Preindustrial-Control and Twentieth-Century Carbon Cycle Experiments with the Earth System Model CESM1(BGC)". Section: Journal of Climate. DOI: 10.1175/JCLI-D-12-00565.1.

Liu, M., B. J. Soden, G. A. Vecchi, and C. Wang (2023). "The Spread of Ocean Heat Uptake Efficiency Traced to Ocean Salinity". *Geophysical Research Letters* 50:4. _eprint: https://onlinelibrary.wiley.com/doi/pdf/10.1029/2022GL100171, e2022GL100171. ISSN: 1944-8007. DOI: 10.1029/2022GL100171.

Lorenz, E. N. (1963). "Deterministic Nonperiodic Flow". Section: Journal of the Atmospheric Sciences. ISSN: 1520-0469.

– (1965). "A study of the predictability of a 28-variable atmospheric model". *Tellus* 17:3. _eprint: https://onlinelibrary.wiley.com/doi/pdf/10.1111/j.2153-3490.1965.tb01424.x, pp. 321–333. ISSN: 2153-3490. DOI: 10.1111/j.2153-3490.1965.tb01424.x.

– (1969). "The predictability of a flow which possesses many scales of motion". *Tellus* 21:3. _eprint: https://onlinelibrary.wiley.com/doi/pdf/10.1111/j.2153-3490.1969.tb00444.x, pp. 289–307. ISSN: 2153-3490. DOI: 10.1111/j.2153-3490.1969.tb00444.x.

Lyu, K., X. Zhang, and J. A. Church (2021). "Projected ocean warming constrained by the ocean observational record". *Nature Climate Change* 11:10. Number: 10 Publisher: Nature Publishing Group, pp. 834–839. ISSN: 1758-6798. DOI: 10.1038/s41558-021-01151-1.

Ma, L. et al. (2020). "Global rules for translating land-use change (LUH2) to land-cover change for CMIP6 using GLM2". *Geoscientific Model Development* 13:7. Publisher: Copernicus GmbH, pp. 3203–3220. ISSN: 1991-959X. DOI: 10.5194/gmd-13-3203-2020.

MacDougall, A. H. and R. Knutti (2016). "Projecting the release of carbon from permafrost soils using a perturbed parameter ensemble modelling approach". *Biogeosciences* 13:7. Publisher: Copernicus GmbH, pp. 2123–2136. ISSN: 1726-4170. DOI: 10.5194/bg-13-2123-2016.

Maher, N., S. Milinski, and R. Ludwig (2021). "Large ensemble climate model simulations: introduction, overview, and future prospects for utilising multiple types of large ensemble". *Earth System Dynamics* 12:2. Publisher: Copernicus GmbH, pp. 401–418. ISSN: 2190-4979. DOI: 10.5194/esd-12-401-2021.

Manabe, S., R. J. Stouffer, M. J. Spelman, and K. Bryan (1991). "Transient Responses of a Coupled Ocean–Atmosphere Model to Gradual Changes of Atmospheric CO2. Part I. Annual Mean Response". Section: Journal of Climate. ISSN: 1520-0442.

Manabe, S. and K. Bryan (1969). "Climate Calculations with a Combined Ocean-Atmosphere Model". Section: Journal of the Atmospheric Sciences. ISSN: 1520-0469.

Manabe, S., K. Bryan, and M. J. Spelman (1975). "A Global Ocean-Atmosphere Climate Model. Part I. The Atmospheric Circulation". Section: Journal of Physical Oceanography. ISSN: 1520-0485.

Marshall, J. and R. A. Plumb (2008). *Atmosphere, ocean, and climate dynamics: an introductory text*. International geophysics series 93. Elsevier AP, Amsterdam Heidelberg. 319 pp. ISBN: 978-0-12-558691-7.

Marshall, J. and K. Speer (2012). "Closure of the meridional overturning circulation through Southern Ocean upwelling". *Nature Geoscience* 5:3. Bandiera_abtest: a Cg_type: Nature Research Journals Number: 3 Primary_atype: Reviews Publisher: Nature Publishing Group Subject_term: Physical oceanography Subject_term_id: physical-oceanography, pp. 171–180. ISSN: 1752-0908. DOI: 10.1038/ngeo1391.

Marshall, J. et al. (2015). "The ocean's role in the transient response of climate to abrupt greenhouse gas forcing". *Climate Dynamics* 44:7, pp. 2287–2299. ISSN: 1432-0894. DOI: 10.1007/s00382-014-2308-0.

Marvel, K., R. Pincus, G. A. Schmidt, and R. L. Miller (2018). "Internal Variability and Disequilibrium Confound Estimates of Climate Sensitivity From Observations". *Geophysical Research Letters* 45:3. _eprint: https://agupubs.onlinelibrary.wiley.com/doi/pdf/10.1002/2017GL076468, pp. 1595–1601. ISSN: 1944-8007. DOI: 10.1002/2017GL076468.

Maslin, M. and P. Austin (2012). "Climate models at their limit?" *Nature* 486:7402, pp. 183–184. ISSN: 0028-0836, 1476-4687. DOI: 10.1038/486183a.

Masson, D. and R. Knutti (2011). "Climate model genealogy". *Geophysical Research Letters* 38:8. _eprint: https://onlinelibrary.wiley.com/doi/pdf/10.1029/2011GL046864. ISSN: 1944-8007. DOI: 10.1029/2011GL046864.

Masson-Delmotte, V. et al., eds. (2021a). *Climate Change 2021: The Physical Science Basis. Contribution of Working Group I to the Sixth Assessment Report of the Intergovernmental Panel on Climate Change*. Cambridge University Press, Cambridge, United Kingdom and New York, NY, USA. DOI: 10.1017/9781009157896.

"Summary for policymakers" (2021b). In: *Climate Change 2021: The Physical Science Basis. Contribution of Working Group I to the Sixth Assessment Report of the Intergovernmental Panel on Climate Change*. Ed. by V. Masson-Delmotte et al. Cambridge University Press, Cambridge, United Kingdom and New York, NY, USA, pp. 3–32. DOI: 10.1017/9781009157896.001.

Matthes, K. et al. (2017). "Solar forcing for CMIP6 (v3.2)". *Geoscientific Model Development* 10:6. Publisher: Copernicus GmbH, pp. 2247–2302. ISSN: 1991-959X. DOI: 10.5194/gmd-10-2247-2017.

McDougall, T. J. (1987). "Thermobaricity, cabbeling, and water-mass conversion". *Journal of Geophysical Research: Oceans* 92, C5. _eprint: https://onlinelibrary.wiley.com/doi/pdf/10.1029/JC092iC05p05448, pp. 5448–5464. ISSN: 2156-2202. DOI: 10.1029/JC092iC05p05448.

– (2003). "Potential Enthalpy: A Conservative Oceanic Variable for Evaluating Heat Content and Heat Fluxes". Section: Journal of Physical Oceanography. ISSN: 1520-0485.

McDougall, T. J. and P. M. Barker (2011). *Getting started with TEOS-10 and the Gibbs Seawater (GSW) Oceanographic Toolbox*. SCOR/IAPSO WG127. 28 pp. ISBN: 978-0-646-55621-5.

McDougall, T. J. et al. (2021). "The interpretation of temperature and salinity variables in numerical ocean model output and the calculation of heat fluxes and heat content". *Geoscientific Model Development* 14:10. Publisher: Copernicus GmbH, pp. 6445–6466. ISSN: 1991-959X. DOI: 10.5194/gmd-14-6445-2021.

McNeall, D. et al. (2016). "The impact of structural error on parameter constraint in a climate model". *Earth System Dynamics* 7:4. Publisher: Copernicus GmbH, pp. 917–935. ISSN: 2190-4979. DOI: 10.5194/esd-7-917-2016.

Meehl, G. A. (2023). "The Role of the IPCC in Climate Science". In: *Oxford Research Encyclopedia of Climate Science*. ISBN: 978-0-19-022862-0. DOI: 10.1093/acrefore/9780190228620.013.933.

Meehl, G. A., J. M. Arblaster, J. T. Fasullo, A. Hu, and K. E. Trenberth (2011). "Model-based evidence of deep-ocean heat uptake during surface-temperature hiatus periods". *Nature Climate Change* 1:7. Publisher: Nature Publishing Group, pp. 360–364. ISSN: 1758-6798. DOI: 10.1038/nclimate1229.

Meehl, G. A., G. J. Boer, C. Covey, M. Latif, and R. J. Stouffer (1997). "Intercomparison makes for a better climate model". *Eos, Transactions American Geophysical Union* 78:41. _eprint: https://onlinelibrary.wiley.com/doi/pdf/10.1029/97EO00276, pp. 445–451. ISSN: 2324-9250. DOI: 10.1029/97EO00276.

– (2000). "The Coupled Model Intercomparison Project (CMIP)". *Bulletin of the American Meteorological Society* 81:2. Publisher: American Meteorological Society, pp. 313–318. ISSN: 0003-0007.

Meehl, G. A. et al. (2007). "THE WCRP CMIP3 Multimodel Dataset: A New Era in Climate Change Research". Section: Bulletin of the American Meteorological Society. DOI: 10.1175/BAMS-88-9-1383.

Meehl, G. A. et al. (2014). "Climate Model Intercomparisons: Preparing for the Next Phase". *Eos, Transactions American Geophysical Union* 95:9. _eprint: https://onlinelibrary.wiley.com/doi/pdf/10.1002/2014EO090001, pp. 77–78. ISSN: 2324-9250. DOI: 10.1002/2014EO090001.

Meehl, G. A. et al. (2020). "Context for interpreting equilibrium climate sensitivity and transient climate response from the CMIP6 Earth system models". *Science Advances* 6:26. Publisher: American Association for the Advancement of Science, eaba1981. DOI: 10.1126/sciadv.aba1981.

Meinshausen, M. et al. (2017). "Historical greenhouse gas concentrations for climate modelling (CMIP6)". *Geoscientific Model Development* 10:5. Publisher: Copernicus GmbH, pp. 2057–2116. ISSN: 1991-959X. DOI: 10.5194/gmd-10-2057-2017.

Meinshausen, M. et al. (2020). "The shared socio-economic pathway (SSP) greenhouse gas concentrations and their extensions to 2500". *Geoscientific Model Development* 13:8. Publisher: Copernicus GmbH, pp. 3571–3605. ISSN: 1991-959X. DOI: 10.5194/gmd-13-3571-2020.

Meyssignac, B. et al. (2019). "Measuring Global Ocean Heat Content to Estimate the Earth Energy Imbalance". *Frontiers in Marine Science* 6. Publisher: Frontiers. ISSN: 2296-7745. DOI: 10.3389/fmars.2019.00432.

Minière, A., K. von Schuckmann, J.-B. Sallée, and L. Vogt (2023). "Robust acceleration of Earth system heating observed over the past six decades". *Scientific Reports* 13:1. Publisher: Nature Publishing Group, p. 22975. ISSN: 2045-2322. DOI: 10.1038/s41598-023-49353-1.

Müller, J. D. et al. (2023). "Decadal Trends in the Oceanic Storage of Anthropogenic Carbon From 1994 to 2014". *AGU Advances* 4:4. _eprint: https://agupubs.onlinelibrary.wiley.com/doi/pdf/10.1029/2023AV000875, e2023AV000875. ISSN: 2576-604X. DOI: 10.1029/2023AV000875.

Munk, W. H. (1950). "ON THE WIND-DRIVEN OCEAN CIRCULATION". Section: Journal of the Atmospheric Sciences. ISSN: 1520-0469.

Murphy, J. M. (1995). "Transient Response of the Hadley Centre Coupled Ocean-Atmosphere Model to Increasing Carbon Dioxide. Part III: Analysis of Global-Mean Response Using Simple Models". Section: Journal of Climate. ISSN: 1520-0442.

Murphy, J. et al. (2007). "A methodology for probabilistic predictions of regional climate change from perturbed physics ensembles". *Philosophical Transactions of the Royal Society A: Mathematical, Physical and Engineering Sciences* 365:1857. Publisher: Royal Society, pp. 1993–2028. DOI: 10.1098/rsta.2007.2077.

Myers, T. A. et al. (2021). "Observational constraints on low cloud feedback reduce uncertainty of climate sensitivity". *Nature Climate Change* 11:6. Number: 6 Publisher: Nature Publishing Group, pp. 501–507. ISSN: 1758-6798. DOI: 10.1038/s41558-021-01039-0.

National Research Council (1979). *Carbon Dioxide and Climate: A Scientific Assessment*. The National Academies Press, Washington, DC. DOI: 10.17226/12181.

Newsom, E., L. Zanna, and J. Gregory (2023). "Background Pycnocline Depth Constrains Future Ocean Heat Uptake Efficiency". *Geophysical Research Letters* 50:22. _eprint: https://onlinelibrary.wiley.com/doi/pdf/10.1029/2023GL105673, e2023GL105673. ISSN: 1944-8007. DOI: 10.1029/2023GL105673.

Newsom, E., L. Zanna, S. Khatiwala, and J. M. Gregory (2020). "The Influence of Warming Patterns on Passive Ocean Heat Uptake". *Geophysical Research Letters* 47:18. _eprint: https://onlinelibrary.wiley.com/doi/pdf/10.1029/2020GL088429, e2020GL088429. ISSN: 1944-8007. DOI: 10.1029/2020GL088429.

Nguyen, H. M., P. J. Ralph, L. Marín-Guirao, M. Pernice, and G. Procaccini (2021). "Seagrasses in an era of ocean warming: a review". *Biological Reviews* 96:5. _eprint: https://onlinelibrary.wiley.com/doi/pdf/10.1111/brv.12736, pp. 2009–2030. ISSN: 1469-185X. DOI: 10.1111/brv.12736.

North, G. R. (1975). "Theory of Energy-Balance Climate Models". Section: Journal of the Atmospheric Sciences. ISSN: 1520-0469.

North, G. R., R. F. Cahalan, and J. A. Coakley Jr. (1981). "Energy balance climate models". *Reviews of Geophysics* 19:1. _eprint: https://onlinelibrary.wiley.com/doi/pdf/10.1029/RG019i001p00091, pp. 91–121. ISSN: 1944-9208. DOI: 10.1029/RG019i001p00091.

O'Neill, B. C. et al. (2016). "The Scenario Model Intercomparison Project (ScenarioMIP) for CMIP6". *Geoscientific Model Development* 9:9. Publisher: Copernicus GmbH, pp. 3461–3482. ISSN: 1991-959X. DOI: 10.5194/gmd-9-3461-2016.

Oliver, E. C. J. (2019). "Mean warming not variability drives marine heatwave trends". *Climate Dynamics* 53:3, pp. 1653–1659. ISSN: 1432-0894. DOI: 10.1007/s00382-019-04707-2.

Oliver, E. C. J. et al. (2018). "Longer and more frequent marine heatwaves over the past century". *Nature Communications* 9:1. Number: 1 Publisher: Nature Publishing Group, p. 1324. ISSN: 2041-1723. DOI: 10.1038/s41467-018-03732-9.

Oliver, E. C. J. et al. (2021). "Marine Heatwaves". *Annual Review of Marine Science* 13:1. _eprint: https://doi.org/10.1146/annurev-marine-032720-095144, pp. 313–342. DOI: 10.1146/annurev-marine-032720-095144.

Olmedo, E. et al. (2022). "Increasing stratification as observed by satellite sea surface salinity measurements". *Scientific Reports* 12:1. Number: 1 Publisher: Nature Publishing Group, p. 6279. ISSN: 2045-2322. DOI: 10.1038/s41598-022-10265-1.

Oreskes, N., K. Shrader-Frechette, and K. Belitz (1994). "Verification, Validation, and Confirmation of Numerical Models in the Earth Sciences". *Science* 263:5147. Publisher: American Association for the Advancement of Science, pp. 641–646. DOI: 10.1126/science.263.5147.641.

Orr, J. C. et al. (2017). "Biogeochemical protocols and diagnostics for the CMIP6 Ocean Model Intercomparison Project (OMIP)". *Geoscientific Model Development* 10:6. Publisher: Copernicus GmbH, pp. 2169–2199. ISSN: 1991-959X. DOI: 10.5194/gmd-10-2169-2017.

Palmer, M. D. and D. J. McNeall (2014). "Internal variability of Earth's energy budget simulated by CMIP5 climate models". *Environmental Research Letters* 9:3. Publisher: IOP Publishing, p. 034016. ISSN: 1748-9326. DOI: 10.1088/1748-9326/9/3/034016.

Palmer, T. (2024). "The real butterfly effect and maggoty apples". *Physics Today* 77:5, pp. 30–35. ISSN: 0031-9228. DOI: 10.1063/pt.eike.hsbz.

Parker, W. S. (2010). "Whose Probabilities? Predicting Climate Change with Ensembles of Models". *Philosophy of Science* 77:5, pp. 985–997. ISSN: 0031-8248, 1539-767X. DOI: 10.1086/656815.

– (2013). "Ensemble modeling, uncertainty and robust predictions". *WIREs Climate Change* 4:3, pp. 213–223. ISSN: 1757-7780, 1757-7799. DOI: 10.1002/wcc.220.

Pearce, R. (2018). *Timeline: The history of climate modelling*. Carbon Brief. URL: https://www.carbonbrief.org/timeline-history-climate-modelling/ (visited on 08/16/2024).

Peng, Q. et al. (2022). "Surface warming–induced global acceleration of upper ocean currents". *Science Advances* 8:16. Publisher: American Association for the Advancement of Science, eabj8394. DOI: 10.1126/sciadv.abj8394.

Pennell, C. and T. Reichler (2011). "On the Effective Number of Climate Models". Section: Journal of Climate. DOI: 10.1175/2010JCLI3814.1.

Phillips, N. A. (1956). "The general circulation of the atmosphere: A numerical experiment". *Quarterly Journal of the Royal Meteorological Society* 82:352. _eprint: https://onlinelibrary.wiley.com/doi/pdf/10.1002/qj.49708235202, pp. 123–164. ISSN: 1477-870X. DOI: 10.1002/qj.49708235202.

Piani, C., D. J. Frame, D. A. Stainforth, and M. R. Allen (2005). "Constraints on climate change from a multi-thousand member ensemble of simulations". *Geophysical Research Letters* 32:23. _eprint: https://onlinelibrary.wiley.com/doi/pdf/10.1029/2005GL024452. ISSN: 1944-8007. DOI: 10.1029/2005GL024452.

Pritchard, H. D. et al. (2012). "Antarctic ice-sheet loss driven by basal melting of ice shelves". *Nature* 484:7395. Publisher: Nature Publishing Group, pp. 502–505. ISSN: 1476-4687. DOI: 10.1038/nature10968.

Purkey, S. G. and G. C. Johnson (2010). "Warming of Global Abyssal and Deep Southern Ocean Waters between the 1990s and 2000s: Contributions to Global Heat and Sea Level Rise Budgets*". *Journal of Climate* 23:23, pp. 6336–6351. ISSN: 1520-0442, 0894-8755. DOI: 10.1175/2010JCLI3682.1.

Qu, X. and A. Hall (2014). "On the persistent spread in snow-albedo feedback". *Climate Dynamics* 42:1, pp. 69–81. ISSN: 1432-0894. DOI: 10.1007/s00382-013-1774-0.

Raper, S. C. B., J. M. Gregory, and R. J. Stouffer (2002). "The Role of Climate Sensitivity and Ocean Heat Uptake on AOGCM Transient Temperature Response". *Journal of Climate* 15:1. Publisher: American Meteorological Society Section: Journal of Climate, pp. 124–130. ISSN: 0894-8755, 1520-0442. DOI: 10.1175/1520-0442(2002)015<0124:TROCSA>2.0.CO;2.

Rauser, F., P. Gleckler, and J. Marotzke (2015). "Rethinking the Default Construction of Multimodel Climate Ensembles". Section: Bulletin of the American Meteorological Society. DOI: 10.1175/BAMS-D-13-00181.1.

Redi, M. H. (1982). "Oceanic Isopycnal Mixing by Coordinate Rotation". Section: Journal of Physical Oceanography. ISSN: 1520-0485.

Reimann, L., A. T. Vafeidis, and L. E. Honsel (2023). "Population development as a driver of coastal risk: Current trends and future pathways". *Cambridge Prisms: Coastal Futures* 1, e14. ISSN: 2754-7205. DOI: 10.1017/cft.2023.3.

Renoult, M. et al. (2020). "A Bayesian framework for emergent constraints: case studies of climate sensitivity with PMIP". *Climate of the Past* 16:5. Publisher: Copernicus GmbH, pp. 1715–1735. ISSN: 1814-9324. DOI: 10.5194/cp-16-1715-2020.

Riahi, K. et al. (2017). "The Shared Socioeconomic Pathways and their energy, land use, and greenhouse gas emissions implications: An overview". *Global Environmental Change* 42, pp. 153–168. ISSN: 0959-3780. DOI: 10.1016/j.gloenvcha.2016.05.009.

Richardson, L. F. (1922). *Weather prediction by numerical process*. In collab. with University of California Libraries. Cambridge, The University press. 262 pp.

Roe, G. (2009). "Feedbacks, Timescales, and Seeing Red". *Annual Review of Earth and Planetary Sciences* 37, Volume 37, 2009. Publisher: Annual Reviews, pp. 93–115. ISSN: 0084-6597, 1545-4495. DOI: 10.1146/annurev.earth.061008.134734.

Romanou, A., J. Marshall, M. Kelley, and J. Scott (2017). "Role of the ocean's AMOC in setting the uptake efficiency of transient tracers". *Geophysical Research Letters* 44:11. _eprint: https://onlinelibrary.wiley.com/doi/pdf/10.1002/2017GL072972, pp. 5590–5598. ISSN: 1944-8007. DOI: 10.1002/2017GL072972.

Rose, B. E. J., K. C. Armour, D. S. Battisti, N. Feldl, and D. D. B. Koll (2014). "The dependence of transient climate sensitivity and radiative feedbacks on the spatial pattern of ocean heat uptake".

Geophysical Research Letters 41:3. _eprint: https://onlinelibrary.wiley.com/doi/pdf/10.1002/2013GL058955, pp. 1071–1078. ISSN: 1944-8007. DOI: 10.1002/2013GL058955.

Rose, B. E. J. and L. Rayborn (2016). "The Effects of Ocean Heat Uptake on Transient Climate Sensitivity". *Current Climate Change Reports* 2:4, pp. 190–201. ISSN: 2198-6061. DOI: 10.1007/s40641-016-0048-4.

Ruane, A. C. and S. P. McDermid (2017). "Selection of a representative subset of global climate models that captures the profile of regional changes for integrated climate impacts assessment". *Earth Perspectives* 4:1, p. 1. ISSN: 2194-6434. DOI: 10.1186/s40322-017-0036-4.

Rugenstein, M. et al. (2023). "Connecting the SST Pattern Problem and the Hot Model Problem". *Geophysical Research Letters* 50:22. _eprint: https://onlinelibrary.wiley.com/doi/pdf/10.1029/2023GL105488, e2023GL105488. ISSN: 1944-8007. DOI: 10.1029/2023GL105488.

Rugenstein, M. A. A., M. Winton, R. J. Stouffer, S. M. Griffies, and R. Hallberg (2013). "Northern High-Latitude Heat Budget Decomposition and Transient Warming". Section: Journal of Climate. DOI: 10.1175/JCLI-D-11-00695.1.

Sacks, J., W. J. Welch, T. J. Mitchell, and H. P. Wynn (1989). "Design and Analysis of Computer Experiments". *Statistical Science* 4:4. Publisher: Institute of Mathematical Statistics, pp. 409–423. ISSN: 0883-4237, 2168-8745. DOI: 10.1214/ss/1177012413.

Saenko, O. A., D. Yang, and J. M. Gregory (2018). "Impact of Mesoscale Eddy Transfer on Heat Uptake in an Eddy-Parameterizing Ocean Model". *Journal of Climate*. Section: Journal of Climate. DOI: 10.1175/JCLI-D-18-0186.1.

Sallée, J.-B. (2018). "Southern Ocean Warming". *Oceanography* 31:2. ISSN: 10428275. DOI: 10.5670/oceanog.2018.215.

Sallée, J.-B. et al. (2021). "Summertime increases in upper-ocean stratification and mixed-layer depth". *Nature* 591:7851. Bandiera_abtest: a Cg_type: Nature Research Journals Number: 7851 Primary_atype: Research Publisher: Nature Publishing Group Subject_term: Physical oceanography Subject_term_id: physical-oceanography, pp. 592–598. ISSN: 1476-4687. DOI: 10.1038/s41586-021-03303-x.

Sanderson, B. M. and R. Knutti (2012). "On the interpretation of constrained climate model ensembles". *Geophysical Research Letters* 39:16. _eprint: https://onlinelibrary.wiley.com/doi/pdf/10.1029/2012GL052665. ISSN: 1944-8007. DOI: 10.1029/2012GL052665.

Sanderson, B. M., R. Knutti, and P. Caldwell (2015a). "A Representative Democracy to Reduce Interdependency in a Multimodel Ensemble". *Journal of Climate*. Section: Journal of Climate. DOI: 10.1175/JCLI-D-14-00362.1.

– (2015b). "Addressing Interdependency in a Multimodel Ensemble by Interpolation of Model Properties". Section: Journal of Climate. DOI: 10.1175/JCLI-D-14-00361.1.

Sanderson, B. M., M. Wehner, and R. Knutti (2017). "Skill and independence weighting for multi-model assessments". *Geoscientific Model Development* 10:6. Publisher: Copernicus GmbH, pp. 2379–2395. ISSN: 1991-959X. DOI: 10.5194/gmd-10-2379-2017.

Sanderson, B. M. et al. (2021). "The potential for structural errors in emergent constraints". *Earth System Dynamics* 12:3. Publisher: Copernicus GmbH, pp. 899–918. ISSN: 2190-4979. DOI: 10.5194/esd-12-899-2021.

Santana-Falcón, Y. and R. Séférian (2022). "Climate change impacts the vertical structure of marine ecosystem thermal ranges". *Nature Climate Change* 12:10. Publisher: Nature Publishing Group, pp. 935–942. ISSN: 1758-6798. DOI: 10.1038/s41558-022-01476-5.

Santora, J. A. et al. (2020). "Habitat compression and ecosystem shifts as potential links between marine heatwave and record whale entanglements". *Nature Communications* 11:1. Number: 1 Publisher: Nature Publishing Group, p. 536. ISSN: 2041-1723. DOI: 10.1038/s41467-019-14215-w.

Sarmiento, J. L. et al. (2004). "Response of ocean ecosystems to climate warming". *Global Biogeochemical Cycles* 18:3. _eprint: https://onlinelibrary.wiley.com/doi/pdf/10.1029/2003GB002134. ISSN: 1944-9224. DOI: 10.1029/2003GB002134.

Schlund, M., A. Lauer, P. Gentine, S. C. Sherwood, and V. Eyring (2020). "Emergent constraints on equilibrium climate sensitivity in CMIP5: do they hold for CMIP6?" *Earth System Dynamics* 11:4. Publisher: Copernicus GmbH, pp. 1233–1258. ISSN: 2190-4979. DOI: 10.5194/esd-11-1233-2020.

Schmidtko, S., L. Stramma, and M. Visbeck (2017). "Decline in global oceanic oxygen content during the past five decades". *Nature* 542:7641. Number: 7641 Publisher: Nature Publishing Group, pp. 335–339. ISSN: 1476-4687. DOI: 10.1038/nature21399.

Schmitz, W. (1996). "On the world ocean circulation: Volume I". *Some Global Features/North Atlantic Circulation, Woods Hole Oceanographic Institution Technical Report WHOI-96-03*.

Schuckmann, K. von et al. (2020). "Heat stored in the Earth system: where does the energy go?" *Earth System Science Data* 12:3. Publisher: Copernicus GmbH, pp. 2013–2041. ISSN: 1866-3508. DOI: 10.5194/essd-12-2013-2020.

Sellers, W. D. (1969). "A Global Climatic Model Based on the Energy Balance of the Earth-Atmosphere System". *Journal of Applied Meteorology and Climatology* 8:3. Publisher: American Meteorological Society Section: Journal of Applied Meteorology and Climatology, pp. 392–400. ISSN: 1520-0450. DOI: 10.1175/1520-0450(1969)008<0392:AGCMBO>2.0.CO;2.

Senior, C. A. and J. F. B. Mitchell (2000). "The time-dependence of climate sensitivity". *Geophysical Research Letters* 27:17. _eprint: https://onlinelibrary.wiley.com/doi/pdf/10.1029/2000GL011373, pp. 2685–2688. ISSN: 1944-8007. DOI: 10.1029/2000GL011373.

Sherwood, S. C. et al. (2020). "An Assessment of Earth's Climate Sensitivity Using Multiple Lines of Evidence". *Reviews of Geophysics* 58:4. _eprint: https://onlinelibrary.wiley.com/doi/pdf/10.1029/2019RG000678, e2019RG000678. ISSN: 1944-9208. DOI: 10.1029/2019RG000678.

Sherwood, S. C. et al. (2015). "Adjustments in the Forcing-Feedback Framework for Understanding Climate Change". Section: Bulletin of the American Meteorological Society. DOI: 10.1175/BAMS-D-13-00167.1.

Siegenthaler, U. and H. Oeschger (1984). "Transient Temperature Changes Due to Increasing CO2 Using Simple Models". *Annals of Glaciology* 5, pp. 153–159. ISSN: 0260-3055, 1727-5644. DOI: 10.3189/1984AoG5-1-153-159.

Siler, N., S. Po-Chedley, and C. S. Bretherton (2018). "Variability in modeled cloud feedback tied to differences in the climatological spatial pattern of clouds". *Climate Dynamics* 50:3, pp. 1209–1220. ISSN: 1432-0894. DOI: 10.1007/s00382-017-3673-2.

Silvy, Y., J.-B. Sallée, E. Guilyardi, J. Mignot, and C. Rousset (2022). "What Causes Anthropogenic Ocean Warming to Emerge from Internal Variability in a Coupled Model?" *Journal of Climate* 35:22. Publisher: American Meteorological Society Section: Journal of Climate, pp. 7435–7454. ISSN: 0894-8755, 1520-0442. DOI: 10.1175/JCLI-D-22-0074.1.

Smale, D. A. (2020). "Impacts of ocean warming on kelp forest ecosystems". *New Phytologist* 225:4. _eprint: https://onlinelibrary.wiley.com/doi/pdf/10.1111/nph.16107, pp. 1447–1454. ISSN: 1469-8137. DOI: 10.1111/nph.16107.

Smale, D. A. et al. (2019). "Marine heatwaves threaten global biodiversity and the provision of ecosystem services". *Nature Climate Change* 9:4. Number: 4 Publisher: Nature Publishing Group, pp. 306–312. ISSN: 1758-6798. DOI: 10.1038/s41558-019-0412-1.

Smith, C. J. et al. (2020). "Effective radiative forcing and adjustments in CMIP6 models". *Atmospheric Chemistry and Physics* 20:16. Publisher: Copernicus GmbH, pp. 9591–9618. ISSN: 1680-7316. DOI: 10.5194/acp-20-9591-2020.

Smith, K. E. et al. (2021). "Socioeconomic impacts of marine heatwaves: Global issues and opportunities". *Science* 374:6566. Publisher: American Association for the Advancement of Science, eabj3593. DOI: 10.1126/science.abj3593.

Smith, K. E. et al. (2023). "Biological Impacts of Marine Heatwaves". *Annual Review of Marine Science* 15, Volume 15, 2023. Publisher: Annual Reviews, pp. 119–145. ISSN: 1941-1405, 1941-0611. DOI: 10.1146/annurev-marine-032122-121437.

Sohail, T., D. B. Irving, J. D. Zika, and J. M. Gregory (2023). "Anthropogenic Aerosols Offsetting Ocean Warming Less Efficiently Since the 1980s". *Geophysical Research Letters* 50:23. _eprint: https://onlinelibrary.wiley.com/doi/pdf/10.1029/2023GL105374, e2023GL105374. ISSN: 1944-8007. DOI: 10.1029/2023GL105374.

Sokolov, A. P., C. E. Forest, and P. H. Stone (2003). "Comparing Oceanic Heat Uptake in AOGCM Transient Climate Change Experiments". Section: Journal of Climate. ISSN: 1520-0442.

Stocker, T. F. (2013). "The ocean as a component of the climate system". In: *Ocean circulation and climate: a 21st century perspective*. Vol. 103. Elsevier, pp. 3–30.

Stolpe, M. B., I. Medhaug, U. Beyerle, and R. Knutti (2019). "Weak dependence of future global mean warming on the background climate state". *Climate Dynamics* 53:7, pp. 5079–5099. ISSN: 1432-0894. DOI: 10.1007/s00382-019-04849-3.

Stommel, H. (1948). "The westward intensification of wind-driven ocean currents". *Eos, Transactions American Geophysical Union* 29:2. _eprint: https://onlinelibrary.wiley.com/doi/pdf/10.1029/TR029i002p002 pp. 202–206. ISSN: 2324-9250. DOI: 10.1029/TR029i002p00202.

Storch, H. von (2010). "Climate models and modeling: an editorial essay". *WIREs Climate Change* 1:3. _eprint: https://onlinelibrary.wiley.com/doi/pdf/10.1002/wcc.12, pp. 305–310. ISSN: 1757-7799. DOI: 10.1002/wcc.12.

Stouffer, R. J. et al. (2017). "CMIP5 Scientific Gaps and Recommendations for CMIP6". Section: Bulletin of the American Meteorological Society. DOI: 10.1175/BAMS-D-15-00013.1.

Stouffer, R. J. and S. Manabe (1999). "Response of a Coupled Ocean–Atmosphere Model to Increasing Atmospheric Carbon Dioxide: Sensitivity to the Rate of Increase". Section: Journal of Climate. ISSN: 1520-0442.

Stouffer, R. J., J. Russell, and M. J. Spelman (2006). "Importance of oceanic heat uptake in transient climate change". *Geophysical Research Letters* 33:17. _eprint: https://onlinelibrary.wiley.com/doi/pdf/10.1029/2006GL027242. ISSN: 1944-8007. DOI: 10.1029/2006GL027242.

Tagliabue, A. et al. (2021). "Persistent Uncertainties in Ocean Net Primary Production Climate Change Projections at Regional Scales Raise Challenges for Assessing Impacts on Ecosystem Services". *Frontiers In Climate* 3:738224. Publisher: Frontiers Media SA. ISSN: 2624-9553. DOI: 10.3389/fclim.2021.738224.

Talley, L. D. et al. (2016). "Changes in Ocean Heat, Carbon Content, and Ventilation: A Review of the First Decade of GO-SHIP Global Repeat Hydrography". *Annual Review of Marine Science* 8, Volume 8, 2016. Publisher: Annual Reviews, pp. 185–215. ISSN: 1941-1405, 1941-0611. DOI: 10.1146/annurev-marine-052915-100829.

Talley, L. (2013). "Closure of the Global Overturning Circulation Through the Indian, Pacific, and Southern Oceans: Schematics and Transports". *Oceanography* 26:1, pp. 80–97. ISSN: 10428275. DOI: 10.5670/oceanog.2013.07.

Talley, L. D., G. L. Pickard, W. J. Emery, and J. H. Swift, eds. (2011). *Descriptive physical oceanography: an introduction*. 6. ed. Elsevier, AP, Amsterdam Heidelberg. 555 pp. ISBN: 978-0-7506-4552-2.

Taylor, K. E., R. J. Stouffer, and G. A. Meehl (2012). "An Overview of CMIP5 and the Experiment Design". Section: Bulletin of the American Meteorological Society. DOI: 10.1175/BAMS-D-11-00094.1.

Tebaldi, C. and R. Knutti (2007). "The use of the multi-model ensemble in probabilistic climate projections". *Philosophical Transactions of the Royal Society A: Mathematical, Physical and Engineering Sciences* 365:1857. Publisher: Royal Society, pp. 2053–2075. DOI: 10.1098/rsta.2007.2076.

Terhaar, J., L. Kwiatkowski, and L. Bopp (2020). "Emergent constraint on Arctic Ocean acidification in the twenty-first century". *Nature* 582:7812. Number: 7812 Publisher: Nature Publishing Group, pp. 379–383. ISSN: 1476-4687. DOI: 10.1038/s41586-020-2360-3.

Thackeray, C. W. and C. G. Fletcher (2016). "Snow albedo feedback: Current knowledge, importance, outstanding issues and future directions". *Progress in Physical Geography: Earth and Environment* 40:3. Publisher: SAGE Publications Ltd, pp. 392–408. ISSN: 0309-1333. DOI: 10.1177/0309133315620999.

Thomas, M. K., C. T. Kremer, C. A. Klausmeier, and E. Litchman (2012). "A Global Pattern of Thermal Adaptation in Marine Phytoplankton". *Science* 338:6110. Publisher: American Association for the Advancement of Science, pp. 1085–1088. DOI: 10.1126/science.1224836.

Toggweiler, J. R. and B. Samuels (1998). "On the Ocean's Large-Scale Circulation near the Limit of No Vertical Mixing". Section: Journal of Physical Oceanography. ISSN: 1520-0485.

Tokarska, K. B. et al. (2020). "Past warming trend constrains future warming in CMIP6 models". *Science Advances* 6:12. Publisher: American Association for the Advancement of Science, eaaz9549. DOI: 10.1126/sciadv.aaz9549.

Tsujino, H. et al. (2020). "Evaluation of global ocean–sea-ice model simulations based on the experimental protocols of the Ocean Model Intercomparison Project phase 2 (OMIP-2)". *Geoscientific Model Development* 13:8. Publisher: Copernicus GmbH, pp. 3643–3708. ISSN: 1991-959X. DOI: 10.5194/gmd-13-3643-2020.

Uppenbrink, J. (1996). "Arrhenius and Global Warming". *Science* 272:5265. Publisher: American Association for the Advancement of Science, pp. 1122–1122. ISSN: 0036-8075.

Vallis, G. K. (2017). *Atmospheric and oceanic fluid dynamics: Fundamentals and large-scale circulation*. 2nd ed. Cambridge University Press, Cambridge.

Venegas, R. M., J. Acevedo, and E. A. Treml (2023). "Three decades of ocean warming impacts on marine ecosystems: A review and perspective". *Deep Sea Research Part II: Topical Studies in Oceanography* 212, p. 105318. ISSN: 0967-0645. DOI: 10.1016/j.dsr2.2023.105318.

Vuuren, D. P. van et al. (2011). "The representative concentration pathways: an overview". *Climatic Change* 109:1, p. 5. ISSN: 1573-1480. DOI: 10.1007/s10584-011-0148-z.

Wagman, B. M. and C. S. Jackson (2018). "A test of emergent constraints on cloud feedback and climate sensitivity using a calibrated single-model ensemble". *Journal of Climate* 31:18. Place: Boston MA, USA Publisher: American Meteorological Society, pp. 7515–7532. DOI: 10.1175/JCLI-D-17-0682.1.

Wang, C., L. Zhang, S.-K. Lee, L. Wu, and C. R. Mechoso (2014). "A global perspective on CMIP5 climate model biases". *Nature Climate Change* 4:3. Number: 3 Publisher: Nature Publishing Group, pp. 201–205. ISSN: 1758-6798. DOI: 10.1038/nclimate2118.

Wanninkhof, R. (1992). "Relationship between wind speed and gas exchange over the ocean". *Journal of Geophysical Research: Oceans* 97, C5. _eprint: https://onlinelibrary.wiley.com/doi/pdf/10.1029/92JC001 pp. 7373–7382. ISSN: 2156-2202. DOI: 10.1029/92JC00188.

Watanabe, M. et al. (2013). "Strengthening of ocean heat uptake efficiency associated with the recent climate hiatus". *Geophysical Research Letters* 40:12. _eprint: https://onlinelibrary.wiley.com/doi/pdf/10.1002/grl.50541, pp. 3175–3179. ISSN: 1944-8007. DOI: 10.1002/grl.50541.

Watson-Parris, D. (2021). "Machine learning for weather and climate are worlds apart". *Philosophical Transactions of the Royal Society A: Mathematical, Physical and Engineering Sciences* 379:2194. Publisher: Royal Society, p. 20200098. DOI: 10.1098/rsta.2020.0098.

Watterson, I. G. (2000). "Interpretation of Simulated Global Warming Using a Simple Model". Section: Journal of Climate. ISSN: 1520-0442.

Webb, M. J. et al. (2017). "The Cloud Feedback Model Intercomparison Project (CFMIP) contribution to CMIP6". *Geoscientific Model Development* 10:1. Publisher: Copernicus GmbH, pp. 359–384. ISSN: 1991-959X. DOI: 10.5194/gmd-10-359-2017.

Wernberg, T. et al. (2011). "Seaweed Communities in Retreat from Ocean Warming". *Current Biology* 21:21. Publisher: Elsevier, pp. 1828–1832. ISSN: 0960-9822. DOI: 10.1016/j.cub.2011.09.028.

Wigley, T. M. L. and M. E. Schlesinger (1985). "Analytical solution for the effect of increasing CO2 on global mean temperature". *Nature* 315:6021. Publisher: Nature Publishing Group, pp. 649–652. ISSN: 1476-4687. DOI: 10.1038/315649a0.

Williams, K. D., W. J. Ingram, and J. M. Gregory (2008). "Time Variation of Effective Climate Sensitivity in GCMs". *Journal of Climate* 21:19. Publisher: American Meteorological Society Section: Journal of Climate, pp. 5076–5090. ISSN: 0894-8755, 1520-0442. DOI: 10.1175/2008JCLI2371.1.

Williams, R. G., P. Ceppi, and A. Katavouta (2020). "Controls of the transient climate response to emissions by physical feedbacks, heat uptake and carbon cycling". *Environmental Research Letters* 15:9. Publisher: IOP Publishing, p. 0940c1. ISSN: 1748-9326. DOI: 10.1088/1748-9326/ab97c9.

Williamson, M. S., P. M. Cox, and F. J. M. M. Nijsse (2018). "Theoretical foundations of emergent constraints: relationships between climate sensitivity and global temperature variability in conceptual models". *Dynamics and Statistics of the Climate System* 3:1, dzy006. ISSN: 2059-6987. DOI: 10.1093/climsys/dzy006.

Williamson, M. S., P. M. Cox, C. Huntingford, and F. J. M. M. Nijsse (2024). "Testing the assumptions in emergent constraints: why does the "emergent constraint on equilibrium climate sensitivity from global temperature variability" work for CMIP5 and not CMIP6?" *Earth System Dynamics* 15:4. Publisher: Copernicus GmbH, pp. 829–852. ISSN: 2190-4979. DOI: 10.5194/esd-15-829-2024.

Williamson, M. S. et al. (2021). "Emergent constraints on climate sensitivities". *Reviews of Modern Physics* 93:2, p. 025004. ISSN: 0034-6861, 1539-0756. DOI: 10.1103/RevModPhys.93.025004. arXiv: 2012.09468[physics].

Wills, R. C. J., Y. Dong, C. Proistosecu, K. C. Armour, and D. S. Battisti (2022). "Systematic Climate Model Biases in the Large-Scale Patterns of Recent Sea-Surface Temperature and Sea-Level Pressure Change". *Geophysical Research Letters* 49:17. _eprint: https://onlinelibrary.wiley.com/doi/pdf/10.1029/2022GL100011, e2022GL100011. ISSN: 1944-8007. DOI: 10.1029/2022GL100011.

Winder, M. and U. Sommer (2012). "Phytoplankton response to a changing climate". *Hydrobiologia* 698:1, pp. 5–16. ISSN: 1573-5117. DOI: 10.1007/s10750-012-1149-2.

Winkler, A. J., R. B. Myneni, and V. Brovkin (2019). "Investigating the applicability of emergent constraints". *Earth System Dynamics* 10:3. Publisher: Copernicus GmbH, pp. 501–523. ISSN: 2190-4979. DOI: 10.5194/esd-10-501-2019.

Winsberg, E. (2022). "Computer Simulations in Science". In: *The Stanford Encyclopedia of Philosophy*. Ed. by E. N. Zalta and U. Nodelman. Winter 2022. Metaphysics Research Lab, Stanford University.

Winton, M., K. Takahashi, and I. M. Held (2010). "Importance of Ocean Heat Uptake Efficacy to Transient Climate Change". *Journal of Climate* 23:9. Publisher: American Meteorological Society Section: Journal of Climate, pp. 2333–2344. ISSN: 0894-8755, 1520-0442. DOI: 10.1175/2009JCLI3139.1.

Winton, M. et al. (2014). "Has coarse ocean resolution biased simulations of transient climate sensitivity?" *Geophysical Research Letters* 41:23. _eprint: https://onlinelibrary.wiley.com/doi/pdf/10.1002/2014GL061523, pp. 8522–8529. ISSN: 1944-8007. DOI: 10.1002/2014GL061523.

Wittenberg, A. T. (2009). "Are historical records sufficient to constrain ENSO simulations?" *Geophysical Research Letters* 36:12. _eprint: https://onlinelibrary.wiley.com/doi/pdf/10.1029/2009GL038710. ISSN: 1944-8007. DOI: 10.1029/2009GL038710.

Wong, A. P. S. et al. (2020). "Argo Data 1999–2019: Two Million Temperature-Salinity Profiles and Subsurface Velocity Observations From a Global Array of Profiling Floats". *Frontiers in Marine Science* 7. Publisher: Frontiers. ISSN: 2296-7745. DOI: 10.3389/fmars.2020.00700.

Worley, S. J., S. D. Woodruff, R. W. Reynolds, S. J. Lubker, and N. Lott (2005). "ICOADS release 2.1 data and products". *International Journal of Climatology* 25:7, pp. 823–842. ISSN: 0899-8418, 1097-0088. DOI: 10.1002/joc.1166.

Yamaguchi, R. and T. Suga (2019). "Trend and Variability in Global Upper-Ocean Stratification Since the 1960s". *Journal of Geophysical Research: Oceans* 124:12. _eprint: https://onlinelibrary.wiley.com/doi/pdf/10.1029/2019JC015439, pp. 8933–8948. ISSN: 2169-9291. DOI: 10.1029/2019JC015439.

Yoshimori, M. et al. (2016). "A review of progress towards understanding the transient global mean surface temperature response to radiative perturbation". *Progress in Earth and Planetary Science* 3:1, p. 21. ISSN: 2197-4284. DOI: 10.1186/s40645-016-0096-3.

Zanchettin, D. et al. (2016). "The Model Intercomparison Project on the climatic response to Volcanic forcing (VolMIP): experimental design and forcing input data for CMIP6". *Geoscientific Model Development* 9:8. Publisher: Copernicus GmbH, pp. 2701–2719. ISSN: 1991-959X. DOI: 10.5194/gmd-9-2701-2016.

Zelinka, M. D. et al. (2020). "Causes of Higher Climate Sensitivity in CMIP6 Models". *Geophysical Research Letters* 47:1. _eprint: https://onlinelibrary.wiley.com/doi/pdf/10.1029/2019GL085782, e2019GL085782. ISSN: 1944-8007. DOI: 10.1029/2019GL085782.

Zhou, C., M. D. Zelinka, A. E. Dessler, and M. Wang (2021). "Greater committed warming after accounting for the pattern effect". *Nature Climate Change* 11:2. Bandiera_abtest: a Cg_type: Nature Research Journals Number: 2 Primary_atype: Research Publisher: Nature Publishing Group Subject_term: Atmospheric science;Ocean sciences Subject_term_id: atmospheric-science;ocean-sciences, pp. 132–136. ISSN: 1758-6798. DOI: 10.1038/s41558-020-00955-x.

2 Increased future ocean heat uptake constrained by Antarctic sea ice extent

At the time of writing (January 18, 2025), this article is under review at *Science Advances* (submitted on June 6, 2024). Note that the section numbering and citation format has been adapted to the overall style used in this thesis.

Authors

Linus Vogt[1,2], Casimir de Lavergne[1], Jean-Baptiste Sallée[1], Lester Kwiatkowski[1], Thomas L. Frölicher[3,4], Jens Terhaar[2,3,4]

Affiliations

[1] Sorbonne Université, CNRS/IRD/MNHN, Laboratoire d'Océanographie et du Climat Expérimentations et Approches Numériques (LOCEAN), Paris, France.

[2] Woods Hole Oceanographic Institution, Woods Hole, MA, USA.

[3] Climate and Environmental Physics, Physics Institute, University of Bern, Bern, Switzerland.

[4] Oeschger Centre for Climate Change Research, University of Bern, Bern, Switzerland.

Abstract

The ocean moderates global warming by absorbing most of the excess heat from anthropogenic climate change. However, ocean heat uptake (OHU) projections still strongly differ between climate models despite their importance for informing climate policy. Here, we provide improved global OHU projections by identifying a relationship between present-day Antarctic sea ice extent and future OHU across an ensemble of 28 state-of-the-art climate models. Combining this relationship with satellite observations of Antarctic sea ice reduces the uncertainty of OHU projections under future emissions scenarios by 12–33%. Moreover, we show that an underestimation of present-day Antarctic sea ice in the latest generation of climate models results in an underestimation of future OHU by 3–14%, of global cloud feedback by 19–32%, and of global atmospheric warming by 6–7%. Our mechanism-based constraint reveals how the present-day Southern Hemisphere state impacts future climate change, and contrasts with previous constraints based solely on past warming trends.

2.1 Introduction

Since the beginning of the industrial period, the ocean has taken up over 90% of the excess heat generated by human-caused climate change (Forster et al. 2021). This ocean heat uptake (OHU) has limited the rate of atmospheric temperature increase (Liu et al. 2016), but the widespread warming of the ocean (Johnson and Lyman 2020) has had cascading negative consequences for humans and marine ecosystems. Ocean warming contributes to sea level rise through thermal expansion and the melting of marine-terminating glaciers (Cazenave and Llovel 2010). Sea level rise and ocean warming create risks for coastal communities due to increased flooding and more destructive tropical cyclones (Sun et al. 2017; Pörtner et al. 2022). Higher upper ocean temperatures also lead to changes in stratification and the supply of nutrients and oxygen to marine ecosystems (Bopp et al. 2013; Sallée et al. 2021; Morée et al. 2023), impacting fish stocks (Cheung et al. 2016) and perturbing the global carbon cycle (Joos et al. 1999). Furthermore, ocean warming drives more frequent and intense marine heatwaves, potentially causing widespread collapses of foundation species including corals, kelps, and seagrasses (Frölicher et al. 2018; Smith et al. 2023).

The extent of future OHU primarily depends on cumulative greenhouse gas emissions, and thus on the effectiveness of mitigation policies (Fox-Kemper et al. 2021). However, OHU is also influenced by atmospheric feedbacks and warming rates as well as oceanic ventilation and overturning (Marshall et al. 2015; Zelinka et al. 2020). Climate feedbacks such as cloud and albedo feedbacks alter the radiative balance of the Earth and thus affect the transient climate response, climate sensitivity, and future ocean heat storage (Williams et al. 2020; Zelinka et al. 2020). Additionally, the

efficiency at which the ocean transports heat from the surface layer to the deep ocean influences its capacity for heat storage and can modulate climate feedbacks by affecting surface warming patterns (Winton et al. 2010; Armour et al. 2013; Andrews et al. 2022).

The majority of OHU occurs in the Southern Ocean (Frölicher et al. 2015), which accounts for around 67% of global OHU between 1871 and 2017 in an observation-based reconstruction (Zanna et al. 2019). In climate model simulations from phase 6 of the Coupled Model Intercomparison Project (CMIP6; Methods), the Southern Ocean south of 30°S is responsible for 84% (68–99%) of the global historical OHU from 1850 to 2024, 53% (38–62%) of future OHU from 2024 to 2100 under the low-emissions SSP1-2.6 scenario, and 48% (42–52%) under the high-emissions SSP5-8.5 scenario (inter-model uncertainty is expressed as 66% *likely* ranges) (Frölicher et al. 2015; Shi et al. 2018). The disproportionately large heat uptake in the Southern Ocean is a direct consequence of the vigorous deep-reaching overturning in this region (Armour et al. 2016). The overturning in the high-latitude Southern Ocean is driven by strong westerly winds which provoke upwelling of large volumes of cold water from the deep ocean (Marshall and Speer 2012). Much of this upwelled water is warmed by the atmosphere before being subducted back into the ocean interior further northward as mode and intermediate waters, following the upper cell of the Southern Ocean meridional overturning circulation (Armour et al. 2016; Sallée 2018).

2.2 Uncertain future of OHU

Although robust and precise projections of OHU are paramount for informing climate mitigation and adaptation measures, accurately projecting OHU remains challenging (Cheng et al. 2022) (Fig. 2.1). The uncertainty of the future cumulative global OHU from 2024 to 2100 is 23–28% of the multi-model mean (depending on emissions scenario), and the ranges of cumulative OHU projections for 2100 overlap across scenarios (Fig. 2.1). Uncertainties in future OHU are large because cloud feedbacks and oceanic heat sequestration by ocean ventilation and mixing remain notoriously challenging to correctly simulate (Frölicher et al. 2015; Ceppi et al. 2017; Zelinka et al. 2020; Terhaar et al. 2021). The Southern Ocean overturning is particularly difficult to faithfully simulate in Earth system models (ESMs) such as those participating in CMIP6 (Beadling et al. 2020). Biases in the baseline state of ESMs are known to have global repercussions on projected climate change, notably by preconditioning future cloud feedback (Siler et al. 2018; Kajtar et al. 2021; Shin et al. 2023) and Southern Ocean ventilation (Terhaar et al. 2021; Bourgeois et al. 2022).

One approach to reducing inter-model uncertainties is the method of emergent constraints (Hall et al. 2019). An emergent constraint identifies a physically grounded relationship between an observable historical climate variable and an uncertain future climate variable, across an ensemble of models. Combining this quantitative relationship with observations of the historical variable

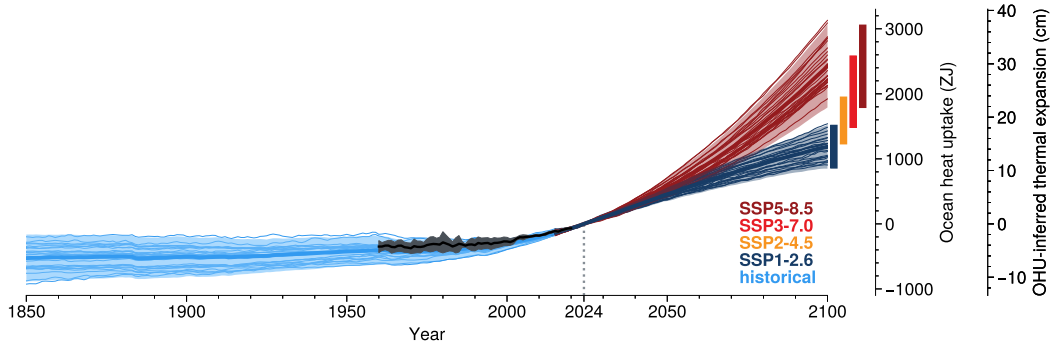

Figure 2.1: Ocean heat uptake in CMIP6 models. Globally integrated cumulative historical and future ocean heat uptake relative to the year 2024 under different scenarios and the associated global mean sea level rise through thermal expansion (see Methods). Thin lines are individual models, while the thick lines and shading depict respectively the ensemble mean and standard deviation for each scenario. The coloured bars on the right indicate the 95% confidence interval around the mean OHU in 2100 for each scenario. Coloured bars are shown for four scenarios (SSP5-8.5 in dark red, SSP3-7.0 in bright red, SSP2-4.5 in orange, SSP1-2.6 in dark blue), whereas the time series are shown only for the historical period and the SSP1-2.6 and SSP5-8.5 scenarios. The black curve and grey shading show the observed changes over 1960–2020.

yields a constrained estimate of the uncertain future variable. Emergent constraints can be broadly divided into three categories (Sanderson et al. 2021): (i) trend-on-trend constraints that assume a time invariant model bias that has existed over the historical period and will continue in the future (Jiménez-de-la-Cuesta and Mauritsen 2019; Nijsse et al. 2020; Tokarska et al. 2020; Lyu et al. 2021), (ii) process-based constraints that identify a physical or biochemical bias that causes a mechanistically linked bias in projections of the considered variable (Terhaar et al. 2020; 2021; Bourgeois et al. 2022), and (iii) sensitivity-based constraints where the sensitivity of a system to changes on short timescales, such as seasonal changes, is related to the response of a system to climate change (Cox et al. 2013; Kwiatkowski et al. 2017). Trend-on-trend constraints have previously indicated smaller future OHU and atmospheric warming compared to the unconstrained mean of CMIP6 projections (Tokarska et al. 2020; Lyu et al. 2021). However, trend-on-trend constraints can fail if the historically-observed trend is not representative of a time invariant bias. This can occur either because the past trend has been strongly affected by a particular phase of natural variability (England et al. 2014; Marvel et al. 2018; Armour et al. 2024), or because the constrained system undergoes a profound change over the 21st century so that the identified past bias does not persist in the future or becomes dwarfed by a larger bias that only emerges in a changing climate (Sanderson et al. 2021). In particular, climate change over recent decades has been characterized by relatively muted radiative feedbacks, likely biasing low constrained estimates of future warming based on observed warming trends (Andrews et al. 2022; Armour et al. 2024).

Here we show that global OHU undergoes such a profound change over the 21st century that model biases in past OHU may be unable to explain differences in projected OHU. To narrow the spread in projected OHU we propose a process-based and mechanistically interpretable emergent relationship. This relationship makes it possible to reduce uncertainties in future OHU by accounting for ESM biases in the baseline state of the Southern Hemisphere as quantified by Antarctic summer sea ice extent.

2.3 Results

2.3.1 Antarctic sea ice as an indicator of Southern Hemisphere climate

Antarctic sea ice extent is an indicator of the climate state of the extratropical Southern Hemisphere. Models with greater sea ice extent under preindustrial conditions tend to have colder sea surface temperatures across the Southern Ocean (Fig. 2.2b) as well as more cloud cover over the mid-latitude Southern Ocean (Kajtar et al. 2021; Shin et al. 2023) (Fig. 2.2a), which modulates radiative heat transfer by reducing downwelling shortwave radiation and enhancing downwelling longwave radiation. Greater sea ice extent is also associated with colder temperatures across the global deep ocean (Fig. 2.2b), including in deep Atlantic layers mainly ventilated from the North Atlantic (Fig. 2.A.1). Biases in the temperature of deep ocean waters, much of which ultimately upwell in the high-latitude Southern Ocean, can thus have cascading effects on Southern Hemisphere sea ice, surface temperatures, and clouds (Luo et al. 2023).

Under future global warming, ESMs with higher present-day sea ice extent have the potential to lose more sea ice (Kajtar et al. 2021). In particular, under the SSP5-8.5 scenario, many ESMs lose virtually all of their Antarctic summer (January–February) sea ice by 2100, so that summer sea ice loss in 2100 is almost equivalent to baseline sea ice extent (Fig. 2.3a). Similarly, models with greater preindustrial extratropical and equatorial cloud cover simulate a greater future reduction in cloud cover at these latitudes (Fig. 2.A.2). As a consequence of these links between preindustrial baseline climate and future changes, ESMs with higher preindustrial Antarctic sea ice extent tend to experience a greater shift in their simulated Southern Hemisphere climate in the future. This shift in climate manifests itself through greater warming of the surface atmosphere and ocean (Fig. 2.3b,c), a more positive global cloud feedback (Fig. 2.3d), and consequently greater OHU (Fig. 2.4). This additional OHU in models with higher preindustrial Antarctic sea ice extent is particularly pronounced in the Southern Hemisphere mode and intermediate waters (Fig. 2.A.3) which tend to transport heat northwards and into the interior ocean (Armour et al. 2016).

The cloud feedback connects Antarctic sea ice extent loss and global OHU. Across the ESM ensemble, this connection is globally apparent by the end of the 21st century as strong correla-

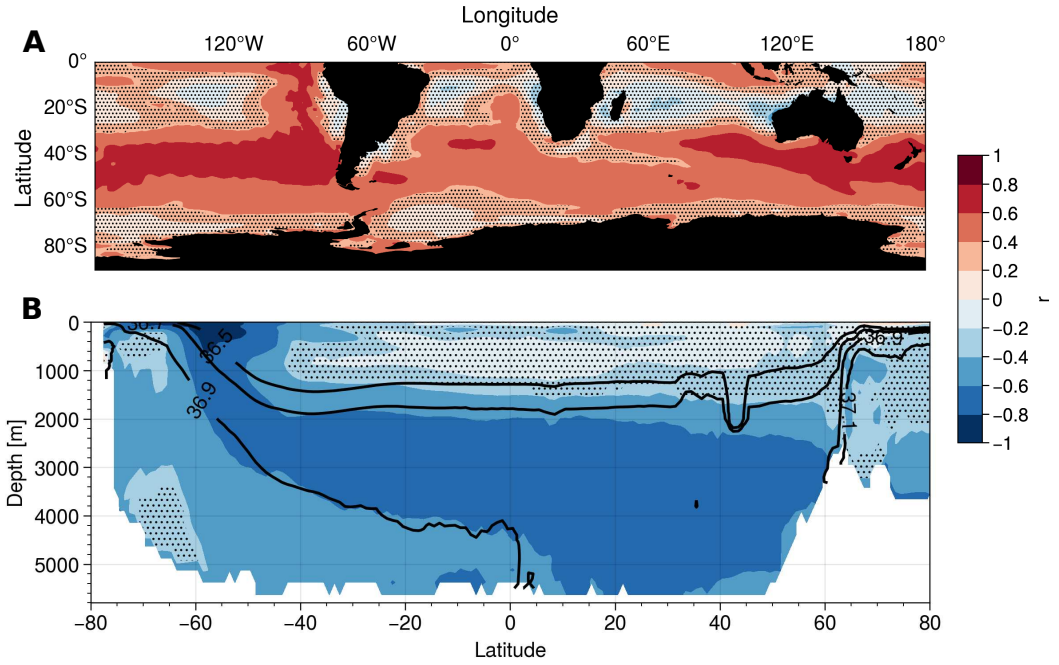

Figure 2.2: Atmospheric and oceanic connections to Antarctic sea ice extent in the preindustrial state. a, Inter-model correlation between preindustrial annual-mean Antarctic sea ice extent and preindustrial total cloud cover in the Southern Hemisphere. In red areas, local cloud cover is increased for models with higher sea ice extent. **b**, Inter-model correlation between preindustrial annual-mean Antarctic sea ice extent and preindustrial zonal mean ocean temperature across all ocean basins. In blue areas, local seawater is colder for models with higher sea ice extent. Black contours show zonal mean potential density relative to a reference pressure of 2000 dbar from observations (Boyer, Tim P. et al. 2023). In both panels, stippling indicates regions where the correlation is not significant ($p \geq 0.05$, two-sided).

tions between cloud feedback and Antarctic sea ice extent loss (Fig. 2.A.4a), and between cloud feedback and global OHU (Fig. 2.A.4b). The global extent of this relationship between Antarctic sea ice loss, cloud feedback and OHU is the result of a northward propagation originating in the Southern Ocean. The surface warming signal in the ocean and atmosphere related to sea ice loss first emerges in the southern high latitudes around 1990–2010, gradually spreading northwards and covering most of the Southern Hemisphere by 2030–2050 under SSP5-8.5 (Fig. 2.A.5). This causes a concomitant spreading of sea ice–related local cloud feedback starting from the Southern Ocean and attaining its near-global extent by mid-century (Fig. 2.A.5). Although cloud feedback is in general controlled by a number of contributions including cloud amount, altitude, and optical depth (Zelinka et al. 2016; Ceppi et al. 2017), the signal is apparent in total cloud amount (Fig. 2.A.2). The northward propagation of these significant inter-model relationships likely results from anomalous heat transport in the ocean and/or the atmosphere (England et al. 2020a; England et al. 2020b; Ayres et al. 2022).

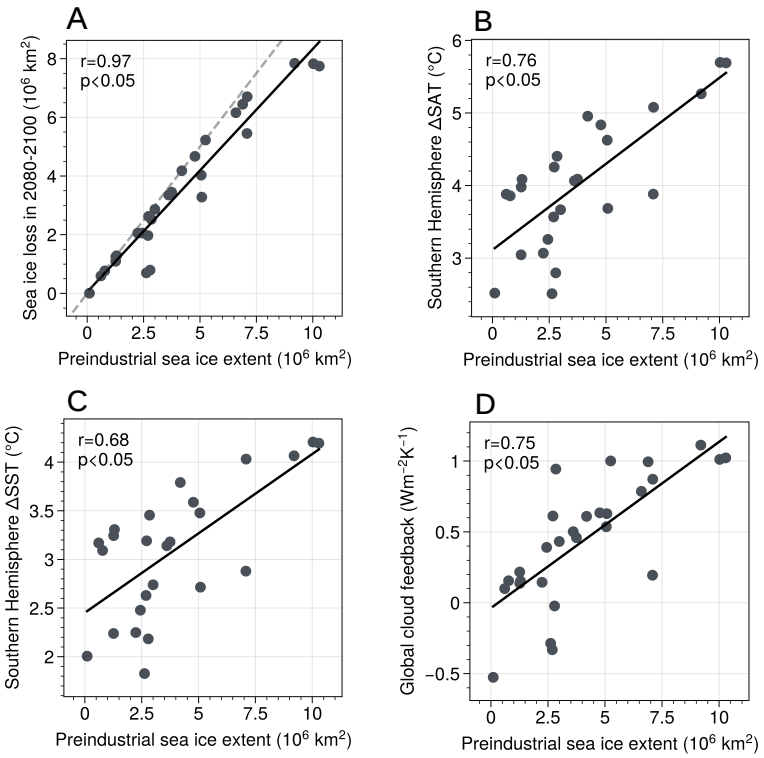

Figure 2.3: Links between preindustrial Antarctic sea ice and Southern Hemisphere climate change. CMIP6 inter-model relationship between preindustrial Antarctic summer (January–February) sea ice extent and future sea ice extent loss (**a**), Southern Hemisphere surface air temperature increase (**b**), Southern Hemisphere sea surface temperature increase (**c**), and global mean cloud feedback parameter (**d**). In each panel, the black line shows the least squares linear regression fit, and the Pearson correlation coefficient r and two-sided p-value are given in the upper left corner. The y-axis of all panels represents anomalies between years 2080–2100 of the high-emissions SSP5-8.5 scenario and the preindustrial state.

Decomposing cloud feedback into its shortwave and longwave radiative components reveals that the global relationship between sea ice loss and cloud feedback is mostly mediated by the shortwave component (Fig. 2.A.4c–d), whereas the longwave component remains restricted to the Southern Ocean by the end of the 21st century. Furthermore, partitioning the excess OHU into its individual air-sea heat flux components demonstrates that the higher OHU in models with greater Antarctic sea ice loss is mainly due to increased shortwave-driven OHU in the Southern Hemisphere and globally increased sensible OHU (Fig. 2.A.6). The increased sensible OHU is a direct consequence of the stronger atmospheric warming in models with more Antarctic sea ice loss. The increased shortwave-induced and sensible OHU associated with larger Antarctic sea ice loss is slightly counteracted by a reduced latent air-sea heat flux at low latitudes (Fig. 2.A.6h). As

sea ice loss strongly accelerates after 2024, these relationships emerge only for future (2024–2100) OHU and are not apparent for OHU over the historical (1850–2024) period.

In addition to the connection of Antarctic sea ice loss with global warming and cloud feedback, the loss of sea ice itself also has direct local influences (Kay et al. 2014). Any reduction of white sea ice cover exposes the underlying ocean, allowing more heat to be absorbed. While the additional OHU under the previously covered sea ice is small compared to the global OHU (about 6% in the multi-model mean), this additional warming close to the sea ice edge further accelerates the loss of sea ice cover through surface albedo feedback.

2.3.2 Emergent constraints on future change

The mechanistic understanding and inter-model relationships presented show that model bias in baseline sea ice extent in austral summer is a physical indicator of future sea ice loss, surface warming, and cloud feedback (Fig. 2.3). As cloud feedback mediates future OHU (Fig. 2.A.4), historical observations of Antarctic sea ice can be used to constrain future OHU (Fig. 2.4). Using the 1980–2020 summer sea ice extent from the OSI SAF satellite observational product (EUMETSAT Ocean and Sea Ice Satellite Application Facility 2024a) of $4.41 \pm 1.00 \times 10^6$ km^2 to constrain future OHU results in an estimate of future global OHU between 2024–2100 of 1244 ± 141 ZJ under SSP1-2.6 (Fig. 2.4a-b) and 2595 ± 209 ZJ under SSP5-8.5 (Fig. 2.4c-d, results for SSP2-4.5 and SSP3-7.0 are shown in Fig. 2.A.7 and detailed in Table 2.A.2). The constrained median estimate is 3% higher and 14% less uncertain than the CMIP6 ensemble prior median under SSP1-2.6, and 14% higher and 33% less uncertain under SSP5-8.5.

In all four SSPs considered, the correlation between 1980–2020 sea ice extent and future OHU is above 0.6 and statistically significant at the $p < 0.05$ level according to a two-sided Student's t-test (Table 2.A.2). This suggests that the presented mechanism is robust and explains a substantial fraction of inter-model spread in future OHU irrespective of the scenario. Given our conservative choice of predictor uncertainty and available model ensemble sizes (Methods), the difference between unconstrained and constrained OHU mean values is statistically significant under SSP2-4.5 and SSP5-8.5 but not under SSP1-2.6 ($p = 0.11$) and SSP3-7.0 ($p = 0.09$) according to a two-sided two-sample Student's t-test (Table 2.A.2).

The higher OHU estimates directly translate to greater than currently anticipated future sea level rise due to thermal expansion. Under SSP1-2.6 the constrained thermosteric global mean sea level rise from 2024 to 2100 is 15.2 ± 1.7 cm, assuming a constant conversion factor between OHU and thermosteric sea level rise (see Methods). Under SSP5-8.5, the constrained estimate is 31.6 ± 2.5 cm. Both estimates are higher and less uncertain than the respective unconstrained estimates of 14.5 ± 2.0 cm and 29.5 ± 3.8 cm (Table 2.A.2).

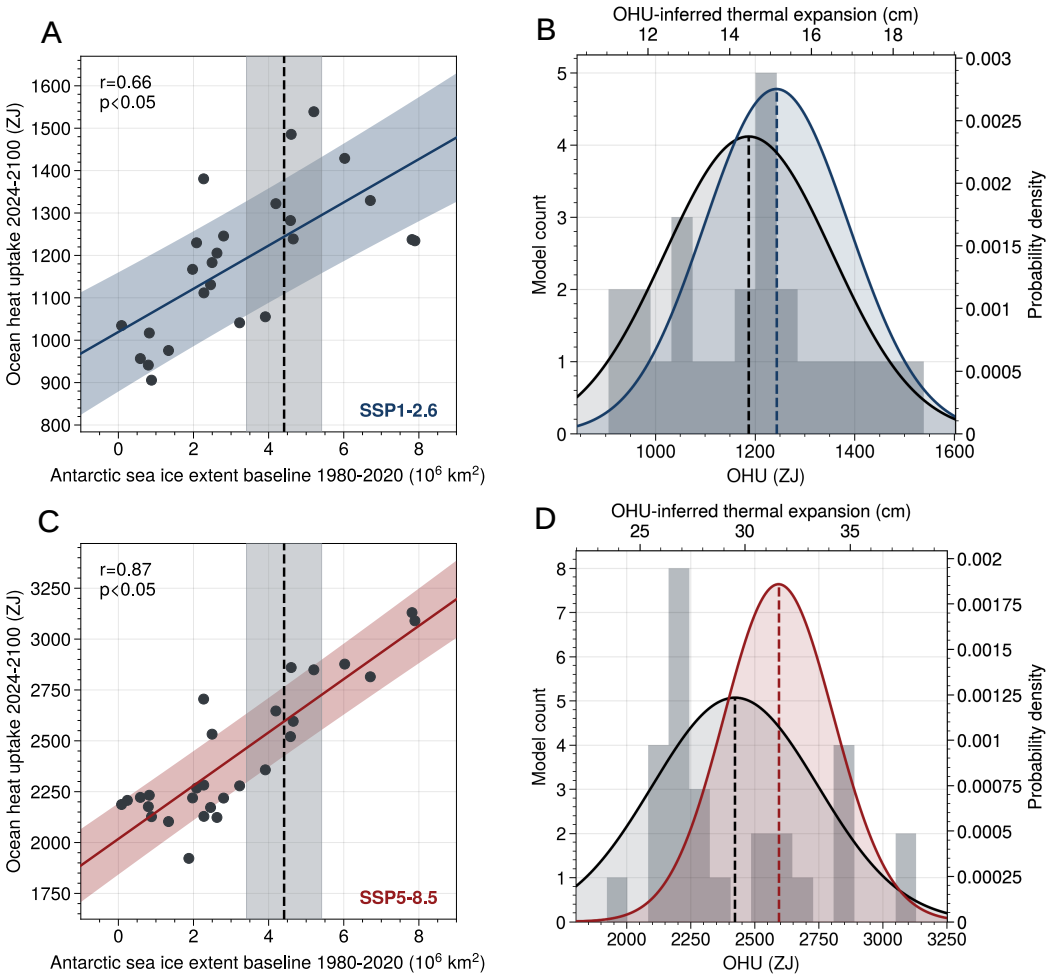

Figure 2.4: Emergent constraint on future global ocean heat uptake. **a**, Inter-model relationship between 1980-2020 Antarctic summer (January–February) sea ice extent and cumulative global OHU over 2024–2100 under the SSP1-2.6 scenario. The blue line and shading show the least squares linear regression fit and its uncertainty (see Methods), with the Pearson's correlation coefficient r and two-sided p-value given in the upper left corner. The dashed vertical line shows satellite observations of Antarctic summer sea ice extent averaged over 1980–2020 (EUMETSAT Ocean and Sea Ice Satellite Application Facility 2024a) and the grey shading shows the associated uncertainty of 1×10^6 km^2; this relatively large observational uncertainty ensures we derive a conservative emergent constraint (Methods). **b**, Unconstrained prior (black) and constrained posterior (blue) probability density functions of 2024–2100 global OHU. In grey we show the prior histogram for 2024–2100 OHU (Methods). **c**, as panel **a** but for the SSP5-8.5 scenario. **d**, as panel **b** but for the SSP5-8.5 scenario.

The mechanism underlying our emergent constraint also has direct implications for the strength of cloud feedback and the magnitude of global warming by the end of the 21st century. Present-day Antarctic sea ice extent is significantly correlated with future cloud feedback and global warming in all four SSPs considered (Table 2.A.2). Using 1980–2020 summer sea ice extent as a predictor, global mean cloud feedback is constrained to be 19% and 31% higher than the CMIP6 median under SSP1-2.6 and SSP5-8.5, respectively (Fig. 2.5b). Future global mean surface air warming is constrained to be 3–7% greater than the CMIP6 median (Fig. 2.5c). The uncertainty in the estimates is reduced by 18% for cloud feedback and by 11% for surface warming under SSP5-8.5 (results for other SSPs are shown in Fig. 2.A.8 and detailed in Table 2.A.2). Present-day sea ice extent is more strongly correlated with future OHU (r = 0.87 under SSP5-8.5) than with end-of-century cloud feedback (r = 0.71) or surface air warming (r = 0.61), which is why the uncertainty reduction is larger for OHU.

The tighter constraint on OHU may be explained by two factors. First, the correlation between Antarctic sea ice extent and local cloud feedback is particularly strong over the southern mid-latitudes where OHU is most efficient (Armour et al. 2016) (Fig. 2.A.4) and where much of the additional OHU occurs (Fig. 2.A.3). Second, larger baseline Antarctic sea ice is associated with colder deep waters (Fig. 2.2b), whose exposure to the warming atmosphere in the Southern Ocean can promote OHU through sensible heat flux (Fig. 2.A.6).

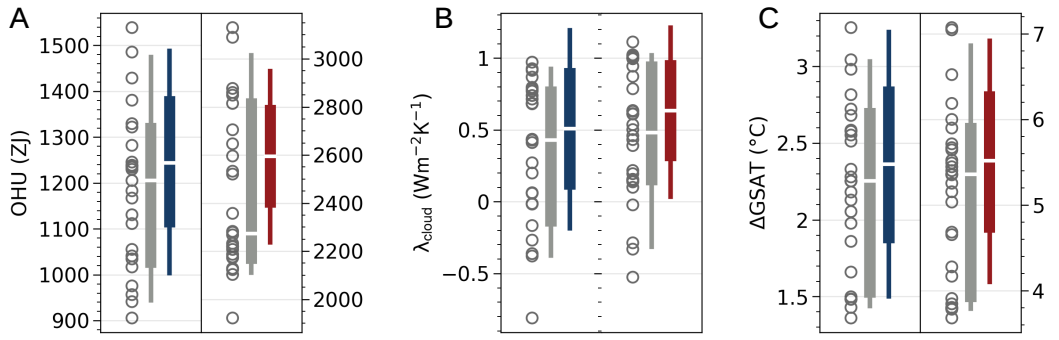

Figure 2.5: Constrained distributions of global OHU, cloud feedback, and warming. Prior and constrained distributions of (**a**) cumulative global OHU from 2024 to 2100, (**b**) global mean cloud feedback parameter in 2080–2100, and (**c**) global mean surface air temperature (GSAT) anomaly in 2080–2100 relative to the preindustrial. In each panel, distributions are shown for SSP1-2.6 (left) and SSP5-8.5 (right). The grey circles and grey boxplots show the prior distribution of model values, and the blue and red boxplots show the constrained distributions for SSP1-2.6 and SSP5-8.5, respectively. In each boxplot, the white line shows the median, the central box spans the likely range (66%), and the whiskers extend to a 95% confidence interval. The constrained values are normally distributed by construction (Methods). Note that the y-axis scale is different between the two SSPs in panels **a** and **c**.

To facilitate comparison with previous studies which used past warming trends as predictors to constrain future OHU (Lyu et al. 2021) or global surface warming (Tokarska et al. 2020), we now

apply our emergent constraint to the same uncertain variables considered in these two studies. For future 0–2000m OHU under SSP5-8.5 in 2081–2100 relative to 2005–2019 as in Lyu et al. (2021), we obtain a constrained estimate which is 16% (9%) higher than the unconstrained CMIP6 median (mean), in contrast to Lyu et al. (2021) whose constrained OHU estimate was lower than the prior mean (Fig. 2.A.9a–b). Historical Antarctic sea ice extent provides higher predictive skill for future 0–2000m OHU ($r = 0.9$) than does past 0–2000m OHU ($r = 0.72$ in Lyu et al. (2021)). For future global surface air temperature warming under SSP5-8.5 in 2081–2100 relative to 1850–1900 as in Tokarska et al. (2020), we obtain a constrained estimate which is 5% (7%) higher than the unconstrained CMIP6 median (mean), again in contrast to the constrained estimate from Tokarska et al. (2020) which was lower than the prior mean (Fig. 2.A.9c–d).

2.3.3 Robustness of the emergent constraint

In these constrained projections we used the satellite-observed summer (January-February) sea ice extent averaged over 1980-2020 as the observable climate variable. Similar results are obtained when alternative definitions of the observable variable are employed (Fig. 2.A.10). Different satellite observational products lead to very minor shifts in the constrained OHU projection, indicating that observational uncertainty in present-day sea ice extent is sufficiently small (much less than the specified uncertainty of 1×10^6 km^2 in Fig. 2.4) to obtain robust uncertainty reduction (Fig. 2.A.10a,d and Methods). Using annual mean sea ice extent or different definitions of the summer season also yield broadly consistent uncertainty reductions (from −13% to −38%) and OHU increases (from +3% to +11%) under SSP5-8.5 (Fig. 2.A.10c).

Antarctic sea ice cover shows both inter-annual and multi-decadal variability over the satellite record (Fig. 2.A.11), so that the choice of baseline period can affect our emergent constraint. Choosing 1980-2000, 1990-2010 or 2000-2020 instead of 1980-2020 as baseline periods within the satellite record yields constrained OHU estimates of +5%, +8% or +9% above the unconstrained mean, respectively. This relatively small sensitivity stems from the large inter-model spread in Antarctic sea ice extent compared to observed variability since 1980 (Fig. 2.A.11). Reconstructions of Antarctic sea ice cover over earlier parts of the 20th century and preceding centuries possess larger uncertainties (Titchner and Rayner 2014; Fogt et al. 2022; Dalaiden et al. 2023), yet they also indicate a negative bias of the multi-model mean annually averaged extent (Fig. 2.A.11). Consequently, choosing different 40-year baseline periods between 1920 and 2000 in these reconstructions (Methods) leads to a constrained heat uptake between 3–12% higher than the CMIP6 mean under the SSP5-8.5 scenario (Fig. 2.A.10b).

For further robustness testing, we examine the correlation between historical sea ice extent and future OHU (Fig. 2.4a,c) in an out-of-sample test using 16 models from the CMIP5 ensemble,

and we probe the sensitivity of this correlation to the chosen OHU time period and sea ice seasonality in both CMIP5 and CMIP6 ensembles (Fig. 2.A.12). In the CMIP6 ensemble, maximal correlation between historical sea ice extent and future OHU under SSP5-8.5 is obtained for summer sea ice extent together with an OHU time period starting at any year after 1850 and ending after approximately 2070 (Fig. 2.A.12a–b). For time periods ending prior to 2030 the correlation becomes statistically insignificant, underlining the fact that the mechanism underlying the emergent relationship occurs only under future forcing. In the CMIP5 ensemble, correlations are higher for annual mean sea ice extent, but the temporal structure is similar to CMIP6 with maximal correlations for OHU periods extending towards the end of the 21st century (Fig. 2.A.12c–d).

The correlation between historical sea ice extent and future OHU is not an artifact of outliers or caused by individual model values of sea ice extent or OHU far from the center of the multi-model distribution (Fig. 2.A.13). A significant positive correlation persists across all considered SSPs even when discarding several models with the highest or lowest values of sea ice extent (Fig. 2.A.13a,c) and OHU (Fig. 2.A.13b,d). Furthermore, using a Huber loss function instead of ordinary least squares (OLS) in order to reduce the influence of outliers yields an almost identical regression slope (131×10^{-6} ZJ/km^2 for OLS, 130×10^{-6} ZJ/km^2 for Huber) and coefficient of determination ($r^2 = 0.75$ for both methods under SSP5-8.5).

The robustness of the constrained results can further be corroborated by observations of cloud cover and deep-ocean temperatures. Though these observations are not readily used as formal predictors in an emergent constraint (see Methods), they show that ensemble mean simulated global deep-ocean temperatures are 7% higher than observations and that simulated mid-latitude Southern Ocean (30–50°S) cloud cover is 7% less than in satellite observations. The underestimation of cloud cover and overestimation of deep ocean temperatures in ESMs concur with a negative bias in Antarctic sea ice extent (Fig. 2.2), and with underestimated cloud feedback, atmospheric warming, and OHU over the 21st century in the unconstrained CMIP6 ensemble mean (Figs. 2.3 and 2.5).

2.4 Discussion

The increased estimates of OHU and global warming found here contrast with previous studies that suggest an overestimation of the future warming by CMIP6 ESMs based on past warming and OHU trends (Jiménez-de-la-Cuesta and Mauritsen 2019; Nijsse et al. 2020; Tokarska et al. 2020; Lyu et al. 2021). A possible explanation for this difference is the limited length and representativeness of the observational records from 1980 to 2015 employed in these studies for the underlying long-term climate change (Andrews et al. 2022; Armour et al. 2024). The 1980-2015 period has been marked by patterns of sea surface temperature change associated with weaker climate feedbacks

than expected under long-term climate change (Andrews et al. 2022). These patterns, which include surface cooling in the eastern tropical Pacific and parts of the Southern Ocean, are less likely than 5% across CMIP5 and CMIP6 simulations (Wills et al. 2022). This mismatch between models and observations can bias emergent constraints that use trends over the 1980-2015 period (Andrews et al. 2022; Armour et al. 2024). More generally, climate variability is a critical confounding factor when short-length observational records are employed to constrain projections. As an example, shifting the 2005–2019 observational period for past OHU trends used in Lyu et al. (2021) only six years earlier (1999–2013) results in statistically insignificant relationship between past OHU trend and future OHU (Fig. 2.A.14).

By the same token, satellite observations of Antarctic sea ice could coincide with a period of anomalously large or small sea ice extent, biasing our emergent constraint. To test our results for such potential bias, we used different baseline periods for sea ice extent, including periods before the satellite era for which reconstructions of Antarctic sea ice are available (Titchner and Rayner 2014; Fogt et al. 2022; Dalaiden et al. 2023). We find that our mechanism-based emergent constraint consistently reduces uncertainty and increases OHU projections, even with the substantial uncertainty we attribute to the predictor (Methods). This robustness of our constraint stems from the use of an observable mean-state variable—instead of observable trends, which tend to be more sensitive to transient (decadal) anomalies—and from the strength of the emergent relationship of Fig. 2.4c (r = 0.87).

Another potential factor for the difference between present and previous estimates of OHU and atmospheric warming (Jiménez-de-la-Cuesta and Mauritsen 2019; Nijsse et al. 2020; Tokarska et al. 2020; Lyu et al. 2021) is the inability of past trends to account for a future regime shift in the climate system (Marvel et al. 2018; Armour et al. 2024; Liang et al. 2024). The climatic relationships and feedbacks underpinning our emergent constraint are dependent on a shift in the Southern Hemisphere climate state under pronounced greenhouse forcing, epitomized by the near-total disappearance of Antarctic summer sea ice under a high-emissions scenario (Fig. 2.3a). Indeed, the constraint is stronger for higher emissions scenarios (Fig. 2.4), and is invalid for past OHU (Methods), indicating that the processes presented here dominate inter-model spread only under moderate to strong forcing. Similarly, the OHU constraint based on past warming trends (Lyu et al. 2021) is insignificant for initial time periods ending before 2010 but becomes stronger for time periods chosen later in the 21st century (Fig. 2.A.14), which suggests that the potential regime shift connected to cloud feedback (Fig. 2.A.5) is necessary for obtaining a strong constraint. Although Antarctic sea ice extent has long seemed relatively unresponsive to anthropogenic forcing, the recently observed abrupt sea ice loss in 2016 and the historical minimum extent anomaly in 2023 have highlighted the possibility of an ongoing regime shift (Hobbs et al. 2024). These ob-

served sea-ice changes could foreshadow stronger Southern Hemisphere climate feedbacks and ocean warming in coming decades (Kang et al. 2023).

While our results suggest higher warming and heat uptake than the CMIP6 multi-model mean and not smaller warming and heat uptake as previously suggested (Nijsse et al. 2020; Tokarska et al. 2020; Lyu et al. 2021), they do not invalidate previous results indicating that the very strong warming, cloud feedback and climate sensitivity of high-end CMIP6 projections is unlikely (Jiménez-de-la-Cuesta and Mauritsen 2019; Nijsse et al. 2020; Tokarska et al. 2020; Cesana and Del Genio 2021; Lyu et al. 2021; Myers et al. 2021). Instead, our results show that accounting for biases in the Southern Ocean mean state in the latest generation of climate models implies larger future climate warming. Other shared biases in CMIP6 models could potentially imply additional positive or negative biases in CMIP6 climate projections. Endeavours to identify and correct such biases thus remain of utmost importance.

The relationships between oceanic, cryospheric and atmospheric variables revealed in this study provide guidance for the reduction of important mean state biases in ESMs. Specifically, they highlight the need for an accurate representation of clouds in ESMs, but also demonstrate the crucial role of the deep-ocean overturning circulation. Deep ocean temperatures explain an important part of differences in present-day Antarctic sea ice and clouds (Fig. 2.2) and thereby influence the future climate change in CMIP6 models. Improving ocean circulation and hydrography for climate projections therefore requires additional attention (Luo et al. 2023), alongside efforts to improve the simulation of clouds (Hyder et al. 2018; Zelinka et al. 2020).

Overall, our results imply that potent feedback mechanisms at mid to high southern latitudes may cause future ocean heat uptake to be higher than expected from previous assessments. Increased ocean heat uptake would cause more thermosteric sea level rise, more damage to marine ecosystems and create additional risks to socio-economic systems. This prospect calls for improved projections of coupled ocean-atmosphere climate feedbacks, as well as continued monitoring of variability and trends across the Southern Ocean.

2.5 Methods

§ Model output We use output from 28 Earth system models participating in the Coupled Model Intercomparison project, phase 6 (CMIP6; Table 2.A.1) (Eyring et al. 2016). We selected one ensemble member per model based on the availability of necessary output variables in the preindustrial, historical and SSP5-8.5 CMIP6 experiments, although output from SSP1-2.6, SSP2-4.5 and SSP3-7.0 scenario experiments is also used. Anomalies relative to the preindustrial state for variables such as heat fluxes, sea ice extent, or thermal expansion were computed by subtracting the matching preindustrial-experiment period from the historical and future variable output starting

from the correct experiment branch point. Note that the raw preindustrial model output was directly subtracted from the historical and SSP output, without prior processing such as fitting a polynomial regression (Silvy et al. 2022). This procedure removes the effect of model drift in the calculated changes (Gupta et al. 2013).

Past and future OHU are defined as OHU over the periods 1850–2024 and 2024–2100, respectively. Since the CMIP6 historical scenario covers 1850–2014 and the SSP scenarios start from 2015, the historical OHU is extended until 2024 using the SSP5-8.5 scenario. Using different future scenarios yields similar results as the differences across SSP experiments are small over the 2015-2024 period (Riahi et al. 2017).

OHU is defined as the anomalous net air-sea heat flux (CMIP variable `hfds`) integrated in space and cumulatively integrated in time:

$$\mathrm{OHU}(t) = \int_{t_0}^{t} \int_{\mathscr{A}} \phi(x, y, t') \, \mathrm{d}x \, \mathrm{d}y \, \mathrm{d}t', \tag{2.1}$$

where ϕ is the anomalous net heat flux into the ocean relative to the preindustrial period (units of $\mathrm{W\,m^{-2}}$), x and y are longitude and latitude, $\mathscr{A}$ is the surface area of the ocean, and $t_0 = 2024$ for future OHU.

Antarctic sea ice extent is defined as the total area in which the monthly mean sea ice concentration (CMIP variable `siconc`) exceeds 15%.

§ Estimation of sea level rise due to thermal expansion We use global mean thermal expansion (CMIP variable `zostoga`) as a measure of the direct effect of OHU on sea level. This variable is available for 20 out of the 28 models. Future global mean sea level rise is strongly correlated to future OHU ($r = 0.97$, $p < 0.05$ two-sided), allowing a direct conversion of OHU to sea level rise based on their ratio of $1.22 \times 10^{-25}\,\mathrm{m\,J^{-1}}$.

§ Climate feedback parameters For the quantification of cloud feedback and other radiative feedbacks, we compute spatially resolved climate feedback parameters under the SSP5-8.5 scenario using the radiative kernel method (Soden and Held 2006) with kernels based on the ERA5 reanalysis (Huang and Huang 2023). The cloud feedback parameter is computed by correcting the cloud radiative effect (CRE) for non-cloud contributions from other feedback terms such as surface albedo and water vapor (Soden et al. 2008).

§ Emergent constraint The posterior probability density functions (PDFs) of ocean heat uptake constrained by sea ice extent observations were calculated using a previously established method (Cox et al. 2013; Kwiatkowski et al. 2017; Cox et al. 2018). Given a set of N response variables

y_i with the predictors x_i and their least-squares linear fit $f(x) = a + by$, the prediction error is (Cox et al. 2018)

$$\sigma_f(x) = s\sqrt{1 + \frac{1}{N} + \frac{(x - \bar{x})^2}{N\sigma_x^2}}. \tag{2.2}$$

In the above equation, s^2 is the quantity minimized by the linear fit,

$$s^2 = \frac{1}{N-2}\sum_{i=1}^{N}\big(y_i - f(x_i)\big)^2, \tag{2.3}$$

while $\bar{x}$ and σ_x^2 are the ensemble mean and variance of the predictors, respectively. Finally, the constrained PDF $P(y)$ can be calculated as

$$P(y) = \int_{-\infty}^{\infty} P(y|x)P(x)\,\mathrm{d}x, \tag{2.4}$$

where $P(x)$ is the observational distribution of the predictor, and

$$P(y|x) = \frac{1}{\sqrt{2\pi}\sigma_f(x)}\exp\left(-\frac{(y - f(x))^2}{2\sigma_f(x)^2}\right) \tag{2.5}$$

is the conditional probability density of y given x.

The observational distribution $P(x)$ is assumed to be normal with mean and standard deviation from observations. Where the uncertainty of the observations is not available, an uncertainty is conservatively estimated. For the emergent constraint on future OHU using summer sea ice extent from OSI SAF satellite observations (Fig. 2.4), we use $\sigma_{\mathrm{obs}} = 1 \times 10^6\ \mathrm{km}^2$ (see below for a discussion of this uncertainty). Our results are robust to reasonable changes of this parameter (Fig. 2.A.10d).

§ Observational data Our principal source of sea ice extent observations for use in the emergent constraint is the OSI SAF Sea Ice index (EUMETSAT Ocean and Sea Ice Satellite Application Facility 2024b) which is based on Advanced Microwave Scanning Radiometer (AMSR) and Special Sensor Microwave Imager/Sounder (SSMIS) instruments, with daily data available starting in 1978. For the sensitivity analysis (Fig. 2.A.10), we use two additional satellite microwave radiometry products covering the period 1978–2023 (the NASA Team (DiGirolamo et al. 2022) and Bootstrap (Comiso and Gersten 2023) products), as well as reconstructions of past sea ice extent from HadISST2.2 (Titchner and Rayner 2014; Hobbs et al. 2016) and refs. (Fogt et al. 2022; Dalaiden et al. 2023).

Interior ocean temperature and salinity were obtained from the World Ocean Atlas 2018 (Boyer, Tim P. et al. 2023), and potential density calculated from these variables using the Gibbs Seawater (GSW) toolbox for Python (McDougall and Barker 2011).

Ocean heat uptake estimates are from a recent analysis of ocean heat content products (Minière et al. 2023) including the Global Climate Observing System (Schuckmann et al. 2020).

§ Uncertainty in sea ice extent observations An estimate of the total uncertainty in daily sea ice concentration due to algorithm and 'smearing' effects from grid interpolation is provided in the OSI SAF sea ice concentration data (EUMETSAT Ocean and Sea Ice Satellite Application Facility 2024a). However, this uncertainty cannot be simply propagated to the calculation of sea ice extent due to spatial and temporal error correlations (Wernecke et al. 2022). An assessment of Arctic sea ice extent uncertainty from a similar satellite observation product has found that the uncertainty in minimum sea ice area in the Arctic is only half of the inter-product spread. Additionally, instrument uncertainties have previously been found to be only 0.036×10^6 km^2 for Antarctic February sea ice extent in comparable satellite-based sea ice products (Meier and Stewart 2019).

An alternative approach to gauge the uncertainty of the sea ice extent estimate is to assess the spread of estimates computed from different products. The three satellite-based sea ice concentration products we tested which use the OSI SAF (EUMETSAT Ocean and Sea Ice Satellite Application Facility 2024a), Bootstrap (Comiso and Gersten 2023), and NASA Team (DiGirolamo et al. 2022) algorithms only differ by $0.38 \pm 0.23 \times 10^6$ km^2 in their January-February sea ice extent on average.

Reconstructions of sea ice extent covering decades and centuries preceding the satellite era have larger uncertainties, as illustrated by the spread across the three products (Fig. 2.A.11). Nonetheless, there is good agreement between the reconstruction of Fogt et al. (2022) and that of Dalaiden et al. (2023) over the overlapping period, whereas the HadISST2.2 reconstruction shows large, likely spurious step-like variability. We therefore deem the reconstructions of refs. (Fogt et al. 2022; Dalaiden et al. 2023) to be the most reliable. We use these two reconstructions of annual mean sea ice extent to estimate the range of multi-decadal variability across 40-year periods. We find a maximum difference in sea ice extent between 40-year periods of 0.23×10^6 km^2 for the period 1850–1980 in the reconstruction of Dalaiden et al. (2023), and a maximum difference of 0.13×10^6 km^2 for the period 1905–1980 in the reconstruction of Fogt et al. (2022). This is comparable to the CMIP6 multi-model average of historical sea ice extent standard deviation across 40-year periods between 1850–1980 of 0.26×10^6 km^2. This measure of sea ice multi-decadal internal variability in observations and models is an order of magnitude smaller than the inter-model standard deviation of 1850–1980 mean sea ice extent of 3.3×10^6 km^2.

In summary, our best estimate of the uncertainty of sea ice extent would be the sum of the uncertainty estimated from the spread between different products ($0.38 \pm 0.23 \times 10^6$ km^2) and the

uncertainty that arises from internal variability (0.23×10^6 km^2). Here we choose a rather large observational uncertainty of $\sigma_{obs} = 1 \times 10^6$ km^2 to derive a conservative emergent constraint. Varying this parameter does not change the central constrained estimate but influences the uncertainty reduction (Fig. 2.A.10d).

§ Constraint on past ocean heat uptake We find no significant emergent relationship between baseline Antarctic sea ice and past historical OHU. The inter-model correlation coefficient between January-February Antarctic sea ice extent and 1850–2024 OHU is $r = -0.03$ for preindustrial mean sea ice extent and $r = -0.04$ for 1980–2020 mean sea ice extent.

§ Alternative predictors The robustness of the constrained result could further be tested by using Southern Ocean cloud cover or deep-ocean temperatures as predictors to constrain OHU, as both are mechanistically linked to Antarctic sea ice extent (Fig. 2.2). However, a direct comparison between observed and modelled cloud cover requires sampling the CMIP6 ESMs at the same time and location as satellites do. Although this can be done with satellite simulators in ESMs, only 5 out of the 28 ESMs considered here provide this output. In the case of mean deep-ocean temperature, the limited spatio-temporal density of historical temperature measurements below 2000 meters depth entails that such a predictor would have sizeable uncertainty. Moreover, we find that the relationship between mean deep-ocean temperature and future OHU across the model ensemble ($r = -0.44$, $p < 0.05$) is not as strong and linear as the presently used emergent relationship.

Acknowledgements

The authors thank Juliette Mignot and Ric Williams for discussions, as well as Martin Vancoppenolle, Ted Maksym and Kenza Himmich for help with sea ice extent data.

Funding

Swiss National Science Foundation Ambizione project ArcticECO - PZ00P2_209044 (JT)
Woods Hole Oceanographic Institution postdoctoral scholarship (JT, LV)
Woods Hole Oceanographic Institution guest student program (LV)
EU Horizon 2020 research and innovation programme, grant agreement no. 101137673 (TipESM) (LK, TLF)
ENS Chanel research chair (LK)
EU Horizon 2020 research and innovation programme, grant agreement no. 821001 (SO-CHIC) (JBS, CDL, LV)

Authors' contributions

Conceptualization: JT, LV, TLF, LK
Methodology: LV, JT
Investigation: all authors
Visualization: LV
Supervision: JT, JBS, CdL
Funding acquisition: JBS, JT
Project administration: JT
Writing—original draft: LV
Writing—review & editing: all authors

Competing interests

The authors declare that they have no competing interests.

Data availability

Observational and model data used in this study are available at the following locations:

- CMIP6 model output: https://esgf-node.llnl.gov/projects/cmip6/
- World Ocean Atlas ocean temperature and salinity data: https://www.ncei.noaa.gov/archive/accession/NCEI-WOA18
- Radiative kernels from Huang and Huang (2023): https://doi.org/10.17632/vmg3s67568
- Ocean heat content dataset from Minière et al. (2023): available from the corresponding author upon request.
- Cloud cover observational data: https://doi.org/10.24381/cds.68653055
- OSI SAF sea ice extent data: https://doi.org/10.24381/cds.3cd8b812
- HadISST2.2 sea ice extent data: https://www.metoffice.gov.uk/hadobs/hadisst2/data/download.html
- Sea ice extent reconstruction from Fogt et al. (2022): https://doi.org/10.6084/m9.figshare.c.5709767.v1.
- Bootstrap algorithm sea ice extent data: https://nsidc.org/data/nsidc-0079/versions/4#anchor-1.

- NASA Team algorithm sea ice extent data: https://climatedataguide.ucar.edu/climate-data/sea-ice-concentration-data-nasa-goddard-and-nsidc-based-nasa-team-algorithm

2.A Supplementary Information

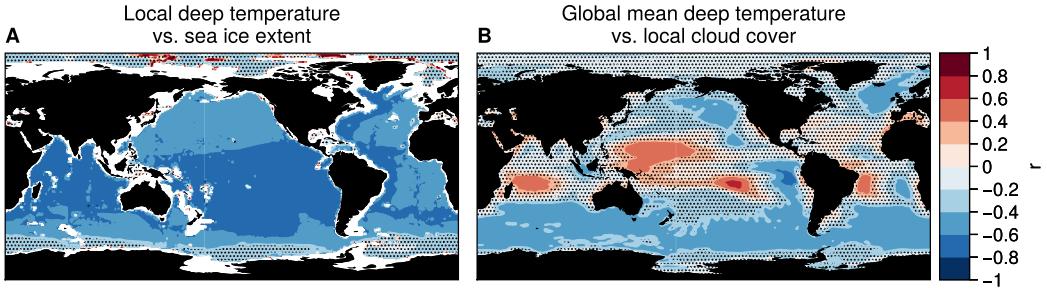

Figure 2.A.1: Relationship between deep ocean temperature and preindustrial surface climate. a, Inter-model correlation between preindustrial local deep ocean temperature (averaged over 2000-4000 m depth) and preindustrial Antarctic annual mean sea ice extent. **b**, Inter-model correlation between preindustrial global mean deep ocean temperature (averaged over 2000-4000 m depth) and preindustrial local total cloud cover. In both panels, stippling indicates regions where the correlation is not significant ($p \geq 0.05$, two-sided).

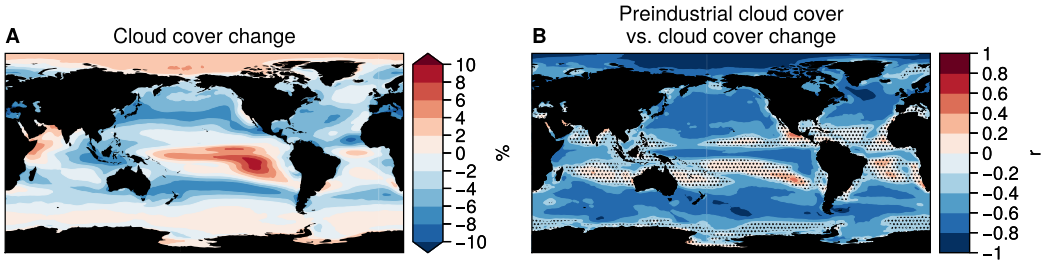

Figure 2.A.2: Changes in cloud cover. a, Change in total cloud cover in 2080-2100 under SSP5-8.5 relative to preindustrial. **b**, Inter-model correlation between local preindustrial cloud cover and local cloud cover change. Blue regions indicate that models with high local initial cloud cover lose more local cloud cover. In panel **a**, the unit of % is the unit of total cloud cover and does not refer to a relative change. In panel **b**, stippling indicates regions where the correlation is not significant ($p \geq 0.05$, two-sided).

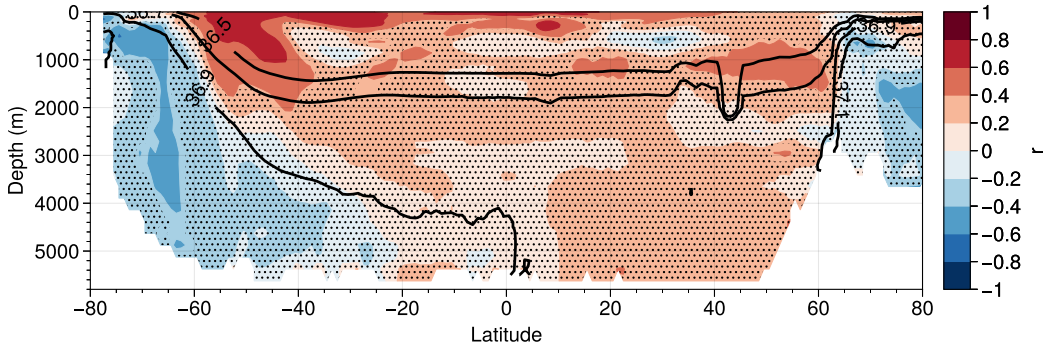

Figure 2.A.3: Zonal mean ocean warming related to preindustrial sea ice. Correlation coefficient across the ensemble of CMIP6 models between preindustrial annual mean Antarctic sea ice extent and zonal mean ocean warming in 2080–2100 under SSP5-8.5 relative to preindustrial. Red shading indicates regions where models with more preindustrial sea ice tend to have more ocean warming in the future scenario. Stippling indicates regions where the correlation is not significant ($p \geq 0.05$, two-sided).

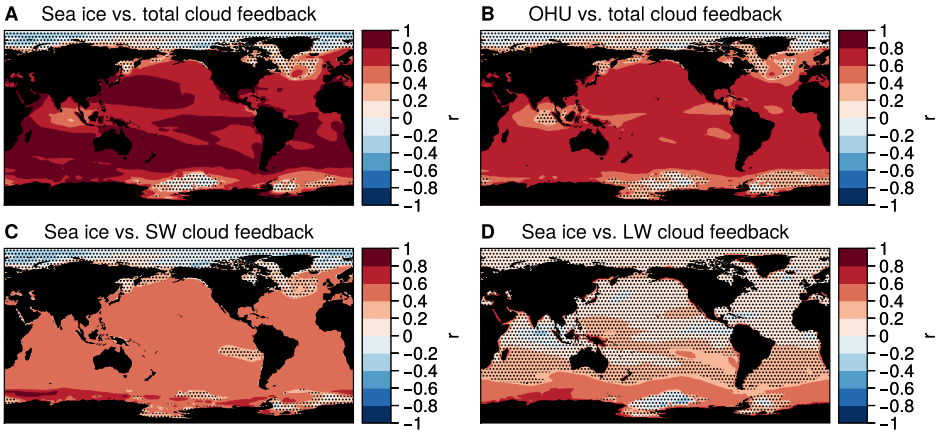

Figure 2.A.4: Relationship between the local cloud feedback and anomalies in sea ice extent and OHU. Inter-model correlation across CMIP6 models under SSP5-8.5 between **a**, local net cloud feedback parameter and Antarctic summer sea ice extent loss by 2080-2100; **b**, local net cloud feedback parameter and total ocean heat uptake from 2024–2100; **c**, as for **a** but with shortwave cloud feedback parameter; and **d**, as for **a** but with longwave cloud feedback parameter. Stippling indicates regions where the correlation is not significant ($p \geq 0.05$, two-sided). In panels **a**, **c** and **d**, red areas indicate locations where models with greater Antarctic sea ice loss tend to have more positive local cloud feedback. In panel **b**, red areas indicate locations where models with more positive local cloud feedback tend to have greater global 2024–2100 OHU.

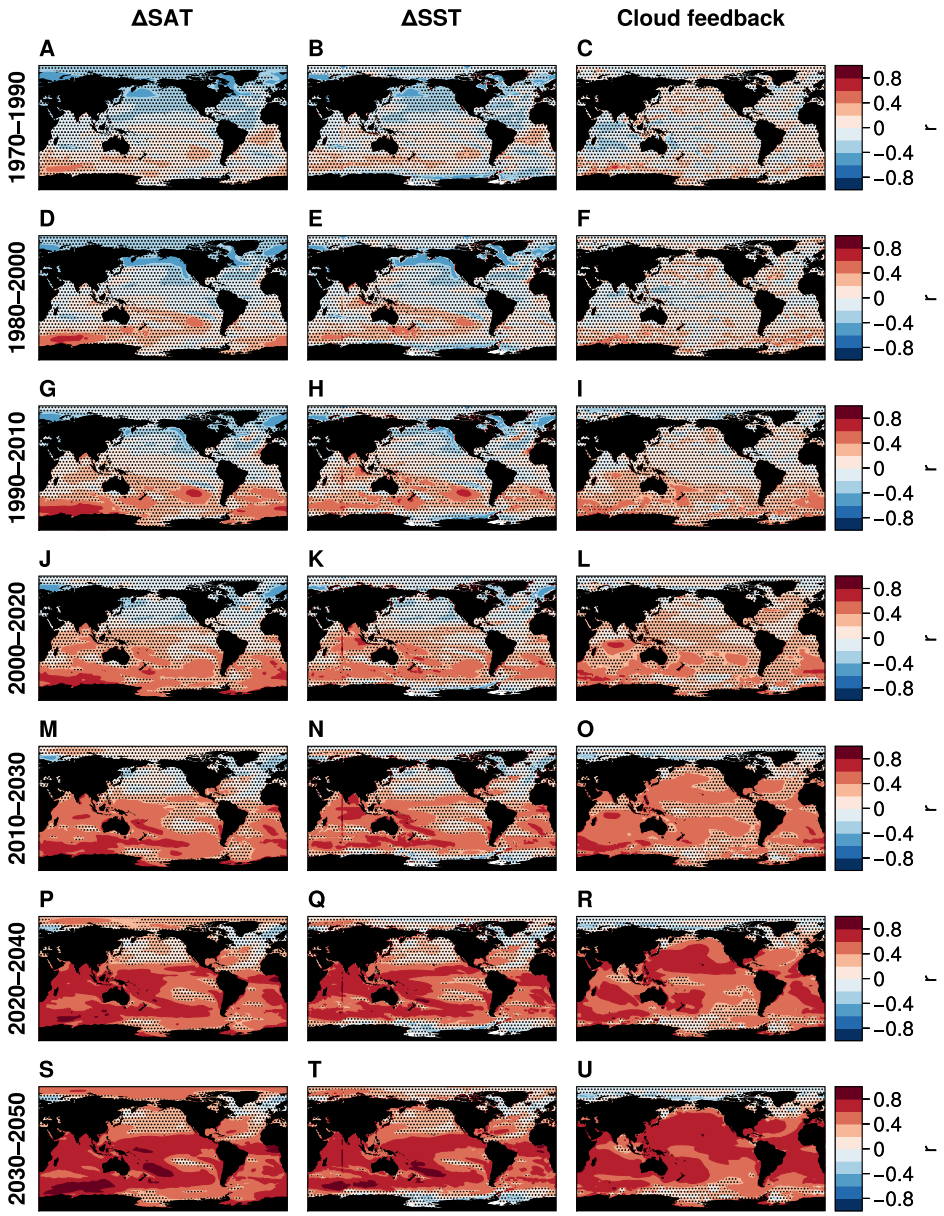

Figure 2.A.5: Time evolution of sea ice–related climate change. Inter-model correlation across CMIP6 models under SSP5-8.5 between preindustrial Antarctic summer sea ice extent and (left column) local surface air temperature anomaly, (middle column) local sea surface temperature anomaly, and (right column) local cloud feedback parameter during progressive 20-year periods between 1970 and 2050. In all panels, stippling indicates regions where the correlation is not significant ($p \geq 0.05$, two-sided).

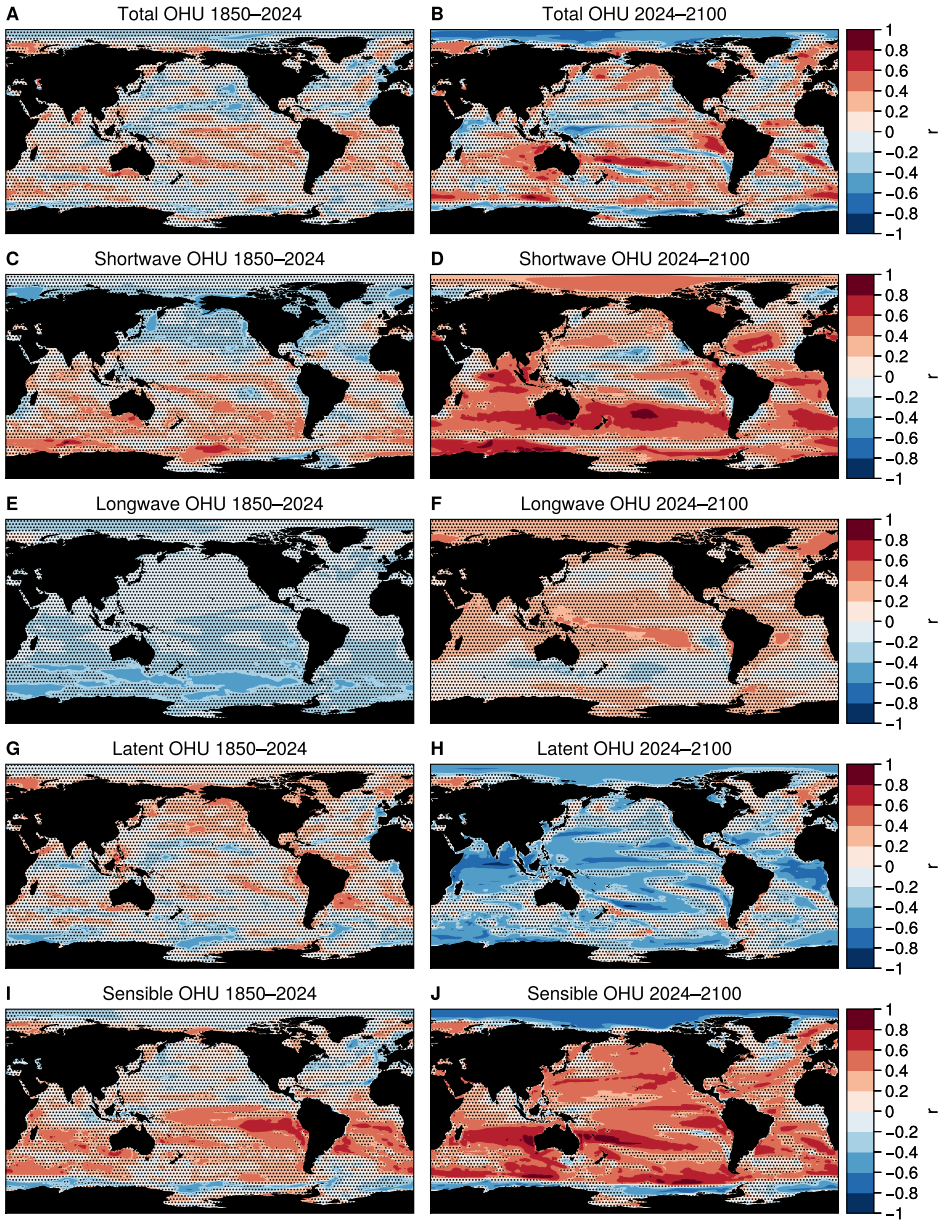

Figure 2.A.6: Relationship between sea ice loss and historical and future OHU components. Left column: Inter-model correlation between total Antarctic summer sea ice loss and historical 1850–2024 total OHU (**a**) as well as OHU from shortwave (**c**), longwave (**e**), latent (**g**), and sensible heat fluxes (**i**). Right column: As left column, but for the future 2024–2100 period. In all panels, stippling indicates regions where the correlation is not significant ($p \geq 0.05$, two-sided).

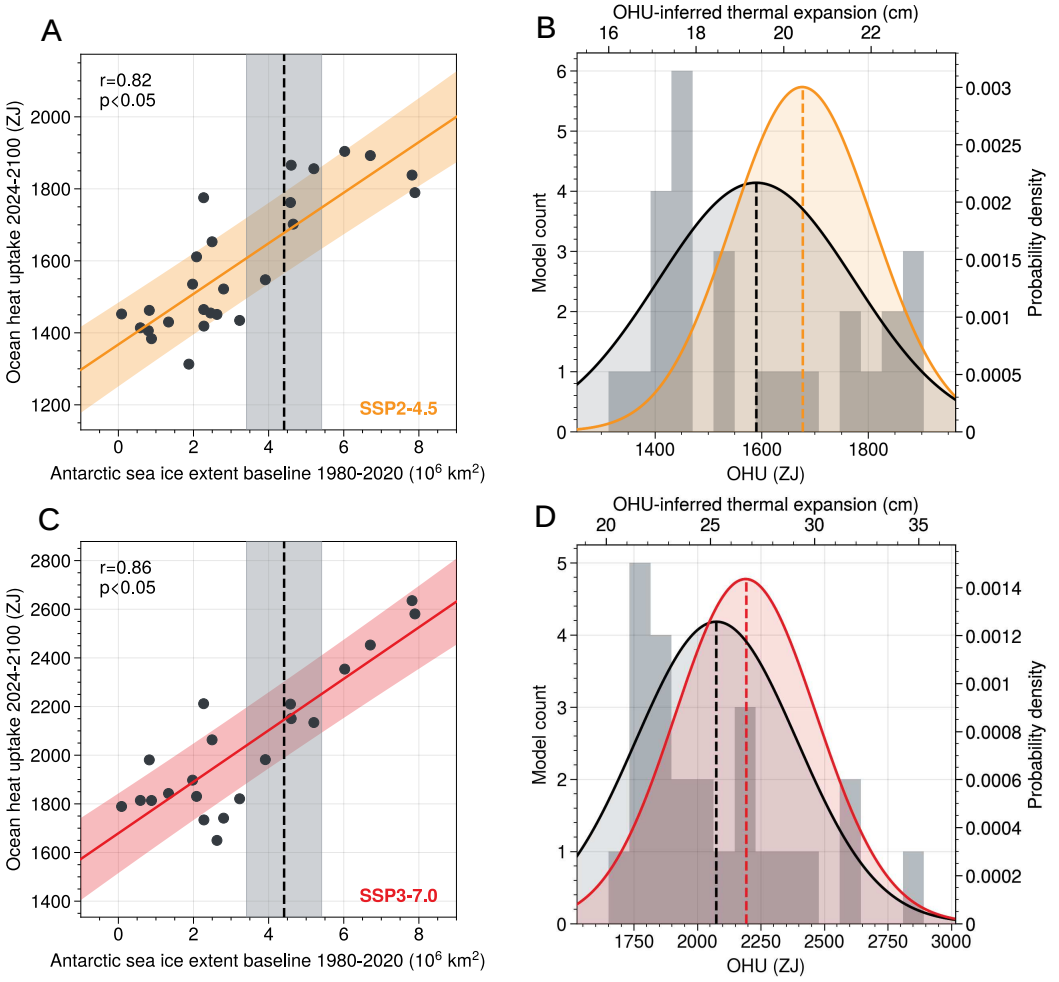

Figure 2.A.7: Emergent constraint on future global ocean heat uptake under SSP2-4.5 and SSP3-7.0. a, Inter-model relationship between 1980-2020 Antarctic summer (January–February) sea ice extent and cumulative global OHU over 2024–2100 under the SSP2-4.5 scenario. The orange line and shading show the least squares linear regression fit and its uncertainty (see Methods), with the Pearson's correlation coefficient r and two-sided p-value given in the upper left corner. The dashed vertical line shows satellite observations of Antarctic summer sea ice extent averaged over 1980–2020 EUMETSAT Ocean and Sea Ice Satellite Application Facility 2024a and the grey shading shows the associated uncertainty of 1×10^6 km^2; this relatively large observational uncertainty ensures we derive a conservative emergent constraint (Methods). **b**, Unconstrained prior (black) and constrained posterior (orange) probability density functions of 2024–2100 global OHU. In grey we show the prior histogram for 2024–2100 OHU (Methods). **c**, as panel **a** but for the SSP3-7.0 scenario. **d**, as panel **b** but for the SSP3-7.0 scenario.

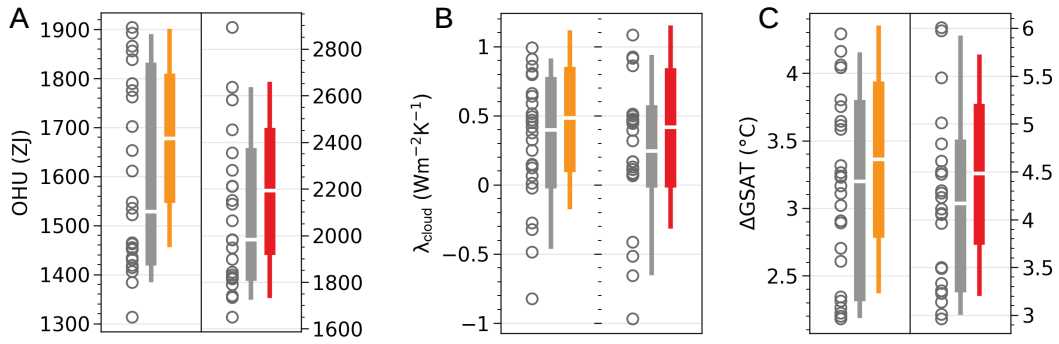

Figure 2.A.8: Constrained distributions of global OHU, cloud feedback, and warming under SSP2-4.5 and SSP3-7.0. Prior and constrained distributions of (**a**) cumulative global OHU from 2024 to 2100, (**b**) global mean cloud feedback parameter in 2080–2100, and (**c**) global mean surface air temperature (GSAT) anomaly in 2080–2100 relative to the preindustrial. In each panel, distributions are shown for SSP2-4.5 (left) and SSP3-7.0 (right). The grey circles and grey boxplots show the prior distribution of model values, and the yellow and red boxplots show the constrained distributions for SSP2-4.5 and SSP3-7.0, respectively. In each boxplot, the white line shows the median, the central box spans the likely range (66%), and the whiskers extend to a 95% confidence interval. The constrained values are normally distributed by construction (Methods). Note that the *y*-axis scale is different between the two SSPs in panels **a** and **c**.

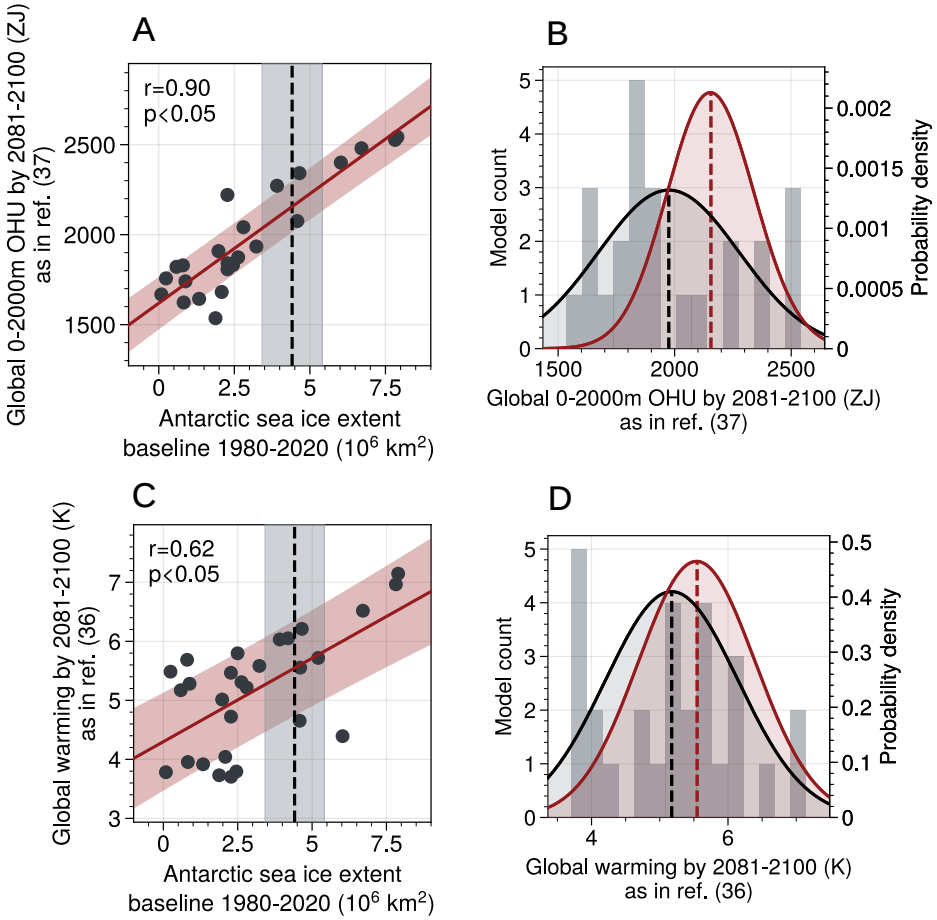

Figure 2.A.9: Emergent constraints on previously published metrics. a, Inter-model relationship between 1980-2020 Antarctic summer (January–February) sea ice extent and 0–2000m OHU in 2081–2100 relative to 2005–2019 under the SSP5-8.5 scenario (as in ref. Lyu et al. 2021). The red line and shading show the least squares linear regression fit and its uncertainty (see Methods), with the Pearson's correlation coefficient r and two-sided p-value given in the upper left corner. The dashed vertical line shows satellite observations of Antarctic summer sea ice extent averaged over 1980–2020 EUMETSAT Ocean and Sea Ice Satellite Application Facility 2024a and the grey shading shows the associated uncertainty of 1×10^6 km^2. **b**, Unconstrained prior (black) and constrained posterior (red) probability density functions of 0–2000m global OHU. In grey we show the prior histogram for 0–2000m OHU. **c**, as panel **a** but for global mean atmospheric surface warming in 2081–2100 relative to 1850–1900 under the SSP5-8.5 scenario (as in ref. Tokarska et al. 2020). **d**, as panel **b** but for global mean atmospheric surface warming as in panel **c**.

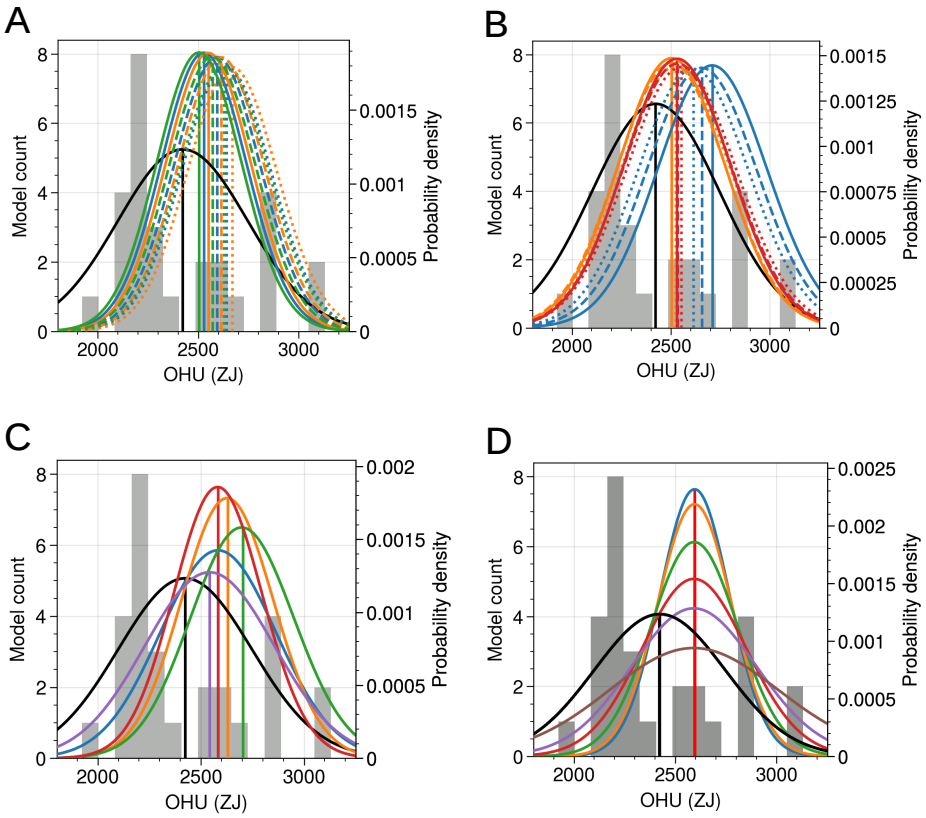

Figure 2.A.10: Robustness of emergent constraint to parameter choices. Prior OHU histograms and probability density functions (PDFs) as in Fig. 2.4, and posterior PDFs obtained from different parameter choices. **a**, Different satellite January–February sea ice extent observation sources: OSI SAF (blue), Bootstrap (orange), and NASA Team (green) using different time periods (solid: 1980–2000, dashed: 1990–2010, dotted: 2000–2020). **b**, Different pre-satellite era yearly sea ice extent observation sources: HadISST2.2 (blue), and reconstructions from ref.Dalaiden et al. 2023 (red) and ref.Fogt et al. 2022 (orange), using different time periods (solid: 1920–1960, dashed: 1940–1980, dotted: 1960–2000). **c**, Different season definitions for sea ice extent baseline from the OSI SAF satellite product EUMETSAT Ocean and Sea Ice Satellite Application Facility 2024a: yearly (blue), January-February–March (orange), February-March (green), January-February (red), July-August-September (purple). **d**, Different observational uncertainties for January–February sea ice extent from the OSI SAF satellite product: 0.2×10^6 km^2 (blue), 0.5×10^6 km^2 (orange), 1×10^6 km^2 (green), 1.5×10^6 km^2 (red), 2×10^6 km^2 (purple), 3×10^6 km^2 (brown).

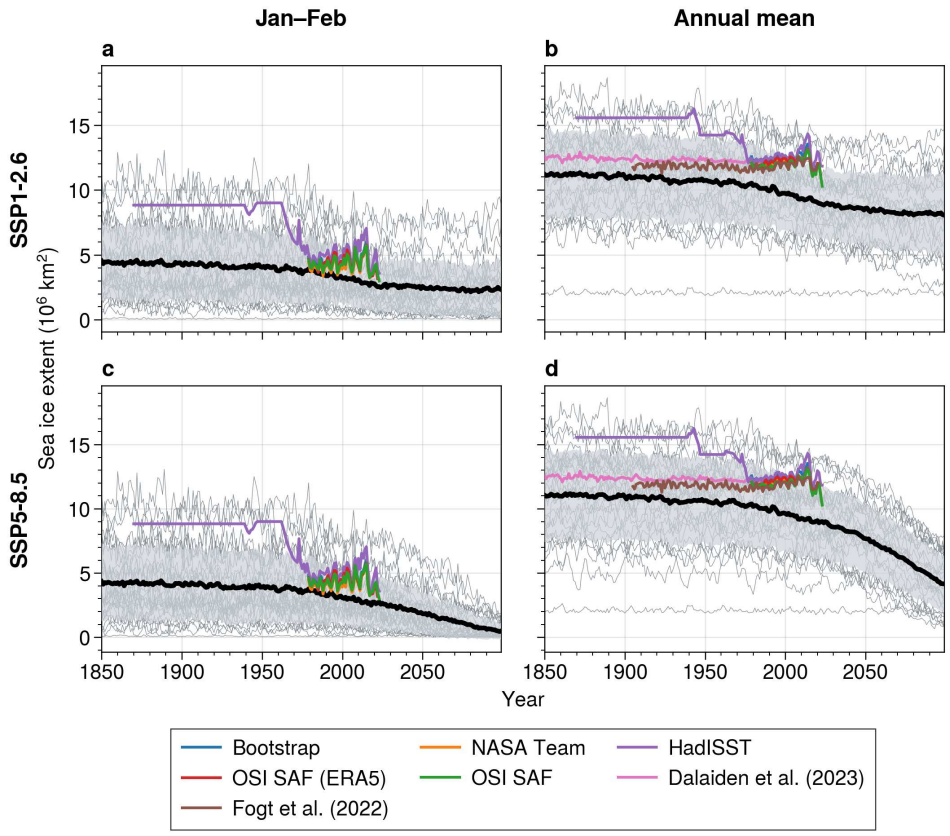

Figure 2.A.11: Time series of observed and simulated Antarctic sea ice extent. Antarctic sea ice extent simulated by individual CMIP6 models (thin grey lines) and in the ensemble mean (bold black line), and in observational products (colored lines). Model time series extend to 2100 under SSP1-2.6 (**a**,**b**) and SSP5-8.5 (**c**,**d**). Yearly values are calculated for (left column) January–February, and (right column) the annual mean.

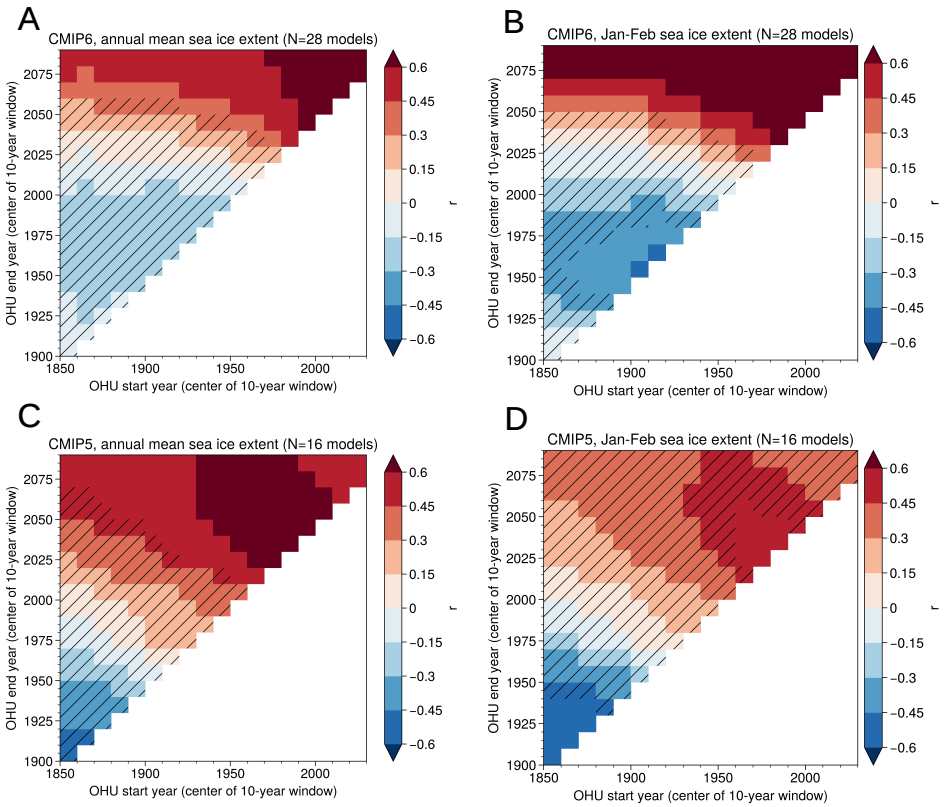

Figure 2.A.12: Sea ice – OHU correlation in CMIP5 and CMIP6 for different values of OHU time period. Heatmaps of the correlation coefficient between 1980–2020 Antarctic (left column) annual or (right column) January–February sea ice extent and global OHU in (**a**–**b**) CMIP5 under RCP8.5 forcing and (**c**–**d**) CMIP6 under SSP5-8.5 forcing, for different OHU time periods. Stippling indicates parameter values where the sea ice – OHU correlation is not statistically significant (p >= 0.05, two-sided).

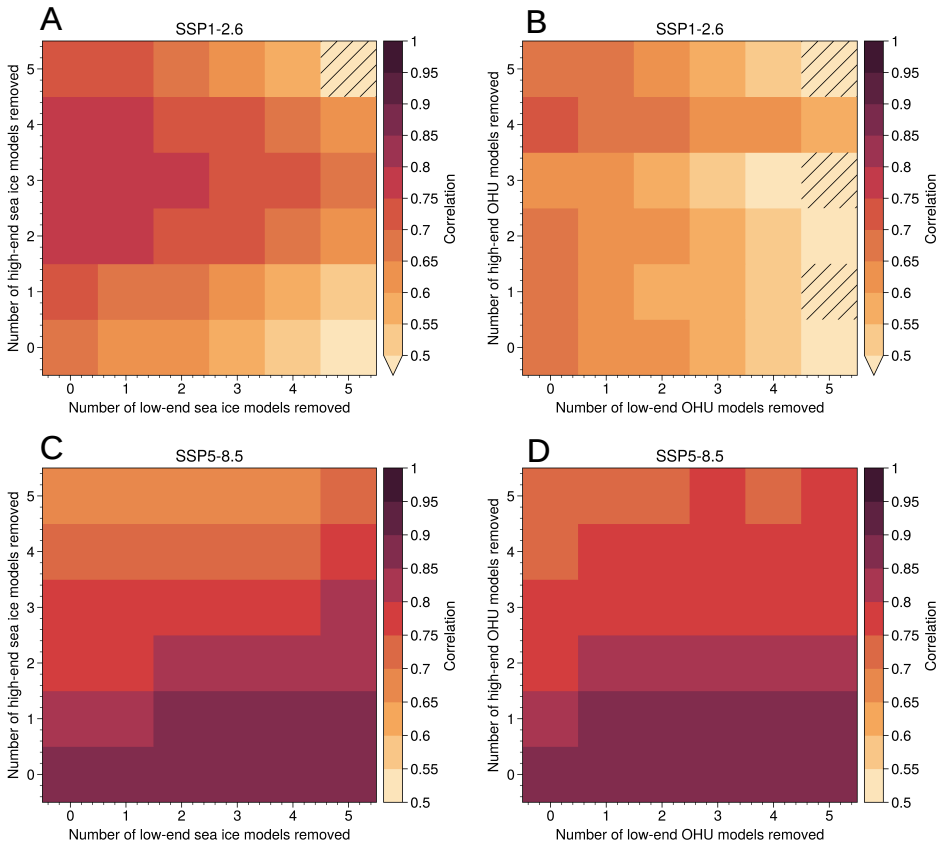

Figure 2.A.13: Robustness of sea ice – OHU correlation to removing extreme model values. Heatmaps of the correlation coefficient between 1980–2020 Antarctic summer sea ice extent and future (2024–2100) global OHU under (**a**–**b**) SSP1-2.6 and (**c**–**d**) SSP5-8.5 when removing a number of models with the highest or lowest sea ice extent (left column), and the highest or lowest future OHU (right column). Stippling indicates parameter values where the sea ice – OHU correlation is not statistically significant (p >= 0.05, two-sided).

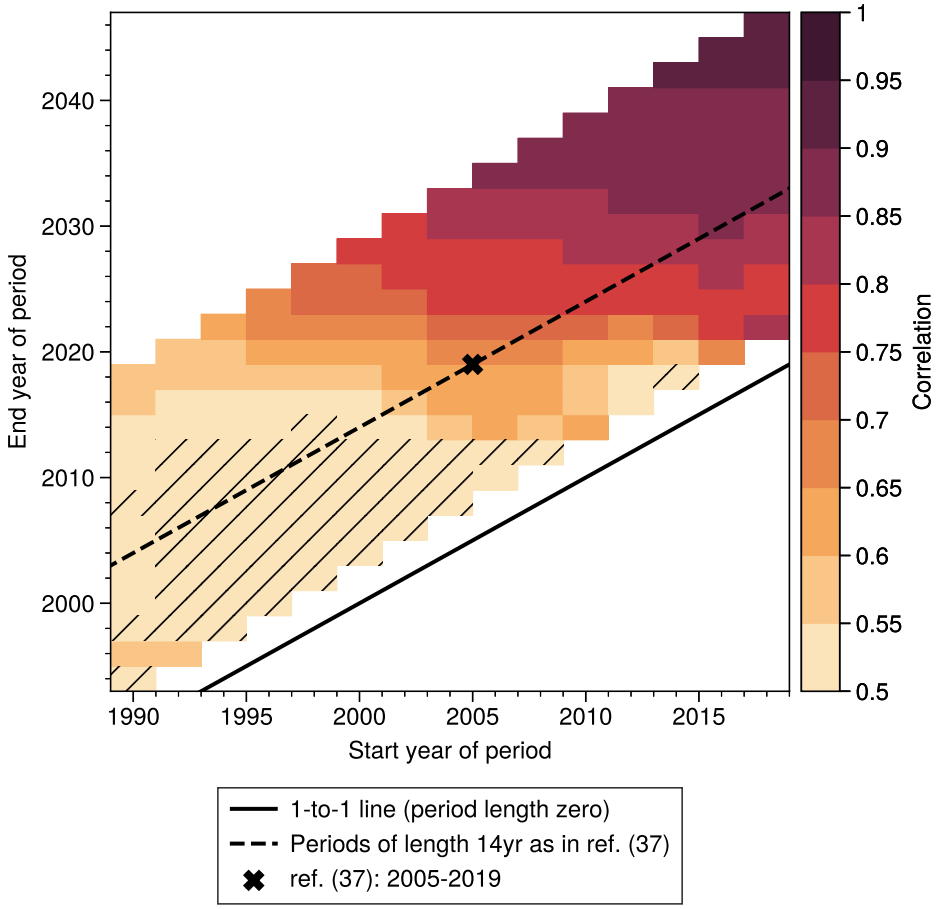

Figure 2.A.14: Sensitivity of OHU constraint based on past warming. Heatmap of the correlation coefficient between past OHU and future (2081–2100 vs. past) OHU among CMIP6 models under SSP5-8.5 forcing for different choices of the start and end year of the past time period.

Model	Modeling center	Reference	missing SSPs[1]
CanESM5	CCCma	Swart et al. 2019	—
CanESM5-CanOE[2]			—
CMCC-CM2-SR5	CMCC	Cherchi et al. 2019	—
CMCC-ESM2		Lovato et al. 2022	—
CNRM-CM6-1	CNRM-CERFACS	Voldoire et al. 2019	—
CNRM-CM6-1-HR			—
CNRM-ESM2-1		Séférian et al. 2019	—
ACCESS-ESM1-5	CSIRO	Ziehn et al. 2020	—
ACCESS-CM2	CSIRO-ARCCSS	Bi et al. 2020	—
EC-Earth3	EC-Earth-Consortium	Döscher et al. 2022	—
EC-Earth3-CC			ssp126, ssp245, ssp370
EC-Earth3-Veg			—
EC-Earth3-Veg-LR			—
IPSL-CM6A-LR	IPSL	Boucher et al. 2020	—
MIROC6	MIROC	Tatebe et al. 2019	—
HadGEM3-GC31-LL	MOHC	Andrews et al. 2020	ssp370
HadGEM3-GC31-MM			ssp245, ssp370
UKESM1-0-LL		Sellar et al. 2019	—
MPI-ESM1-2-HR	MPI-M	Gutjahr et al. 2019	—
MPI-ESM1-2-LR			—
MRI-ESM2-0	MRI	Yukimoto et al. 2019	—
GISS-E2-1-G	NASA-GISS	Kelley et al. 2020	—
CESM2	NCAR	Danabasoglu et al. 2020	—
CESM2-WACCM			—
NorESM2-LM	NCC	Seland et al. 2020	—
NorESM2-MM			—
GFDL-CM4	NOAA-GFDL	Held et al. 2019	ssp126, ssp370
GFDL-ESM4		Dunne et al. 2020	ssp126

Table 2.A.1: CMIP6 models used in this study. [1]Models for which essential output variables (`hfds` and `siconc`) are unavailable for any of the SSP1-2.6, SSP2-4.5, or SSP3-7.0 scenarios.

Future scenario		OHU (ZJ)	SLR (cm)	ΔGSAT (°C)	λ_{cloud} (W m^{-2} K^{-1})
SSP1-2.6 (n = 25)	corr(X, SIE)	r = 0.66*	r = 0.66*	r = 0.45*	r = 0.64*
	prior	1205 ± 163	14.7 ± 2.0	2.25 ± 0.52	0.43 ± 0.47
	constrained	1244 ± 141	15.2 ± 1.7	2.36 ± 0.51	0.51 ± 0.41
SSP2-4.5 (n = 26)	corr(X, SIE)	r = 0.82*	r = 0.82*	r = 0.56*	r = 0.66*
	prior	1528 ± 178	18.6 ± 2.2	3.20 ± 0.63	0.40 ± 0.43
	constrained	1678* ± 129	20.5* ± 1.6	3.36 ± 0.58	0.48 ± 0.37
SSP3-7.0 (n = 24)	corr(X, SIE)	r = 0.64*	r = 0.64*	r = 0.62*	r = 0.63*
	prior	1981 ± 308	24.2 ± 3.8	4.17 ± 0.82	0.24 ± 0.48
	constrained	2193 ± 270	26.7 ± 3.3	4.48 ± 0.73	0.42 ± 0.42
SSP5-8.5 (n = 28)	corr(X, SIE)	r = 0.87*	r = 0.87*	r = 0.61*	r = 0.71*
	prior	2273 ± 314	27.7 ± 3.8	5.36 ± 0.93	0.48 ± 0.42
	constrained	2595* ± 208	31.6* ± 2.5	5.52 ± 0.83	0.63* ± 0.35

Table 2.A.2: Emergent constraints across scenarios. For each variable and each SSP, this table gives the inter-model correlation (Pearson's r-value) between 1980–2020 Antarctic summer sea ice extent (SIE) and the respective future variable (X), as well as the unconstrained and constrained median values of X. Correlation r-values with an asterisk indicate significant correlations at the $p < 0.05$ level according to a two-sided Student's t-test. Constrained values with an asterisk indicate significant difference between unconstrained and constrained mean values at the $p < 0.05$ level according to a two-sided Student's t-test. Uncertainty ranges express the 66% *likely* range. Variable abbreviations stand for ocean heat uptake (OHU), global mean sea level rise from thermal expansion (SLR), global mean surface air temperature warming (ΔGSAT), and global mean cloud feedback parameter (λ_{cloud}); see Methods.

Bibliography

Andrews, M. B. et al. (2020). "Historical Simulations With HadGEM3-GC3.1 for CMIP6". *Journal of Advances in Modeling Earth Systems* 12:6, e2019MS001995. ISSN: 1942-2466. DOI: 10.1029/2019MS001995.

Andrews, T. et al. (2022). "On the Effect of Historical SST Patterns on Radiative Feedback". *Journal of Geophysical Research: Atmospheres* 127:18. _eprint: https://onlinelibrary.wiley.com/doi/pdf/10.1029/2022JD036675, e2022JD036675. ISSN: 2169-8996. DOI: 10.1029/2022JD036675.

Armour, K. C., C. M. Bitz, and G. H. Roe (2013). "Time-Varying Climate Sensitivity from Regional Feedbacks". *Journal of Climate* 26:13. Publisher: American Meteorological Society Section: Journal of Climate, pp. 4518–4534. ISSN: 0894-8755, 1520-0442. DOI: 10.1175/JCLI-D-12-00544.1.

Armour, K. C., J. Marshall, J. R. Scott, A. Donohoe, and E. R. Newsom (2016). "Southern Ocean warming delayed by circumpolar upwelling and equatorward transport". *Nature Geoscience* 9:7. Number: 7 Publisher: Nature Publishing Group, pp. 549–554. ISSN: 1752-0908. DOI: 10.1038/ngeo2731.

Armour, K. C. et al. (2024). "Sea-surface temperature pattern effects have slowed global warming and biased warming-based constraints on climate sensitivity". *Proceedings of the National Academy of Sciences* 121:12. Publisher: Proceedings of the National Academy of Sciences, e2312093121. DOI: 10.1073/pnas.2312093121.

Ayres, H. C., J. A. Screen, E. W. Blockley, and T. J. Bracegirdle (2022). "The Coupled Atmosphere–Ocean Response to Antarctic Sea Ice Loss". *Journal of Climate* 35:14. Publisher: American Meteorological Society Section: Journal of Climate, pp. 4665–4685. ISSN: 0894-8755, 1520-0442. DOI: 10.1175/JCLI-D-21-0918.1.

Beadling, R. L. et al. (2020). "Representation of Southern Ocean Properties across Coupled Model Intercomparison Project Generations: CMIP3 to CMIP6". *Journal of Climate* 33:15. Publisher: American Meteorological Society Section: Journal of Climate, pp. 6555–6581. ISSN: 0894-8755, 1520-0442. DOI: 10.1175/JCLI-D-19-0970.1.

Bi, D. et al. (2020). "Configuration and Spin-up of ACCESS-CM2, the New Generation Australian Community Climate and Earth System Simulator Coupled Model". *Journal of Southern*

Hemisphere Earth Systems Science 70:1, pp. 225–251. ISSN: 2206-5865. DOI: 10.1071/ES19040.

Bopp, L. et al. (2013). "Multiple stressors of ocean ecosystems in the 21st century: projections with CMIP5 models". *Biogeosciences* 10:10. Publisher: Copernicus GmbH, pp. 6225–6245. ISSN: 1726-4170. DOI: 10.5194/bg-10-6225-2013.

Boucher, O. et al. (2020). "Presentation and Evaluation of the IPSL-CM6A-LR Climate Model". *Journal of Advances in Modeling Earth Systems* 12:7, e2019MS002010. ISSN: 1942-2466. DOI: 10.1029/2019MS002010.

Bourgeois, T., N. Goris, J. Schwinger, and J. F. Tjiputra (2022). "Stratification constrains future heat and carbon uptake in the Southern Ocean between 30°S and 55°S". *Nature Communications* 13:1. Bandiera_abtest: a Cc_license_type: cc_by Cg_type: Nature Research Journals Number: 1 Primary_atype: Research Publisher: Nature Publishing Group Subject_term: Biogeochemistry;Carbon cycle;Marine chemistry;Physical oceanography Subject_term_id: biogeochemistry;carbon-cycle;marine-chemistry;physical-oceanography, p. 340. ISSN: 2041-1723. DOI: 10.1038/s41467-022-27979-5.

Boyer, Tim P. et al. (2023). *World Ocean Atlas 2018*.

Cazenave, A. and W. Llovel (2010). "Contemporary Sea Level Rise". *Annual Review of Marine Science* 2, Volume 2, 2010. Publisher: Annual Reviews, pp. 145–173. ISSN: 1941-1405, 1941-0611. DOI: 10.1146/annurev-marine-120308-081105.

Ceppi, P., F. Brient, M. D. Zelinka, and D. L. Hartmann (2017). "Cloud feedback mechanisms and their representation in global climate models". *WIREs Climate Change* 8:4. _eprint: https://onlinelibrary.wiley.com/doi/pdf/10.1002/wcc.465, e465. ISSN: 1757-7799. DOI: 10.1002/wcc.465.

Cesana, G. V. and A. D. Del Genio (2021). "Observational constraint on cloud feedbacks suggests moderate climate sensitivity". *Nature Climate Change* 11:3. Number: 3 Publisher: Nature Publishing Group, pp. 213–218. ISSN: 1758-6798. DOI: 10.1038/s41558-020-00970-y.

Cheng, L. et al. (2022). "Past and future ocean warming". *Nature Reviews Earth & Environment*. Publisher: Nature Publishing Group, pp. 1–19. ISSN: 2662-138X. DOI: 10.1038/s43017-022-00345-1.

Cherchi, A. et al. (2019). "Global Mean Climate and Main Patterns of Variability in the CMCC-CM2 Coupled Model". *Journal of Advances in Modeling Earth Systems* 11:1, pp. 185–209. ISSN: 1942-2466. DOI: 10.1029/2018MS001369.

Cheung, W. W. L., G. Reygondeau, and T. L. Frölicher (2016). "Large Benefits to Marine Fisheries of Meeting the 1.5°C Global Warming Target". *Science* 354:6319, pp. 1591–1594. DOI: 10.1126/science.aag2331.

Comiso, J. C. and R. Gersten (2023). *Bootstrap Sea Ice Concentrations from Nimbus-7 SMMR and DMSP SSM/I-SSMIS, Version 4*. DOI: 10.5067/X5LG68MH013O.

Cox, P. M., C. Huntingford, and M. S. Williamson (2018). "Emergent constraint on equilibrium climate sensitivity from global temperature variability". *Nature* 553:7688. Number: 7688 Publisher: Nature Publishing Group, pp. 319–322. ISSN: 1476-4687. DOI: 10.1038/nature25450.

Cox, P. M. et al. (2013). "Sensitivity of tropical carbon to climate change constrained by carbon dioxide variability". *Nature* 494:7437. Number: 7437 Publisher: Nature Publishing Group, pp. 341–344. ISSN: 1476-4687. DOI: 10.1038/nature11882.

Dalaiden, Q. et al. (2023). "An Unprecedented Sea Ice Retreat in the Weddell Sea Driving an Overall Decrease of the Antarctic Sea-Ice Extent Over the 20th Century". *Geophysical Research Letters* 50:21, e2023GL104666. ISSN: 1944-8007. DOI: 10.1029/2023GL104666.

Danabasoglu, G. et al. (2020). "The Community Earth System Model Version 2 (CESM2)". *Journal of Advances in Modeling Earth Systems* 12:2, e2019MS001916. ISSN: 1942-2466. DOI: 10.1029/2019MS001916.

DiGirolamo, N., C. Parkinson, D. Cavalieri, P. Gloersen, and H. Zwally (2022). *Sea Ice Concentrations from Nimbus-7 SMMR and DMSP SSM/I-SSMIS Passive Microwave Data*. DOI: 10.5067/MPYG15WAA4WX.

Döscher, R. et al. (2022). "The EC-Earth3 Earth system model for the Coupled Model Intercomparison Project 6". *Geoscientific Model Development* 15:7. Publisher: Copernicus GmbH, pp. 2973–3020. ISSN: 1991-959X. DOI: 10.5194/gmd-15-2973-2022.

Dunne, J. P. et al. (2020). "The GFDL Earth System Model Version 4.1 (GFDL-ESM 4.1): Overall Coupled Model Description and Simulation Characteristics". *Journal of Advances in Modeling Earth Systems* 12:11, e2019MS002015. ISSN: 1942-2466. DOI: 10.1029/2019MS002015.

England, M. R., L. M. Polvani, and L. Sun (2020a). "Robust Arctic warming caused by projected Antarctic sea ice loss". *Environmental Research Letters* 15:10. Publisher: IOP Publishing, p. 104005. ISSN: 1748-9326. DOI: 10.1088/1748-9326/abaada.

England, M. R., L. M. Polvani, L. Sun, and C. Deser (2020b). "Tropical climate responses to projected Arctic and Antarctic sea-ice loss". *Nature Geoscience* 13:4. Number: 4 Publisher: Nature Publishing Group, pp. 275–281. ISSN: 1752-0908. DOI: 10.1038/s41561-020-0546-9.

England, M. H. et al. (2014). "Recent intensification of wind-driven circulation in the Pacific and the ongoing warming hiatus". *Nature Climate Change* 4:3. Publisher: Nature Publishing Group, pp. 222–227. ISSN: 1758-6798. DOI: 10.1038/nclimate2106.

EUMETSAT Ocean and Sea Ice Satellite Application Facility (2024a). *OSI SAF Global Sea Ice Concentration (SSMIS)*. DOI: doi:10.15770/EUM_SAF_OSI_NRT_2004.

– (2024b). *OSI SAF Sea Ice Index 1978-Onwards, Version 2.2*.

Eyring, V. et al. (2016). "Overview of the Coupled Model Intercomparison Project Phase 6 (CMIP6) experimental design and organization". *Geoscientific Model Development* 9:5, pp. 1937–1958. ISSN: 1991-9603. DOI: 10.5194/gmd-9-1937-2016.

Fogt, R. L., A. M. Sleinkofer, M. N. Raphael, and M. S. Handcock (2022). "A regime shift in seasonal total Antarctic sea ice extent in the twentieth century". *Nature Climate Change* 12:1. Number: 1 Publisher: Nature Publishing Group, pp. 54–62. ISSN: 1758-6798. DOI: 10.1038/s41558-021-01254-9.

Forster, P. et al. (2021). "The Earth's energy budget, climate feedbacks, and climate sensitivity". In: *Climate Change 2021: The Physical Science Basis. Contribution of Working Group I to the Sixth Assessment Report of the Intergovernmental Panel on Climate Change*. Ed. by V. Masson-Delmotte et al. Cambridge University Press, Cambridge, United Kingdom and New York, NY, USA, pp. 923–1054. DOI: 10.1017/9781009157896.001.

Fox-Kemper, B. et al. (2021). "Ocean, cryosphere, and sea level change". In: *Climate Change 2021: The Physical Science Basis. Contribution of Working Group I to the Sixth Assessment Report of the Intergovernmental Panel on Climate Change*. Ed. by V. Masson-Delmotte et al. Cambridge University Press, Cambridge, United Kingdom and New York, NY, USA, pp. 1211–1362. DOI: 10.1017/9781009157896.001.

Frölicher, T. L., E. M. Fischer, and N. Gruber (2018). "Marine heatwaves under global warming". *Nature* 560:7718. Number: 7718 Publisher: Nature Publishing Group, pp. 360–364. ISSN: 1476-4687. DOI: 10.1038/s41586-018-0383-9.

Frölicher, T. L. et al. (2015). "Dominance of the Southern Ocean in Anthropogenic Carbon and Heat Uptake in CMIP5 Models". *Journal of Climate* 28:2. Publisher: American Meteorological Society Section: Journal of Climate, pp. 862–886. ISSN: 0894-8755, 1520-0442. DOI: 10.1175/JCLI-D-14-00117.1.

Gupta, A. S., N. C. Jourdain, J. N. Brown, and D. Monselesan (2013). "Climate Drift in the CMIP5 Models". *Journal of Climate* 26:21, pp. 8597–8615. ISSN: 0894-8755, 1520-0442. DOI: 10.1175/JCLI-D-12-00521.1.

Gutjahr, O. et al. (2019). "Max Planck Institute Earth System Model (MPI-ESM1.2) for the High-Resolution Model Intercomparison Project (HighResMIP)". *Geoscientific Model Development* 12:7, pp. 3241–3281. ISSN: 1991-959X. DOI: 10.5194/gmd-12-3241-2019.

Hall, A., P. Cox, C. Huntingford, and S. Klein (2019). "Progressing emergent constraints on future climate change". *Nature Climate Change* 9:4. Number: 4 Publisher: Nature Publishing Group, pp. 269–278. ISSN: 1758-6798. DOI: 10.1038/s41558-019-0436-6.

Held, I. M. et al. (2019). "Structure and Performance of GFDL's CM4.0 Climate Model". *Journal of Advances in Modeling Earth Systems* 11:11, pp. 3691–3727. ISSN: 1942-2466. DOI: 10.1029/2019MS001829.

Hobbs, W. et al. (2024). "Observational Evidence for a Regime Shift in Summer Antarctic Sea Ice". *Journal of Climate* -1:aop. ISSN: 0894-8755, 1520-0442. DOI: 10.1175/JCLI-D-23-0479.1.

Hobbs, W. R. et al. (2016). "A review of recent changes in Southern Ocean sea ice, their drivers and forcings". *Global and Planetary Change* 143, pp. 228–250. ISSN: 0921-8181. DOI: 10.1016/j.gloplacha.2016.06.008.

Huang, H. and Y. Huang (2023). "Radiative sensitivity quantified by a new set of radiation flux kernels based on the ECMWF Reanalysis v5 (ERA5)". *Earth System Science Data* 15:7. Publisher: Copernicus GmbH, pp. 3001–3021. ISSN: 1866-3508. DOI: 10.5194/essd-15-3001-2023.

Hyder, P. et al. (2018). "Critical Southern Ocean climate model biases traced to atmospheric model cloud errors". *Nature Communications* 9:1. Number: 1 Publisher: Nature Publishing Group, p. 3625. ISSN: 2041-1723. DOI: 10.1038/s41467-018-05634-2.

Jiménez-de-la-Cuesta, D. and T. Mauritsen (2019). "Emergent constraints on Earth's transient and equilibrium response to doubled CO2 from post-1970s global warming". *Nature Geoscience* 12:11. Number: 11 Publisher: Nature Publishing Group, pp. 902–905. ISSN: 1752-0908. DOI: 10.1038/s41561-019-0463-y.

Johnson, G. C. and J. M. Lyman (2020). "Warming trends increasingly dominate global ocean". *Nature Climate Change* 10:8. Number: 8 Publisher: Nature Publishing Group, pp. 757–761. ISSN: 1758-6798. DOI: 10.1038/s41558-020-0822-0.

Joos, F., G.-K. Plattner, T. F. Stocker, O. Marchal, and A. Schmittner (1999). "Global Warming and Marine Carbon Cycle Feedbacks on Future Atmospheric CO2". *Science* 284:5413, pp. 464–467. DOI: 10.1126/science.284.5413.464.

Kajtar, J. B. et al. (2021). "CMIP5 Intermodel Relationships in the Baseline Southern Ocean Climate System and With Future Projections". *Earth's Future* 9:6, e2020EF001873. ISSN: 2328-4277. DOI: 10.1029/2020EF001873.

Kang, S. M., P. Ceppi, Y. Yu, and I.-S. Kang (2023). "Recent global climate feedback controlled by Southern Ocean cooling". *Nature Geoscience* 16:9. Number: 9 Publisher: Nature Publishing Group, pp. 775–780. ISSN: 1752-0908. DOI: 10.1038/s41561-023-01256-6.

Kay, J. E. et al. (2014). "Processes controlling Southern Ocean shortwave climate feedbacks in CESM". *Geophysical Research Letters* 41:2. _eprint: https://onlinelibrary.wiley.com/doi/pdf/10.1002/2013GL058315, pp. 616–622. ISSN: 1944-8007. DOI: 10.1002/2013GL058315.

Kelley, M. et al. (2020). "GISS-E2.1: Configurations and Climatology". *Journal of Advances in Modeling Earth Systems* 12:8. _eprint: https://onlinelibrary.wiley.com/doi/pdf/10.1029/2019MS002025, e2019MS002025. ISSN: 1942-2466. DOI: 10.1029/2019MS002025.

Kwiatkowski, L. et al. (2017). "Emergent constraints on projections of declining primary production in the tropical oceans". *Nature Climate Change* 7:5. Number: 5 Publisher: Nature Publishing Group, pp. 355–358. ISSN: 1758-6798. DOI: 10.1038/nclimate3265.

Liang, Y., N. P. Gillett, and A. H. Monahan (2024). "Accounting for Pacific climate variability increases projected global warming". *Nature Climate Change* 14:6. Publisher: Nature Publishing Group, pp. 608–614. ISSN: 1758-6798. DOI: 10.1038/s41558-024-02017-y.

Liu, W., S.-P. Xie, and J. Lu (2016). "Tracking Ocean Heat Uptake during the Surface Warming Hiatus". *Nature Communications* 7:1, p. 10926. ISSN: 2041-1723. DOI: 10.1038/ncomms10926.

Lovato, T. et al. (2022). "CMIP6 Simulations With the CMCC Earth System Model (CMCC-ESM2)". *Journal of Advances in Modeling Earth Systems* 14:3, e2021MS002814. ISSN: 1942-2466. DOI: 10.1029/2021MS002814.

Luo, F., J. Ying, T. Liu, and D. Chen (2023). "Origins of Southern Ocean warm sea surface temperature bias in CMIP6 models". *npj Climate and Atmospheric Science* 6:1. Number: 1 Publisher: Nature Publishing Group, pp. 1–8. ISSN: 2397-3722. DOI: 10.1038/s41612-023-00456-6.

Lyu, K., X. Zhang, and J. A. Church (2021). "Projected ocean warming constrained by the ocean observational record". *Nature Climate Change* 11:10. Number: 10 Publisher: Nature Publishing Group, pp. 834–839. ISSN: 1758-6798. DOI: 10.1038/s41558-021-01151-1.

Marshall, J. and K. Speer (2012). "Closure of the meridional overturning circulation through Southern Ocean upwelling". *Nature Geoscience* 5:3. Bandiera_abtest: a Cg_type: Nature Research Journals Number: 3 Primary_atype: Reviews Publisher: Nature Publishing Group Subject_term: Physical oceanography Subject_term_id: physical-oceanography, pp. 171–180. ISSN: 1752-0908. DOI: 10.1038/ngeo1391.

Marshall, J. et al. (2015). "The ocean's role in the transient response of climate to abrupt greenhouse gas forcing". *Climate Dynamics* 44:7, pp. 2287–2299. ISSN: 1432-0894. DOI: 10.1007/s00382-014-2308-0.

Marvel, K., R. Pincus, G. A. Schmidt, and R. L. Miller (2018). "Internal Variability and Disequilibrium Confound Estimates of Climate Sensitivity From Observations". *Geophysical Research Letters* 45:3. _eprint: https://agupubs.onlinelibrary.wiley.com/doi/pdf/10.1002/2017GL076468, pp. 1595–1601. ISSN: 1944-8007. DOI: 10.1002/2017GL076468.

McDougall, T. J. and P. M. Barker (2011). *Getting started with TEOS-10 and the Gibbs Seawater (GSW) Oceanographic Toolbox*. SCOR/IAPSO WG127. 28 pp. ISBN: 978-0-646-55621-5.

Meier, W. N. and J. S. Stewart (2019). "Assessing Uncertainties in Sea Ice Extent Climate Indicators". *Environmental Research Letters* 14:3, p. 035005. ISSN: 1748-9326. DOI: 10.1088/1748-9326/aaf52c.

Minière, A., K. von Schuckmann, J.-B. Sallée, and L. Vogt (2023). "Robust acceleration of Earth system heating observed over the past six decades". *Scientific Reports* 13:1. Publisher: Nature Publishing Group, p. 22975. ISSN: 2045-2322. DOI: 10.1038/s41598-023-49353-1.

Morée, A. L., T. M. Clarke, W. W. L. Cheung, and T. L. Frölicher (2023). "Impact of Deoxygenation and Warming on Global Marine Species in the 21st Century". *Biogeosciences* 20:12, pp. 2425–2454. ISSN: 1726-4170. DOI: 10.5194/bg-20-2425-2023.

Myers, T. A. et al. (2021). "Observational constraints on low cloud feedback reduce uncertainty of climate sensitivity". *Nature Climate Change* 11:6. Number: 6 Publisher: Nature Publishing Group, pp. 501–507. ISSN: 1758-6798. DOI: 10.1038/s41558-021-01039-0.

Nijsse, F. J. M. M., P. M. Cox, and M. S. Williamson (2020). "Emergent constraints on transient climate response (TCR) and equilibrium climate sensitivity (ECS) from historical warming in CMIP5 and CMIP6 models". *Earth System Dynamics* 11:3. Publisher: Copernicus GmbH, pp. 737–750. ISSN: 2190-4979. DOI: 10.5194/esd-11-737-2020.

Pörtner, H.-O. et al., eds. (2022). *Climate Change 2022: Impacts, Adaptation and Vulnerability. Contribution of Working Group II to the Sixth Assessment Report of the Intergovernmental Panel on Climate Change*. Cambridge University Press.

Riahi, K. et al. (2017). "The Shared Socioeconomic Pathways and their energy, land use, and greenhouse gas emissions implications: An overview". *Global Environmental Change* 42, pp. 153–168. ISSN: 0959-3780. DOI: 10.1016/j.gloenvcha.2016.05.009.

Sallée, J.-B. (2018). "Southern Ocean Warming". *Oceanography* 31:2. ISSN: 10428275. DOI: 10.5670/oceanog.2018.215.

Sallée, J.-B. et al. (2021). "Summertime increases in upper-ocean stratification and mixed-layer depth". *Nature* 591:7851. Bandiera_abtest: a Cg_type: Nature Research Journals Number: 7851 Primary_atype: Research Publisher: Nature Publishing Group Subject_term: Physical oceanography Subject_term_id: physical-oceanography, pp. 592–598. ISSN: 1476-4687. DOI: 10.1038/s41586-021-03303-x.

Sanderson, B. M. et al. (2021). "The potential for structural errors in emergent constraints". *Earth System Dynamics* 12:3. Publisher: Copernicus GmbH, pp. 899–918. ISSN: 2190-4979. DOI: 10.5194/esd-12-899-2021.

Schuckmann, K. von et al. (2020). "Heat stored in the Earth system: where does the energy go?" *Earth System Science Data* 12:3. Publisher: Copernicus GmbH, pp. 2013–2041. ISSN: 1866-3508. DOI: 10.5194/essd-12-2013-2020.

Séférian, R. et al. (2019). "Evaluation of CNRM Earth System Model, CNRM-ESM2-1: Role of Earth System Processes in Present-Day and Future Climate". *Journal of Advances in Modeling Earth Systems* 11:12, pp. 4182–4227. ISSN: 1942-2466. DOI: 10.1029/2019MS001791.

Seland, Ø. et al. (2020). "Overview of the Norwegian Earth System Model (NorESM2) and Key Climate Response of CMIP6 DECK, Historical, and Scenario Simulations". *Geoscientific Model Development* 13:12, pp. 6165–6200. ISSN: 1991-959X. DOI: 10.5194/gmd-13-6165-2020.

Sellar, A. A. et al. (2019). "UKESM1: Description and Evaluation of the U.K. Earth System Model". *Journal of Advances in Modeling Earth Systems* 11:12, pp. 4513–4558. ISSN: 1942-2466. DOI: 10.1029/2019MS001739.

Shi, J.-R., S.-P. Xie, and L. D. Talley (2018). "Evolving Relative Importance of the Southern Ocean and North Atlantic in Anthropogenic Ocean Heat Uptake". *Journal of Climate* 31:18. Publisher: American Meteorological Society Section: Journal of Climate, pp. 7459–7479. ISSN: 0894-8755, 1520-0442. DOI: 10.1175/JCLI-D-18-0170.1.

Shin, S.-J. et al. (2023). "Southern Ocean Control of 2°C Global Warming in Climate Models". *Earth's Future* 11:1. _eprint: https://onlinelibrary.wiley.com/doi/pdf/10.1029/2022EF003212, e2022EF003212. ISSN: 2328-4277. DOI: 10.1029/2022EF003212.

Siler, N., S. Po-Chedley, and C. S. Bretherton (2018). "Variability in modeled cloud feedback tied to differences in the climatological spatial pattern of clouds". *Climate Dynamics* 50:3, pp. 1209–1220. ISSN: 1432-0894. DOI: 10.1007/s00382-017-3673-2.

Silvy, Y., J.-B. Sallée, E. Guilyardi, J. Mignot, and C. Rousset (2022). "What Causes Anthropogenic Ocean Warming to Emerge from Internal Variability in a Coupled Model?" *Journal of Climate* 35:22. Publisher: American Meteorological Society Section: Journal of Climate, pp. 7435–7454. ISSN: 0894-8755, 1520-0442. DOI: 10.1175/JCLI-D-22-0074.1.

Smith, K. E. et al. (2023). "Biological Impacts of Marine Heatwaves". *Annual Review of Marine Science* 15, Volume 15, 2023. Publisher: Annual Reviews, pp. 119–145. ISSN: 1941-1405, 1941-0611. DOI: 10.1146/annurev-marine-032122-121437.

Soden, B. J. and I. M. Held (2006). "An Assessment of Climate Feedbacks in Coupled Ocean–Atmosphere Models". *Journal of Climate* 19:14, pp. 3354–3360. ISSN: 1520-0442, 0894-8755. DOI: 10.1175/JCLI3799.1.

Soden, B. J. et al. (2008). "Quantifying Climate Feedbacks Using Radiative Kernels". *Journal of Climate* 21:14. Publisher: American Meteorological Society Section: Journal of Climate, pp. 3504–3520. ISSN: 0894-8755, 1520-0442. DOI: 10.1175/2007JCLI2110.1.

Sun, Y. et al. (2017). "Impact of Ocean Warming on Tropical Cyclone Size and Its Destructiveness". *Scientific Reports* 7:1. Publisher: Nature Publishing Group, p. 8154. ISSN: 2045-2322. DOI: 10.1038/s41598-017-08533-6.

Swart, N. C. et al. (2019). "The Canadian Earth System Model version 5 (CanESM5.0.3)". *Geoscientific Model Development* 12:11. Publisher: Copernicus GmbH, pp. 4823–4873. ISSN: 1991-959X. DOI: 10.5194/gmd-12-4823-2019.

Tatebe, H. et al. (2019). "Description and Basic Evaluation of Simulated Mean State, Internal Variability, and Climate Sensitivity in MIROC6". *Geoscientific Model Development* 12:7, pp. 2727–2765. ISSN: 1991-959X. DOI: 10.5194/gmd-12-2727-2019.

Terhaar, J., T. L. Frölicher, and F. Joos (2021). "Southern Ocean anthropogenic carbon sink constrained by sea surface salinity". *Science Advances* 7:18. Publisher: American Association for the Advancement of Science, eabd5964. DOI: 10.1126/sciadv.abd5964.

Terhaar, J., L. Kwiatkowski, and L. Bopp (2020). "Emergent constraint on Arctic Ocean acidification in the twenty-first century". *Nature* 582:7812. Number: 7812 Publisher: Nature Publishing Group, pp. 379–383. ISSN: 1476-4687. DOI: 10.1038/s41586-020-2360-3.

Titchner, H. A. and N. A. Rayner (2014). "The Met Office Hadley Centre Sea Ice and Sea Surface Temperature Data Set, Version 2: 1. Sea Ice Concentrations". *Journal of Geophysical Research: Atmospheres* 119:6, pp. 2864–2889. ISSN: 2169-8996. DOI: 10.1002/2013JD020316.

Tokarska, K. B. et al. (2020). "Past warming trend constrains future warming in CMIP6 models". *Science Advances* 6:12. Publisher: American Association for the Advancement of Science, eaaz9549. DOI: 10.1126/sciadv.aaz9549.

Voldoire, A. et al. (2019). "Evaluation of CMIP6 DECK Experiments With CNRM-CM6-1". *Journal of Advances in Modeling Earth Systems* 11:7, pp. 2177–2213. ISSN: 1942-2466. DOI: 10.1029/2019MS001683.

Wernecke, A., D. Notz, S. Kern, and T. Lavergne (2022). "Estimating the Uncertainty of Sea-Ice Area and Sea-Ice Extent from Satellite Retrievals". *EGUsphere*, pp. 1–19. DOI: 10.5194/egusphere-2022-1189.

Williams, R. G., P. Ceppi, and A. Katavouta (2020). "Controls of the transient climate response to emissions by physical feedbacks, heat uptake and carbon cycling". *Environmental Research Letters* 15:9. Publisher: IOP Publishing, p. 0940c1. ISSN: 1748-9326. DOI: 10.1088/1748-9326/ab97c9.

Wills, R. C. J., Y. Dong, C. Proistosecu, K. C. Armour, and D. S. Battisti (2022). "Systematic Climate Model Biases in the Large-Scale Patterns of Recent Sea-Surface Temperature and Sea-Level Pressure Change". *Geophysical Research Letters* 49:17. _eprint: https://onlinelibrary.wiley.com/doi/pdf/10.1029/2022GL100011, e2022GL100011. ISSN: 1944-8007. DOI: 10.1029/2022GL100011.

Winton, M., K. Takahashi, and I. M. Held (2010). "Importance of Ocean Heat Uptake Efficacy to Transient Climate Change". *Journal of Climate* 23:9. Publisher: American Meteorological Society Section: Journal of Climate, pp. 2333–2344. ISSN: 0894-8755, 1520-0442. DOI: 10.1175/2009JCLI3139.1.

Yukimoto, S. et al. (2019). "The Meteorological Research Institute Earth System Model Version 2.0, MRI-ESM2.0: Description and Basic Evaluation of the Physical Component". *Journal of the Meteorological Society of Japan. Ser. II* 97:5, pp. 931–965. DOI: 10.2151/jmsj.2019-051.

Zanna, L., S. Khatiwala, J. M. Gregory, J. Ison, and P. Heimbach (2019). "Global Reconstruction of Historical Ocean Heat Storage and Transport". *Proceedings of the National Academy of Sciences* 116:4, pp. 1126–1131. DOI: 10.1073/pnas.1808838115.

Zelinka, M. D., C. Zhou, and S. A. Klein (2016). "Insights from a refined decomposition of cloud feedbacks". *Geophysical Research Letters* 43:17. _eprint: https://onlinelibrary.wiley.com/doi/pdf/10.1002/2016GL0 pp. 9259–9269. ISSN: 1944-8007. DOI: 10.1002/2016GL069917.

Zelinka, M. D. et al. (2020). "Causes of Higher Climate Sensitivity in CMIP6 Models". *Geophysical Research Letters* 47:1. _eprint: https://onlinelibrary.wiley.com/doi/pdf/10.1029/2019GL085782, e2019GL085782. ISSN: 1944-8007. DOI: 10.1029/2019GL085782.

Ziehn, T. et al. (2020). "The Australian Earth System Model: ACCESS-ESM1.5". *Journal of Southern Hemisphere Earth Systems Science* 70:1, pp. 193–214. ISSN: 2206-5865. DOI: 10.1071/ES19035.

3 Stratification and overturning circulation are intertwined controls on ocean heat uptake efficiency in climate models

At the time of writing (January 18, 2025), this article is under review at *Ocean Science* (submitted on November 5, 2024). Note that the section numbering and citation format has been adapted to the overall style used in this thesis.

Authors

Linus Vogt[1], Casimir de Lavergne[1], Jean-Baptiste Sallée[1]

Affiliation

[1] Sorbonne Université, CNRS/IRD/MNHN, Laboratoire d'Océanographie et du Climat Expérimentations et Approches Numériques (LOCEAN), Paris, France.

Abstract

The global ocean takes up over 90% of the added heat in the climate system due to anthropogenic emissions, thereby buffering climate change at the Earth's surface. A key metric to quantify the role of the oceanic processes removing this heat from the atmosphere and storing it in the ocean is the ocean heat uptake efficiency (OHUE), defined as the amount of ocean heat uptake per degree of global surface warming. Despite the importance of OHUE, there remain substantial uncertainties concerning the physical mechanisms controlling its magnitude in global climate model simulations: ocean mixed layer depth, Atlantic meridional overturning circulation (AMOC) strength, and upper ocean stratification strength have all been previously proposed as controlling factors.

In this study, we analyze model output from an ensemble of 28 climate models from the Coupled Model Intercomparison Project, phase 6 (CMIP6), in order to resolve these apparently divergent explanations. We find that stratification in the mid-latitude Southern Ocean is a key model property setting the value of OHUE due to its influence on Southern Ocean overturning. The previously proposed role of the AMOC for OHUE is explained by a linkage of stratification model biases between the subpolar North Atlantic and the Southern Ocean. Our analysis thus reconciles previous attempts at explaining controls on OHUE, and highlights the importance of interlinked model biases across variables and geographical regions.

3.1 Introduction

The global ocean buffers anthropogenic climate change by taking up excess heat and carbon from the atmosphere. Since the preindustrial era, over 90% of the additional heat that has entered the Earth system as a result of changes in the Earth's radiative balance has been stored in the ocean (Schuckmann et al. 2020; Forster et al. 2021). This ocean heat uptake (OHU) is a key process determining the sensitivity of the climate system to external perturbations, in particular to radiative forcing from increased atmospheric greenhouse gas concentrations.

More than half of the observed increase in ocean heat content (OHC) is concentrated in waters shallower than 700 m depth (Schuckmann et al. 2020). Under increased radiative forcing, anomalous air-sea heat fluxes enter the ocean through its surface and quickly warm the ocean mixed layer on seasonal to interannual timescales, whereas the deep ocean (below 2000 m depth) is more isolated from the atmosphere and is warmed on timescales of decades to centuries (Cheng et al. 2022). Heat is fluxed towards the deep ocean through a multitude of processes, including subduction from the mixed layer (Marzocchi et al. 2021), mean downwelling flows and vertical mixing (Exarchou et al. 2015), and (sub-)mesoscale eddy processes contributing notably to isopycnal mixing (Gregory 2000; Morrison et al. 2016).

A key metric to quantify the efficiency of these processes at hiding heat from the atmosphere under transient climate change is the *OHU efficiency* (OHUE), defined as the rate of global OHU per degree of global mean surface warming (e.g., Gregory and Mitchell 1997; Gregory et al. 2023), with units of $\mathrm{Wm^{-2}K^{-1}}$:

$$\mathrm{OHUE} = \mathrm{OHU}/\Delta T, \tag{3.1}$$

where OHU is the increase in OHC relative to preindustrial levels expressed as a flux of energy per unit global surface area, and ΔT is the global mean surface air temperature anomaly relative to preindustrial levels.

In global climate model (GCM) simulations of transient climate change, OHUE estimates span a factor of two across different models (Gregory et al. 2023), due to inter-model spread in both OHU (e.g., Vogt et al. 2024) and transient surface warming projections (e.g., Meehl et al. 2020). In an attempt to determine the source of this uncertainty and to find potential observational constraints on OHUE, previous studies have proposed a number of oceanic metrics that control OHUE in GCMs participating in successive phases of the Coupled Model Intercomparison Project ((CMIP; Eyring et al. 2016)). High-latitude ocean mixed layer depths were first identified as a possible control of transient warming rates in the ocean and atmosphere using the CMIP3 ensemble (Boé et al. 2009). Subsequently, the strength of the Atlantic Meridional Overturning Circulation (AMOC) in the preindustrial baseline climate has been found to correlate well with OHUE across CMIP5 multi-model ensembles (Kostov et al. 2014; Winton et al. 2014) as well as across parameter perturbation ensembles (Romanou et al. 2017; Saenko et al. 2018) and initial condition ensembles (He et al. 2017), each based on a single model. However, the actual amount of anomalous heat entering the North Atlantic and being subducted by the AMOC is small compared to the OHU occurring in the mid-latitude Southern Ocean (Frölicher et al. 2015; Cheng et al. 2022). This is explained by aerosol-induced cooling in the North Atlantic and higher subduction rates in the Southern Ocean (Williams et al. 2024). Furthermore, OHUE actually decreases when the AMOC strengthens under transient forcing (Stolpe et al. 2018). Gregory et al. (2023) have thus postulated that the correlation between AMOC and OHUE may originate from a common dependence on a third factor that would characterize the preindustrial ocean state of a model and influence both AMOC and OHUE.

A promising candidate that potentially controls both AMOC and OHUE is the strength of the upper ocean stratification (Kuhlbrodt and Gregory 2012), i.e. the density difference between the upper and deeper ocean, which is the main reason for the deep ocean's relative isolation from other parts of the climate system. Because large-scale ocean currents and smaller-scale mixing processes occur preferentially along isopycnal surfaces, stratification impedes the exchange of properties between the upper and deep oceans (e.g., McDougall et al. 2014). Recent studies have highlighted

the impact of upper ocean stratification on OHUE in GCMs. Bourgeois et al. (2022) constrained oceanic heat and carbon uptake in the Southern Ocean using observed and CMIP6-simulated stratification profiles in the region between 30°S and 55°S. Similarly, Liu et al. (2023) underscored the importance of salinity stratification in influencing OHUE in CMIP6 models and used global sea surface salinity observations to estimate OHU efficiency through an emergent constraint. Finally, Newsom et al. (2023) showed that the depth of the global pycnocline, used as a metric to quantify upper ocean stratification, is strongly correlated with OHUE across CMIP5/6 models and across a parameter perturbation ensemble of a single model.

It remains unclear, however, how to reconcile these proposed OHUE controls based on AMOC strength, mixed layer depth (MLD), and stratification. This is not least due to the fact that these variables are interconnected: a deeper mixed layer translates to reduced stratification and vice versa, and North Atlantic MLD and stratification condition the AMOC (Jackson et al. 2023; Nayak et al. 2024). Furthermore, climate model biases can be linked between remote regions of the Earth (Wang et al. 2014; Luo et al. 2023), complicating the analysis and interpretation of regional climate metrics in GCMs. For instance, the extratropical oceans, in particular the subpolar North Atlantic and the Southern Ocean, have an outsize role in ventilating the global ocean and in storing heat and carbon (Frölicher et al. 2015; Shi et al. 2018). In these regions, the stratification is directly related to the large-scale global ocean circulation since the upper and deep oceans are connected via upwards-sloping isopycnals (Kuhlbrodt et al. 2007; Kamenkovich and Radko 2011; Morrison et al. 2022). A potential link between Southern Ocean and subpolar North Atlantic stratification could therefore provide insight into the control of upper ocean stratification on OHUE in GCMs.

In this study, we use an ensemble of CMIP6 models under idealized CO_2 forcing as well as a global ocean state estimate in order to analyze the inter-model relationships and biases in upper ocean properties (stratification and mixed layer depth) and meridional overturning metrics (AMOC and Southern Ocean overturning strength), as well as their combined influence on OHUE.

In particular, we aim to answer the following questions:

- In which oceanic regions does stratification control OHUE?
- How do temperature and salinity stratification differ in their control on OHUE?
- How are local stratification biases linked across geographically distant regions, and how does this influence OHUE?
- What explains the positive correlation between AMOC strength and OHUE across CMIP6 models?
- What is the role of meridional overturning in the Southern Ocean for OHUE?

The remainder of this article is organized as follows: In Sect. 3.2, we present the data and methods used in this study. In Sect. 3.3, we analyze the dependence of OHUE on upper ocean properties and meridional overturning metrics both from a global (Sect. 3.3.1) and a local perspective (Sect. 3.3.2). In Sect. 3.4, we then present the inter-model relationships between these upper ocean properties on one hand and the meridional overturning metrics on the other hand. In Sect. 3.5, we analyze the ensemble mean and inter-model spread of historical stratification and its bias relative to observations, including a link between GCM stratification biases between the Southern Ocean and the subpolar North Atlantic (Sect. 3.5.2). Finally, in Sect. 3.6 we offer a schematic picture of all major inter-model relationships explored in this study and conclude by answering the five questions posed above.

3.2 Methods

3.2.1 CMIP6 model output

We use model output from a set of 28 climate models from 14 modeling centers run in two CMIP6 experiments: a baseline experiment with preindustrial forcings (piControl experiment), and a perturbed scenario forced by an idealized CO_2 increase of 1% per year during 150 years (1pctCO2 experiment). We use one ensemble member per model, with the 1pctCO2 run branching off from the piControl run (Table 3.A.1). All model output used for the analysis (principally ocean potential temperature and ocean salinity) is regridded onto a regular 1°× 1°latitude–longitude grid in order to allow the calculation of local inter-model correlations at each grid cell. Anomalies of variables in the 1pctCO2 experiment relative to the piControl run are calculated by subtracting the appropriate piControl period from the 1pctCO2 data; since piControl runs are extended over the 150-year period of the 1pctCO2 experiment, this method removes the effect of model drift.

3.2.2 Calculation of ocean variables

Ocean heat content per unit volume is defined as $\mathrm{OHC} = \rho_0 C_p \theta$, where $\rho_0 = 1035\ \mathrm{kg\,m^{-3}}$ is a reference density, $C_p = 3992.1\ \mathrm{J\,kg^{-1}\,K^{-1}}$ is a reference heat capacity ((as in e.g. Huguenin et al. 2022)), and θ is potential temperature. Global OHU in the 1pctCO2 experiment is then calculated as the time derivative of the three-dimensional integral of the OHC anomaly relative to the preindustrial state.

Ocean heat uptake efficiency (OHUE) is defined as in Gregory et al. 2023: the total OHU divided by 1.5 times the global mean sea surface temperature anomaly at years 60–80 in the 1pctCO2 run, which is the 20-year period around the time of CO_2 doubling relative to the preindustrial.

The AMOC strength is calculated using the overturning streamfunction variables in latitude–depth coordinates from the CMIP6 output and is defined as the streamfunction maximum in the Atlantic basin at 26.5°N and below 500 m depth.

Stratification is defined as the squared buoyancy frequency N^2 integrated in depth between 0 and 1500 m, resulting in units of m s^{-2}. The squared buoyancy frequency N^2 is calculated using the TEOS-10 software toolbox (McDougall and Barker 2011). The depth of 1500 m is chosen to encompass the mixed layer as well as the internal pycnocline (Gnanadesikan 1999; Klocker et al. 2023). The main results of this study are tested with different values of this maximal depth (spanning a range from 400 m to 2500 m and will be shown to be only weakly sensitive to this particular choice. The stratification is further decomposed into contributions from temperature and salinity, according to

$$N^2 = N_T^2 + N_S^2 = -g\alpha\frac{\partial\theta}{\partial z} + g\beta\frac{\partial S}{\partial z} \tag{3.2}$$

where α is the thermal expansion coefficient, β the haline contraction coefficient, g the vertical acceleration due to gravity, and S salinity. The sum of these two terms reproduces the total N^2 exactly.

Mixed layer depth is defined as the minimum depth where the monthly potential density σ_0 deviates by 0.03 kg m^{-3} from its value at 5 m depth (Boyer Montégut et al. 2004). For consistency, this definition is used even for models that have the MLD variable `mlotst` available as part of their CMIP output.

To calculate the strength of the upper Southern Ocean overturning cell, we first calculate the time-mean overturning streamfunction in latitude–density coordinates from time-mean meridional ocean velocity and potential density referenced to 2000 dbars (σ_2) ((e.g. Farneti et al. 2015)):

$$\overline{\Psi}_{\mathrm{SO}}(y,\sigma_2) = -\int\int_{-H}^{\tilde{z}(x,y,\sigma_2)} \bar{v}(x,y,z')\,\mathrm{d}z'\mathrm{d}x, \tag{3.3}$$

where x, y, and z are longitude, latitude, and depth; $H(x,y)$ is the depth of the ocean bottom; v is residual mean meridional mass transport (CMIP variable `vmo`, including resolved and parameterized transport); and $\tilde{z}(x,y,\sigma_2)$ is the local depth of the isopycnal σ_2. The strength of the upper cell M_{SO} is then defined as the time-mean streamfunction maximum within the 1034 kg m^{-3} < σ_2 < 1038 kg m^{-3} density range and between 35°S and 40°S.

For a complementary quantification of Southern Ocean overturning, we compute surface flux water mass transformation (SFWMT), a measure of overturning inferred from surface buoyancy

fluxes, following Jackson and Petit (2023). The SFWMT is the derivative of the area-integrated surface buoyancy flux into the Southern Ocean south of 30°S with respect to density:

$$\Psi(\sigma_2) = \frac{\partial}{\partial \sigma_2} B_A(\sigma_2), \tag{3.4}$$

where the surface buoyancy flux into the area A is a sum of heat and freshwater terms:

$$B_A(\sigma_2) = \int \mathrm{d}A' \left(-\alpha \frac{Q}{C_p} - \beta \frac{sW}{1-s} \right). \tag{3.5}$$

In this equation, s is non-dimensional sea surface salinity, and W is the surface freshwater flux (CMIP variable `wfo`) in units of kg m^{-2} s^{-1}. As a single measure of Southern Ocean overturning strength inferred from surface buoyancy fluxes, we choose the difference

$$M_{\mathrm{WMT}} = \max_{\sigma_2} \Psi - \min_{\sigma_2} \Psi. \tag{3.6}$$

3.2.3 Observation-based data

For comparison of model fields with observationally constrained data, we use potential temperature and salinity data from the ECCO Version 4 global state estimate (Forget et al. 2015; ECCO Consortium et al. 2024) with data coverage from 1992 to 2017. To calculate stratification strength and MLD, the ECCO output fields are regridded and processed in the same way as the CMIP6 model output.

3.2.4 Inter-model empirical orthogonal function analysis

An empirical orthogonal function (EOF) algorithm (Dawson 2016) is applied to two-dimensional model fields to construct inter-model EOF patterns, expressed as the correlation across models between the principal component value and the input field at each grid cell. This corresponds to a standard EOF analysis, but with the variance maximized by each EOF being measured across models instead of in time (e.g. Hu et al. 2020).

For the EOF analysis of preindustrial mixed layer depth (Fig. 3.A.8), a number of outlier models with extreme values of the first principal component were identified and removed from the analysis in order to facilitate interpretation. For this, the EOF algorithm was iteratively applied five times to the preindustrial annual mean MLD fields of all models and the model with the most extreme value of the first principal component was removed.

3.2.5 Classification of vertical stratification profiles

An unsupervised ocean profile classification algorithm (Maze et al. 2017; Maze 2020) is applied to vertical profiles of N_T^2 and N_S^2 to obtain a pre-specified number of 8 representative classes characterized by the shape and amplitude of temperature and salinity stratification profiles. As input to the classification procedure, the preindustrial time-mean N_T^2 and N_S^2 profiles are pooled together from all grid cells and from all models.

3.3 Global and local controls on ocean heat uptake efficiency

We begin by investigating the main proposed controls on OHUE in our set of 28 CMIP6 GCMs in the preindustrial state. These variables belong to two categories: upper ocean properties (i.e., stratification and mixed layer depth), and meridional overturning strength (i.e., AMOC, M_{SO}, and M_{WMT}).

3.3.1 Global controls on OHUE

We first establish how the two upper ocean properties are related to OHUE in the global mean (Fig. 3.1a–b). Preindustrial global mean upper ocean stratification is not significantly correlated with OHUE at the $p = 0.05$ level across our ensemble of 28 CMIP6 models (Fig. 3.1a). In contrast, preindustrial global mean MLD is positively correlated with OHUE with a linear correlation coefficient of $r = 0.56$ (Fig. 3.1b), i.e., models with a deeper global mean mixed layer tend to have a higher OHUE.

Turning now to the three overturning strength metrics (Fig. 3.1c–e), preindustrial AMOC strength is positively correlated across models with OHUE (Fig. 3.1c, $r = 0.61$). This is consistent with previous findings, but we obtain a smaller correlation coefficient for our ensemble of 28 CMIP6 models than for the mixed model ensemble of Gregory et al. (2023) which included 19 CMIP5 models and 14 CMIP6 models (their $r = 0.81$). A slightly stronger relationship is found for the Southern Ocean upper cell (Fig. 3.1d): M_{SO} and OHUE are also positively correlated ($r = 0.64$). The model MRI-ESM2-0 is an outlier with high OHUE but only moderate M_{SO}, removing this model from the linear fit results in a correlation of $r = 0.86$. As an alternative to the overturning metric M_{SO} computed in latitude–density coordinates, we also consider the Southern Ocean overturning strength inferred from surface buoyancy fluxes, M_{WMT} (Fig. 3.1e). This metric is not significantly correlated with OHUE at the $p = 0.05$ level in our model ensemble ($r = 0.39$, $p = 0.08$).

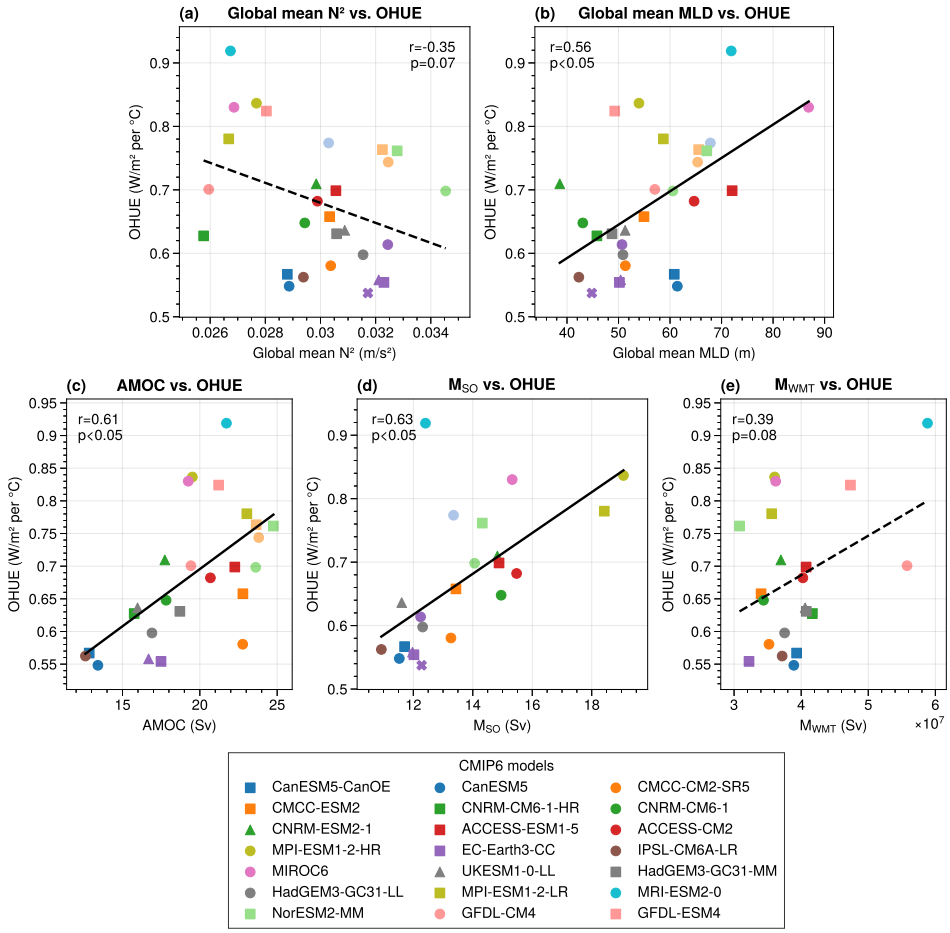

Figure 3.1: Proposed controls on ocean heat uptake efficiency (OHUE). Scatter plot between OHUE and **(a)** preindustrial global mean upper ocean (0–1500 m) stratification (N^2), **(b)** preindustrial global mean mixed layer depth (MLD), **(c)** preindustrial mean AMOC strength, **(d)** Southern Ocean upper cell strength, and **(e)** Southern Ocean surface buoyancy flux inferred overturning. In panels (c)–(e), only a subset of models is included due to output availability (see Table 3.A.1).

3.3.2 Local upper ocean controls on OHUE

The fact that global mean upper ocean stratification is not significantly correlated with OHUE across models may at first sight appear to contradict previous findings highlighting the importance of stratification for OHUE (Bourgeois et al. 2022; Liu et al. 2023; Newsom et al. 2023). This is because globally averaged stratification or MLD are relatively crude bulk measures of the simulated upper ocean state. We now therefore extend this analysis to the local level by considering inter-model correlations between the two upper ocean variables and OHUE at each model grid cell (Fig. 3.2).

Figure 3.2a shows the inter-model correlation coefficient between OHUE and local preindustrial annual mean upper ocean (0–1500 m) stratification. Unlike global average stratification

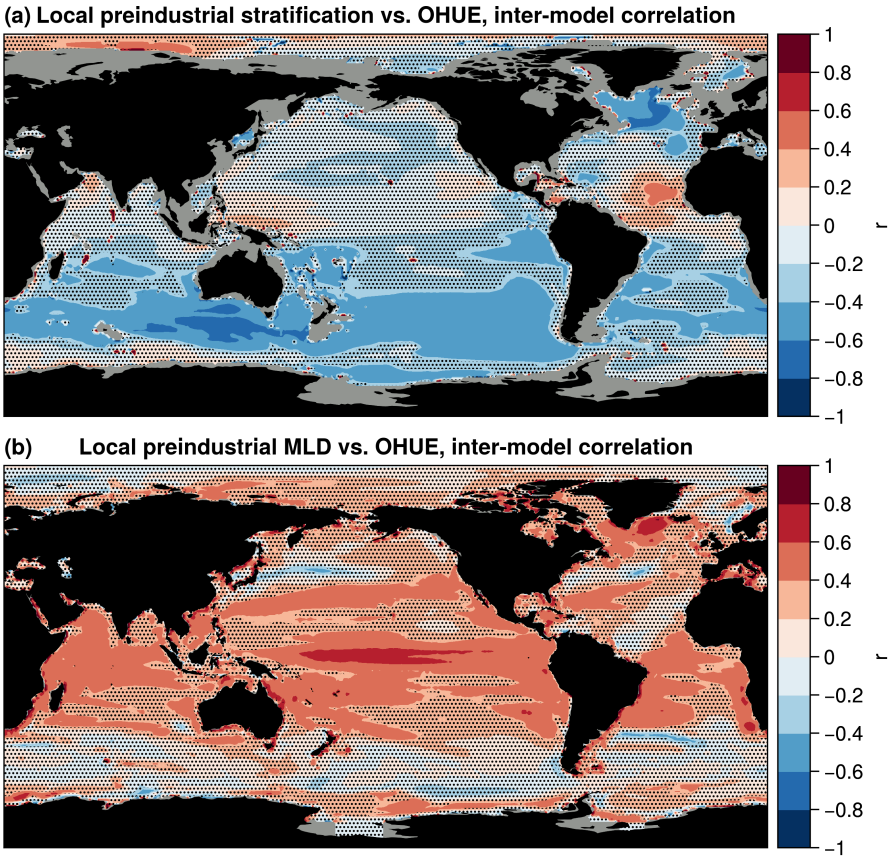

Figure 3.2: Local upper-ocean controls on ocean heat uptake efficiency (OHUE). Maps of inter-model Pearson correlation coefficient across 28 CMIP6 models between OHUE and local preindustrial annual mean **(a)** upper ocean (0–1500 m) stratification and **(b)** mixed layer depth. Stippling indicates region where the least squares linear regression slope is not significantly different from zero ($p \geq 0.05$, Wald test with t-distribution). In panel (a), regions where the bathymetry is less than 1500 m deep are shaded in grey.

(Fig. 3.2a), local stratification is significantly anticorrelated with OHUE in several locations. Significant correlations ($p < 0.05$) are found in two primary regions: the subpolar North Atlantic and the mid-latitude Southern Ocean. In both regions, the correlation is negative, indicating that models with greater (more stable) preindustrial stratification in these regions have a lower OHUE. In the Southern Ocean, significant negative correlations are found particularly in the Pacific and Indian sectors, whereas the signal in the southern Atlantic Ocean is less widespread. This zonally asymmetric pattern is consistent with the geography of Subantarctic Mode Water formation (McCartney 1979; Hanawa and D.Talley 2001) and subduction (Sallée et al. 2010). Apart from these two regions, a smaller patch of significant negative correlations is found in the eastern tropical Pacific. These patterns are partly dependent on the choice of the depth range over which the squared buoyancy frequency N^2 is integrated (Fig. 3.A.1). The negative correlation in the subpolar North

Atlantic is present for all depth choices from 0–400 m to 0–2500 m, but the negative correlation in the mid-latitude Southern Ocean is absent for 0–400 m stratification and only emerges gradually for 0–1500 m and deeper depth ranges. The decomposition of stratification into its temperature and salinity contributions (Eq. 3.2) shows that the subpolar North Atlantic control on OHUE is due to salinity stratification, whereas temperature stratification in this region is positively correlated with OHUE (Fig. 3.A.1). In the Southern Ocean, both temperature and salinity contribute to the negative correlation with OHUE (Fig. 3.A.1), and only their combination to total stratification results in the broad-scale signal found across the Southern Ocean in Fig. 3.2a.

An analogous analysis for local preindustrial annual mean MLD is shown in Figure 3.2b. Significant positive correlations are found in the subpolar North Atlantic as well as at low latitudes in all ocean basins; higher OHUE is thus associated with deeper mixed layers in these regions. However, in contrast to stratification, there are no significant correlations between MLD and OHUE in the mid-latitude Southern Ocean.

3.4 Upper ocean controls on meridional overturning

In the previous section, we have found significant inter-model correlations with OHUE not only for meridional overturning metrics (Fig. 3.1c,d), but also for regional upper ocean properties (Fig. 3.2). It is therefore worthwhile to investigate the potential linkages between these two categories of variables across the model ensemble, i.e. between stratification and MLD on the one hand, and overturning metrics on the other hand, as shown in Figure 3.3.

The left column of Figure 3.3 shows the inter-model correlations between local preindustrial mean upper ocean stratification and preindustrial AMOC, M_{SO} or M_{WMT}. Preindustrial AMOC strength is anticorrelated with subpolar North Atlantic total stratification, and weakly positively correlated with total stratification in the western Pacific (Fig. 3.3a). While the signal in the western Pacific is unclear and due to both temperature and salinity stratification, the negative correlation in the subpolar North Atlantic can be attributed to salinity stratification, since the temperature contribution is of the opposite sign (Fig. 3.A.2b–c).

The Southern Ocean upper cell strength, M_{SO}, computed in latitude–density coordinates is anticorrelated with total stratification mostly in the Southern Ocean at the latitudes of the Antarctic Circumpolar Current (ACC; Fig. 3.3c). This can mostly be attributed to temperature stratification (Fig. 3.A.2e), which has significant negative correlations extending up to subtropical latitudes in the Pacific and Indian oceans.

The Southern Ocean upper cell strength M_{WMT} inferred from surface buoyancy fluxes is also negatively correlated with total stratification in the Southern Ocean, and its correlations are higher and extend over a greater surface area (Fig. 3.3e) than for the upper cell computed in latitude–

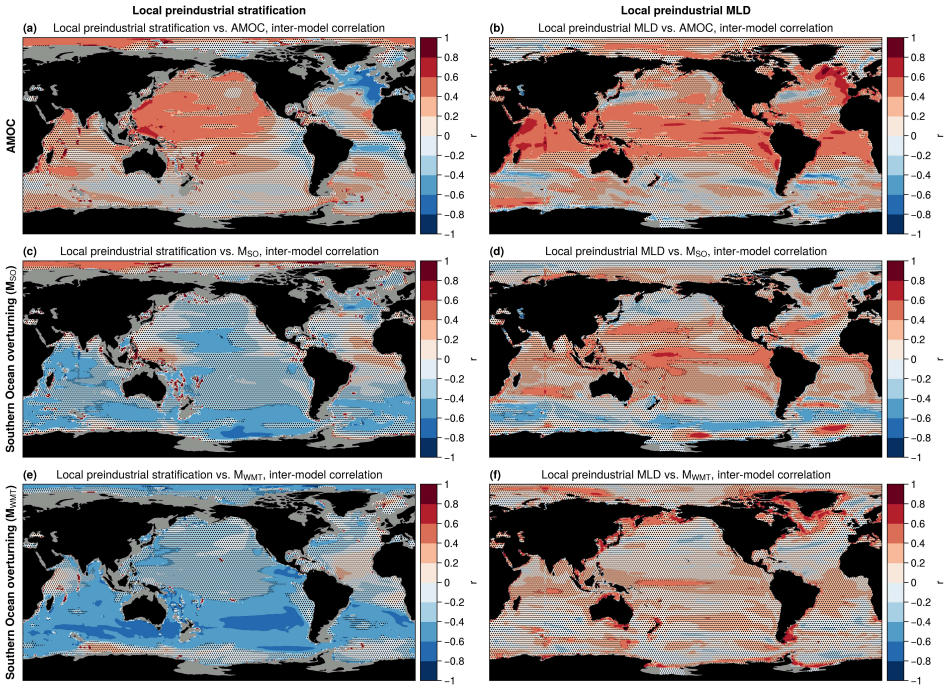

Figure 3.3: Local upper-ocean controls on meridional overturning strength in CMIP6. Left column: maps of inter-model Pearson correlation coefficient across 28 CMIP6 models between local preindustrial annual mean upper ocean (0–1500 m) stratification and **(a)** preindustrial mean AMOC strength, **(c)** Southern Ocean upper cell strength, and **(e)** Southern Ocean surface buoyancy flux inferred overturning. Right column [**(b)**, **(d)**, **(f)**]: as left column, but for local preindustrial annual mean mixed layer depth.

density coordinates. However, for this metric, the inter-model link to stratification can be attributed solely to salinity stratification (Fig. 3.A.2i), while temperature stratification shows no significant correlation to M_{WMT} in any of the major ocean basins (Fig. 3.A.2h).

We now turn to the links between these overturning strength metrics and local preindustrial mean MLD, shown in the right column of Figure 3.3. AMOC strength is positively correlated with MLD in the subpolar North Atlantic as well as at tropical latitudes in all ocean basins. This closely resembles the pattern found for the MLD–OHUE link in Figure 3.2b, which is a point to which we will return in the conclusions (Sect. 3.6).

For the two Southern Ocean overturning metrics M_{SO} and M_{WMT}, a potential link to MLD is overall much less clear than for the AMOC. While M_{SO} is positively correlated with MLD in some regions in the tropical and subtropical Pacific, it is negatively correlated with MLD along the Polar Front in the Southern Ocean. Furthermore, the Southern Ocean overturning metric inferred from surface buoyancy fluxes, M_{WMT}, exhibits no large-scale regions of significant correlations with MLD.

3.5 Stratification model bias and inter-model spread

3.5.1 Ensemble mean stratification and bias relative to observations

Although we found global mean stratification to be unrelated to OHUE (Fig. 3.1), there are significant links between regional stratification and OHUE in the subpolar North Atlantic and the mid-latitude Southern Ocean (Fig. 3.2a). In addition, stratification in each of these two regions is in turn related to the AMOC and Southern Ocean overturning, respectively (Fig. 3.4). Potential model biases in these regions would thus have direct implications for OHUE. Beyond the foregoing analysis of inter-model relationships between variables, it is thus insightful to investigate also the mean state, inter-model spread, and bias relative to observations of simulated upper ocean stratification; this is shown in Figure 3.4.

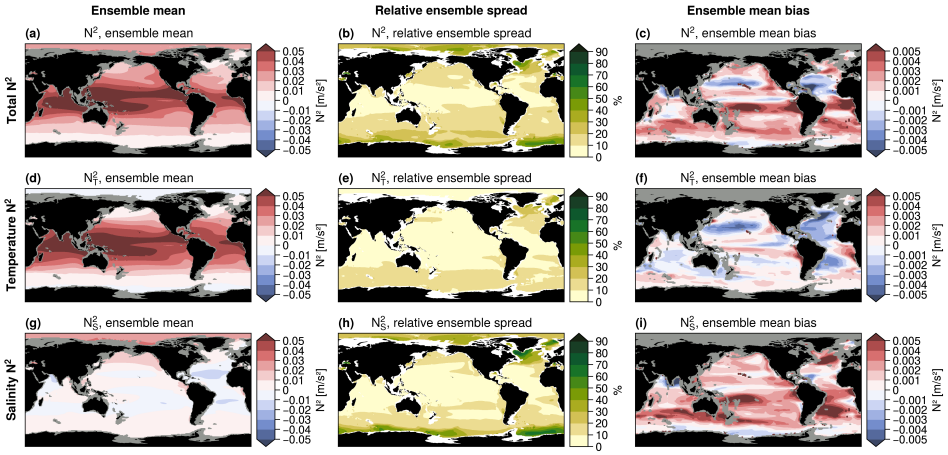

Figure 3.4: Ensemble mean stratification and bias relative to observations. **(a)** CMIP6 ensemble mean total historical stratification integrated over the 0–1500 m depth range. **(b)**, Inter-model coefficient of variation (ratio of ensemble standard deviation to ensemble mean) of total stratification. **(c)**, Bias in total stratification between CMIP6 ensemble mean and the ECCO state estimate. **(d)–(f)**, As (a)–(c) but for temperature stratification. **(g)–(i)**, As (a)–(c) but for salinity stratification. For both the model ensemble and the state estimate, stratification is averaged over the historical period 1992–2017.

The ensemble mean total stratification (Fig. 3.4a) has a distinct equator-to-pole gradient, with a highly stratified water column in the tropics, and lowest stratification in the Southern Ocean and subpolar North Atlantic. Consequently, the largest relative inter-model spread in total stratification (Fig. 3.4b) is found in regions with low stratification commonly associated with deep convection: the Weddell and Ross Seas in the Southern Hemisphere and the subpolar North Atlantic and Nordic Seas in the Northern Hemisphere, where the inter-model standard deviation is larger than 50% of the ensemble mean. Compared to the ECCO state estimate, the CMIP6 ensemble is too stratified over most of the ocean (Fig. 3.4c), especially in the equatorial Pacific and

Atlantic, where the bias reaches values of up to 10% of the ensemble mean, and in the mid-latitude Southern Ocean.

The temperature contribution to stratification dominates the magnitude and pattern of the ensemble mean total stratification in the low-to-mid latitudes (Fig. 3.4d), while the mean salinity contribution is responsible for stabilizing the high latitude oceans (Fig. 3.4g). This is a consequence of the nonlinear equation of state for seawater which diminishes the influence of temperature on density in cold water (Roquet et al. 2015). Relative to the average total stratification, there is a larger inter-model spread in salinity stratification than in temperature stratification (Fig. 3.4e,h), especially in the high-latitude Southern Ocean around Antarctica and in the North Atlantic subpolar gyre and Nordic Seas. Despite its subordinate role in setting the mean global stratification, the salinity contribution is thus a deciding factor in the inter-model spread in total stratification. Furthermore, salinity stratification also dominates the model bias relative to the state estimate (Fig. 3.4i), with relatively large positive salinity stratification biases in the Southern Ocean and subpolar North Atlantic, while temperature stratification biases are small in magnitude except for a negative bias in the Atlantic basin (Fig. 3.4f). It should be recalled that the biases documented here are those of the CMIP6 ensemble mean; individual model biases may differ.

3.5.2 Regional coherence of stratification inter-model links

The fact that OHUE is unrelated to global mean stratification (Fig. 3.1a) and instead sensitive to stratification in disconnected regions of both the Northern and Southern Hemispheres (Fig. 3.2a) which additionally exhibit common biases relative to observations (Fig. 3.4) motivates a closer analysis of the inter-model spread in regional stratification patterns.

An inter-model empirical orthogonal function (EOF) analysis on the model ensemble's preindustrial annual mean stratification patterns reveals two principal modes of inter-model spread (Fig. 3.5), which together explain 55% of the inter-model variance (the third leading mode explains only 5.6% of the variance). The first EOF (Fig. 3.5a) explains 39% of the inter-model variance and consists of a broadly uniform large-scale coherence including the Pacific and Indian ocean basins and the Southern Ocean, but with no signal in the North Atlantic. This means that, to first order, model biases in preindustrial stratification in the Pacific, Indian, and Southern oceans tend to covary across models, whereas the North Atlantic stratification varies independently. The first-order independence of North Atlantic stratification from other regions can also be seen from an unsupervised classification of vertical stratification profiles (Fig. 3.A.7), where the North Atlantic is associated with a stratification profile not found in any other ocean basin or in the Southern Hemisphere. The same pattern as in the first EOF can be seen by considering the preindustrial inter-model correlation of local stratification with global mean stratification (Fig. 3.5b). Global

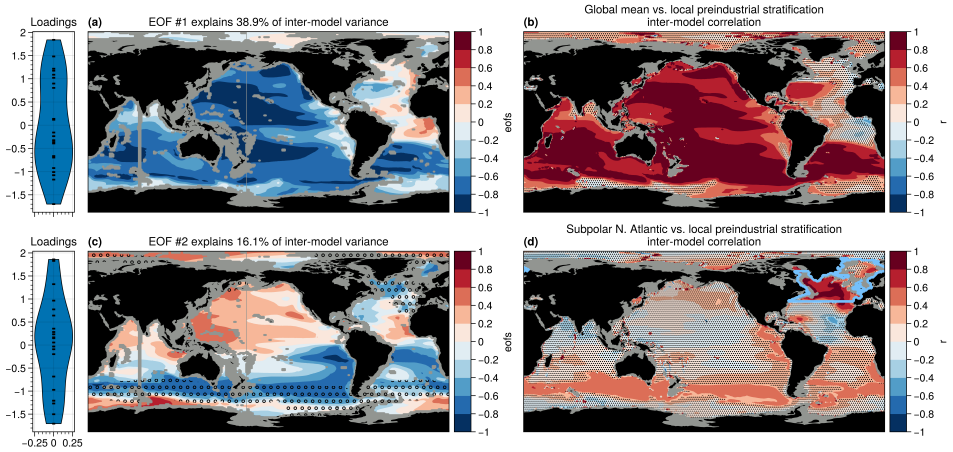

Figure 3.5: Regional coherence of inter-model stratification spread. Panels **(a)** and **(c)** show respectively the first and second mode of inter-model EOF analysis on preindustrial annual mean upper ocean stratification (see Methods). The violin plots in panels (a) and (c) show the ensemble distribution of the normalized loadings for each EOF. In panel (c), stippling indicates areas with surface density in the range $25.75\ \mathrm{kg\,m^{-3}} < \sigma_0 < 27\ \mathrm{kg\,m^{-3}}$. Panels **(b)** and **(d)** show the inter-model correlation between the local preindustrial stratification and either **(b)** the global mean preindustrial stratification or **(d)** the subpolar North Atlantic mean preindustrial stratification. The subpolar North Atlantic region used in panel (d) is indicated by the blue contour.

mean stratification is correlated with local stratification across the Pacific, Indian, and Southern oceans, but not in the North Atlantic. This shows that the principal component associated with the first EOF (Fig. 3.5a) is strongly correlated to the global mean stratification (Fig. 3.A.3).

The second EOF (Fig. 3.5c) explains 16% of the inter-model variance in preindustrial stratification. It mainly consists of a coherence including the mid-latitude Southern Ocean, subpolar North Atlantic, and eastern tropical Pacific, and a signal of opposite sign in the western tropical Pacific. This suggests that, to second order, preindustrial stratification model biases in the Southern Ocean and subpolar North Atlantic tend to be linked. Although these two regions are geographically far apart, they are physically connected by the outcropping of the same isopycnals in the range $25.75\ \mathrm{kg\,m^{-3}} < \sigma_0 < 27\ \mathrm{kg\,m^{-3}}$, as indicated by the stippling of sea surface density in Figure 3.5c. This link is further illustrated by the inter-model correlation of local stratification with stratification averaged over the subpolar North Atlantic (indicated by the contour in Figure 3.5d). Apart from a trivial positive correlation in the subpolar North Atlantic itself, we find a circumpolar band of positive inter-model correlation in the mid-latitude Southern Ocean.

Further EOF modes are not explored in detail here since they each explain less than 6% of the inter-model variance. Still, the three following EOFs all have a signal of the same sign in the Southern Ocean and subpolar North Atlantic (Fig. 3.A.4), strengthening the inter-model link between these regions found in the second EOF.

The distinct role of temperature and salinity stratification at setting these patterns of inter-model spread can be seen by applying the EOF analysis to temperature and salinity stratification separately (Fig. 3.A.5). It is apparent that the first two inter-model EOFs in total stratification (Fig. 3.5a,c) resemble the first two EOFs of salinity stratification (Fig. 3.A.5b,d). In contrast, the first EOF of temperature stratification (Fig. 3.A.5a) consists of a broad low- to mid-latitude pattern including the North Atlantic, and the second EOF (Fig. 3.A.5c) shows an approximate hemispheric dipole signal with opposite sign between the Southern Ocean and the Northern Hemisphere oceans. This implies that inter-model spread in patterns of salinity stratification are decisive for setting the patterns of total stratification, which in turn control OHUE (Fig. 3.2a).

It is furthermore interesting to note that temperature and salinity stratification (N_T^2 and N_S^2) do not vary independently across the model ensemble: inter-model biases in temperature and salinity stratification tend to compensate each other in the high-latitude Southern Ocean and in the North Atlantic, meaning that models with strong salinity stratification tend to have weak temperature stratification at these locations, and vice versa (Fig. 3.A.6a). In addition, a difference in total stratification between two models tends to coincide with a difference in salinity stratification of the same sign across almost all of the global ocean (Fig. 3.A.6c), while temperature stratification is positively correlated with total stratification only over of the low- to mid-latitude oceans (Fig. 3.A.6b). These findings partly explain the success of the emergent constraint by Liu et al. (2023) between sea surface salinity as a proxy for N_S^2 and OHUE.

3.6 Discussion and conclusions

3.6.1 Schematic summary of principal inter-model relationships between variables controlling OHUE

The schematic in Figure 3.6 summarizes the inter-model relationships found in this study between local upper ocean stratification, local mixed layer depth, various meridional overturning strength metrics, and OHUE. We now summarize our findings for the most important connections, depicted as arrows and labelled with lowercase letters in Figure 3.6.

a) Subpolar North Atlantic stratification ($N^2_{\text{N.Atl.}}$) and Southern Ocean stratification (N^2_{SO})

We have identified a coherent pattern of inter-model spread in preindustrial stratification linking the subpolar North Atlantic and the mid-latitude Southern Ocean (Fig. 3.5c,d). Although this mode of inter-model variability explains only 16% of inter-model variance in preindustrial stratification (compared to 39% for the leading mode), it is key for driving differences in OHUE between

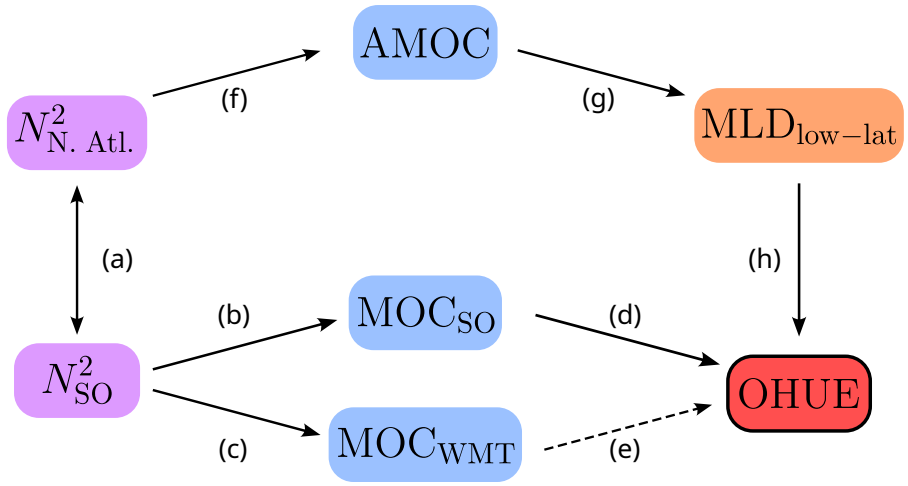

Figure 3.6: Schematic illustrating the inter-model links between key ocean properties. Arrows indicate the identified physically-based inter-model relationships, and the dashed arrow labelled (e) indicates the unclear relationship between M_{WMT} and OHUE.

models. Indeed, the loadings of this second EOF are correlated with OHUE across the model ensemble (Pearson $r = 0.57$, $p < 0.05$). This pattern of North Atlantic–Southern Ocean coherence is also found in the inter-model correlation between total preindustrial stratification and OHUE (Fig. 3.2a), and in the ensemble mean bias of historical total and salinity stratification with respect to observations (Fig. 3.4c,i).

The physical link between stratification in the mid-latitude Southern Ocean and the subpolar North Atlantic is illustrated by the outcropping of the same isopycnals in these two regions (Fig. 3.5c). In both regions, permanent stratification is dominated by the internal pycnocline of the global ocean, which separates the shallow northward and deep southward limbs of the AMOC (Gnanadesikan 1999; Klocker et al. 2023). An inter-hemispheric connection via the AMOC has also been shown to explain common temperature biases in the Southern Ocean of CMIP6 models (Luo et al. 2023). Certain characteristics of the subpolar North Atlantic can thus be proxies for those of the Southern Ocean and vice versa.

b) Southern Ocean stratification (N^2_{SO}) and upper cell strength (MOC_{SO})

Southern Ocean stratification impacts the strength of the Southern Ocean upper overturning cell M_{SO} computed in latitude–density coordinates (Fig. 3.3c). However, this correlation is relatively weak ($r < 0.6$ at most locations) and its spatial pattern is rather discontinuous, although consistent with the documented regions of water-mass formation feeding the upper overturning cell (east Indian and east Pacific basins in the latitude range 40°S–60°S; e.g., Sallée et al. 2010).

c) Southern Ocean stratification (N^2_{SO}) and upper cell strength inferred from surface buoyancy fluxes (MOC_{WMT})

The upper cell strength inferred from surface buoyancy fluxes, M_{WMT}, was used as an alternative measure of Southern Ocean overturning. It is impacted by stratification across the Southern Ocean and from latitudes of the ACC up to the subtropics (Fig. 3.3g), with higher correlations than for the alternative metric M_{SO}.

d) Upper cell strength (MOC_{SO}) and OHUE

The strength of the Southern Ocean upper overturning cell M_{SO} computed in latitude–density coordinates is well correlated with OHUE (Fig. 3.1d), and when ignoring the outlier model MRI-ESM2-0, the correlation coefficient ($r = 0.86$) is much higher than that for AMOC ($r = 0.61$). (In a different model ensemble, Gregory et al. (2023) found a correlation coefficient between AMOC and OHUE of $r = 0.83$.)

e) Upper cell strength inferred from surface buoyancy fluxes (MOC_{WMT}) and OHUE

The upper cell strength inferred from surface buoyancy fluxes, M_{WMT}, was found to be not significantly correlated with OHUE ($r = 0.39$, $p = 0.08$).

f) Subpolar North Atlantic stratification ($N^2_{N.Atl.}$) and AMOC

Preindustrial upper ocean stratification in the subpolar North Atlantic is anticorrelated with preindustrial AMOC strength (Fig. 3.3a). This is consistent with theoretical understanding and modeling results from previous studies which have shown that AMOC strength in CMIP6 is influenced by North Atlantic stratification (Nayak et al. 2024), especially in the Labrador Sea and due to salinity stratification (Jackson and Petit 2023; Jackson et al. 2023; Lin et al. 2023). This is because stratification in this region inhibits the formation of North Atlantic Deep Water which feeds the southward branch of the AMOC, mostly via open ocean deep convection in these models (Heuzé 2021).

g) AMOC and low-latitude mixed layer depth ($MLD_{low-lat}$)

Preindustrial AMOC strength is positively correlated with preindustrial MLD in the subpolar North Atlantic as well as in the low latitudes in all ocean basins (Fig. 3.3b). Subpolar North Atlantic MLD is a proxy for deep convection (Heuzé 2021; Jackson and Petit 2023), and its connection to AMOC strength is consistent with process understanding and related to point f) above (Jackson et al. 2023).

However, the reason for the link between AMOC and low-latitude mixed layer depths is unclear. Since significant positive correlations are not only found in the Atlantic, but also extend across the Pacific and Indian basins, it is possible that this relationship is not directly caused by a physical mechanism, but rather due to the spatial coherence of inter-model MLD spread, analogous to stratification in Section 3.5.2. Indeed, an inter-model EOF analysis applied to preindustrial annual mean MLD reveals a first-order coherence between subpolar North Atlantic MLD and global MLDs including the tropics (Fig. 3.A.8a), with the second- and third-order EOFs respectively containing the variance in the high and low latitudes separately (Fig. 3.A.8b–c).

h) Low–latitude mixed layer depth ($MLD_{low-lat}$) and OHUE

Preindustrial mixed layer depth in the low latitudes is positively correlated to OHUE (Fig. 3.2b). One hypothesis to explain this is that the mixed layer depth at these latitudes quantifies the thermal capacity of the ocean, since most of the radiative forcing is applied to the ocean surface at these latitudes (Gregory et al. 2023) and deeper mixed layers have a higher heat capacity. Furthermore, since sea surface temperatures are high and vertical temperature gradients are strong in the low latitudes, the modeled mixed layer depth there may be sensitive to the parameterization of vertical mixing of heat in these models. The representation of this mixing also impacts OHUE (Newsom et al. 2023), possibly contributing to the link between low-latitude MLD and OHUE.

3.6.2 Synthesis

We are now in a position to answer the questions posed in the Introduction of this study.

3.6.2.1 In which oceanic regions does stratification control OHUE?

The key regions where preindustrial stratification controls OHUE are the subpolar North Atlantic and the mid-latitude Southern Ocean (Fig. 3.2a). These two regions are linked together via the second-order mode of inter-model stratification spread (Fig. 3.5), and they are precisely the regions where ensemble mean historical stratification is biased high (Fig. 3.4c) due to biased salinity stratification (Fig. 3.4i). This is consistent with the findings of Liu et al. (2023) who showed that CMIP6 models tend to overestimate salinity stratification, particularly in these regions (their Figure 3a), and that salinity stratification approximated via sea surface salinity can be used to constrain OHUE. Our results demonstrate that it is possible that only the Southern Ocean stratification has a direct effect on OHUE through its influence on the large scale overturning circulation (Fig. 3.3d–i); the subpolar North Atlantic stratification could be anticorrelated with OHUE due to its connection with Southern Ocean stratification (Fig. 3.5) rather than due to a direct influence on OHUE. This would be consistent with previous findings showing that the actual amount

of anomalous heat entering the North Atlantic and being subducted by the AMOC is small compared to the OHU occurring in the mid-latitude Southern Ocean (Frölicher et al. 2015; Cheng et al. 2022), and that changes in the strength of OHUE and AMOC under transient forcing are uncorrelated (Stolpe et al. 2018). The direct link between OHUE and Southern Ocean stratification, rather than North Atlantic stratification, is further illustrated by a comparison of the upper ocean stratification definition used here with the pycnocline depth index defined by Newsom et al. (2023) (Fig. 3.A.9). This near-global (60°S–60°N) pycnocline depth index has been shown to nicely constrain OHUE (Newsom et al. 2023), and we show here that it is strongly anticorrelated with local stratification in the Southern Ocean but not in the subpolar North Atlantic (Fig. 3.A.9a).

3.6.2.2 How do temperature and salinity stratification differ in their control on OHUE?

Salinity stratification has a dominant role for OHUE due to several reasons. First, the inter-model spread in total stratification in key regions is dominated by spread in salinity stratification (Fig. 3.4h). Second, salinity stratification sets the spatial patterns of inter-model stratification spread as determined by the inter-model EOF analysis (Figs. 3.5 and 3.A.5). Finally, the pattern of the bias of CMIP6 ensemble mean stratification with respect to the ECCO state estimate is driven by the bias in salinity stratification (Fig. 3.4c,i). This is consistent with the dominant role of salinity stratification for OHUE found by Liu et al. (2023). However, temperature stratification also plays a role, in particular for setting the mean strength of global total stratification.

3.6.2.3 Is there any regional coherence of the inter-model spread in stratification, and how does this influence OHUE?

The inter-model EOF analysis has revealed two dominant modes of inter-model variation in preindustrial stratification (Fig. 3.5). The first mode consists of a broad coherence between all ocean basins except the North Atlantic and dominates inter-model variance. However, it is the second mode which connects stratification biases in the Southern Ocean and the North Atlantic, and which allows to interpret the meaning of North Atlantic stratification for OHUE (Section 3.6.2.1).

3.6.2.4 What explains the positive correlation between AMOC strength and OHUE across CMIP6 models?

AMOC strength is directly controlled by subpolar North Atlantic stratification. The positive correlation of AMOC with OHUE can be explained by two factors: i) North Atlantic stratification is connected to Southern Ocean stratification physically via the internal pycnocline (separating

shallow northward and deep southward limbs of the global overturning) and statistically via the second EOF of inter-model stratification spread. We argue that Southern Ocean stratification influences in turn OHUE via the overturning circulation; ii) both AMOC and OHUE are related to low-latitude MLD as a proxy of thermal capacity.

These two factors represent the upper and lower branches connecting AMOC to OHUE in the schematic in Figure 3.6, and presumably they both contribute to the positive correlation between AMOC and OHUE. Our analysis thus supports the hypothesis that the AMOC is not the mechanism actively controlling OHUE (Gregory et al. 2023). This hypothesis concurs with the observation that the amount of heat entering the North Atlantic and being subducted by the AMOC is relatively small compared to Southern Ocean OHU (Frölicher et al. 2015; Cheng et al. 2022), due to aerosol-induced cooling in the North Atlantic and larger subduction rates in the Southern Ocean (Williams et al. 2024).

3.6.2.5 What is the role of meridional overturning in the Southern Ocean for OHUE?

Our results make it clear that the AMOC might not be the ocean circulation directly affecting OHUE by transporting heat into the ocean interior, and that, instead, it is the Southern Ocean upper overturning cell which has a direct impact on OHUE. However, the link between Southern Ocean stratification to OHUE via Southern Ocean overturning is difficult to quantify. The connection between Southern Ocean stratification and Southern Ocean overturning is clearest when using an overturning metric inferred from surface buoyancy fluxes (M_{WMT}, Fig. 3.3c,e), but the link from Southern Ocean overturning to OHUE is only significant when using an overturning metric calculated directly from meridional velocities in latitude–density coordinates (Fig. 3.1d,e). This highlights the fundamental difficulties in pinning down the physical controls on Southern Ocean overturning in global climate models, especially at the regional level, and calls for the inclusion of more detailed overturning metrics in future CMIP exercises.

3.6.2.6 Code and data availability

All model output and observational data used in this study are freely available. CMIP6 model output is available from the Earth System Grid Federation at `https://esgf-node.llnl.gov/projects/cmip6/`. Data from the ECCO state estimate are available at `https://www.ecco-group.org/products-ECCO-V4r4.htm`.

The processed data and Python code used to produce the figures in this study are available at *<Zenodo URL to be provided upon acceptance>*

3.6.2.7 Author contributions

LV conceived the study, performed the data processing and analysis, and wrote the initial draft. JBS and CdL were responsible for supervision and funding acquisition. All authors contributed to interpreting the results and revising the paper.

3.6.2.8 Competing interests

The authors declare that they have no conflict of interest.

3.6.2.9 Acknowledgements

The authors thank Juliette Mignot, Ric Williams, and Robin Waldman for discussions. LV, JBS, and CdL received funding from the European Union's Horizon 2020 research and innovation programme under grant agreement no. 821001 (SO-CHIC).

3.A Supplementary Information

Model	piControl	1pctCO2	Data available for AMOC/M_{SO}/M_{WMT}
CanESM5	r1i1p1f1	r1i1p1f1	Y/Y/Y
CanESM5-CanOE	r1i1p2f1	r1i1p2f1	Y/Y/Y
CMCC-CM2-SR5	r1i1p1f1	r1i1p1f1	Y/Y/Y
CMCC-ESM2	r1i1p1f1	r1i1p1f1	Y/Y/Y
CNRM-CM6-1	r1i1p1f2	r1i1p1f2	Y/Y/Y
CNRM-CM6-1-HR	r1i1p1f2	r1i1p1f2	Y/N/Y
CNRM-ESM2-1	r1i1p1f2	r1i1p1f2	Y/Y/Y
ACCESS-ESM1-5	r1i1p1f1	r1i1p1f1	Y/Y/Y
ACCESS-CM2	r1i1p1f1	r1i1p1f1	Y/Y/Y
EC-Earth3	r1i1p1f1	r3i1p1f1	N/Y/N
EC-Earth3-CC	r1i1p1f1	r1i1p1f1	Y/Y/Y
EC-Earth3-Veg	r1i1p1f1	r1i1p1f1	Y/Y/N
EC-Earth3-Veg-LR	r1i1p1f1	r1i1p1f1	N/Y/N
IPSL-CM6A-LR	r1i1p1f1	r1i1p1f1	Y/Y/Y
MIROC6	r1i1p1f1	r1i1p1f1	Y/Y/Y
HadGEM3-GC31-LL	r1i1p1f1	r1i1p1f3	Y/Y/Y
HadGEM3-GC31-MM	r1i1p1f1	r1i1p1f3	Y/N/Y
UKESM1-0-LL	r1i1p1f2	r1i1p1f2	Y/Y/Y
MPI-ESM1-2-HR	r1i1p1f1	r1i1p1f1	Y/Y/Y
MPI-ESM1-2-LR	r1i1p1f1	r1i1p1f1	Y/Y/Y
MRI-ESM2-0	r1i1p1f1	r1i1p1f1	Y/Y/Y
GISS-E2-1-G	r1i1p1f2	r1i1p1f1	N/Y/N
CESM2	r1i1p1f1	r1i1p1f1	Y/N/N
CESM2-WACCM	r1i1p1f1	r1i1p1f1	Y/N/N
NorESM2-LM	r1i1p1f1	r1i1p1f1	Y/Y/N
NorESM2-MM	r1i1p1f1	r1i1p1f1	Y/Y/Y
GFDL-CM4	r1i1p1f1	r1i1p1f1	Y/N/Y
GFDL-ESM4	r1i1p1f1	r1i1p1f1	Y/N/Y

Table 3.A.1: CMIP6 models used in this study.

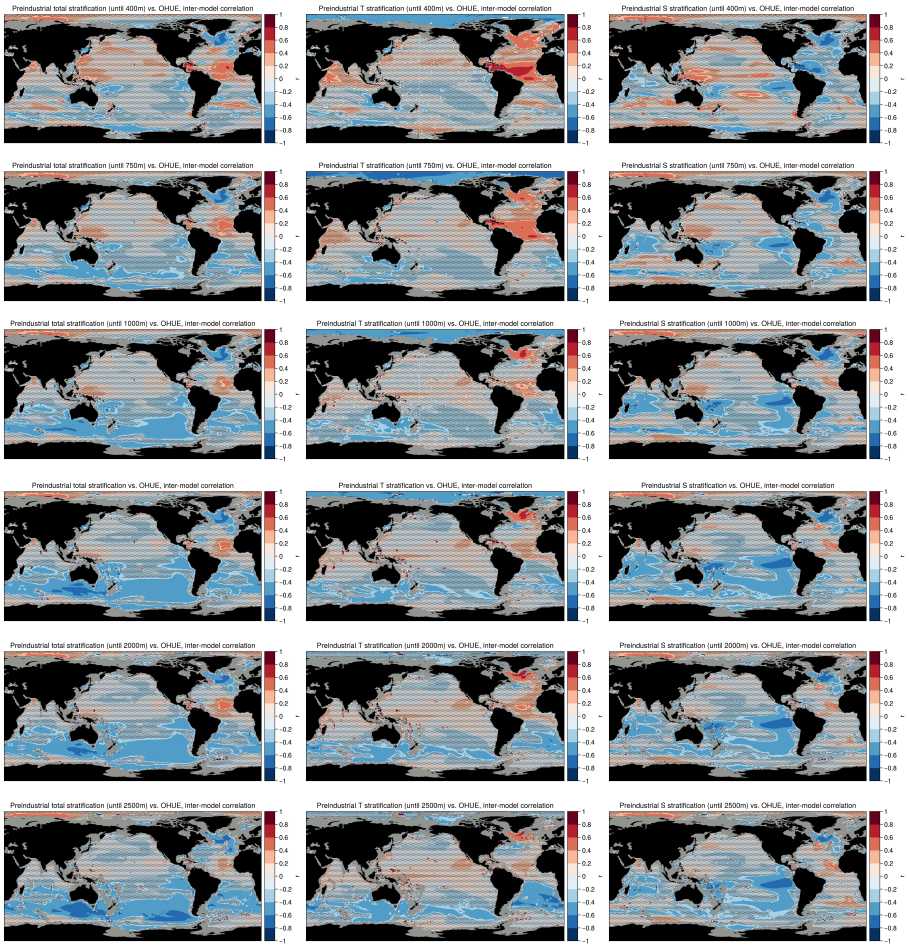

Figure 3.A.1: Maps of inter-model Pearson correlation coefficient between OHUE and local preindustrial annual mean total (left column), temperature (middle column), and total (right column) stratification across 28 CMIP6 models, with stratification in the depth ranges **(a)–(c)** 0–400 m, **(d)–(f)** 0–750 m, **(g)–(i)** 0–1000 m, **(j)–(l)** 0–1500 m, **(m)–(o)** 0–2000 m, and **(p)–(r)** 0–2500 m. Stippling indicates region where the linear slope is not significantly different from zero ($p \geq 0.05$, Wald test with t-distribution). Regions where the bathymetry is less than 1500 m deep are shaded in grey.

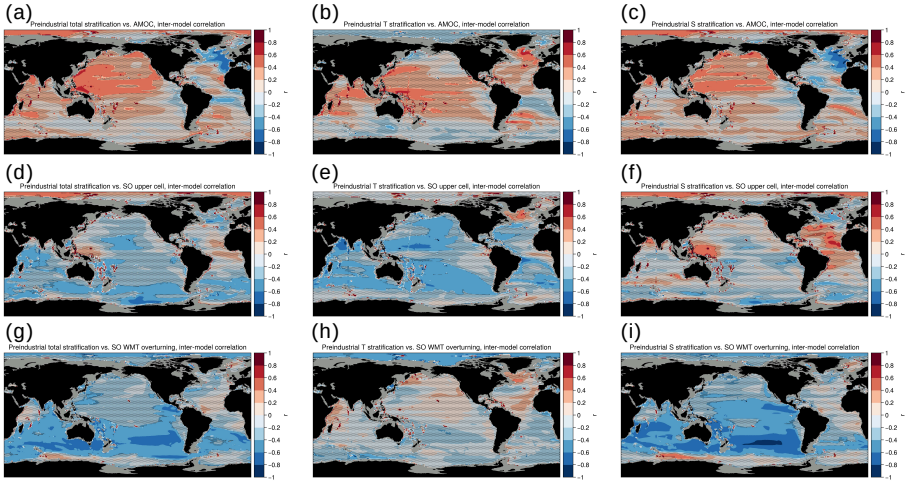

Figure 3.A.2: Inter-model relation between stratification and overturning cells. **(a)–(c)**: inter-model correlation between preindustrial 0–1500 m stratification and AMOC for total (left column), temperature (middle column), and salinity (right column) stratification. **(d)–(f)**: as in (a)–(c) but for the Southern Ocean upper cell in density coordinates. **(g)–(i)**: as in (a)–(c) but for the Southern Ocean overturning strength inferred from surface buoyancy fluxes (see Methods). Note that the first column of this figure is the same as the first column of Fig. 3.3 in the main text.

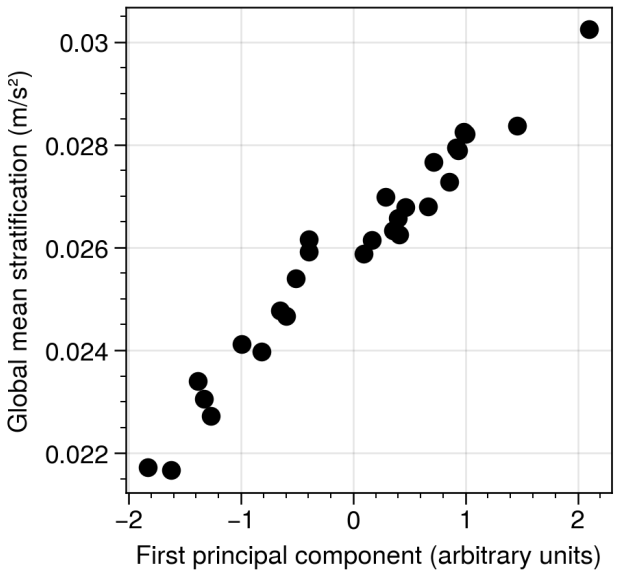

Figure 3.A.3: Scatter plot between the first principal component of the inter-model EOF analysis on preindustrial stratification (see Sect. 3.5.2) and global mean preindustrial stratification for each CMIP6 model.

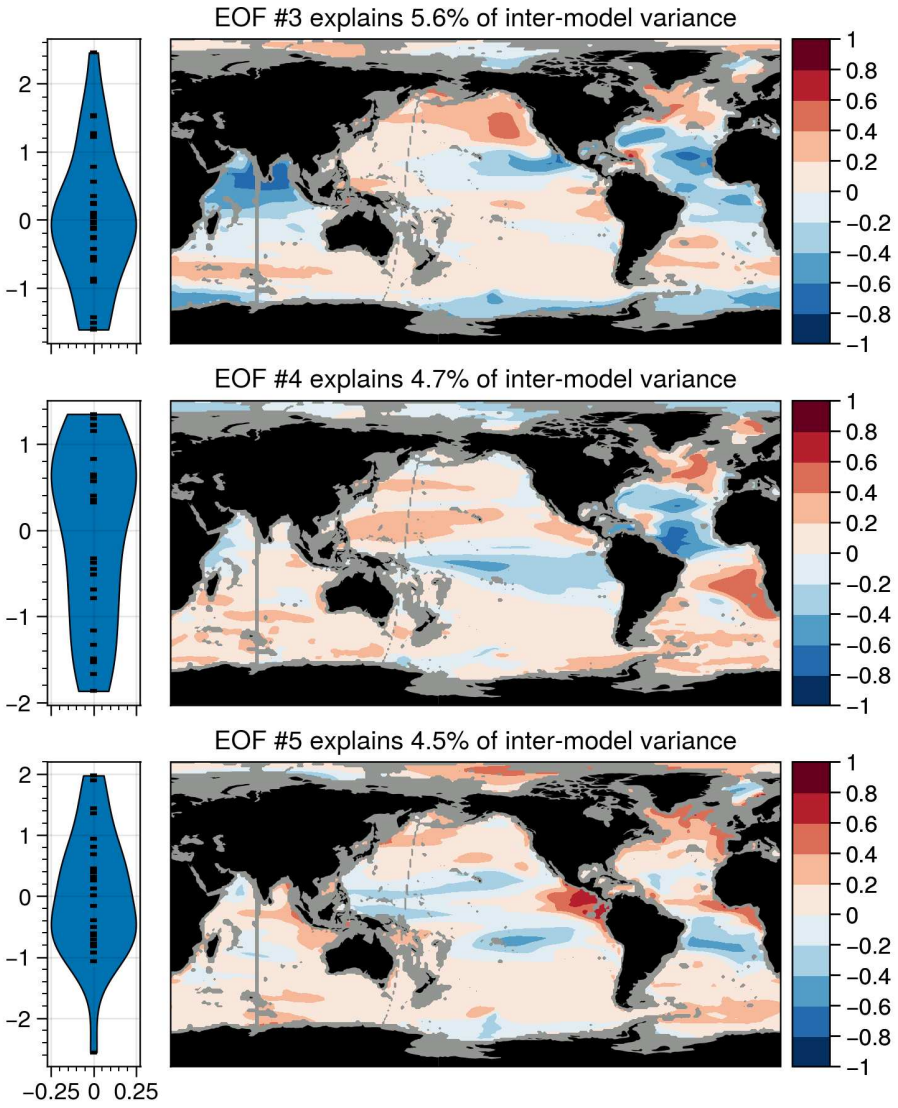

Figure 3.A.4: Modes 3 to 5 of inter-model empirical orthogonal function analysis on preindustrial annual mean upper ocean stratification.

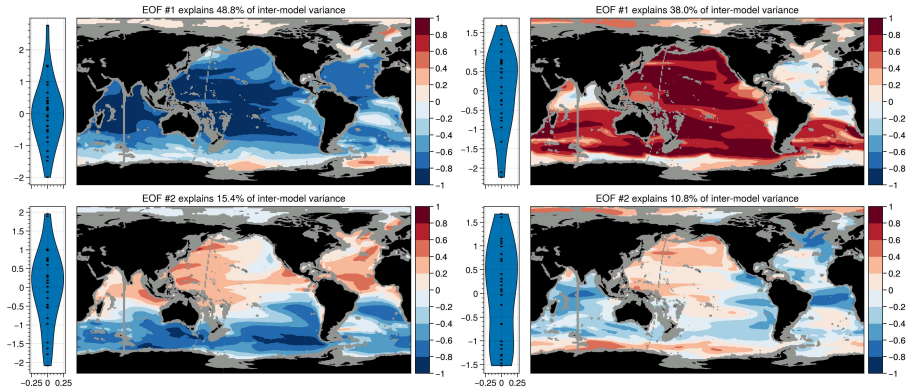

Figure 3.A.5: Left column: first and second mode of inter-model empirical orthogonal function analysis on preindustrial annual mean upper ocean temperature stratification. Right column: as left column, but for salinity stratification.

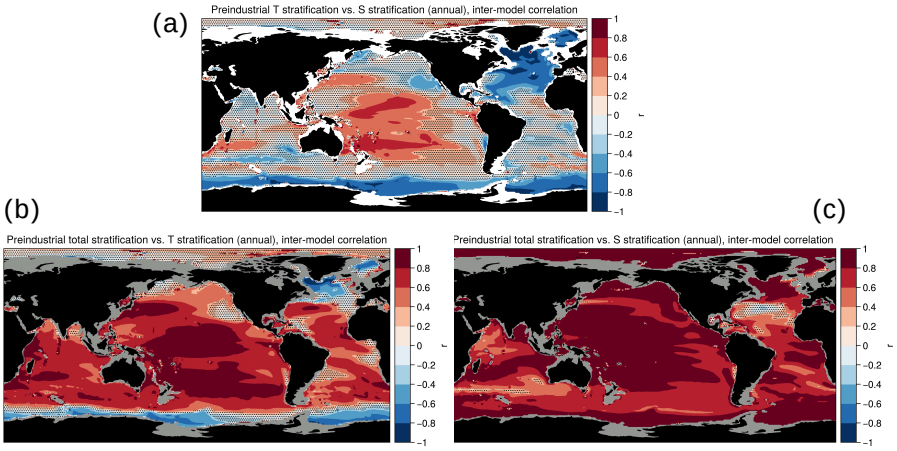

Figure 3.A.6: **(a)**, Map of inter-model correlation between preindustrial local 0–1500 m temperature stratification and salinity stratification. **(b)**, Same as (a) but between total stratification and temperature stratification. **(c)**, Same as (a) but between total stratification and salinity stratification.

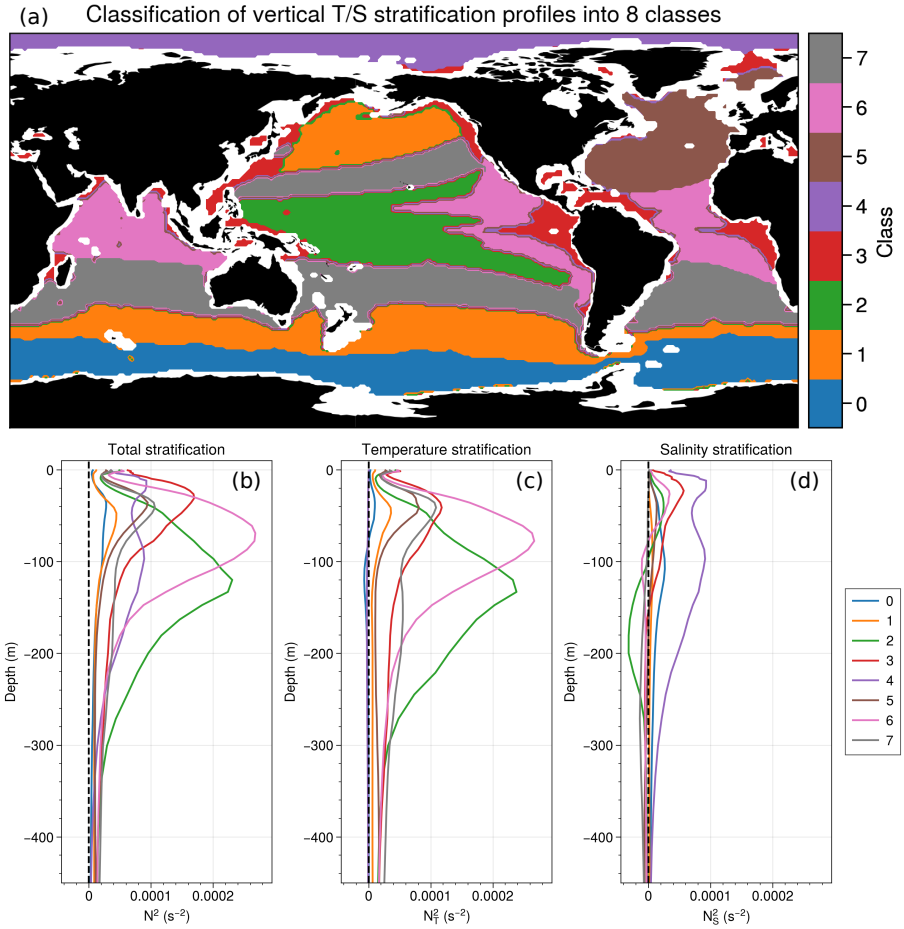

Figure 3.A.7: Classification of vertical stratification profiles. **(a)**, map showing the geographical location of identified classes. **(b)**–**(d)**, median vertical stratification profiles of each class (for total, temperature, and salinity stratification).

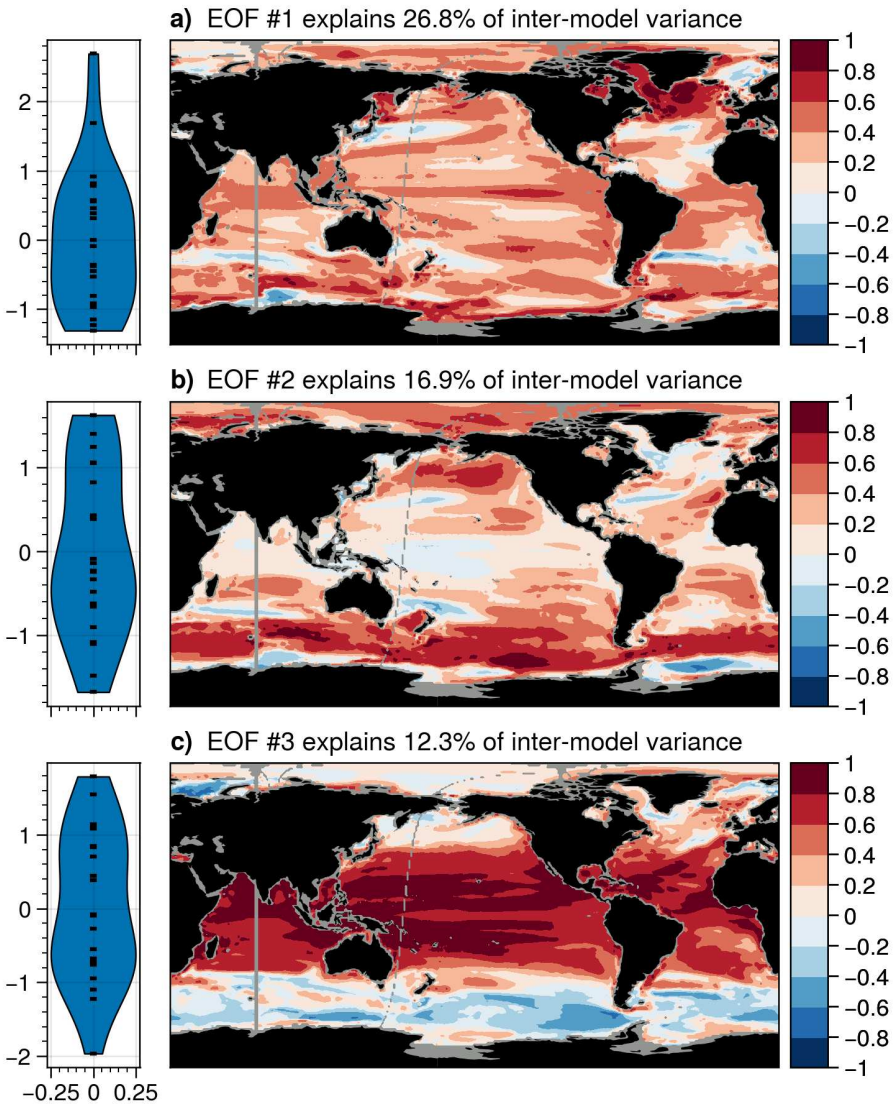

Figure 3.A.8: EOF analysis on preindustrial MLD. First three modes of inter-model empirical orthogonal function analysis on preindustrial annual mean MLD after removing 5 outlier models (see Methods).

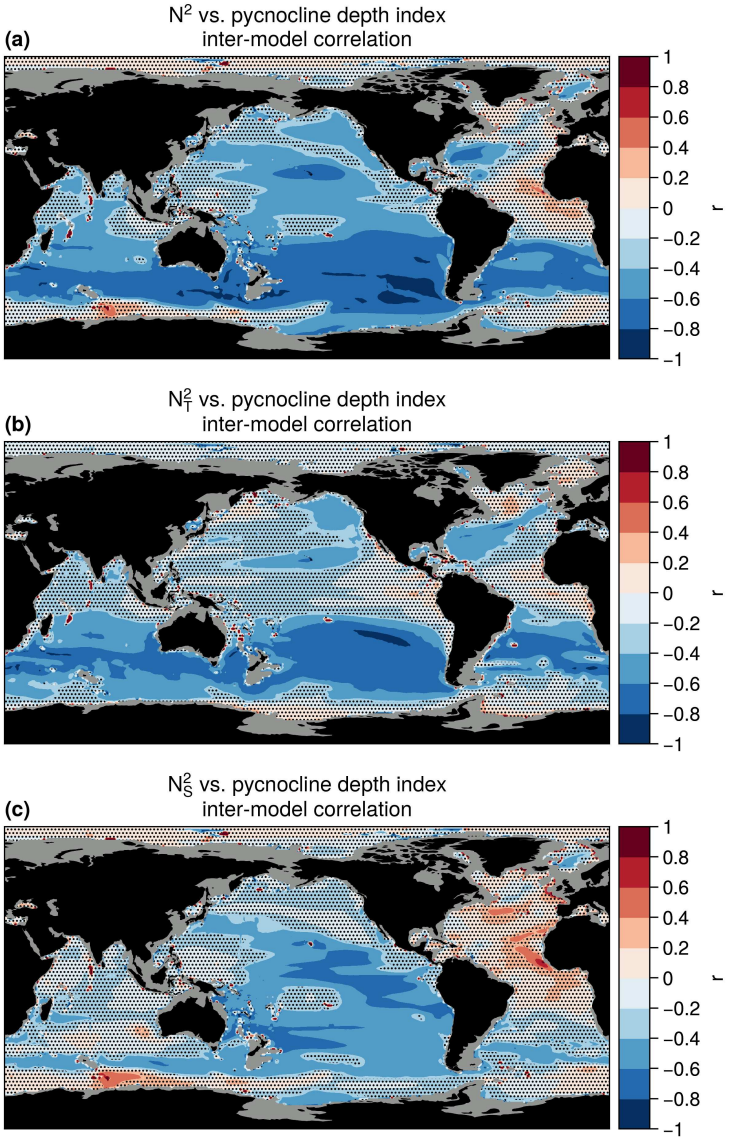

Figure 3.A.9: Inter-model correlation across 28 CMIP6 models between the pycnocline depth metric defined by Newsom et al. (2023) and local preindustrial annual mean **(a)** total, **(b)** temperature, and **(c)** salinity stratification.

Bibliography

Boé, J., A. Hall, and X. Qu (2009). "Deep ocean heat uptake as a major source of spread in transient climate change simulations". *Geophysical Research Letters* 36:22. _eprint: https://onlinelibrary.wiley.com/doi/pdf/10.1029/2009GL040845. ISSN: 1944-8007. DOI: 10.1029/2009GL040845.

Bourgeois, T., N. Goris, J. Schwinger, and J. F. Tjiputra (2022). "Stratification constrains future heat and carbon uptake in the Southern Ocean between 30°S and 55°S". *Nature Communications* 13:1. Bandiera_abtest: a Cc_license_type: cc_by Cg_type: Nature Research Journals Number: 1 Primary_atype: Research Publisher: Nature Publishing Group Subject_term: Biogeochemistry;Carbon cycle;Marine chemistry;Physical oceanography Subject_term_id: biogeochemistry;carbon-cycle;marine-chemistry;physical-oceanography, p. 340. ISSN: 2041-1723. DOI: 10.1038/s41467-022-27979-5.

Boyer Montégut, C. de, G. Madec, A. S. Fischer, A. Lazar, and D. Iudicone (2004). "Mixed layer depth over the global ocean: An examination of profile data and a profile-based climatology". *Journal of Geophysical Research: Oceans* 109, C12. _eprint: https://onlinelibrary.wiley.com/doi/pdf/10.1029/2004JC002378. ISSN: 2156-2202. DOI: 10.1029/2004JC002378.

Cheng, L. et al. (2022). "Past and future ocean warming". *Nature Reviews Earth & Environment*. Publisher: Nature Publishing Group, pp. 1–19. ISSN: 2662-138X. DOI: 10.1038/s43017-022-00345-1.

Dawson, A. (2016). "eofs: A Library for EOF Analysis of Meteorological, Oceanographic, and Climate Data". *Journal of Open Research Software* 4:1, e14. DOI: https://doi.org/10.5334/jors.122.

ECCO Consortium et al. (2024). *ECCO Central Estimate*. Version Version 4 Release 4.

Exarchou, E., T. Kuhlbrodt, J. M. Gregory, and R. S. Smith (2015). "Ocean Heat Uptake Processes: A Model Intercomparison". *Journal of Climate* 28:2. Publisher: American Meteorological Society Section: Journal of Climate, pp. 887–908. ISSN: 0894-8755, 1520-0442. DOI: 10.1175/JCLI-D-14-00235.1.

Eyring, V. et al. (2016). "Overview of the Coupled Model Intercomparison Project Phase 6 (CMIP6) experimental design and organization". *Geoscientific Model Development* 9:5, pp. 1937–1958. ISSN: 1991-9603. DOI: 10.5194/gmd-9-1937-2016.

Farneti, R. et al. (2015). "An assessment of Antarctic Circumpolar Current and Southern Ocean meridional overturning circulation during 1958–2007 in a suite of interannual CORE-II simulations". *Ocean Modelling* 93, pp. 84–120. ISSN: 1463-5003. DOI: 10.1016/j.ocemod.2015.07.009.

Forget, G. et al. (2015). "ECCO version 4: an integrated framework for non-linear inverse modeling and global ocean state estimation". *Geoscientific Model Development* 8:10. Publisher: Copernicus GmbH, pp. 3071–3104. ISSN: 1991-959X. DOI: 10.5194/gmd-8-3071-2015.

Forster, P. et al. (2021). "The Earth's energy budget, climate feedbacks, and climate sensitivity". In: *Climate Change 2021: The Physical Science Basis. Contribution of Working Group I to the Sixth Assessment Report of the Intergovernmental Panel on Climate Change*. Ed. by V. Masson-Delmotte et al. Cambridge University Press, Cambridge, United Kingdom and New York, NY, USA, pp. 923–1054. DOI: 10.1017/9781009157896.001.

Frölicher, T. L. et al. (2015). "Dominance of the Southern Ocean in Anthropogenic Carbon and Heat Uptake in CMIP5 Models". *Journal of Climate* 28:2. Publisher: American Meteorological Society Section: Journal of Climate, pp. 862–886. ISSN: 0894-8755, 1520-0442. DOI: 10.1175/JCLI-D-14-00117.1.

Gnanadesikan, A. (1999). "A Simple Predictive Model for the Structure of the Oceanic Pycnocline". *Science* 283:5410. Publisher: American Association for the Advancement of Science, pp. 2077–2079. DOI: 10.1126/science.283.5410.2077.

Gregory, J. M. (2000). "Vertical heat transports in the ocean and their effect on time-dependent climate change". *Climate Dynamics* 16:7, pp. 501–515. ISSN: 0930-7575, 1432-0894. DOI: 10.1007/s003820000059.

Gregory, J. M. and J. F. B. Mitchell (1997). "The climate response to CO2 of the Hadley Centre coupled AOGCM with and without flux adjustment". *Geophysical Research Letters* 24:15. _eprint: https://onlinelibrary.wiley.com/doi/pdf/10.1029/97GL01930, pp. 1943–1946. ISSN: 1944-8007. DOI: 10.1029/97GL01930.

Gregory, J. M. et al. (2023). "A new conceptual model of global ocean heat uptake". *Climate Dynamics*. ISSN: 1432-0894. DOI: 10.1007/s00382-023-06989-z.

Hanawa, K. and L. D.Talley (2001). "Chapter 5.4 Mode waters". In: *International Geophysics*. Ed. by G. Siedler, J. Church, and J. Gould. Vol. 77. Ocean Circulation and Climate. Academic Press, pp. 373–386. DOI: 10.1016/S0074-6142(01)80129-7.

He, J., M. Winton, G. Vecchi, L. Jia, and M. Rugenstein (2017). "Transient Climate Sensitivity Depends on Base Climate Ocean Circulation". *Journal of Climate* 30:4. Publisher: American Meteorological Society Section: Journal of Climate, pp. 1493–1504. ISSN: 0894-8755, 1520-0442. DOI: 10.1175/JCLI-D-16-0581.1.

Heuzé, C. (2021). "Antarctic Bottom Water and North Atlantic Deep Water in CMIP6 models". *Ocean Science* 17:1. Publisher: Copernicus GmbH, pp. 59–90. ISSN: 1812-0784. DOI: 10.5194/os-17-59-2021.

Hu, X. et al. (2020). "A less cloudy picture of the inter-model spread in future global warming projections". *Nature Communications* 11:1. Number: 1 Publisher: Nature Publishing Group, p. 4472. ISSN: 2041-1723. DOI: 10.1038/s41467-020-18227-9.

Huguenin, M. F., R. M. Holmes, and M. H. England (2022). "Drivers and distribution of global ocean heat uptake over the last half century". *Nature Communications* 13:1. Number: 1 Publisher: Nature Publishing Group, p. 4921. ISSN: 2041-1723. DOI: 10.1038/s41467-022-32540-5.

Jackson, L. C. and T. Petit (2023). "North Atlantic overturning and water mass transformation in CMIP6 models". *Climate Dynamics* 60:9, pp. 2871–2891. ISSN: 1432-0894. DOI: 10.1007/s00382-022-06448-1.

Jackson, L. C. et al. (2023). "Challenges simulating the AMOC in climate models". *Philosophical Transactions of the Royal Society A: Mathematical, Physical and Engineering Sciences* 381:2262. Publisher: Royal Society, p. 20220187. DOI: 10.1098/rsta.2022.0187.

Kamenkovich, I. and T. Radko (2011). "Role of the Southern Ocean in setting the Atlantic stratification and meridional overturning circulation". *Journal of Marine Research* 69:2, pp. 277–308. DOI: 10.1357/002224011798765286.

Klocker, A., A. C. Naveira Garabato, F. Roquet, C. de Lavergne, and S. R. Rintoul (2023). "Generation of the Internal Pycnocline in the Subpolar Southern Ocean by Wintertime Sea Ice Melting". *Journal of Geophysical Research: Oceans* 128:3. _eprint: https://onlinelibrary.wiley.com/doi/pdf/10.1029/2022JC019113, e2022JC019113. ISSN: 2169-9291. DOI: 10.1029/2022JC019113.

Kostov, Y., K. C. Armour, and J. Marshall (2014). "Impact of the Atlantic meridional overturning circulation on ocean heat storage and transient climate change". *Geophysical Research Letters* 41:6. _eprint: https://onlinelibrary.wiley.com/doi/pdf/10.1002/2013GL058998, pp. 2108–2116. ISSN: 1944-8007. DOI: 10.1002/2013GL058998.

Kuhlbrodt, T. and J. M. Gregory (2012). "Ocean heat uptake and its consequences for the magnitude of sea level rise and climate change". *Geophysical Research Letters* 39:18. _eprint: https://onlinelibrary.wiley.com/doi/pdf/10.1029/2012GL052952. ISSN: 1944-8007. DOI: 10.1029/2012GL052952.

Kuhlbrodt, T. et al. (2007). "On the driving processes of the Atlantic meridional overturning circulation". *Reviews of Geophysics* 45:2. _eprint: https://onlinelibrary.wiley.com/doi/pdf/10.1029/2004RG000166. ISSN: 1944-9208. DOI: 10.1029/2004RG000166.

Lin, Y.-J., B. E. J. Rose, and Y.-T. Hwang (2023). "Mean state AMOC affects AMOC weakening through subsurface warming in the Labrador Sea". *Journal of Climate* -1, aop. Publisher: American Meteorological Society Section: Journal of Climate, pp. 1–44. ISSN: 0894-8755, 1520-0442. DOI: 10.1175/JCLI-D-22-0464.1.

Liu, M., B. J. Soden, G. A. Vecchi, and C. Wang (2023). "The Spread of Ocean Heat Uptake Efficiency Traced to Ocean Salinity". *Geophysical Research Letters* 50:4. _eprint: https://onlinelibrary.wiley.com/doi/pdf/10.1029/2022GL100171, e2022GL100171. ISSN: 1944-8007. DOI: 10.1029/2022GL100171.

Luo, F., J. Ying, T. Liu, and D. Chen (2023). "Origins of Southern Ocean warm sea surface temperature bias in CMIP6 models". *npj Climate and Atmospheric Science* 6:1. Number: 1 Publisher: Nature Publishing Group, pp. 1–8. ISSN: 2397-3722. DOI: 10.1038/s41612-023-00456-6.

Marzocchi, A., A. J. G. Nurser, L. Clément, and E. L. McDonagh (2021). "Surface atmospheric forcing as the driver of long-term pathways and timescales of ocean ventilation". *Ocean Science* 17:4, pp. 935–952. ISSN: 1812-0792. DOI: 10.5194/os-17-935-2021.

Maze, G. (2020). *Ocean Profile Classification Model in python*. Version 0.4.1. DOI: 10.5281/zenodo.3906236.

Maze, G. et al. (2017). "Coherent heat patterns revealed by unsupervised classification of Argo temperature profiles in the North Atlantic Ocean". *Progress in Oceanography* 151, pp. 275–292. ISSN: 0079-6611. DOI: 10.1016/j.pocean.2016.12.008.

McCartney, M. S. (1979). *Subantarctic mode water*. Woods Hole Oceanographic Institution.

McDougall, T. J. and P. M. Barker (2011). *Getting started with TEOS-10 and the Gibbs Seawater (GSW) Oceanographic Toolbox*. SCOR/IAPSO WG127. 28 pp. ISBN: 978-0-646-55621-5.

McDougall, T. J., S. Groeskamp, and S. M. Griffies (2014). "On Geometrical Aspects of Interior Ocean Mixing". *Journal of Physical Oceanography* 44:8, pp. 2164–2175. ISSN: 0022-3670, 1520-0485. DOI: 10.1175/JPO-D-13-0270.1.

Meehl, G. A. et al. (2020). "Context for interpreting equilibrium climate sensitivity and transient climate response from the CMIP6 Earth system models". *Science Advances* 6:26. Publisher: American Association for the Advancement of Science, eaba1981. DOI: 10.1126/sciadv.aba1981.

Morrison, A. K., S. M. Griffies, M. Winton, W. G. Anderson, and J. L. Sarmiento (2016). "Mechanisms of Southern Ocean Heat Uptake and Transport in a Global Eddying Climate Model". *Journal of Climate* 29:6. Publisher: American Meteorological Society Section: Journal of Climate, pp. 2059–2075. ISSN: 0894-8755, 1520-0442. DOI: 10.1175/JCLI-D-15-0579.1.

Morrison, A. K., D. W. Waugh, A. M. Hogg, D. C. Jones, and R. P. Abernathey (2022). "Ventilation of the Southern Ocean Pycnocline". *Annual Review of Marine Science* 14:1. _eprint:

https://doi.org/10.1146/annurev-marine-010419-011012, pp. 405–430. DOI: 10.1146/annurev-marine-010419-011012.

Nayak, M. S., D. B. Bonan, E. R. Newsom, and A. F. Thompson (2024). "Controls on the Strength and Structure of the Atlantic Meridional Overturning Circulation in Climate Models". *Geophysical Research Letters* 51:11. _eprint: https://onlinelibrary.wiley.com/doi/pdf/10.1029/2024GL109055, e2024GL109055. ISSN: 1944-8007. DOI: 10.1029/2024GL109055.

Newsom, E., L. Zanna, and J. Gregory (2023). "Background Pycnocline Depth Constrains Future Ocean Heat Uptake Efficiency". *Geophysical Research Letters* 50:22. _eprint: https://onlinelibrary.wiley.com/doi/pdf/10.1029/2023GL105673, e2023GL105673. ISSN: 1944-8007. DOI: 10.1029/2023GL105673.

Romanou, A., J. Marshall, M. Kelley, and J. Scott (2017). "Role of the ocean's AMOC in setting the uptake efficiency of transient tracers". *Geophysical Research Letters* 44:11. _eprint: https://onlinelibrary.wiley.com/doi/pdf/10.1002/2017GL072972, pp. 5590–5598. ISSN: 1944-8007. DOI: 10.1002/2017GL072972.

Roquet, F., G. Madec, L. Brodeau, and J. Nycander (2015). "Defining a Simplified Yet "Realistic" Equation of State for Seawater". *Journal of Physical Oceanography* 45:10. Publisher: American Meteorological Society Section: Journal of Physical Oceanography, pp. 2564–2579. ISSN: 0022-3670, 1520-0485. DOI: 10.1175/JPO-D-15-0080.1.

Saenko, O. A., D. Yang, and J. M. Gregory (2018). "Impact of Mesoscale Eddy Transfer on Heat Uptake in an Eddy-Parameterizing Ocean Model". *Journal of Climate*. Section: Journal of Climate. DOI: 10.1175/JCLI-D-18-0186.1.

Sallée, J. B., K. G. Speer, and S. R. Rintoul (2010). "Zonally asymmetric response of the Southern Ocean mixed-layer depth to the Southern Annular Mode". *Nature Geoscience* 3:4. Number: 4 Publisher: Nature Publishing Group, pp. 273–279. ISSN: 1752-0908. DOI: 10.1038/ngeo812.

Schuckmann, K. von et al. (2020). "Heat stored in the Earth system: where does the energy go?" *Earth System Science Data* 12:3. Publisher: Copernicus GmbH, pp. 2013–2041. ISSN: 1866-3508. DOI: 10.5194/essd-12-2013-2020.

Shi, J.-R., S.-P. Xie, and L. D. Talley (2018). "Evolving Relative Importance of the Southern Ocean and North Atlantic in Anthropogenic Ocean Heat Uptake". *Journal of Climate* 31:18. Publisher: American Meteorological Society Section: Journal of Climate, pp. 7459–7479. ISSN: 0894-8755, 1520-0442. DOI: 10.1175/JCLI-D-18-0170.1.

Stolpe, M. B., I. Medhaug, J. Sedláček, and R. Knutti (2018). "Multidecadal Variability in Global Surface Temperatures Related to the Atlantic Meridional Overturning Circulation". *Journal of Climate* 31:7, pp. 2889–2906. ISSN: 0894-8755, 1520-0442. DOI: 10.1175/JCLI-D-17-0444.1.

Vogt, L. et al. (2024). *Increased future ocean heat uptake constrained by Antarctic sea ice extent*. ISSN: 2693-5015. DOI: 10.21203/rs.3.rs-3982037/v1.

Wang, C., L. Zhang, S.-K. Lee, L. Wu, and C. R. Mechoso (2014). "A global perspective on CMIP5 climate model biases". *Nature Climate Change* 4:3. Number: 3 Publisher: Nature Publishing Group, pp. 201–205. ISSN: 1758-6798. DOI: 10.1038/nclimate2118.

Williams, R. G. et al. (2024). "Asymmetries in the Southern Ocean contribution to global heat and carbon uptake". *Nature Climate Change* 14:8. Publisher: Nature Publishing Group, pp. 823–831. ISSN: 1758-6798. DOI: 10.1038/s41558-024-02066-3.

Winton, M. et al. (2014). "Has coarse ocean resolution biased simulations of transient climate sensitivity?" *Geophysical Research Letters* 41:23. _eprint: https://onlinelibrary.wiley.com/doi/pdf/10.1002/2014GL061 pp. 8522–8529. ISSN: 1944-8007. DOI: 10.1002/2014GL061523.

4 Outlook: Improved constraints through statistical analysis of a large multi-model ensemble

4.1 Introduction

In Chapter 2, we have already found an emergent constraint on total future OHU, and in Chapter 3, we determined the most important variables and regions controlling the inter-model spread in OHUE. A natural extension of these results would thus be to search for an emergent constraint on OHUE in the CMIP6 ensemble. Although related by definition, total OHU and OHUE are not controlled by the same processes: total OHU integrates the strength of radiative forcing and climate feedbacks (Sec. 1.1.2) and correlates with global warming (Gregory et al. 2023), while OHUE is defined by scaling total OHU by this global warming (Eq. 1.10), thus removing some of this atmospheric influence and yielding a more purely oceanic metric. Indeed, total OHU and OHUE are not correlated across CMIP5/6 models, and only OHUE correlates with preindustrial AMOC strength (Gregory et al. 2023).

Future OHUE has been previously constrained using global mean sea surface salinity (SSS) as a predictor chosen as a proxy for upper ocean stratification (Liu et al. 2023), but the underlying correlation was rather dependent on outlier models, and global mean SSS is a rather crude physical metric considering the rich spatial structure and multivariate nature of inter-model controls on OHUE spread shown in Chapter 3; it also does not explicitly take into account the much-discussed relation between AMOC strength and OHUE (Winton et al. 2014). Similarly, the OHUE constraint of Bourgeois et al. (2022) based on Southern Ocean stratification is, although consistent with the conclusions of Chapter 3, only regional in nature and thus not directly applicable for a global OHUE constraint. In this outlook chapter, we therefore attempt to leverage the multivariate and spatially resolved information gained in Chapter 3 to search for a potential emergent constraint on OHUE.

The analysis in this chapter is very loosely inspired by an (unpublished) collaboration with B.B. Cael and J. Terhaar.

In Chapters 2 and 3, only one initial condition ensemble member was used per CMIP6 model, under the implicit assumption (also widely employed in multi-model studies in the literature) that initial condition and parameter uncertainty are less important than structural uncertainty on long time scales (Fig. 1.17 in the Introduction). In this chapter, we instead choose to use the maximum number of initial condition and parameter perturbation members available for each model in the CMIP6 archive in order to better sample these sources of uncertainty. The vast majority of archived single-model ensembles for individual CMIP6 models are initial condition ensembles, although a few models provide ensembles with members differing in the choice of certain model components (e.g., for aerosol chemistry) and therefore sample a form of parameter uncertainty. We choose to use only widely available output variables (SST, SSS and meridional overturning streamfunctions) as predictors, since the full-depth ocean temperature and salinity fields needed for the calculation of stratification and MLD are often not included in the archived model output of all ensemble members. We also include total OHU and global mean surface warming as predictands to be potentially constrained, since these variables are related by definition to OHUE.

With the greater number of members per model compared to the previous chapters, structural similarities can be investigated among and across members originating from the same climate model, modeling center, or sharing the same ocean or atmospheric model component. Furthermore, the greater total number of members retained (ca. 120 members per SSP, see below) allows for a more robust application of statistical analysis techniques, both to understand the ensemble structure of the predictors as well as to perform regression to constrain the predictands.

The rest of this chapter is structured into two parts: Section 4.2 details the regional predictor variables and global predictand variables used in Section 4.3, which presents preliminary results of an analysis of this data.

4.2 Model output for predictor and target variables

We use 127 members from 21 models for SSP1-2.6, 160 members from 21 models for SSP2-4.5, 115 members from 11 models for SSP3-7.0, and 130 members from 23 models for SSP5-8.5, according to the availability of the necessary model output (including the predictor variables of Sec. 4.2.2) in the CMIP6 archive (the number of members shown in the figures below can slightly differ from these a priori available members due to minor issues in the archived model output.) These members are mostly initial condition ensemble members as described above, but also include different versions of the GISS-E2-1-G model (with the aerosol chemistry component set to different versions or omitted; NASA/GISS 2018), as well as the CanESM5 large ensemble with 50 members in total, which is split into two 25-member sub-ensembles each employing one of two

choices for remapping wind stress onto the ocean model grid, which can influence local ocean dynamics (Swart et al. 2019).

4.2.1 Predictand variables

We use total OHU, global mean surface air temperature anomaly ΔSAT, and OHUE as predictors to be potentially constrained in this Chapter; these variables are detailed in Table 4.1. Anomalies of OHU and surface air temperature are computed by subtracting the average over the full preindustrial experiment for the parent simulation of each historical and SSP member, since the preindustrial period exactly corresponding to each historical or SSP member (as in Chapters 2 and 3) is not available for all models. Anomalies are averaged over the years 2080–2100 in each SSP scenario, and OHUE is defined as OHUE = OHU/ΔSAT (unlike OHUE = OHU/(1.5 · ΔSST) as in Chapter 3 and Gregory et al. 2023) for a more direct definitional relationship between the three predictands (OHU, ΔSAT, and OHU/ΔSAT).

Predictand	Description
OHU	Global ocean heat uptake defined as global mean air-sea heat flux anomaly, in $\mathrm{W\,m^{-2}}$
ΔSAT	Global mean surface air temperature anomaly, in K
OHUE	Ocean heat uptake efficiency defined as OHU/ΔSAT, in $\mathrm{W\,m^{-2}\,K^{-1}}$

Table 4.1: Variables used as predictands/targets for the statistical analysis in this chapter. All variables are annual mean anomalies relative to the preindustrial mean averaged over the years 2080–2100 in a given SSP scenarios.

4.2.1.1 Global surface warming and ocean heat uptake

Figure 4.1 shows time series of global mean ΔSAT for the high-mitigation SSP1-2.6 and the low-mitigation SSP5-8.5 scenarios (here and in the following, the SSP2-4.5 and SSP3-7.0 scenarios are depicted in corresponding figures in Appendix B). In each panel, the simulations over the CMIP6 `historical` period (until 2014) are identical and branch off into different scenario projections after 2014. Under SSP1-2.6, the increase in global mean ΔSAT stagnates after around 2050 in most members and even reverses towards the end of the century in some members (Fig. 4.1a), while it continues increasing under the other three SSP scenarios (Figs. 4.1b and B.1). The ensemble mean ΔSAT over 2080–2100 under SSP1-2.6 averaged over all members is 2.51 ± 0.99 K (95% confidence interval approximated as $1.96 \cdot \hat{\sigma}$, where $\hat{\sigma}$ is the sample standard deviation), and under SSP5-8.5 it is 5.89 ± 2.34 K. The relative inter-model spread ($\hat{\sigma}$ divided by the ensemble mean) is relatively constant across the four SSPs considered with values from 0.19 to 0.24. However, these estimates are biased since climate models with more members (such as CanESM5) are

overrepresented. Calculating the multi-model mean after averaging over each model's members separately first leads to an ensemble mean ΔSAT projections of 2.27 ± 1.07 K for SSP1-2.6 and 5.17 ± 2.00 K for SSP5-8.5, which are both smaller than the raw average over all members, while the relative inter-model spread remains in the same range as for the raw members.

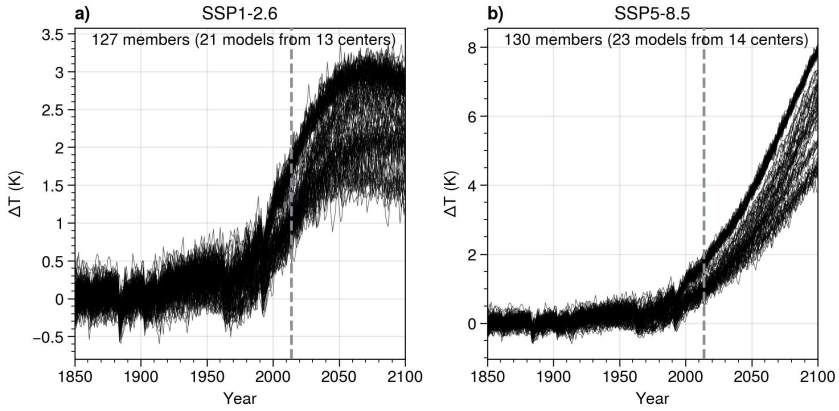

Figure 4.1: Global mean surface air temperature anomaly ΔSAT under the SSP1-2.6 and SSP5-8.5 scenarios. The dashed vertical line indicates the year 2014 where the SSP runs branch off from the historical run in each ensemble member. The corresponding figure for SSP2-4.5 and SSP3-7.0 is shown in Fig. B.1 in Appendix B.

Figure 4.2 shows the analogous time series for global OHU, where the ensemble mean in 2080–2100 over all members is 1.10 ± 0.35 W m^{-2} for SSP1-2.6 and 4.31 ± 1.21 W m^{-2} for SSP5-8.5. The relative inter-model spread in OHU is smaller than for ΔSAT and is between 0.12 and 0.16 across the four SSPs. The multi-model mean obtained after averaging each model's members separately first is 1.19 ± 0.44 W m^{-2} for SSP1-2.6 and 3.89 ± 1.09 W m^{-2} for SSP5-8.5 (i.e., higher than the raw average for SSP1-2.6 and lower for SSP5-8.5), and the relative inter-model spread is generally higher (between 0.13 and 0.19). The increase in global OHU stagnates towards the end of the century under SSP1-2.6 and SSP2-4.5, while it continues to increase under SSP3-7.0 and SSP5-8.5.

4.2.1.2 Ocean heat uptake efficiency

The OHUE time series resulting from these ΔSAT and OHU time series is shown in Fig. 4.3. OHUE generally declines over time (Figs. 4.3 and B.3). Under SSP5-8.5, the ensemble mean OHUE over 2080–2100 is 0.76 ± 0.16 W m^{-2} K^{-1} averaged over all members and 0.80 ± 0.21 W m^{-2} K^{-1} averaged over separate model means, with a relative inter-model spread of 0.11. For the scenarios with weaker forcing (SSP1-2.6 and potentially SSP2-4.5), the OHUE concept is not applicable, since both ΔSAT and OHU cease their steady increase at some point after 2050. This can be seen

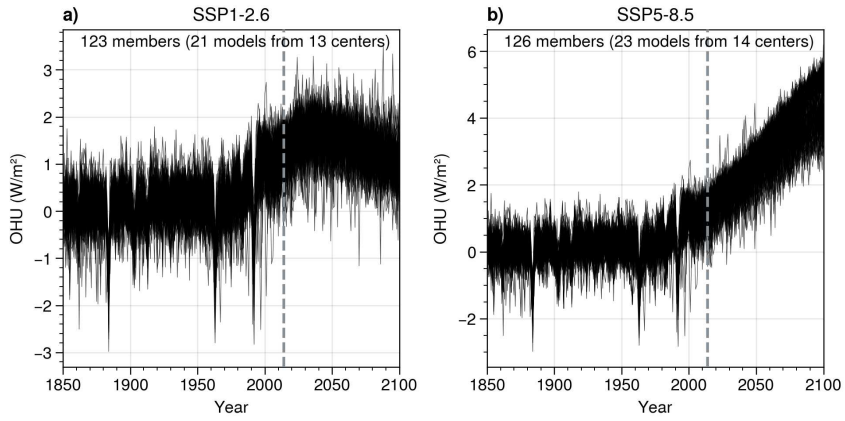

Figure 4.2: Global ocean heat uptake (OHU) under the SSP1-2.6 and SSP5-8.5 scenarios. The dashed vertical line indicates the year 2014 where the SSP runs branch off from the historical run in each ensemble member. The corresponding figure for SSP2-4.5 and SSP3-7.0 is shown in Fig. B.2 in Appendix B.

in a visualization of OHU plotted against ΔSAT (Fig. 4.4, where the slope of each curve is OHUE, and the underlying blue shading are the same as in Fig. 4.3): under SSP1-2.6, ΔSAT approaches a (model-dependent) equilibrium value while OHU continues to decrease, which is shown by the "fingers" in Fig. 4.4a descending at values of ΔSAT between 1.5 and 3 K. A similar but less drastic behavior is seen for SSP2-4.5 (Fig. B.4). Under the stronger forcing of SSP3-7.0 and SSP5-8.5, on the other hand, both ΔSAT and OHU continually increase through to 2100, and the OHUE concept is valid. The decrease in OHUE with time can be seen in Fig. 4.4b as the decrease in the slope of OHU as a function of ΔSAT with increasing ΔSAT.

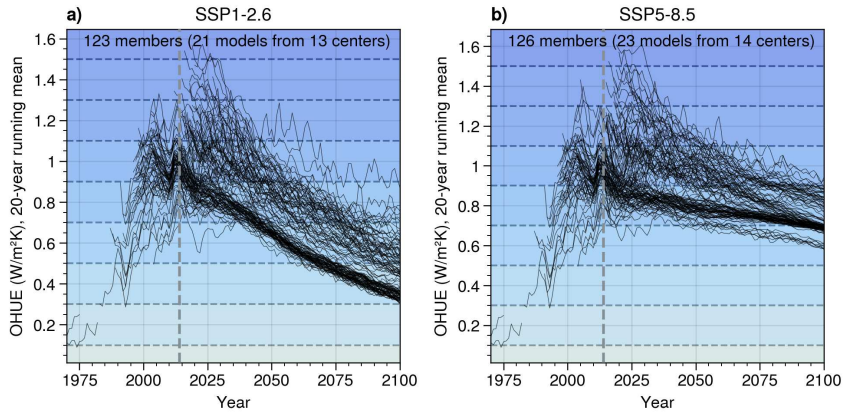

Figure 4.3: Ocean heat uptake efficiency (OHUE) under the SSP1-2.6 and SSP5-8.5 scenarios (20-year running mean). The dashed vertical line indicates the year 2014 where the SSP runs branch off from the historical run in each ensemble member. The corresponding figure for SSP2-4.5 and SSP3-7.0 is shown in Fig. B.3 in Appendix B.

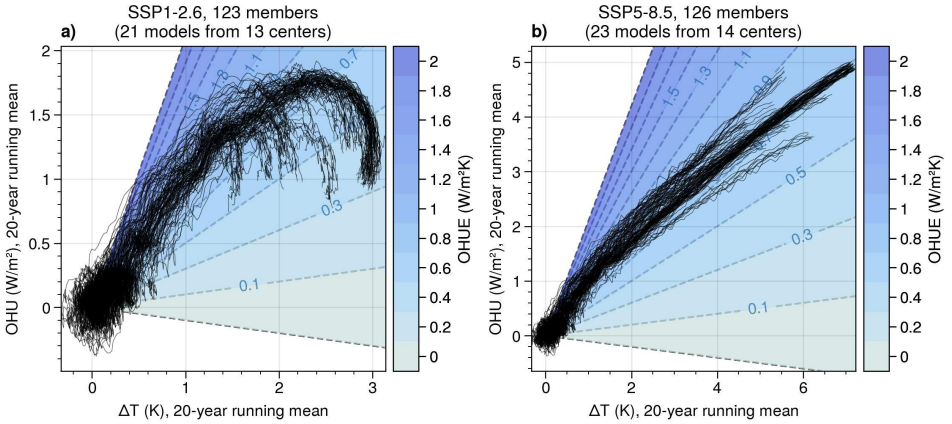

Figure 4.4: Global OHU plotted against global ΔSAT under the SSP1-2.6 and SSP5-8.5 scenarios (20-year running mean). The blue shading and labeled contours indicate the resulting OHU efficiency (OHUE = OHU/ΔSAT). The corresponding figure for SSP2-4.5 and SSP3-7.0 is shown in Fig. B.4 in Appendix B.

Figure 4.5 shows a scatter plot of OHU versus ΔSAT averaged over 2080–2100 for SSP3-7.0 and SSP5-8.5 (the two SSP scenarios for which the OHUE concept is fully applicable throughout the 21st century). The markers are colored according to the climate model of each member, and the marker shape corresponds to the ocean model component used in each climate model (see the legend in Fig. 4.5). Since more models have supplied output for SSP5-8.5 than for SSP3-7.0, we will focus on the low-mitigation SSP5-8.5 scenario here, additionally benefitting from a larger signal-to-noise ratio. An inspection of Figure 4.5b permits several observations: (i) there is substantial inter-model spread along directions of constant OHUE, meaning that OHU and ΔSAT partly compensate each other across models; (ii) at least visually, intra-model spread (i.e., among members of a single model) is generally contained in OHU, while ΔSAT variations are smaller (leading to vertical spreading of model members in the ΔSAT–OHU plane of Fig. 4.5); (iii) intra-model spread is generally smaller than inter-model spread, but can be comparable (e.g., the intra-model spread of CNRM-ESM2-1 is greater than the inter-model distance between NorESM2-MM and MPI-ESM1-2-LR); and finally, (iv) members with NEMO ocean components generally have smaller OHUE, although with greatly varying (and compensating) values of OHU and ΔSAT.

4.2.2 Predictor variables

We now turn to the predictor variables used in this chapter, i.e., the variables used to potentially constrain the future predictand variables ΔSAT, OHU, and OHUE introduced above. Fig. 4.6 shows a schematic of the employed predictor variables, which are also detailed in Table 4.3: re-

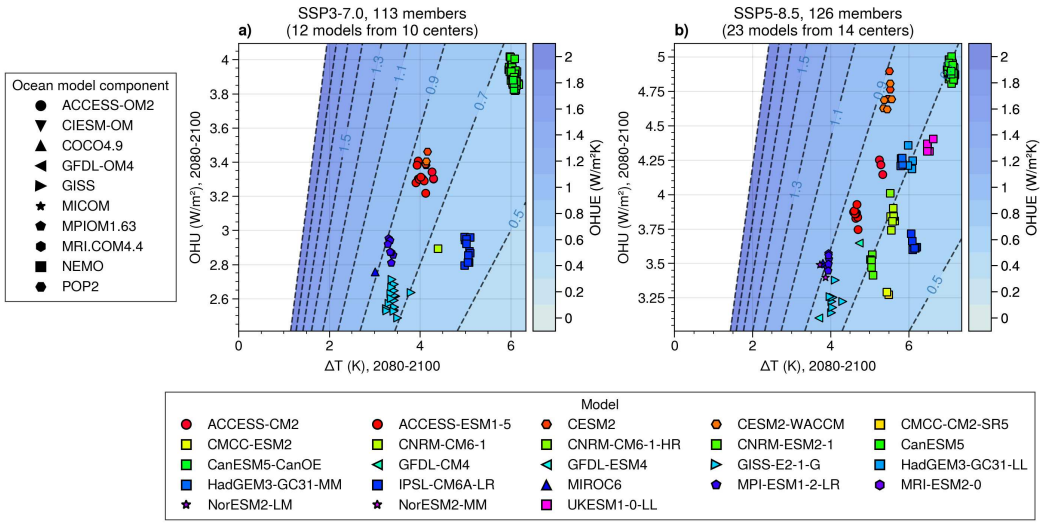

Figure 4.5: Global OHU plotted against global ΔSAT (averaged over 2080–2100 in the SSP3-7.0 and SSP5-8.5 scenarios). The blue shading and labeled contours indicate the resulting OHU efficiency (OHUE = OHU/ΔSAT). The marker colors indicate the different climate models, and the marker shape indicate their ocean model component. The corresponding figure for SSP1-2.6 and SSP2-4.5 is shown in Fig. B.5 in Appendix B.

gional SST (in six regions detailed in Tab. 4.2), regional SSS, and AMOC strength. These variables are evaluated over 1850–1900 in each model's `historical` experiment, since the greater number of historical over preindustrial simulations yields a larger sample size. As an example, Fig. B.6 shows AMOC time series for SSP1-2.6 and SSP5-8.5. The reasoning for choosing these variables as potential predictors is that, for each of them, there is a plausible connection to at least one of the predictands (ΔSAT, OHU, or OHUE): (i) AMOC strength is related to OHUE (Chapter 3) and to ΔSAT (Gregory et al. 2023); (ii) SST and SSS in the Southern Ocean and subpolar North Atlantic contribute to stratification and are thus related to OHUE (Chapter 3); (iii) SST in the tropical Pacific and Southern Ocean influences climate feedback (e.g., Ceppi and Gregory 2017; Kang et al. 2023, as well as Chapter 2) and thus ΔSAT as well as OHU (see also the Perspective section 5.2.1 in the Discussion).

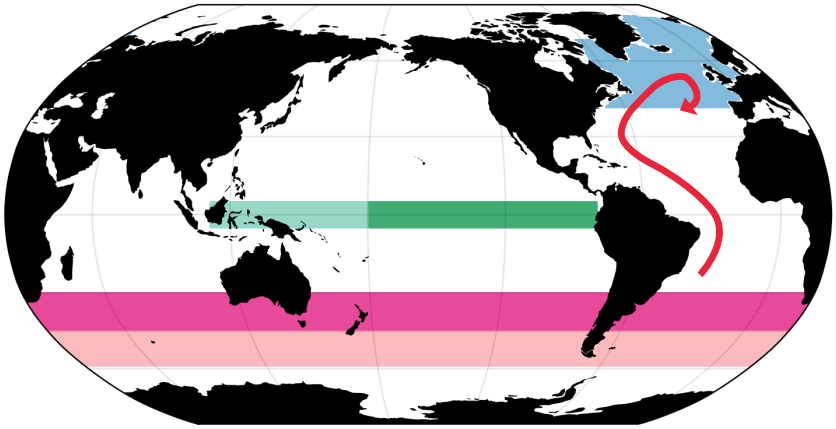

Figure 4.6: Schematic of potential predictors used for the statistical analysis in this chapter. The colored areas indicate the longitude–latitude boxes defined in Table 4.2 as well as the North Atlantic region, and the thick red arrow represents the AMOC.

Region name	Definition
`global`	global mean
`natl`	North Atlantic north of 40°N, see Fig. 4.6.
`SO-60-45`	Southern Ocean, 60–45°S, 0–360°E.
`SO-45-30`	Southern Ocean, 45–30°S, 0–360°E.
`EEP`	Eastern Equatorial Pacific, 5°S–5°N, 180–80°W, as in Rugenstein et al. (2023).
`WEP`	Western Equatorial Pacific, 5°S–5°N, 110°E–180°, as in Rugenstein et al. (2023).

Table 4.2: Definition of geographical regions used to compute sea surface temperature and salinity time series in this chapter.

Predictor	Description
AMOC	AMOC strength at 26°N from overturning streamfunction model output below 500 m.
Regional SST	Sea surface temperature averaged over the regions specified in Table 4.2.
Regional SSS	Sea surface salinity averaged over the regions specified in Table 4.2, except for `EEP` and `WEP`.

Table 4.3: Variables used as potential predictors/features for the statistical analysis in this chapter. All variables are annual means averaged over the years 1850–1900 in the historical experiment.

4.3 Exploratory analysis

In this section, we present a preliminary analysis of the inter-member spread and relationships of the 11 predictor variables (SST in 6 regions, SSS in 4 regions, and AMOC), as well as the three predictand variables (ΔSAT, OHU, and OHUE).

4.3.1 Principal component analysis

Since the chosen predictors are clearly expected to be correlated (e.g., model SST bias in the nearby `SO-60-45` and `SO-45-30` regions), we first perform a principal component analysis (PCA) on the 11 predictor variables. The input variables are first standardized to unit variance to account for their different scales and units. The resulting principal components (PCs) are uncorrelated by construction and determine the most important directions (in predictor space) of inter-member variance. The PCs can then also themselves be used as a more restricted set of predictors for the predictands of interest, a method known as principal component regression (however, although the PCs are constructed to contain maximal inter-member variance in the predictors, this is not guaranteed to translate to maximal inter-member variance in the predictands; Hastie et al. 2009).

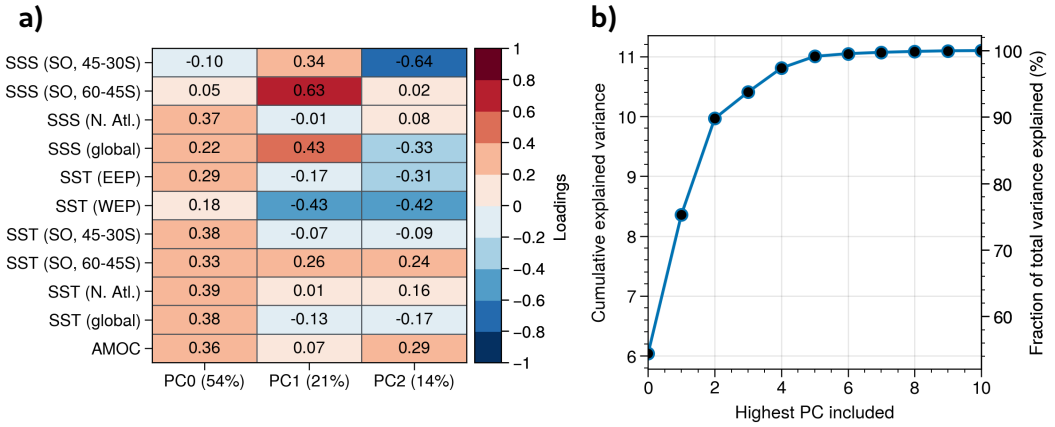

Figure 4.7: Principal component analysis of the predictor variables. **a)** Principal component loadings for the first three PCs. The numbers in parentheses at the bottom give the fraction of total variance explained by each PC. **b)** Cumulative variance explained by principal components. A corresponding figure where the predictor variables are first averaged over each multi-member ensemble for individual climate models is shown in Fig. B.7 in Appendix B.

Fig. 4.7a shows the loadings (i.e., how each of the 11 original variables contributes to each PC) for the first three PCs. The first PC (PC0) accounts for 54% of inter-member variance and represents a broad contribution of most predictors except Southern Ocean SSS and SST in the `WEP` region. This indicates (as is indeed the case) that many of these variables are pairwise correlated, and that their common inter-member spread already accounts for more than half of the predictor

variance. The next two PCs (PC1 with 21% of variance and PC2 with 14% of variance) are more heterogeneous: positive values of both PC1 and PC2 are associated with a colder `WEP` region, but PC1 has a more saline `SO-60-45` region, while PC2 has a fresher `SO-45-30` region. The next PC (PC3) accounts for only 4% of inter-member variance, and the remaining PCs together for 11% (Fig. 4.7b). These characteristics do not change qualitatively when the predictor variables are first averaged over each multi-member ensemble for individual climate models (Fig. B.7), although the quantitative values of the loadings for individual variables are different.

4.3.2 Clustering

In order to identify similarities among members of this large multi-model ensemble, we apply the k-means clustering algorithm to the principal components obtained above for the set of historical (1850–1900) predictor variables. Using the PCs (obtained from normalized predictors) as input variables to the clustering procedure avoids potential issues due to pairwise correlations among predictor variables. The resulting clusters (for a choice of $k = 7$) are shown in a two-dimensional view in Fig. 4.8, where each cluster is shown in a different color, and marker shapes are chosen to represent each climate model. The loadings of the first two PCs (given in Fig. 4.7), which span the two axes in this figure, are shown as arrows in Fig. 4.8.

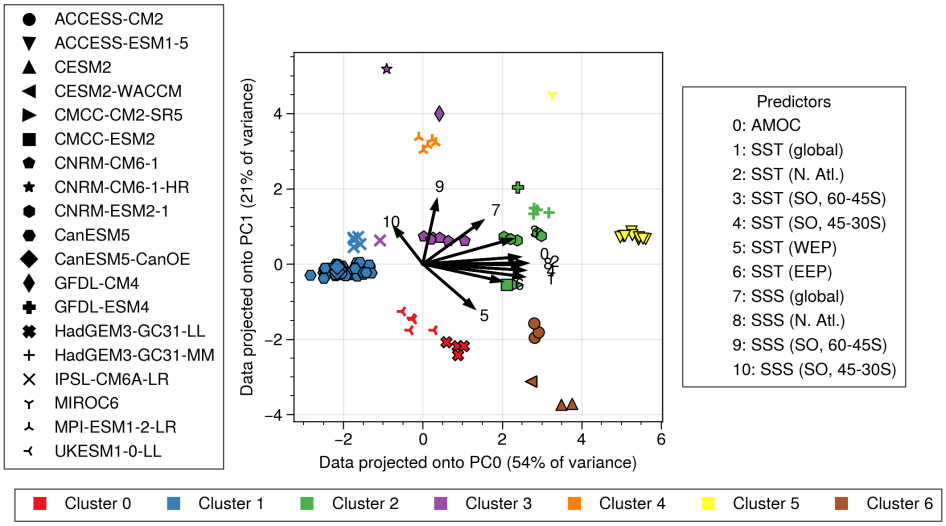

Figure 4.8: Clustering of principal components projected onto the first two PCs. $k = 7$ clusters were obtained through K-means clustering on the first 10 principal components of the predictors. A corresponding figure where the predictor variables are first averaged over each multi-member ensemble for individual climate models is shown in Fig. B.9, and using spectral clustering instead of K-means in Fig. B.8, both in Appendix B.

The k-means clustering is clearly successful in identifying a number of visually distinct clusters ("visually" to be understood here in this two-dimensional space spanned by the first two PCs). Since the chosen number of clusters ($k = 7$) is smaller than the number of climate models, some clusters necessarily contain members from different climate models, such as cluster 0 which contains all ensemble members from the UKESM1-0-LL and HadGEM3-GC31-LL climate models. Nevertheless, there is a clear tendency for members of the same climate model to be assigned to the same cluster. For example, all 50 CanESM5 members belong to cluster 1 (colored in blue in Fig. 4.8), and the five MPI-ESM1-2-LR form a separte cluster (cluster 4, colored in orange).

Although most clusters form visually distinct units in this two-dimensional space, some clusters are spread relatively far apart (such as cluster 5 with a large distance between the nine ACCESS-ESM1-5 members and the single MIROC6 member), while some members that are nearby on Fig. 4.8 are assigned to different clusters (such as the GFDL-CM4 member and the MPI-ESM1-2-LR members belonging to clusters 3 and 4, respectively). This is because all of the first ten PCs were used as input to the clustering procedure, such that members from a single cluster can also differ in their scores in higher-order PCs; this can be seen by projecting the clusters onto the first three PCs as in Fig. 4.9.

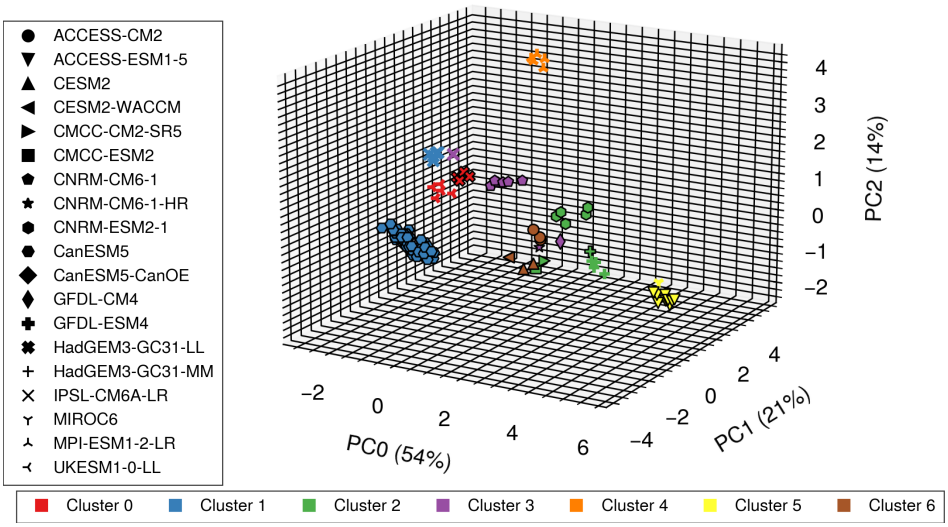

Figure 4.9: Clustering of principal components projected onto the first three PCs. $k = 7$ clusters were obtained through K-means clustering on the first 10 principal components of the predictors. These are the same clusters as the ones shown in Fig. 4.8.

The three-dimensional view of Fig. 4.9 shows why the GFDL-CM4 member and the MPI-ESM1-2-LR members were not assigned to the same cluster, since they greatly differ in their value of the third PC (PC2; the vertical axis in Fig. 4.9). Further spread apparent in Fig. 4.9 of members

belonging to the same cluster may similarly be explained by higher-order PCs, although this can not be easily visualized in analogy to Figs. 4.8 and 4.9.

The cluster sizes resulting from the *k*-means procedure are clearly uneven, and this is quantified in Fig. 4.10: cluster 1 is by far the largest cluster and contains 58 members, while the remaining clusters all contain between five and twelve members. This is because, as noted above, cluster 1 contains all 50 members of the CanESM5 ensemble, while other models in the multi-model ensemble used here have each provided a smaller number of ensemble members.

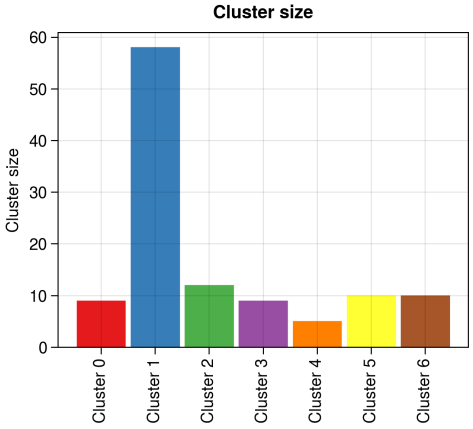

Figure 4.10: Cluster sizes (number of members assigned to each cluster).

Although simulation output from 18 distinct climate models was included, the identified clusters contain members from at most five different climate models (Fig. 4.11). Furthermore, only the IPSL-CM6A-LR ensemble is spread over multiple clusters (clusters 1 and 3), while members from all other climate models are uniquely assigned to single clusters. This highlights the fact that, although information concerning the climate models having produced each simulation was not used in the clustering procedure, the resulting clusters can still clearly identify similarities in ensemble members originating from the same model, implying that inter-member differences due to internal variability are subordinate to structural differences across models.

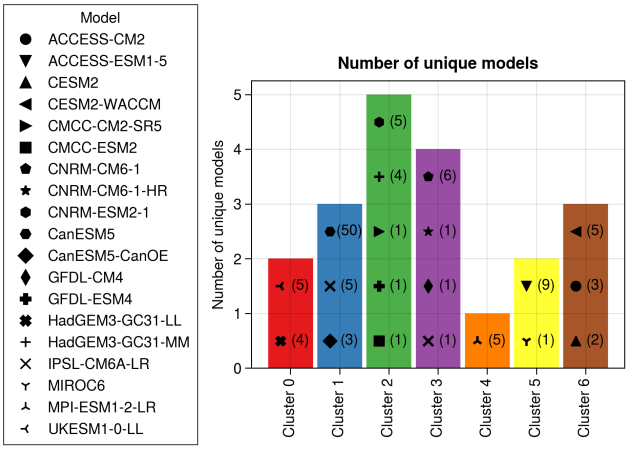

Figure 4.11: Number of unique climate models in each cluster.

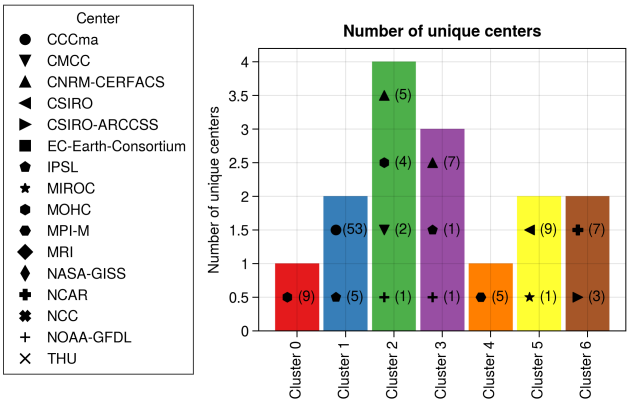

Figure 4.12: Number of unique climate modeling centers in each cluster.

Similar considerations hold for the number of distinct modeling centers (such as IPSL for the IPSL-CM6A-LR model, or NOAA-GFDL for the GFDL-CM4 model) present in each cluster (Fig. 4.12). The identified clusters contain members from at most four different modeling centers (cluster 2), with cluster 0 and cluster 4 each containing members from only one center. This is because both the UKESM1-0-LL model and the HadGEM3-GC31-LL model are developed by the Met Office Hadley Center (MOHC), although this modeling center is also present in cluster 2 for the HadGEM3-GC31-MM model. This illustrates that two versions of the same model differing in their spatial resolution (in this case, LL for low resolution and MM for medium resolution) can be more dissimilar in their simulation output of major climate variables than two distinct models developed at the same institution.

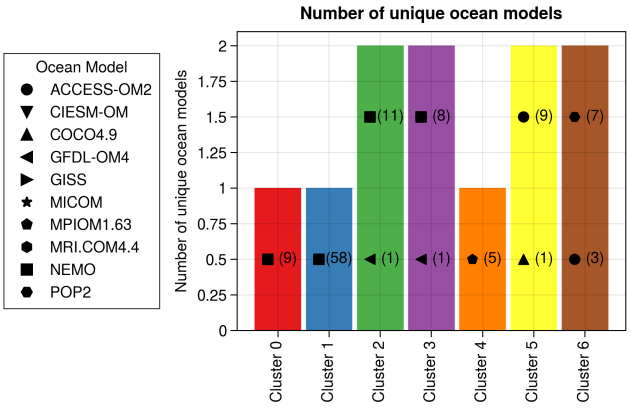

Figure 4.13: Number of unique ocean model components in each cluster.

Beyond climate model and modeling center membership, more detailed information can be considered to compare intra- and inter-cluster similarities across ensemble members. An example for this is given in Fig. 4.13, which shows the number of unique ocean model components present in each cluster. This data was obtained from Annex 2 to the IPCC AR6 WG1 report (Gutiérrez and Treguier 2021), which among other details also contains information about atmospheric model components and spatial model resolution of the CMIP6 members used here. For the present purposes, different versions of the same ocean model (such as the NEMO model; Madec et al. 2023) were considered to represent the same model component. Although ten different ocean model components are employed by members of the model ensemble of this chapter, the identified clusters contain

members from at most two different ocean models, with three clusters (clusters 1, 2, and 4) containing members using a single ocean model each. This is likely at least in part due to the relatively small number of distinct ocean models present in the model ensemble as well as the disproportionately large number of members employing the NEMO ocean model, but nevertheless suggests that models sharing the same ocean model also share certain behavior, as was already found for the case of OHUE above (Fig. 4.5).

4.3.3 Linear regression

Following the above analysis of inter-model spread and ensemble structure in the predictor variables, we now consider their application to potential constraints of the future predictand variables of interest (OHU, ΔSAT, and OHUE). Since the analysis in this chapter is of a preliminary nature, we will limit ourselves to a selection of salient univariate inter-model relationships in the SSP5-8.5 scenario, especially those relating to the results of chapters 2 and 3.

4.3.3.1 Link to chapter 2

We first consider inter-model links relevant to chapter 2, i.e., between the baseline Southern Ocean climate and future OHU and global warming. In Chapter 2, we showed that the preindustrial baseline climate state in the Southern Ocean is linked to future global OHU and ΔSAT in a CMIP6 ensemble of 28 models. Here, we can replicate some of this analysis in a multi-model ensemble with a much greater number of members, although the number of distinct climate models considered here is smaller than in Chapter 2 due to data availability constraints. Fig. 4.14 shows a scatter plot of preindustrial SST averaged over the Southern Ocean `SO-60-45` region (Table 4.2) against future global OHU in 2080–2100 under the SSP5-8.5 scenario. These two variables are anticorrelated across the ensemble, i.e., models with warmer preindustrial Southern Ocean SSTs simulate less global OHU in the future. The coefficient of determination for an ordinary least squares linear regression across all members is $R^2 = 0.68$, although this fit is biased due to the overrepresentation of models supplying more members to our ensemble (e.g., the 50 CanESM5 members). Averaging ensemble members for each climate model before performing the regression yields $R^2 = 0.23$, and averaging over members from each modeling center results in linear slope that is statstically not significantly different from zero at the $p = 0.05$ level, with $R^2 = 0.22$. This result is consistent with Chapter 2, and correlations using local preindustrial SSTs are higher (more negative) than the ones captured by the relatively broad latitude range of 60°S–45°S used here. As most climate models have produced only one or two preindustrial `piControl` runs, intra-model spread for any given climate model is mostly along the OHU axis (i.e., vertically in Fig. 4.14), and can be attributed to internal variability.

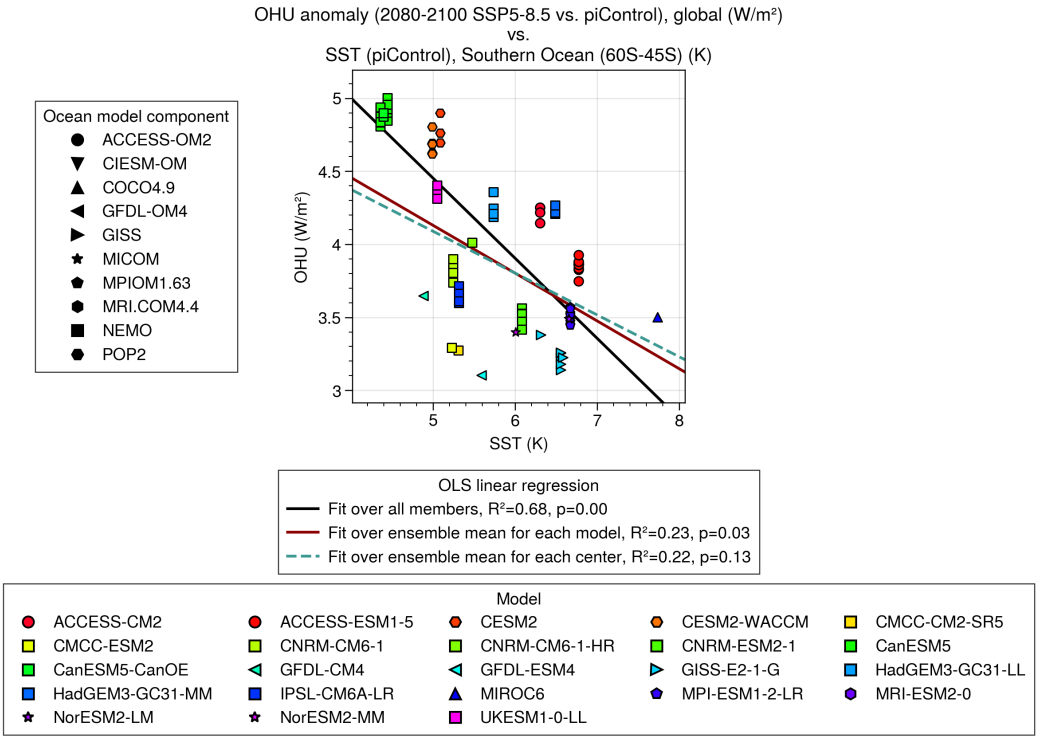

Figure 4.14: Preindustrial mean SST in the `SO-60-45` region scattered against future global OHU across the model ensemble. The marker colors indicate the climate models which generated each ensemble member simulation, and the marker shapes indicate the ocean model component used in each model. The straight lines show the ordinary least squares (OLS) regression obtained from all members (black), from averages over members from each climate model (red), and from averages over members from each modeling center (blue). The given p-values are for a two-sided Wald test with t-distribution for the hypothesis that the linear slope is different from zero.

Fig. 4.15 shows a similar plot for preindustrial Southern Ocean SST scattered against future global ΔSAT in 2080–2100 under the SSP5-8.5 scenario. As for future global OHU, the inter-member correlation is negative, i.e., models with warmer preindustrial Southern Ocean SST simulate smaller future global ΔSAT, consistent with Chapter 2. The linear regression fit over all members has $R^2 = 0.82$, and the regressions obtained after averaging over climate models or modeling centers remain statistically significant at the $p = 0.05$ level (with $R^2 = 0.52$ and $R^2 = 0.58$, respectively). Notably, all members using the NEMO ocean component have ΔSAT > 5 °C.

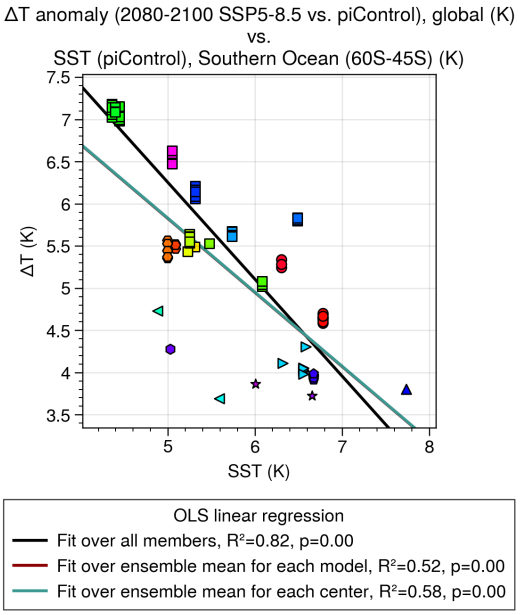

Figure 4.15: Preindustrial mean SST in the `SO-60-45` region scattered against future global ΔSAT across the model ensemble. Marker colors and shapes correspond to climate models and ocean model components, respectively, as given in the legend of Fig. 4.14.

4.3.3.2 Link to chapter 3

We now consider inter-member relationships relevant to Chapter 3, i.e., between baseline ocean circulation and stratification metrics and future OHUE.

Fig. 4.16 shows the inter-member relationship between preindustrial AMOC strength at 26°N and future projected OHUE in 2080–2100 under the SSP5-8.5 scenario. Future OHUE is positively correlated with AMOC across the ensemble, consistent with Chapter 3 and e.g. Gregory et al. (2023). However, the linear regression slope is strongly influenced by the GISS-E2-1-G model, which was not included in Chapter 3 due to data availability issues and whose members are outliers to the linear relationship with a strong AMOC but an OHUE only slightly above the multi-model average. The reason for this behavior would require more in-depth analysis of this model's full simulation output (as in Chapter 3) and is therefore outside of the scope of this exploratory outlook chapter.

In order to study the influence of mid- to high-latitude ocean stratification on overturning circulation, sea surface salinity (SSS) can be used as a proxy for upper ocean stratification (e.g., Terhaar et al. 2021; Liu et al. 2023). Fig. 4.17 shows the inter-member relationship between historical (1850–1900) mean SSS in the subpolar North Atlantic `natl` region against historical (1850–1900) AMOC strength. Here we use historical averages instead of averages over the preindustrial simu-

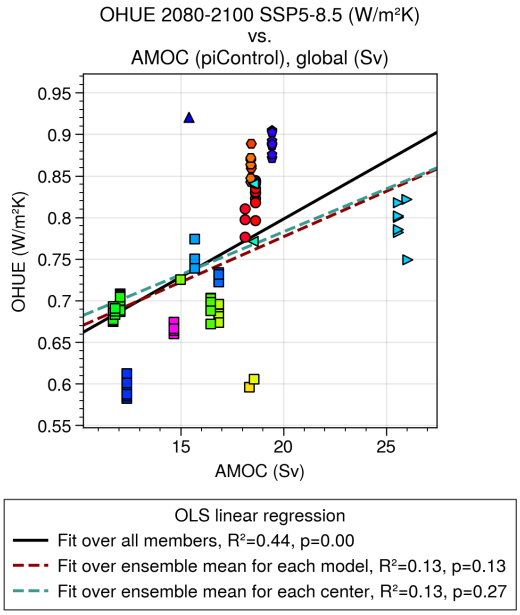

Figure 4.16: Preindustrial mean AMOC scattered against future OHUE across the model ensemble. Marker colors and shapes correspond to climate models and ocean model components, respectively, as given in the legend of Fig. 4.14.

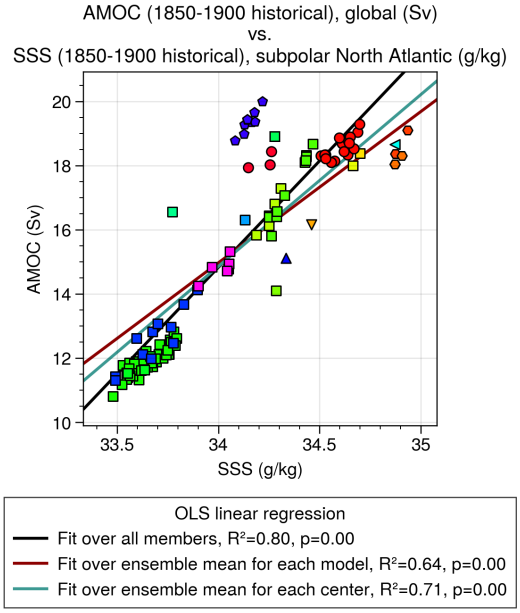

Figure 4.17: Historical (1850–1900) mean SSS in the `natl` region scattered against historical (1850–1900) AMOC strength across the model ensemble. Marker colors and shapes correspond to climate models and ocean model components, respectively, as given in the legend of Fig. 4.14.

lation for each member in order to reveal also the inter-member relationship between these variables for different members of single climate models which typically only supply one preindustrial simulation. Consistent with Chapter 3, Fig. 4.17 reveals a high correlation between SSS_{natl} and AMOC strength, i.e., higher surface salinity is associated with a stronger AMOC, with $R^2 = 0.80$ for the linear fit across all members. Interestingly, this correlation also holds for several initial condition ensembles of single models, such as for the large CanESM5 ensemble (green squares in the lower left quadrant of Fig. 4.17) and the MPI-ESM1-2-LR ensemble (dark blue pentagons in the upper part of Fig. 4.17).

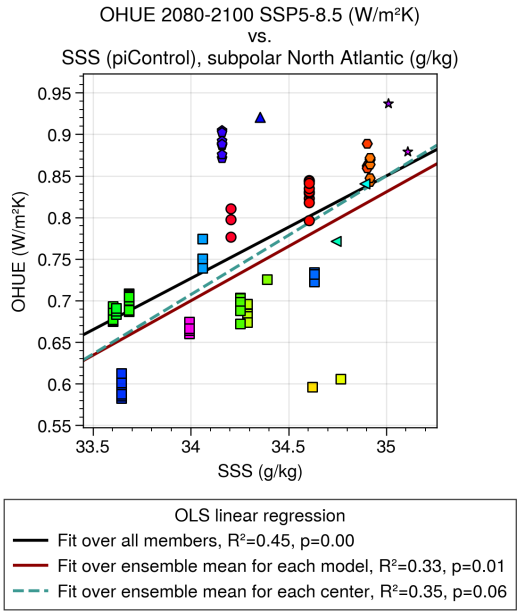

Figure 4.18: Preindustrial mean SST in the `natl` region scattered against future OHUE across the model ensemble. Marker colors and shapes correspond to climate models and ocean model components, respectively, as given in the legend of Fig. 4.14.

As explored in depth in Chapter 3, the link between AMOC and OHUE arises from the common dependence of AMOC and OHUE on stratification in the subpolar North Atlantic and mid-latitude Southern Ocean. Fig. 4.18 shows the inter-member relationship between preindustrial subpolar North Atlantic SSS and future OHUE. Consistent with Chapter 3, there is a significant positive inter-member correlation, indicating that models with weaker subpolar North Atlantic stratification (quantified by higher SSS_{natl}) have greater OHUE. As already noted for Fig. 4.5, the models using the NEMO ocean component all have relatively low OHUE and thus almost exclusively lie in the lower half of Fig. 4.18. An analogous analysis for Southern Ocean SSS in the `SO-60-45` region (Fig. B.10) shows a much weaker correlation, with statistically insignificant linear slopes for regressions of model and modeling center averages. This is likely due

to the relatively broad definition of the `SO-60-45` region and represents a fundamental weakness of the large-scale regional approach of this chapter compared to the local analysis of Chapter 3 of inter-model relationships at the grid cell level.

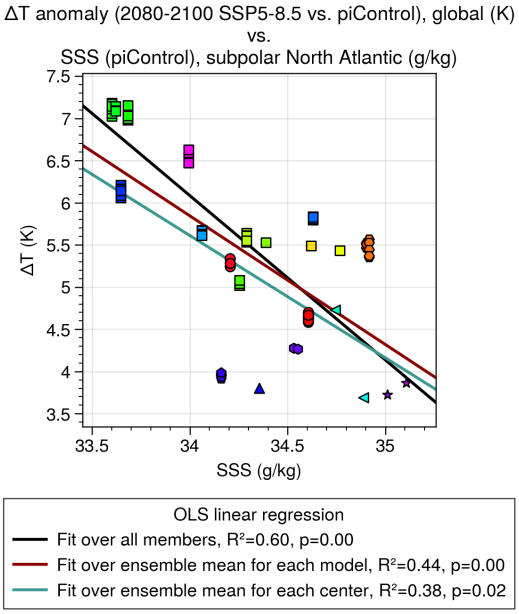

Figure 4.19: Preindustrial mean SSS in the `natl` region scattered against future global ΔSAT across the model ensemble. Marker colors and shapes correspond to climate models and ocean model components, respectively, as given in the legend of Fig. 4.14.

Going beyond the impact of stratification metrics on OHUE (OHU/ΔSAT) as in Chapter 3, we can also consider their role for ΔSAT and OHU separately. Scatter plots between subpolar SSS_{natl} and ΔSAT (Fig. 4.19) and between subpolar North Atlantic SSS_{natl} and OHU (Fig.4.20) show negative correlations for both variables, i.e., a less stratified subpolar North Atlantic translates to both lower ΔSAT and less OHU, although the correlation for OHU is weaker than for ΔSAT. The stratification–OHUE link must thus arise from the control of (salinity) stratification on surface warming and not OHU, as already noted by Liu et al. (2023).

4.3.4 Cross-validation

If the framework developed in this chapter is to be combined with observational data to obtain constrained projections of future OHU, ΔSAT, and OHUE, a systematic cross-validation procedure is needed to ensure the robustness of the multiple linear regression of these predictands onto the 11 predictors. An adequate validation procedure would need to take into account the ensemble structure information revealed in the clustering analysis above. A potential such ap-

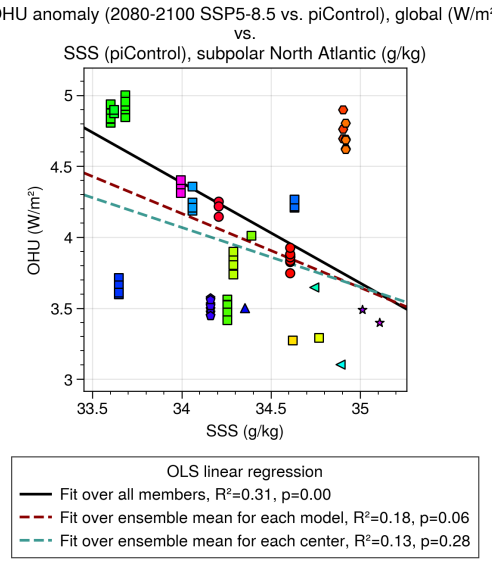

Figure 4.20: Preindustrial mean SSS in the `natl` region scattered against future global OHU across the model ensemble. Marker colors and shapes correspond to climate models and ocean model components, respectively, as given in the legend of Fig. 4.14.

proach is offered by grouped k-fold cross-validation, as depicted schematically in Fig. 4.21. In this approach, the set of $p = 11$ predictands for $N \approx 100$ ensemble members is repeatedly split ($k = 5$ times in the case of Fig. 4.21) into a training set and a test set. The regression model is then fit to the training set and evaluated on the test set. The information of climate model membership (or modeling center membership and ocean component) can be used to ensure that ensemble members belonging to the same climate model are not present in both the training set and the test set to avoid an overestimation of the quality of the regression fit. In Fig. 4.21, the "Group" label corresponds to climate model membership, and the training/test split over the $k = 5$ iterations clearly respects these group boundaries.

4.4 Discussion

As mentioned in the introduction, the analysis conducted in this chapter is of an exploratory nature, and its findings are preliminary. We have presented a number of results which could form the foundation for a systematic approach to constraining future OHU, ΔSAT, and OHUE.

The clustering analysis in Section 4.3.2 has shown systematic features of the structure of CMIP6 multi-model ensembles: simulations of key quantities tend to behave similarly for ensemble members belonging to the same climate model or modeling center, or using the same ocean model. This analysis could be extended to include further pieces of information characterizing each ensem-

ble member, including other model components (e.g., the atmospheric component), measures of model complexity, or of code similarity. Furthermore, instead of k-means clustering, a hierarchical clustering method could be used, which would allow the identification of sub-groups of ensemble members at different levels of granularity (e.g., as in the "model genealogy" of Masson and Knutti 2011).

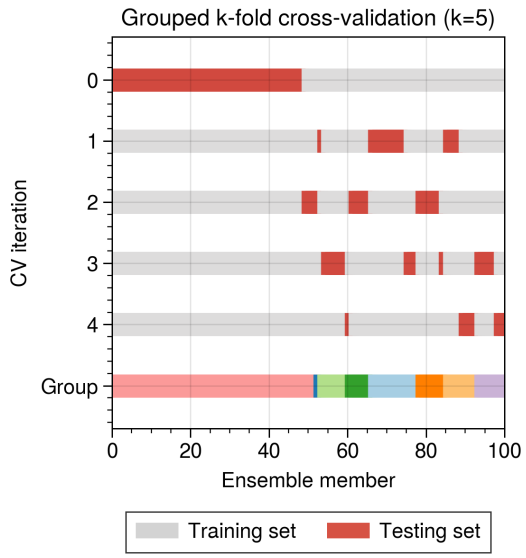

Figure 4.21: Schematic of grouped k-fold cross validation. Adapted from `https://scikit-learn.org/stable/auto_examples/model_selection/plot_cv_indices.html`

The findings obtained from the clustering analysis could also be used to inform the regression of the predictands onto the set of predictors. For instance, after having obtained and carefully analyzed a set of meaningful ensemble member clusters, the predictands could be first averaged over these clusters (instead of averaging over members of the same model or modeling center). This could potentially reduce problems associated with model interdependence (see Sec. 1.2.3). Additionally, instead of ordinary least squares (OLS), more sophisticated versions of linear regression could be used to predict the future variables of interest, such as Lasso or Ridge regression. These methods differ from OLS by introducing a penalty term for the size of the regression coefficients, which can yield more stable models, and in the case of Lasso regression can improve model interpretability by setting some coefficients to zero (Hastie et al. 2009).

Bibliography

Bourgeois, T., N. Goris, J. Schwinger, and J. F. Tjiputra (2022). "Stratification constrains future heat and carbon uptake in the Southern Ocean between 30°S and 55°S". *Nature Communications* 13:1. Bandiera_abtest: a Cc_license_type: cc_by Cg_type: Nature Research Journals Number: 1 Primary_atype: Research Publisher: Nature Publishing Group Subject_term: Biogeochemistry;Carbon cycle;Marine chemistry;Physical oceanography Subject_term_id: biogeochemistry;carbon-cycle;marine-chemistry;physical-oceanography, p. 340. ISSN: 2041-1723. DOI: 10.1038/s41467-022-27979-5.

Ceppi, P. and J. M. Gregory (2017). "Relationship of tropospheric stability to climate sensitivity and Earth's observed radiation budget". *Proceedings of the National Academy of Sciences* 114:50. Publisher: Proceedings of the National Academy of Sciences, pp. 13126–13131. DOI: 10.1073/pnas.1714308114.

Gregory, J. M. et al. (2023). "A new conceptual model of global ocean heat uptake". *Climate Dynamics*. ISSN: 1432-0894. DOI: 10.1007/s00382-023-06989-z.

Gutiérrez, J. M. and A.-M. Treguier (2021). "Annex II: Models". In: *Climate Change 2021: The Physical Science Basis. Contribution of Working Group I to the Sixth Assessment Report of the Intergovernmental Panel on Climate Change*. Ed. by V. Masson-Delmotte et al. Cambridge University Press, Cambridge, United Kingdom and New York, NY, USA, pp. 2087–2138. DOI: 10.1017/9781009157896.001.

Hastie, T., R. Tibshirani, and J. Friedman (2009). *The Elements of Statistical Learning*. Springer Series in Statistics. Springer New York, New York, NY. ISBN: 978-0-387-84857-0 978-0-387-84858-7. DOI: 10.1007/978-0-387-84858-7.

Kang, S. M., P. Ceppi, Y. Yu, and I.-S. Kang (2023). "Recent global climate feedback controlled by Southern Ocean cooling". *Nature Geoscience* 16:9. Number: 9 Publisher: Nature Publishing Group, pp. 775–780. ISSN: 1752-0908. DOI: 10.1038/s41561-023-01256-6.

Liu, M., B. J. Soden, G. A. Vecchi, and C. Wang (2023). "The Spread of Ocean Heat Uptake Efficiency Traced to Ocean Salinity". *Geophysical Research Letters* 50:4. _eprint: https://onlinelibrary.wiley.com/doi/pdf/10.1029/2022GL100171, e2022GL100171. ISSN: 1944-8007. DOI: 10.1029/2022GL100171.

Madec, G. et al. (2023). "NEMO Ocean Engine Reference Manual". Publisher: Zenodo. DOI: 10.5281/zenodo.8167700.

Masson, D. and R. Knutti (2011). "Climate model genealogy". *Geophysical Research Letters* 38:8. _eprint: https://onlinelibrary.wiley.com/doi/pdf/10.1029/2011GL046864. ISSN: 1944-8007. DOI: 10.1029/2011GL046864.

NASA/GISS (2018). *NASA-GISS GISS-E2.1G model output prepared for CMIP6 CMIP*. DOI: 10.22033/ESGF/CMIP6.1400.

Rugenstein, M. et al. (2023). "Connecting the SST Pattern Problem and the Hot Model Problem". *Geophysical Research Letters* 50:22. _eprint: https://onlinelibrary.wiley.com/doi/pdf/10.1029/2023GL10548 e2023GL105488. ISSN: 1944-8007. DOI: 10.1029/2023GL105488.

Swart, N. C. et al. (2019). "The Canadian Earth System Model version 5 (CanESM5.0.3)". *Geoscientific Model Development* 12:11. Publisher: Copernicus GmbH, pp. 4823–4873. ISSN: 1991-959X. DOI: 10.5194/gmd-12-4823-2019.

Terhaar, J., T. L. Frölicher, and F. Joos (2021). "Southern Ocean anthropogenic carbon sink constrained by sea surface salinity". *Science Advances* 7:18. Publisher: American Association for the Advancement of Science, eabd5964. DOI: 10.1126/sciadv.abd5964.

Winton, M. et al. (2014). "Has coarse ocean resolution biased simulations of transient climate sensitivity?" *Geophysical Research Letters* 41:23. _eprint: https://onlinelibrary.wiley.com/doi/pdf/10.1002/2014GL061 pp. 8522–8529. ISSN: 1944-8007. DOI: 10.1002/2014GL061523.

5 Discussion

5.1 Summary and discussion of main results

In this section, we will summarize the main results found in chapters 2–4 of this thesis, and provide responses to the scientific questions posed at the end of the Introduction chapter (Sec. 1.3).

5.1.1 Chapter 2: How can we constrain future global OHU?

We answered this question in Chapter 2 by explicitly identifying and applying an emergent constraint on future OHU. We found a strong inter-model correlation between historical Antarctic sea ice extent and future global OHU by the end of the 21st century in an ensemble of 28 CMIP6 models. This relationship allowed us to use satellite observations of sea ice concentrations to constrain future OHU, leading to OHU estimates that are 12–33% less uncertain than the unconstrained prior model average, depending on emissions scenario. Our constraint fulfils the three validity criteria for emergent constraints introduced in Sec. 1.2.5.5: (i) the predictor–predictand relationship is based on a verifiable physical mechanism, as summarized below; (ii) the observational data is sufficiently well constrained to allow meaningful uncertainty reduction (as confirmed with substantial robustness testing in Chapter 2); and (iii) the constraint is robust to out-of-sample testing (as confirmed by a replication in an ensemble of 16 CMIP5 models in Chapter 2).

The emergent constraint is supported by a physical mechanism originating from model biases in the extratropical Southern Hemisphere. We found that, in the preindustrial state across the model ensemble, there is a strong connection between deep ocean temperatures, Southern Ocean surface temperatures, Southern Ocean cloud cover, and Antarctic sea ice extent. These variables are physically linked and together quantify the baseline climate state of the Southern Hemisphere in each model. Crucially, we showed that this baseline state influences the modelled climate evolution under anthropogenic forcing: models with an initially colder state have higher cloud feedback, more OHU, and stronger global warming under future emissions scenarios than models with an initially warmer state. The initial climate state represents a *potential* for the amplitude of future climate changes, and sea ice extent was essentially used as a "thermometer" of this initial

state. Using observed Antarctic sea ice extent over 1980–2020 as a predictor therefore amounted to measuring the potential of the actual climate system for these changes, thus constraining the amplitude of these changes expected under various future emissions scenarios.

Chapter 2 thus offers a partial answer to the question of constraining future global OHU. It is only partial because mechanisms other than the one we have identified might influence future OHU, cloud feedback, and global warming in amplifying or compensating ways. However, our constraint is likely more robust than a number of major previously published constraints which were based on the use of warming trends over the recent past as predictors for future (ocean) warming (e.g., Tokarska et al. 2020; Lyu et al. 2021). The observational time periods employed in these studies coincide with a period of anomalously weak observed climate feedback due to surface warming patterns not captured in climate models, leading to biased trend-on-trend emergent constraints (Wills et al. 2022; Alessi and Rugenstein 2023; Armour et al. 2024, see also the perspective on the "pattern effect" in Sec. 5.2.1 below). This is less critical for our constraint since it is based on a physical mechanism and uses a long time-average instead of shorter-term trends as a predictor (and this was shown in extensive sensitivity tests). Furthermore, constraints based on past trends cannot incorporate the possibility of potential regime shifts in the climate system, such as the progression to a future warm state in the Southern Hemispere in initially "cold" models shown in Chapter 2.

5.1.2 Chapter 3: What processes control the OHU efficiency?

We addressed this question in Chapter 3 by considering the major controlling factors on OHU efficiency (OHUE) previously proposed in the literature (e.g.; Boé et al. 2009; Winton et al. 2014; Liu et al. 2023; Newsom et al. 2023, and others) and systematically analyzing their inter-model relationships at the global and regional levels. These proposed controlling factors include the depth of the upper ocean mixed layer, the strength of upper ocean (0–1500 m) density stratification, as well as the magnitude of the meridional overturning cells of the Atlantic and Southern Ocean.

By calculating inter-model correlations across an ensemble of 28 CMIP6 models, we showed that the global mean MLD as well as the strength of the AMOC and Southern Ocean upper cell in the preindustrial climate are all correlated with the magnitude of OHUE under an idealized scenario with exponentially increasing atmospheric CO_2 concentrations. Although the global mean upper ocean stratification is uncorrelated with OHUE, local correlations at the grid cell level revealed that stronger stratification in the subpolar North Atlantic and mid-latitude Southern Ocean is associated with a smaller OHUE, suggesting physical links to the overturning circulations generated in these regions. This was further supported by an analysis of the links between local stratification and overturning strength across the model ensemble, which showed a link between

subpolar North Atlantic stratification and AMOC, and between Southern Ocean stratification and the Southern Ocean upper cell. A closer look at the ensemble mean bias and inter-model spread in regional stratification then revealed the existence of salient salinity stratification biases in the North Atlantic and Southern Ocean – the two key regions for overturning and OHUE.

The synthesis of these results supports a central control on OHUE of upper ocean stratification, primarily through the key subpolar North Atlantic and mid-latitude Southern Ocean regions which are the gatekeepers of the global overturning circulations. Our analysis added a regional focus to the importance of salinity stratification for OHUE (Liu et al. 2023) despite its subordinate role to temperature in setting the mean stratification strength. Furthermore, our findings give more detailed insight to the suggestion by Gregory et al. (2023) that the AMOC is not the active process determining OHUE, but that AMOC and OHUE are both controlled by stratification. The key role of preindustrial model biases in geographically distant regions highlights the complexity of the inter-model spread in currently available climate models, and calls for renewed focus on the parameterization and tuning choices affecting ocean stratification (Newsom et al. 2023).

5.1.3 Chapter 4: Can we use this process understanding to constrain OHU (efficiency)?

In Chapter 4, we attempted to provide an answer to this question by performing an exploratory analysis of inter-member linkages in a large CMIP6 multi-model ensemble. We defined a set of 11 variables (AMOC strength, regional SST, and regional SSS) which could potentially serve as predictors in a multi-variable emergent constraint on future global OHU, surface air temperature anomaly (ΔSAT), and OHUE. As these variables are more commonly available from the CMIP archive than the detailed model output used in Chapters 2 and 3, we obtained over 110 ensemble members for both the historical period and each of four SSP scenarios. This relatively large number of simulations compared to the previous chapters more easily lends itself to popular statistical analysis procedures, both in the "unsupervised" setting (i.e., to analyze the statistical properties and ensemble structure of the predictors themselves), as well as in the "supervised" setting (i.e., to perform regression of the predictands onto these predictors; Hastie et al. 2009).

In the unsupervised setting, we applied a clustering algorithm on the 11 predictors across the model ensemble which revealed clear links between cluster assignment and climate model membership, modeling center, and the ocean model component employed in each ensemble member. Even though the clustering procedure was applied without reference to this additional information, it revealed how ensemble members from the same climate model, from the same modeling center, and using the same ocean model component all tend to exhibit similar characteristics in

their simulation of crucial ocean variables. Notably, we found that climate models employing the NEMO ocean model as their ocean component (the most common ocean model in our ensemble; Madec et al. 2023) tend to have a lower OHUE than climate models with different ocean components.

In the supervised setting, we revisited the analysis of Chapters 2 and 3 by calculating univariate correlations between salient predictor–predictand pairs, which confirmed the previously obtained results summarized above. For example, beyond correlations computed across single members of different climate models, we found that the relationship between subpolar North Atlantic salinity stratification and AMOC also holds for initial condition members of individual climate models, further supporting the interpretation of the results of Chapter 3.

5.1.4 Overarching question: What is the effect of climate model biases on future projections, and how do different biases relate to each other?

Throughout this thesis, we have performed extensive analyses of simulation output from a range of numerical climate models, in order to both produce projections of future climate changes and to obtain an improved understanding of the involved physical climate system processes. No climate model is perfect, and different climate models are biased with respect to the true climate system in different ways. Although this fact introduces uncertainties in the projections obtained from model ensembles (see Sec. 1.2.3), the systematic comparison of climate model biases across ensemble members also provides a unique opportunity to understand and constrain climate variables of interest. In particular, emergent inter-model relationships between variables across multi-model ensembles (Sec. 1.2.3.3) can be used to infer behavior not explicitly contained in any single climate model. We used this idea in Chapter 2 where we combined such an emergent relationship involving oceanic, atmospheric, and cryospheric climate variables with observational data in order to constrain future OHU projections, and in Chapter 3 where we disentangled a number of previously reported inter-model relationships that control OHU efficiency in climate models.

Future climate models, such as those being prepared for the upcoming CMIP7 exercise, are expected to improve on current models on many fronts including increased spatial resolution (Fox-Kemper et al. 2019), the inclusion of previously unresolved processes (e.g., Schmidt et al. 2023), as well as the use of improved parameterizations and hybrid machine learning-based modeling approaches (Eyring et al. 2024). These developments will alleviate some of the biases plaguing current models, but will certainly not eradicate them all, and may even lead to new biases appearing in previously well-simulated areas (e.g., Meehl et al. 2020). As new ensembles of increasingly complex Earth system models will become available in the future, the approaches adopted in this thesis will

therefore remain vital for model intercomparison, climate projections, and process understanding.

5.2 Perspectives

In this last section, we will discuss a number of potential extensions of the present work to related questions.

5.2.1 Pattern effects on ocean heat uptake

As we have seen throughout this thesis, the ocean plays not only a passive role in climate change by responding to atmospheric changes, but also an eminently active role through its direct involvement in climate feedbacks (Chapter 2) and its buffering effect on surface warming (Chapter 3). One aspect of this active oceanic influence on climate change which has garnered major scientific interest in recent years is the *influence of sea surface warming patterns on global climate feedback*. As the ocean takes up heat from the atmosphere, the resulting surface warming is not spatially uniform (see Fig. 5.1a for the period 1981–2014). For example, the observed warming is amplified in the Western Equatorial Pacific (WEP), while the Eastern Equatorial Pacific (EEP) and parts of the Southern Ocean have shown muted warming and even cooling trends over this period. Warming at the Southern Ocean surface is slowed by the upwelling of century-old water masses and the efficient transport of heat into the ocean interior (Armour et al. 2016), and the zonally heterogeneous warming in the Pacific is characteristic of the Pacific Decadal Oscillation (PDO) mode of internal variability (although the full picture is more complicated and not of primary importance for this discussion; e.g., McGregor et al. 2014). In the tropical Pacific, the atmosphere and ocean are tightly coupled through atmospheric convection, giving rise to phenomena such as ENSO. This coupling also has implications for climate feedback: zonal temperature gradients in the tropical Pacific influence the stability of the troposphere, which affects cloud feedback, mainly through changes in marine low cloud coverage, as well as the lapse-rate feedback (e.g., Ceppi and Gregory 2017). Warming trends in the Southern Ocean can further feed into this effect through teleconnections via the Southeast Pacific involving cloud feedback (Kang et al. 2023a; b).

5.2.1.1 The atmospheric pattern effect

Despite this importance of SST warming patterns for climate feedback (and ultimately climate sensitivity), current climate models are unable to correcly simulate these observed trends (Wills et al. 2022). Under historical forcing, CMIP5/6 models simulate warming patterns which are much more spatially uniform than observed, with some muted warming in the Southern Ocean but an

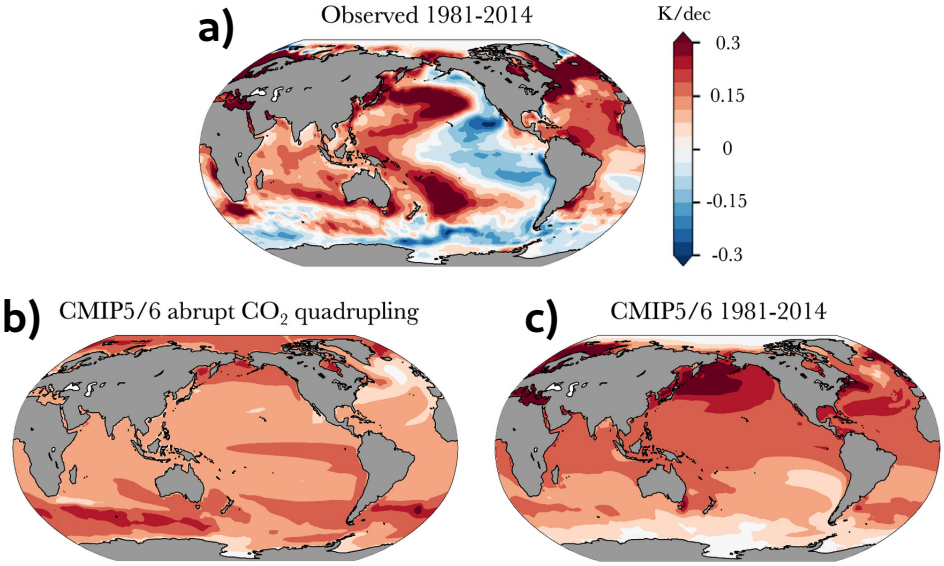

Figure 5.1: Sea surface temperature trends in observations and CMIP5/6 models. **a)** Observed trends over 1981–2014. **b)** Trends simulated by CMIP5/6 models over years 1–150 of the `abrupt-4xCO2` experiment. **c)** Trends simulated by CMIP5/6 models over years 1981–2014 of the `historical` experiment. Adapted from Armour et al. (2024) (Fig. 2).

almost completely absent zonal warming gradient in the tropical Pacific (Fig. 5.1c). This pattern is similar to the eventual equilibrium warming pattern as simulated in abrupt CO_2 quadrupling experiments (Fig. 5.1b), where maximal warming is expected to be found in the Southern Ocean and the EEP, which are precisely the regions with the smallest observed warming. This model-observation mismatch in surface warming patterns over the recent historical period thus leads to a simulated historical climate feedback parameter which is too weak (with the inferred climate sensitivity too low), an issue which has been termed the "pattern effect" (e.g., Andrews et al. 2018; 2022; Alessi and Rugenstein 2023; Armour et al. 2024).

5.2.1.2 An oceanic pattern effect

Since the surface ocean is the interface between the atmosphere and the deep ocean, changes at the surface do not only impact the atmosphere above, but also the deeper ocean layers below. In particular, patterns of ocean surface warming can influence the efficiency of heat transport to the deep ocean, since surface warming in regions of efficient vertical exchange (such as the Southern Ocean) lead to more heat subduction than surface warming in highly stratified regions (such as the tropical oceans). This effect was quantified in a study by Newsom et al. (2020), who forced a Green's function representation of the steady-state ocean circulation with varying surface warming patterns, and found that the pattern simulated by CMIP5 models (see Fig. 5.1c) damps the

"passive" ocean heat uptake efficiency by 24% compared to spatially uniform warming, since regions of strong ventilation tend to have smaller surface warming. A similar approach using a full 3D ocean model proved a substantial sensitivity of modelled AMOC strength and total OHU to imposed surface heat fluxes (Huber and Zanna 2017), but Newsom et al. (2020) did not find a significant control of inter-model variation in warming patterns on passive OHUE in CMIP5. Although Newsom et al. (2020) did not investigate the implications of model biases relative to observed warming as discussed for the atmospheric case above, it can be hypothesized that, for example, the enhanced Southern Ocean warming in models compared to observations should lead to an overestimation of OHUE from model simulations (compare Figs. 5.1a,c), giving rise to an oceanic "pattern effect". (It should be noted that both pattern effects introduced here are intrinsically coupled phenomena since both the atmosphere and ocean contribute to the establishment of warming patterns, but we stress here the distinction between the effect of these patterns on either atmospheric or oceanic processes in each case.) An oceanic pattern effect of this type has recently been shown to have played an important role in the deglaciation after the last glacial maximum, ca. 21 ka ago (Zhu et al. 2024).

5.2.1.3 Combining atmospheric and oceanic pattern effects on ocean heat uptake

In light of this dual influence of surface warming patterns on both atmospheric feedbacks above and oceanic heat uptake below, it would be interesting to investigate the combined effect of these two pattern effects on both total OHU and OHUE (see the schematic in Fig. 5.2). A potential study of this combined effect could adopt a systematic approach of forcing steady-state representations of both the ocean and atmosphere with a specified set of surface warming patterns, including the observed pattern (Fig. 5.1a), the ensemble mean simulated pattern (Fig. 5.1c), the simulated patterns from individual CMIP5/6 models, as well as a baseline spatially uniform pattern. The steady-state representations of the ocean and atmosphere could be either the same for all experiments, or created for each model individually to also incorporate inter-model differences in ocean circulation, although this approach would be more complex (for model-specific Green's functions, see e.g. Kang et al. (2023a) for the atmosphere and Chamberlain et al. (2019) for the ocean).

The OHU and OHUE estimates resulting from these different imposed surface warming patterns (and potentially different ocean circulation representations) would show whether the two pattern effects amplify or compensate each other at the global scale. Since both the tropical Pacific and Southern Ocean are key regions for the atmospheric pattern effect, but only the Southern Ocean is key for the oceanic effect, it would be interesting to investigate the potential coupling of SST model biases in these two regions, and to see how this impacts the amplification or compensation of the two pattern effects on OHU(E).

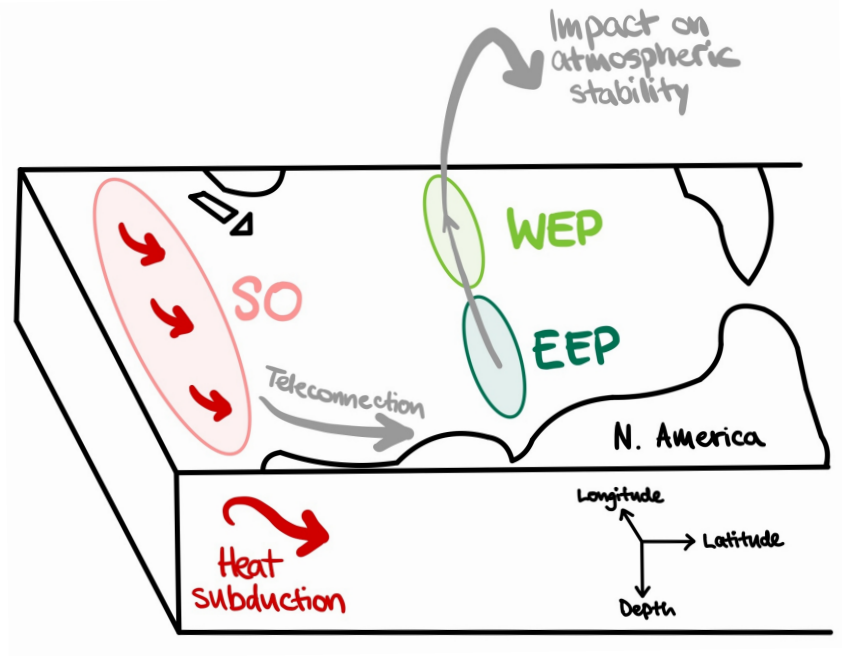

Figure 5.2: Schematic of the proposed combination of atmospheric and oceanic pattern effects on OHU. Surface ocean warming trends in the Western and Eastern Equatorial Pacific (WEP and EEP) impact atmospheric stability, cloud feedback, and ultimately OHU (Ceppi and Gregory 2017). Southern Ocean (SO) warming trends control OHU through heat subduction, and communicate with the EEP via atmospheric teleconnections (Kang et al. 2023a).

5.2.2 Lagrangian approaches to model analysis

All analyses in this thesis were conducted in an Eulerian reference frame, that is, on model grids which are fixed in space and where fluid and tracer fluxes are represented as exchanges between fixed grid boxes. An alternative to this framework is offered by the Lagrangian viewpoint, where the reference frame follows each fluid parcel as it moves through space. Although these two viewpoints are equivalent, this second viewpoint is in some ways more natural than the Eulerian case, since the equations of motion fundamentally apply to each fluid parcel itself (Vallis 2017), and not to arbitrary fluid regions fixed by a model grid. Importantly, the Lagrangian approach can be used to analyze velocity fields obtained from observational data or model output, and can yield information on the physics and statistics of flow trajectories and timescales that are hard or impossible to obtain from a purely Eulerian standpoint (the major Eulerian alternative to study such questions is the use of purposeful dye tracers in model simulations; e.g., Marzocchi et al. 2021). Ocean models can be constructed in a native Lagrangian fashion (e.g., Haertel and Fedorov 2012), but a more common approach is to "release" *virtual particles* into Eulerian models, which are then advected by the resolved currents (and potentially by imposed subgrid-scale diffusion; Sebille et al. 2018). These particles

can be added either "online" during the model integration, or "offline" using the velocity fields output by the model run.

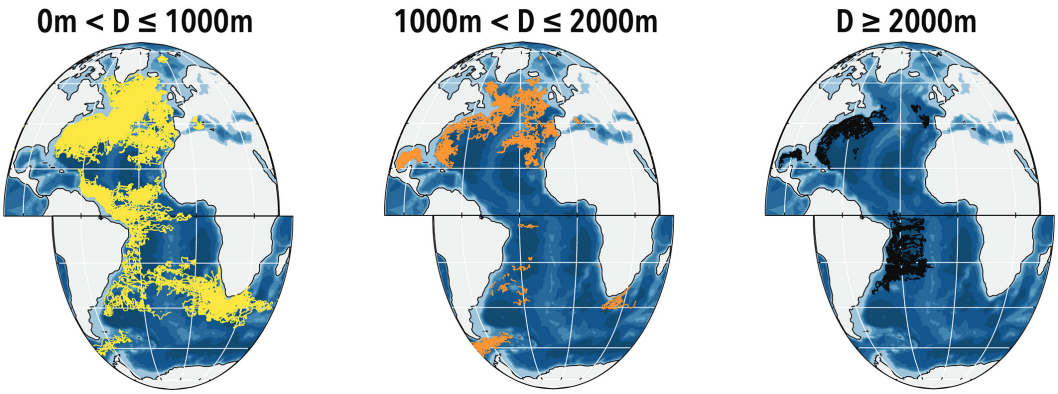

Figure 5.3: Observational subsurface float trajectories in the Atlantic binned by depth range from the AOML PhOD subsurface drifter database (Ramsey et al. 2018). These floats are advected by ocean currents and thus naturally follow Langrangian pathways. Reprinted from Bower et al. (2019) (Fig. 12).

Models participating in CMIP generally provide output for Eulerian overturning streamfunctions computed online on the model grid. This output is commonly used to calculate the AMOC strength at specific latitudes in the Atlantic. However, it is potentially unsuitable for calculating overturning strength in e.g. the subpolar North Atlantic or the Southern Ocean, where the density surfaces, along which the circulation is mostly aligned, are tilted vertically in the meridional direction, such that zonal integration yields unphysical overturning cells not associated with tracer transport (e.g., the Deacon cell in the Southern Ocean; Döös and Webb 1994). In Chapter 3, we thus resorted to overturning streamfunctions computed in density coordinates, which circumvents this issue. These streamfunctions are only supplied by a limited number of CMIP6 models and thus had to be calculated from monthly-resolution velocity, temperature, and salinity model output. Furthermore, this overturning metric proved to be problematic for model intercomparison, not least because it is unclear how to identify a single suitable metric for "overturning strength" given these streamfunctions.

Lagrangian analysis provides a potential solution to these problems. It has been successfully used to study the ventilation of the Southern Ocean (Viglione and Thompson 2016; Tamsitt et al. 2017; Drake et al. 2018; Tamsitt et al. 2018; Styles et al. 2024; Xie et al. 2024) as well as the AMOC and global overturning circulation (e.g., Speich et al. 2007; Bower et al. 2019; Rousselet et al. 2021). A potential Lagrangian multi-model study of OHU and OHUE could inject offline particles into ocean model velocity fields from the CMIP archive, and build a global inventory of Lagrangian overturning and subduction pathways and their relation to OHU(E). This would require an implementation of subgrid-scale heat diffusion for a correct heat budget (e.g., using the

Parcels framework in Python; Delandmeter and Sebille 2019), although an analysis of resolved pathways and timescales could already prove instructive. The issue of Southern Ocean overturning encountered in Chapter 3 and discussed above could then more easily be interpreted through an inspection of the precise heat subduction pathways exhibited by each model, which could be compared to available estimates from observational drifters (Fig. 5.3) which naturally follow Lagrangian trajectories. As the spatial resolution of ocean models is expected to increase in future CMIP generations, this approach will be able to more accurate resolve the ventilation of heat and other tracers from the surface to the deep ocean (MacGilchrist et al. 2017).

5.2.3 Extending parameter perturbation experiments to the multi-model setting

In Chapters 2 and 3 of this thesis, we used a single member per climate model to conduct multi-model analyses, and in Chapter 4 we included several initial condition members per model to enhance statistical robustness and include the effect of internal variability. Recalling our discussion of model ensemble uncertainty in the Introduction (Sec. 1.2.3), it would be interesting to explicitly consider also the impact of parameter uncertainty for each model in a multi-model ensemble (MME). A majority of climate modeling studies aimed at process understanding typically employ one of two types of model ensemble: (i) MMEs with either one or several initial condition members per model, or (ii) parameter perturbation ensembles from a single model. However, the usage of systematic parameter perturbation for each member of an MME is less common. In particular, while the CMIP6 archive contains some simulations with different physical setups for a given model (as indicated by the physics index "p" in the CMIP6 `member_id`, e.g. "r1i1p1f1"), these simulations typically only differ in their specification of certain model components (e.g., for aerosol chemistry), and do not represent systematic parameter perturbation ensembles (PPEs).

Single-model PPEs have been used to study OHU in the simulations of Huber and Zanna (2017) and Newsom et al. (2023), which explored the impact of varying the vertical diffusivity parameter κ_v and the Gent-McWilliams parameter κ_{GM}. Generalizing this approach to the multi-model setting, perhaps through a coordinated MIP in a future CMIP cycle, would enable much enhanced process understanding that would not be limited to the particular structure of a single model. As model resolution will increase with increasing computing power in the future, some models may choose to disable or modify some of their subgrid-scale parameterizations (e.g., Styles et al. 2023), calling for a more detailed investigation of the ensuing implications for stratification and ocean heat uptake.

5.2.4 The ocean heat-carbon nexus

The focus of this thesis has been on ocean heat uptake, but there is a second major way in which the ocean regulates climate change: through the uptake of anthropogenic carbon (C_{ant}). Since 1850, the ocean has taken up 180 ± 35 GtC (gigatonnes of carbon, i.e., 10^{12} kg of carbon), which is 26% of the cumulative C_{ant} emissions due to the burning of fossil fuels and land-use change over this period (Friedlingstein et al. 2023, see Fig. 5.4). Over the same period, the terrestrial carbon sink (i.e., the land biosphere) has taken up 225 ± 55 GtC or 32% of the total emissions (Friedlingstein et al. 2023). Taken together, the land and ocean sinks have therefore removed 58% of the cumulative anthropogenic carbon emissions from the atmosphere, thus substantially reducing the anthropogenic greenhouse effect that would result if all emissions remained in the atmosphere. The dual role of the ocean in taking up both anthropogenic heat and carbon (including related climate and carbon feedbacks, as discussed below) has been termed the "ocean heat-carbon nexus" (Canadell et al. 2021; Séférian et al. 2024).

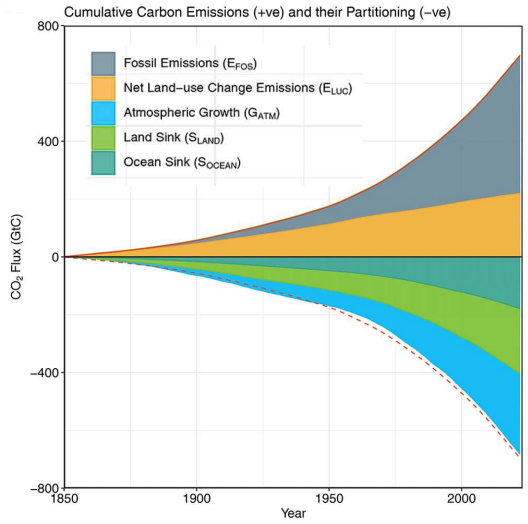

Figure 5.4: The cumulative global carbon budget as a function of time from 1850 to 2022. CO_2 emissions from fossil and land-use change contributions are balanced by increasing atmospheric CO_2 and by the land and ocean carbon sinks. The dashed red line mirrors the total CO_2 emissions indicated by the soldi red line. Adapted from Friedlingstein et al. (2023) (Fig. 3).

Ocean heat and C_{ant} uptake share a number of similarities, but they are not completely analogous. Both heat and CO_2 enter the ocean through air-sea fluxes at the surface, and are then transported by large-scale currents and mixing processes into the ocean interior. However, due to the distinctive carbonate chemistry of seawater, only 0.5% of C_{ant} is stored in the ocean in the form of dissolved CO_2 or carbonic acid (H_2CO_3), since almost all of the CO_2 is dissociated into bicarbonate (HCO_3^-) and carbonate (CO_3^{2-}) ions (Sarmiento and Gruber 2006), and this fact greatly enhances the carbon storage capacity of the ocean. A further difference stems from the fact that, unlike C_{ant}, heat is an active tracer, meaning that it influences the density of seawater, which is why OHU leads to changes in ocean circulation and stratification. These circulation changes then impact both heat and C_{ant} uptake and storage by redistributing these tracers across preexisting gradients in their oceanic inventories (e.g., Banks and Gregory 2006), although this effect is more pronounced for heat than for C_{ant} (Winton et al. 2013).

Nevertheless, there is a fundamental similarity between the oceanic uptake of heat and C_{ant}, and this was used in a study by Bronselaer and Zanna (2020) who showed that the spatial patterns of C_{ant} storage are closely related to patterns of "added heat" (i.e., the OHU resulting from transport by the preexisting ocean circulation), such that observations of C_{ant} storage can be exploited to infer the patterns of added and "redistributed heat" (i.e., the OHU resulting from changes in ocean circulation alone).

Heat and carbon uptake are not only connected through their oceanic storage patterns, but also, and perhaps more importantly, through their combined effect on climate. The effect of C_{ant} emissions on global warming can be quantified by the transient climate response to emissions (TCRE), which quantifies the global mean surface warming resulting for a given quantity of cumulative anthropogenic carbon emissions (in units of e.g. $\mathrm{K\,GtC^{-1}}$). It has been shown that the relationship between cumulative emissions and global warming is nearly linear (Allen et al. 2009; Matthews et al. 2009; Zickfeld et al. 2009) and path-independent (Krasting et al. 2014; MacDougall 2017), implying that the TCRE is nearly constant and thus a useful and policy-relevant metric, e.g., to prescribe remaining carbon budgets for a given warming target (Zickfeld et al. 2009; Lahn 2020). (This linearity may break down on millenial time scales (Paynter and Frölicher 2015) or under negative emissions from carbon dioxide removal; Zickfeld et al. 2016.) Despite being a simple climate change metric to define (or perhaps because of this), the TCRE is controlled by a complex set of processes involving the whole Earth system. A number of complementary frameworks have been proposed to decompose the TCRE into its controlling factors (e.g., Goodwin et al. 2015; Williams et al. 2016), emphasizing both the role of the atmosphere and ocean (Katavouta et al. 2018). Here we cite the form used by Williams et al. (2020):

$$\mathrm{TCRE} = \frac{\Delta T(t)}{I_{\mathrm{em}}(t)} = \underbrace{\left(\frac{\Delta T(t)}{\Delta F(t)}\right)}_{\text{thermal processes}} \cdot \underbrace{\left(\frac{\Delta F(t)}{\Delta I_{\mathrm{atmos}}(t)}\right)}_{\text{radiative forcing}} \cdot \underbrace{\left(\frac{\Delta I_{\mathrm{atmos}}(t)}{I_{\mathrm{em}}}\right)}_{\text{airborne fraction}}. \tag{5.1}$$

In this equation, ΔT is the global mean surface temperature anomaly in K, I_{em} the cumulative carbon emissions in GtC, ΔF the radiative forcing in $\mathrm{W\,m^{-2}}$, and I_{atmos} the atmospheric carbon inventory in GtC. Although this decomposition is mathematically trivial, it is highly useful and reveals the influence of distinct processes on TCRE as depicted in Fig. 5.5: (i) the term $\Delta T/\Delta F$ represents the surface warming resulting from a given radiative forcing and is therefore controlled by thermal processes such as climate feedbacks and OHU; (ii) the term $\Delta F/\Delta I_{\mathrm{atmos}}$ represents the radiative forcing arising from a given atmospheric CO_2 concentration; and (iii) the term $\Delta I_{\mathrm{atmos}}/\Delta I_{\mathrm{em}}$ is the airborne fraction, i.e., the fraction of C_{ant} emissions remaining in the atmosphere, and is thus controlled by the biogeochemical processes that set the land and ocean carbon sinks. In particular, the constancy of TCRE has been found to arise from a compensation

between a strengthening of the thermal part (i.e., weaker OHU and stronger climate feedbacks over time) and a weakening of the radiative forcing part (i.e., a saturation of radiative forcing with increasing atmospheric CO_2 concentrations; Williams et al. 2016). This further underlines the central connection between the ocean heat and carbon sinks, as well as the climatic importance of the "ocean heat-carbon nexus".

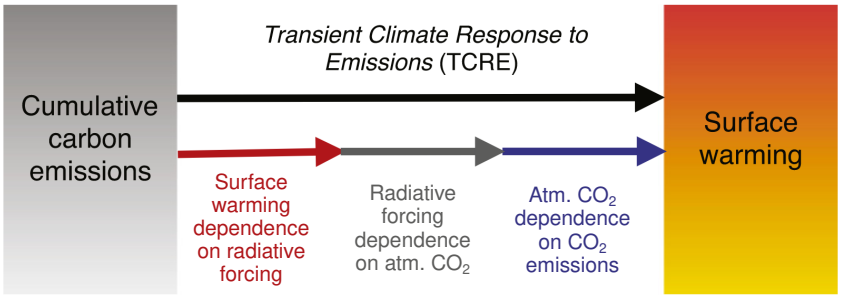

Figure 5.5: Schematic representation of the link between carbon emissions and warming. Adapted from Williams et al. (2016) (Fig. 1b).

There remains uncertainty in the processes contributing to each of three terms in Eq. (5.1). The first term is affected by uncertainties in cloud feedback (Zelinka et al. 2020) and OHU, whose inter-model spread only partly compensate each other, and represent the dominant uncertainty on a 100-year time scale (Williams et al. 2020). The second term results from the absorbtion spectrum of CO_2 and can be approximated as a logarithmic function of CO_2 concentration (Romps et al. 2022), but is still variable across models due to differences in carbon sink efficiency and radiative forcing. The last term (the airborne fraction) is affected by carbon cycle feedbacks which modulate the amount of carbon remaining in the atmosphere and can make the TCRE rate dependent (MacDougall and Friedlingstein 2015). These feedbacks are overall stable and result from a combination of negative (e.g., increased carbon sinks under increasing atmospheric CO_2) and positive contributions (e.g., decreased carbon sinks due to warming; Williams et al. 2019; Arora et al. 2020; Katavouta and Williams 2021), but they require interactive carbon cycle models and emissions-driven scenarios to be appropriately quantified, and this is not yet standard in the current generation of CMIP models.

A potential study on these uncertainties in the TCRE could extend the approaches used in this thesis—observational constraints as in Chapter 2 and mechanistic inter-model analyses as in Chapter 3—to include the effects of oceanic carbon uptake, redistribution, and storage on global warming. The analogies between ocean heat and carbon uptake identified by Bronselaer and Zanna (2020) could be further investigated by incorporating new observations of further tracers such as oxygen or chlorofluorocarbon (CFC) species. This would potentially allow a more mechanistic understanding of the biogeochemical processes affecting the efficiency of carbon and oxygen

fluxes (which are irrelevant for heat), as well as the physical processes affecting all tracers similarly. By eventually constraining the storage patterns of these tracers, this information could then also feed back into the pattern effect issue discussed above (Sec. 5.2.1).

Bibliography

Alessi, M. J. and M. A. A. Rugenstein (2023). "Surface Temperature Pattern Scenarios Suggest Higher Warming Rates Than Current Projections". *Geophysical Research Letters* 50:23. _eprint: https://onlinelibrary.wiley.com/doi/pdf/10.1029/2023GL105795, e2023GL105795. ISSN: 1944-8007. DOI: 10.1029/2023GL105795.

Allen, M. R. et al. (2009). "Warming caused by cumulative carbon emissions towards the trillionth tonne". *Nature* 458:7242. Publisher: Nature Publishing Group, pp. 1163–1166. ISSN: 1476-4687. DOI: 10.1038/nature08019.

Andrews, T. et al. (2018). "Accounting for Changing Temperature Patterns Increases Historical Estimates of Climate Sensitivity". *Geophysical Research Letters* 45:16. _eprint: https://onlinelibrary.wiley.com/doi/pdf/10.1029/2018GL078887, pp. 8490–8499. ISSN: 1944-8007. DOI: 10.1029/2018GL078887.

Andrews, T. et al. (2022). "On the Effect of Historical SST Patterns on Radiative Feedback". *Journal of Geophysical Research: Atmospheres* 127:18. _eprint: https://onlinelibrary.wiley.com/doi/pdf/10.1029/2022JD036675, e2022JD036675. ISSN: 2169-8996. DOI: 10.1029/2022JD036675.

Armour, K. C., J. Marshall, J. R. Scott, A. Donohoe, and E. R. Newsom (2016). "Southern Ocean warming delayed by circumpolar upwelling and equatorward transport". *Nature Geoscience* 9:7. Number: 7 Publisher: Nature Publishing Group, pp. 549–554. ISSN: 1752-0908. DOI: 10.1038/ngeo2731.

Armour, K. C. et al. (2024). "Sea-surface temperature pattern effects have slowed global warming and biased warming-based constraints on climate sensitivity". *Proceedings of the National Academy of Sciences* 121:12. Publisher: Proceedings of the National Academy of Sciences, e2312093121. DOI: 10.1073/pnas.2312093121.

Arora, V. K. et al. (2020). "Carbon–concentration and carbon–climate feedbacks in CMIP6 models and their comparison to CMIP5 models". *Biogeosciences* 17:16. Publisher: Copernicus GmbH, pp. 4173–4222. ISSN: 1726-4170. DOI: 10.5194/bg-17-4173-2020.

Banks, H. T. and J. M. Gregory (2006). "Mechanisms of ocean heat uptake in a coupled climate model and the implications for tracer based predictions of ocean heat uptake". *Geophysical Re-*

search Letters 33:7. _eprint: https://onlinelibrary.wiley.com/doi/pdf/10.1029/2005GL025352. ISSN: 1944-8007. DOI: 10.1029/2005GL025352.

Boé, J., A. Hall, and X. Qu (2009). "Deep ocean heat uptake as a major source of spread in transient climate change simulations". *Geophysical Research Letters* 36:22. _eprint: https://onlinelibrary.wiley.com/doi/pdf/10.1029/2009GL040845. ISSN: 1944-8007. DOI: 10.1029/2009GL040845.

Bower, A. et al. (2019). "Lagrangian Views of the Pathways of the Atlantic Meridional Overturning Circulation". *Journal of Geophysical Research: Oceans* 124:8. _eprint: https://onlinelibrary.wiley.com/doi/pdf/10.1029/2019JC015014, pp. 5313–5335. ISSN: 2169-9291. DOI: 10.1029/2019JC015014.

Bronselaer, B. and L. Zanna (2020). "Heat and carbon coupling reveals ocean warming due to circulation changes". *Nature* 584:7820. Bandiera_abtest: a Cg_type: Nature Research Journals Number: 7820 Primary_atype: Research Publisher: Nature Publishing Group Subject_term: Attribution;Physical oceanography;Projection and prediction Subject_term_id: attribution;physical-oceanography;projection-and-prediction, pp. 227–233. ISSN: 1476-4687. DOI: 10.1038/s41586-020-2573-5.

Canadell, J. G. et al. (2021). "Global carbon and other biogeochemical cycles and feedbacks". In: *Climate Change 2021: The Physical Science Basis. Contribution of Working Group I to the Sixth Assessment Report of the Intergovernmental Panel on Climate Change*. Ed. by V. Masson-Delmotte et al. Cambridge University Press, Cambridge, United Kingdom and New York, NY, USA, pp. 673–816. DOI: 10.1017/9781009157896.001.

Ceppi, P. and J. M. Gregory (2017). "Relationship of tropospheric stability to climate sensitivity and Earth's observed radiation budget". *Proceedings of the National Academy of Sciences* 114:50. Publisher: Proceedings of the National Academy of Sciences, pp. 13126–13131. DOI: 10.1073/pnas.1714308114.

Chamberlain, M. A., R. J. Matear, M. Holzer, D. Bi, and S. J. Marsland (2019). "Transport matrices from standard ocean-model output and quantifying circulation response to climate change". *Ocean Modelling* 135, pp. 1–13. ISSN: 1463-5003. DOI: 10.1016/j.ocemod.2019.01.005.

Delandmeter, P. and E. van Sebille (2019). "The Parcels v2.0 Lagrangian framework: new field interpolation schemes". *Geoscientific Model Development* 12:8. Publisher: Copernicus GmbH, pp. 3571–3584. ISSN: 1991-959X. DOI: 10.5194/gmd-12-3571-2019.

Döös, K. and D. J. Webb (1994). "The Deacon Cell and the Other Meridional Cells of the Southern Ocean". *Journal of Physical Oceanography* 24:2. Publisher: American Meteorological Society Section: Journal of Physical Oceanography, pp. 429–442. ISSN: 0022-3670, 1520-0485. DOI: 10.1175/1520-0485(1994)024<0429:TDCATO>2.0.CO;2.

Drake, H. F. et al. (2018). "Lagrangian Timescales of Southern Ocean Upwelling in a Hierarchy of Model Resolutions". *Geophysical Research Letters* 45:2. _eprint: https://onlinelibrary.wiley.com/doi/pdf/10.1002/2017GL076045, pp. 891–898. ISSN: 1944-8007. DOI: 10.1002/2017GL076045.

Eyring, V. et al. (2024). "Pushing the frontiers in climate modelling and analysis with machine learning". *Nature Climate Change* 14:9. Publisher: Nature Publishing Group, pp. 916–928. ISSN: 1758-6798. DOI: 10.1038/s41558-024-02095-y.

Fox-Kemper, B. et al. (2019). "Challenges and Prospects in Ocean Circulation Models". *Frontiers in Marine Science* 6. Publisher: Frontiers. ISSN: 2296-7745. DOI: 10.3389/fmars.2019.00065.

Friedlingstein, P. et al. (2023). "Global Carbon Budget 2023". *Earth System Science Data* 15:12. Publisher: Copernicus GmbH, pp. 5301–5369. ISSN: 1866-3508. DOI: 10.5194/essd-15-5301-2023.

Goodwin, P., R. G. Williams, and A. Ridgwell (2015). "Sensitivity of climate to cumulative carbon emissions due to compensation of ocean heat and carbon uptake". *Nature Geoscience* 8:1. Publisher: Nature Publishing Group, pp. 29–34. ISSN: 1752-0908. DOI: 10.1038/ngeo2304.

Gregory, J. M. et al. (2023). "A new conceptual model of global ocean heat uptake". *Climate Dynamics*. ISSN: 1432-0894. DOI: 10.1007/s00382-023-06989-z.

Haertel, P. and A. Fedorov (2012). "The Ventilated Ocean". Section: Journal of Physical Oceanography. DOI: 10.1175/2011JPO4590.1.

Hastie, T., R. Tibshirani, and J. Friedman (2009). *The Elements of Statistical Learning*. Springer Series in Statistics. Springer New York, New York, NY. ISBN: 978-0-387-84857-0 978-0-387-84858-7. DOI: 10.1007/978-0-387-84858-7.

Huber, M. B. and L. Zanna (2017). "Drivers of uncertainty in simulated ocean circulation and heat uptake". *Geophysical Research Letters* 44:3. _eprint: https://onlinelibrary.wiley.com/doi/pdf/10.1002/2016GL071587, pp. 1402–1413. ISSN: 1944-8007. DOI: 10.1002/2016GL071587.

Kang, S. M., P. Ceppi, Y. Yu, and I.-S. Kang (2023a). "Recent global climate feedback controlled by Southern Ocean cooling". *Nature Geoscience* 16:9. Number: 9 Publisher: Nature Publishing Group, pp. 775–780. ISSN: 1752-0908. DOI: 10.1038/s41561-023-01256-6.

Kang, S. M. et al. (2023b). "Global impacts of recent Southern Ocean cooling". *Proceedings of the National Academy of Sciences* 120:30. Publisher: Proceedings of the National Academy of Sciences, e2300881120. DOI: 10.1073/pnas.2300881120.

Katavouta, A. and R. G. Williams (2021). "Ocean carbon cycle feedbacks in CMIP6 models: contributions from different basins". *Biogeosciences* 18:10. Publisher: Copernicus GmbH, pp. 3189–3218. ISSN: 1726-4170. DOI: 10.5194/bg-18-3189-2021.

Katavouta, A., R. G. Williams, P. Goodwin, and V. Roussenov (2018). "Reconciling Atmospheric and Oceanic Views of the Transient Climate Response to Emissions". *Geophysical Research Letters* 45:12. _eprint: https://agupubs.onlinelibrary.wiley.com/doi/pdf/10.1029/2018GL077849, pp. 6205–6214. ISSN: 1944-8007. DOI: 10.1029/2018GL077849.

Krasting, J. P., J. P. Dunne, E. Shevliakova, and R. J. Stouffer (2014). "Trajectory sensitivity of the transient climate response to cumulative carbon emissions". *Geophysical Research Letters* 41:7. _eprint: https://onlinelibrary.wiley.com/doi/pdf/10.1002/2013GL059141, pp. 2520–2527. ISSN: 1944-8007. DOI: 10.1002/2013GL059141.

Lahn, B. (2020). "A history of the global carbon budget". *WIREs Climate Change* 11:3. _eprint: https://onlinelibrary.wiley.com/doi/pdf/10.1002/wcc.636, e636. ISSN: 1757-7799. DOI: 10.1002/wcc.636.

Liu, M., B. J. Soden, G. A. Vecchi, and C. Wang (2023). "The Spread of Ocean Heat Uptake Efficiency Traced to Ocean Salinity". *Geophysical Research Letters* 50:4. _eprint: https://onlinelibrary.wiley.com/doi/pdf/10.1029/2022GL100171, e2022GL100171. ISSN: 1944-8007. DOI: 10.1029/2022GL100171.

Lyu, K., X. Zhang, and J. A. Church (2021). "Projected ocean warming constrained by the ocean observational record". *Nature Climate Change* 11:10. Number: 10 Publisher: Nature Publishing Group, pp. 834–839. ISSN: 1758-6798. DOI: 10.1038/s41558-021-01151-1.

MacDougall, A. H. (2017). "The oceanic origin of path-independent carbon budgets". *Scientific Reports* 7:1. Publisher: Nature Publishing Group, p. 10373. ISSN: 2045-2322. DOI: 10.1038/s41598-017-10557-x.

MacDougall, A. H. and P. Friedlingstein (2015). "The Origin and Limits of the Near Proportionality between Climate Warming and Cumulative CO2 Emissions". *Journal of Climate* 28:10, pp. 4217–4230. ISSN: 0894-8755, 1520-0442. DOI: 10.1175/JCLI-D-14-00036.1.

MacGilchrist, G. A., D. P. Marshall, H. L. Johnson, C. Lique, and M. Thomas (2017). "Characterizing the chaotic nature of ocean ventilation". *Journal of Geophysical Research: Oceans* 122:9. _eprint: https://onlinelibrary.wiley.com/doi/pdf/10.1002/2017JC012875, pp. 7577–7594. ISSN: 2169-9291. DOI: 10.1002/2017JC012875.

Madec, G. et al. (2023). "NEMO Ocean Engine Reference Manual". Publisher: Zenodo. DOI: 10.5281/zenodo.8167700.

Marzocchi, A., A. J. G. Nurser, L. Clément, and E. L. McDonagh (2021). "Surface atmospheric forcing as the driver of long-term pathways and timescales of ocean ventilation". *Ocean Science* 17:4, pp. 935–952. ISSN: 1812-0792. DOI: 10.5194/os-17-935-2021.

Matthews, H. D., N. P. Gillett, P. A. Stott, and K. Zickfeld (2009). "The proportionality of global warming to cumulative carbon emissions". *Nature* 459:7248. Publisher: Nature Publishing Group, pp. 829–832. ISSN: 1476-4687. DOI: 10.1038/nature08047.

McGregor, S. et al. (2014). "Recent Walker circulation strengthening and Pacific cooling amplified by Atlantic warming". *Nature Climate Change* 4:10. Publisher: Nature Publishing Group, pp. 888–892. ISSN: 1758-6798. DOI: 10.1038/nclimate2330.

Meehl, G. A. et al. (2020). "Context for interpreting equilibrium climate sensitivity and transient climate response from the CMIP6 Earth system models". *Science Advances* 6:26. Publisher: American Association for the Advancement of Science, eaba1981. DOI: 10.1126/sciadv.aba1981.

Newsom, E., L. Zanna, and J. Gregory (2023). "Background Pycnocline Depth Constrains Future Ocean Heat Uptake Efficiency". *Geophysical Research Letters* 50:22. _eprint: https://onlinelibrary.wiley.com/doi/pdf/10.1029/2023GL105673, e2023GL105673. ISSN: 1944-8007. DOI: 10.1029/2023GL105673.

Newsom, E., L. Zanna, S. Khatiwala, and J. M. Gregory (2020). "The Influence of Warming Patterns on Passive Ocean Heat Uptake". *Geophysical Research Letters* 47:18. _eprint: https://onlinelibrary.wiley.com/doi/pdf/10.1029/2020GL088429, e2020GL088429. ISSN: 1944-8007. DOI: 10.1029/2020GL088429.

Paynter, D. and T. L. Frölicher (2015). "Sensitivity of radiative forcing, ocean heat uptake, and climate feedback to changes in anthropogenic greenhouse gases and aerosols". *Journal of Geophysical Research: Atmospheres* 120:19. _eprint: https://onlinelibrary.wiley.com/doi/pdf/10.1002/2015JD023364, pp. 9837–9854. ISSN: 2169-8996. DOI: 10.1002/2015JD023364.

Ramsey, A. L., H. H. Furey, and A. S. Bower (2018). "Deep Floats Reveal Complex Ocean Circulation Patterns". *Eos* 99. ISSN: 2324-9250. DOI: 10.1029/2018EO105549.

Romps, D. M., J. T. Seeley, and J. P. Edman (2022). "Why the Forcing from Carbon Dioxide Scales as the Logarithm of Its Concentration". Section: Journal of Climate. DOI: 10.1175/JCLI-D-21-0275.1.

Rousselet, L., P. Cessi, and G. Forget (2021). "Coupling of the mid-depth and abyssal components of the global overturning circulation according to a state estimate". *Science Advances*. Publisher: American Association for the Advancement of Science. DOI: 10.1126/sciadv.abf5478.

Sarmiento, J. L. and N. Gruber (2006). *Ocean Biogeochemical Dynamics*. Princeton University Press. ISBN: 978-1-4008-4907-9 978-0-691-01707-5. DOI: 10.2307/j.ctt3fgxqx.

Schmidt, G. A. et al. (2023). "Anomalous Meltwater From Ice Sheets and Ice Shelves Is a Historical Forcing". *Geophysical Research Letters* 50:24. _eprint: https://onlinelibrary.wiley.com/doi/pdf/10.1029/2023GL106530, e2023GL106530. ISSN: 1944-8007. DOI: 10.1029/2023GL106530.

Sebille, E. van et al. (2018). "Lagrangian ocean analysis: Fundamentals and practices". *Ocean Modelling* 121, pp. 49–75. ISSN: 1463-5003. DOI: 10.1016/j.ocemod.2017.11.008.

Séférian, R. et al. (2024). "Physical inconsistencies in the representation of the ocean heat-carbon nexus in simple climate models". *Communications Earth & Environment* 5:1. Publisher: Nature Publishing Group, pp. 1–10. ISSN: 2662-4435. DOI: 10.1038/s43247-024-01464-x.

Speich, S., B. Blanke, and W. Cai (2007). "Atlantic meridional overturning circulation and the Southern Hemisphere supergyre". *Geophysical Research Letters* 34:23. _eprint: https://onlinelibrary.wiley.com/doi/pdf/10.1029/2007GL031583. ISSN: 1944-8007. DOI: 10.1029/2007GL031583.

Styles, A. F., M. J. Bell, and D. P. Marshall (2023). "The Sensitivity of an Idealized Weddell Gyre to Horizontal Resolution". *Journal of Geophysical Research: Oceans* 128:10. _eprint: https://onlinelibrary.wiley.com/doi/pdf/10.1029/2023JC019711, e2023JC019711. ISSN: 2169-9291. DOI: 10.1029/2023JC019711.

Styles, A. F., G. A. MacGilchrist, M. J. Bell, and D. P. Marshall (2024). "Spatial and Temporal Patterns of Southern Ocean Ventilation". *Geophysical Research Letters* 51:4. _eprint: https://onlinelibrary.wiley.com/doi/pdf/10.1029/2023GL106716, e2023GL106716. ISSN: 1944-8007. DOI: 10.1029/2023GL106716.

Tamsitt, V., R. P. Abernathey, M. R. Mazloff, J. Wang, and L. D. Talley (2018). "Transformation of Deep Water Masses Along Lagrangian Upwelling Pathways in the Southern Ocean". *Journal of Geophysical Research: Oceans* 123:3. _eprint: https://onlinelibrary.wiley.com/doi/pdf/10.1002/2017JC013409, pp. 1994–2017. ISSN: 2169-9291. DOI: 10.1002/2017JC013409.

Tamsitt, V. et al. (2017). "Spiraling pathways of global deep waters to the surface of the Southern Ocean". *Nature Communications* 8:1. Number: 1 Publisher: Nature Publishing Group, p. 172. ISSN: 2041-1723. DOI: 10.1038/s41467-017-00197-0.

Tokarska, K. B. et al. (2020). "Past warming trend constrains future warming in CMIP6 models". *Science Advances* 6:12. Publisher: American Association for the Advancement of Science, eaaz9549. DOI: 10.1126/sciadv.aaz9549.

Vallis, G. K. (2017). *Atmospheric and oceanic fluid dynamics: Fundamentals and large-scale circulation*. 2nd ed. Cambridge University Press, Cambridge.

Viglione, G. A. and A. F. Thompson (2016). "Lagrangian pathways of upwelling in the Southern Ocean". *Journal of Geophysical Research: Oceans* 121:8. _eprint: https://onlinelibrary.wiley.com/doi/pdf/10.1002/2016JC011773, pp. 6295–6309. ISSN: 2169-9291. DOI: 10.1002/2016JC011773.

Williams, R. G., P. Ceppi, and A. Katavouta (2020). "Controls of the transient climate response to emissions by physical feedbacks, heat uptake and carbon cycling". *Environmental Research Letters* 15:9. Publisher: IOP Publishing, p. 0940c1. ISSN: 1748-9326. DOI: 10.1088/1748-9326/ab97c9.

Williams, R. G., P. Goodwin, V. M. Roussenov, and L. Bopp (2016). "A framework to understand the transient climate response to emissions". *Environmental Research Letters* 11:1. Publisher: IOP Publishing, p. 015003. ISSN: 1748-9326. DOI: 10.1088/1748-9326/11/1/015003.

Williams, R. G., A. Katavouta, and P. Goodwin (2019). "Carbon-Cycle Feedbacks Operating in the Climate System". *Current Climate Change Reports* 5:4, pp. 282–295. ISSN: 2198-6061. DOI: 10.1007/s40641-019-00144-9.

Wills, R. C. J., Y. Dong, C. Proistosecu, K. C. Armour, and D. S. Battisti (2022). "Systematic Climate Model Biases in the Large-Scale Patterns of Recent Sea-Surface Temperature and Sea-Level Pressure Change". *Geophysical Research Letters* 49:17. _eprint: https://onlinelibrary.wiley.com/doi/pdf/10.1029/2022GL100011, e2022GL100011. ISSN: 1944-8007. DOI: 10.1029/2022GL100011.

Winton, M., S. M. Griffies, B. L. Samuels, J. L. Sarmiento, and T. L. Frölicher (2013). "Connecting Changing Ocean Circulation with Changing Climate". *Journal of Climate* 26:7. Publisher: American Meteorological Society Section: Journal of Climate, pp. 2268–2278. ISSN: 0894-8755, 1520-0442. DOI: 10.1175/JCLI-D-12-00296.1.

Winton, M. et al. (2014). "Has coarse ocean resolution biased simulations of transient climate sensitivity?" *Geophysical Research Letters* 41:23. _eprint: https://onlinelibrary.wiley.com/doi/pdf/10.1002/2014GL061523, pp. 8522–8529. ISSN: 1944-8007. DOI: 10.1002/2014GL061523.

Xie, Y. et al. (2024). "Euphotic Zone Residence Time of Antarctic Bottom Water". *Geophysical Research Letters* 51:10. _eprint: https://agupubs.onlinelibrary.wiley.com/doi/pdf/10.1029/2023GL106342, e2023GL106342. ISSN: 1944-8007. DOI: 10.1029/2023GL106342.

Zelinka, M. D. et al. (2020). "Causes of Higher Climate Sensitivity in CMIP6 Models". *Geophysical Research Letters* 47:1. _eprint: https://onlinelibrary.wiley.com/doi/pdf/10.1029/2019GL085782, e2019GL085782. ISSN: 1944-8007. DOI: 10.1029/2019GL085782.

Zhu, C. et al. (2024). "Enhanced ocean heat storage efficiency during the last deglaciation". *Science Advances* 10:38. Publisher: American Association for the Advancement of Science, eadp5156. DOI: 10.1126/sciadv.adp5156.

Zickfeld, K., M. Eby, H. D. Matthews, and A. J. Weaver (2009). "Setting cumulative emissions targets to reduce the risk of dangerous climate change". *Proceedings of the National Academy of Sciences* 106:38. Publisher: Proceedings of the National Academy of Sciences, pp. 16129–16134. DOI: 10.1073/pnas.0805800106.

Zickfeld, K., A. H. MacDougall, and H. D. Matthews (2016). "On the proportionality between global temperature change and cumulative CO2 emissions during periods of net negative CO2 emissions". *Environmental Research Letters* 11:5. Publisher: IOP Publishing, p. 055006. ISSN: 1748-9326. DOI: 10.1088/1748-9326/11/5/055006.

A Appendix to front matter

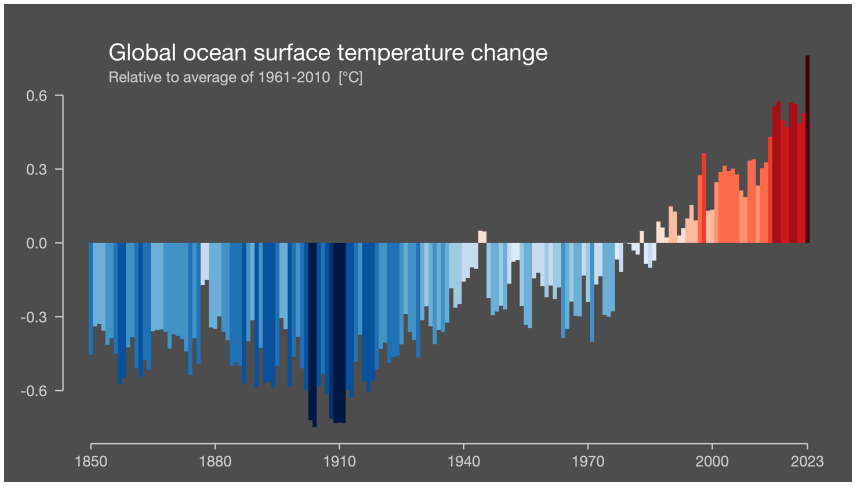

Figure A.1: Global mean sea surface temperature anomalies from 1850 to 2023 relative to a 1961–2010 mean baseline, from https://showyourstripes.info/c/ocean/all (Prof. Ed Hawkins, University of Reading). This is the original figure that was adapted for the title pages of this thesis.

B Appendix to Chapter 4

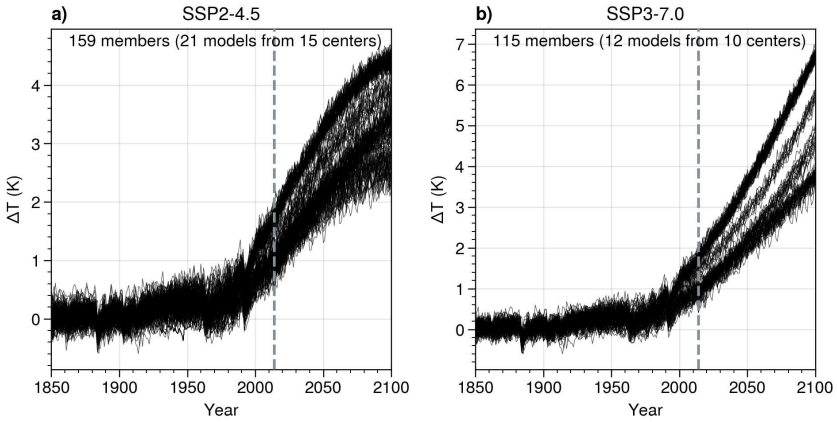

Figure B.1: Global mean surface air temperature anomaly ΔSAT under the SSP2-4.5 and SSP3-7.0 scenarios. The dashed vertical line indicates the year 2014 where the SSP runs branch off from the historical run in each ensemble member.

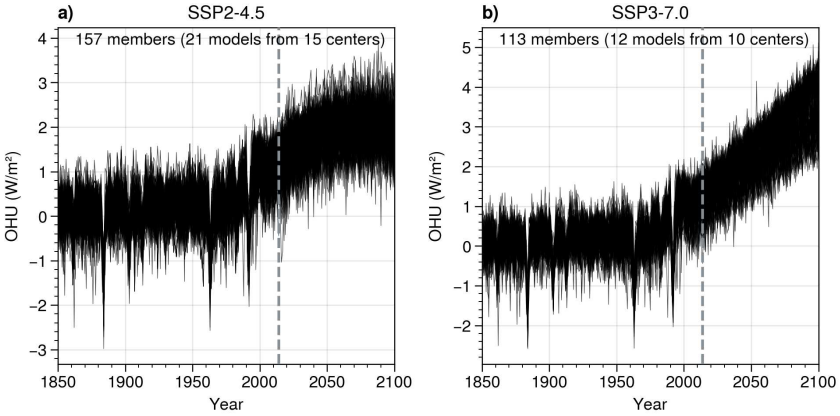

Figure B.2: Global ocean heat uptake (OHU) under the SSP2-4.5 and SSP3-7.0 scenarios. The dashed vertical line indicates the year 2014 where the SSP runs branch off from the historical run in each ensemble member.

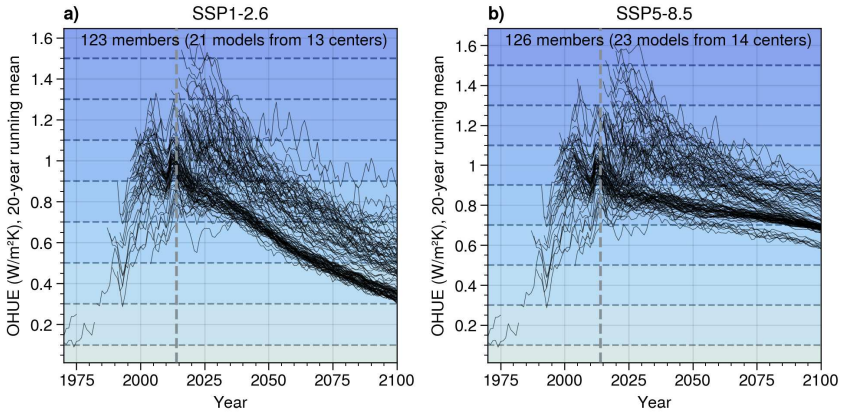

Figure B.3: Ocean heat uptake efficiency (OHUE) under the SSP2-4.5 and SSP3-7.0 scenarios (20-year running mean). The dashed vertical line indicates the year 2014 where the SSP runs branch off from the historical run in each ensemble member.

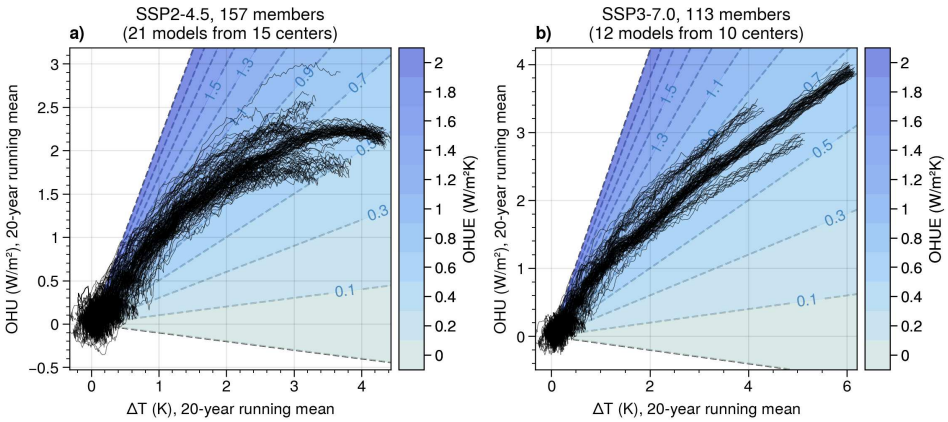

Figure B.4: Global OHU plotted against global ΔSAT under the SSP2-4.5 and SSP3-7.0 scenarios (20-year running mean). The blue shading and labeled contours indicate the resulting OHU efficiency (OHUE = OHU/ΔSAT).

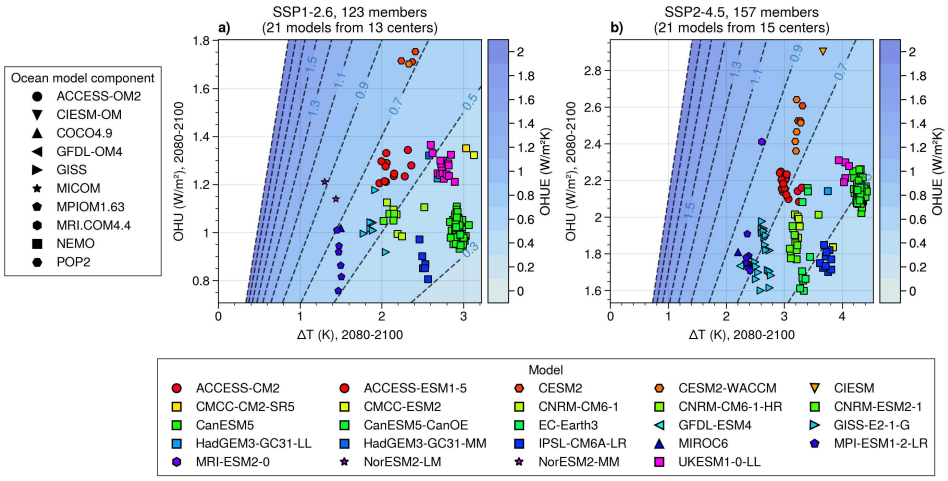

Figure B.5: Global OHU plotted against global ΔSAT (averaged over 2080–2100 in the SSP1-2.6 and SSP2-4.5 scenarios). The blue shading and labeled contours indicate the resulting OHU efficiency (OHUE = OHU/ΔSAT). The marker colors indicate the different climate models, and the marker shape indicate their ocean model component.

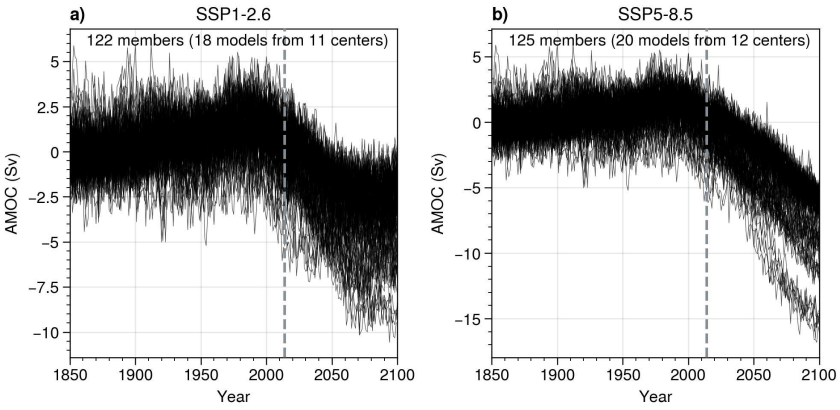

Figure B.6: AMOC strength anomaly at 26°N under the SSP1-2.6 and SSP5-8.5 scenarios. The dashed vertical line indicates the year 2014 where the SSP runs branch off from the historical run in each ensemble member.

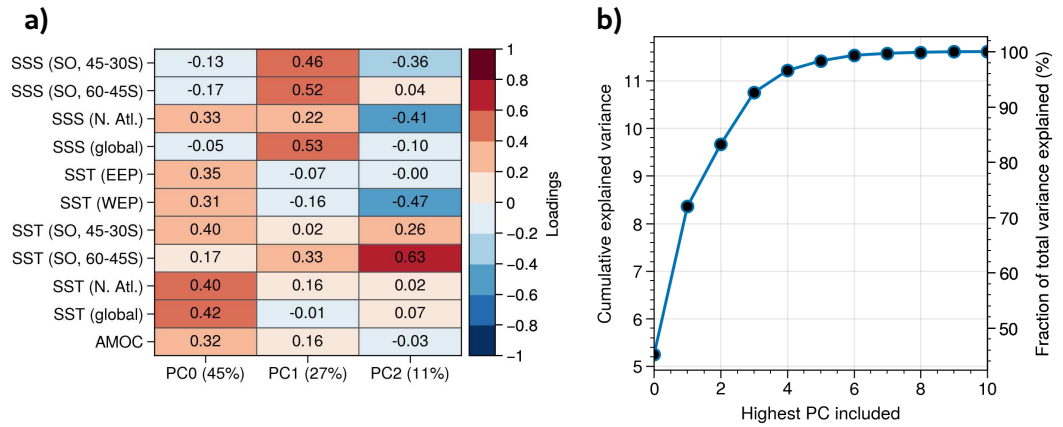

Figure B.7: Principal component analysis of the predictor variables. As in Fig. 4.7, but the predictor variables were first averaged over multi-member ensembles for individual climate models. **a)** Principal component loadings for the first four PCs. The numbers in parentheses give the fraction of total variance explained by each PC. **b)** Cumulative variance explained by principal components.

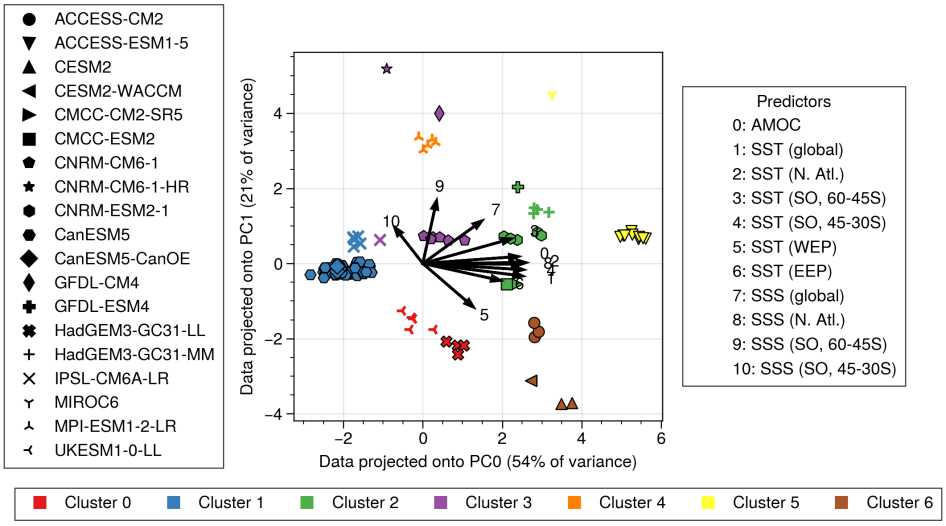

Figure B.8: Clustering of principal components. As in Fig. 4.8, but with spectral clustering instead of K-means clustering.

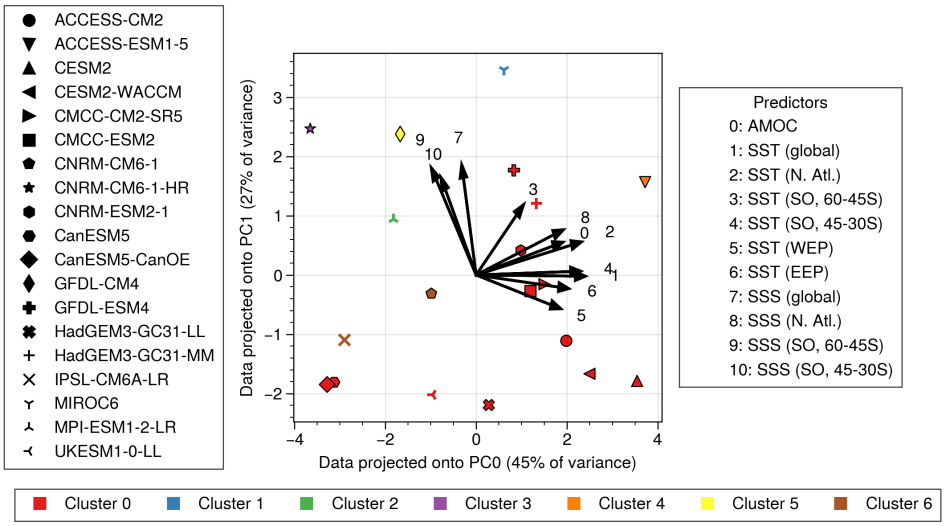

Figure B.9: Clustering of principal components. As in Fig. 4.8, but with input variables first averaged over each multi-member ensemble for individual climate models.

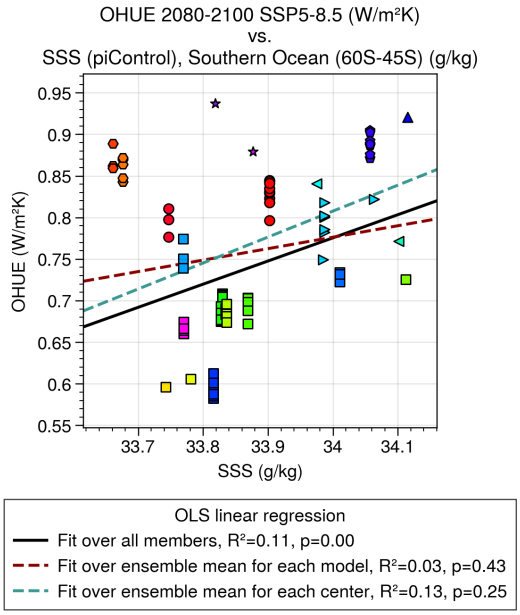

Figure B.10: Preindustrial mean SSS in the `SO-60-45` region scattered against future OHUE across the model ensemble. Marker colors and shapes correspond to climate models and ocean model components, respectively, as given in the legend of Fig. 4.14.


The End.